

Numerical simulations of accretion discs

Miljenko Čemeljić

SGMK, College of Astronomy and Natural Sciences, Torun
Nicolaus Copernicus Astronomical Center, Polish Academy of Sciences,
Warsaw

Monday 13:30-15:30 CET

Part I: Newtonian simulations of accretion discs (M. Čemeljić)

- **Lect. 1:** General introduction to accretion and types of objects where accretion is important, jets, Linux shell commands, text editors, ecology of computing
- **Lect. 2:** Accretion energetics, spherical (Bondi) accretion, stationary thin accretion disc, fluid eqs, (M)HD eqs, viscosity, resistivity, turbulence, MRI, Alfven waves, code PLUTO, structure of the code, hands-on installation and testing, visualization with gnuplot
- **Lect. 3:** Shakura-Sunyaev 1973 disc, initial and boundary conditions for Orszag-Tang test problem in PLUTO in 2D and 3D, visualization in 2D and 3D with Paraview & VisIt
- **Lect. 4:** KK 3D solution for thin disc in HD, Vertically averaged solutions for thin disc, setup and running of 2.5D HD KK disc in PLUTO, analysis of the results from 2.5D runs with Paraview and Python
- **Lect. 5:** Euler equations, Finite difference, volume and elements methods, Godunov's scheme, Riemann problem, CFL condition, Magnetized thin KK disc, setup and running of 2.5D disc in MHD in PLUTO, visualization of magnetic field lines with Paraview.
- **Lect. 6:** Approximate Riemann solvers, reconstruction methods, MHD numerics, astrophysical jets, simulations of jets from disc as a b.c. and with the disc evolution included, streamlines in Paraview in 2D and 3D
- **Lect. 7:** Different modules in PLUTO, cooling, radiative transfer, hot discs, post-processing of the results, DUSTER, Python script for analysis
- **Lect. 8:** Pseudo-Newtonian potential and its use in numerical simulations of a disk or torus around black hole or naked singularity, star-planet simulations, running jobs on a linux cluster

- **Part II: General relativity simulations of accretion discs (obligatory for Geoplanet students) by Debora Lančová (6 lectures)+1 lecture on Cosmological simulations by Tomasz Krajewski**

Outline, Lect. 1: Introduction to accretion

- General intro on lectures, literature, well-being...
- What is accretion and why do we need it?
- History of accretion, disks, jets
- Observational material on accretion, cosmic magnetic fields
- Roche equipotential surfaces, PyAstro package
- Motivation and examples of accr. disk simulations
- Intro to Linux, shell commands, text editors
- Ecology of computing

Lectures time is Mondays 13:30-15:30 CET, on-site for residents in Warsaw, online on Zoom. Attendance of 70% is expected. Exam by preparing a report on chosen simulation setup and discussion of that report with the lecturer.

Literature for this course:

- **Books:**

Frank, King & Raine, „Accretion power in astrophysics”

Kato, Fukue & Mineshige, „Black-Hole Accretion Disks: Towards a New Paradigm”

M. Čemeljić lecture scripts from the Silesian University in Opava, (2022), “Thin accretion disks” part I: Basic concepts and solutions, Part II: Numerical simulations

User manual of PLUTO code, available in PLUTO/Doc/userguide.pdf directory

Linux booklet “Linux Pocket Guide”, D.J.Barrett, O’Reilly Media

Douglas Adams, “The Hitchhiker’s Guide to the Galaxy”

- **Journal papers:**

Shakura & Sunyaev, 1973, “Black holes in binary systems”, A&A, 24, 337

Novikov & Thorne, 1973, general relativistic disk

Pringle, 1981, “Accretion discs in astrophysics”, ARAA, 19, 137

M. Čemeljić, 2019, "Atlas" of numerical solutions for star-disk magnetospheric interaction, A&A, 624, A31

Čemeljić, Kluźniak, Parthasarathy, 2023, „Magnetically threaded accretion disks in resistive magnetohydrodynamic simulations and asymptotic expansion”, A&A 678, A57

Zhu & Stone, 2018, „Global Evolution of an Accretion Disk with a Net Vertical Field: Coronal Accretion, Flux Transport, and Disk Winds”, ApJ, 867, 34

B. Mishra, 2016, .”Strongly magnetized accretion discs: structure and accretion from global magnetohydrodynamic simulation”, MNRAS 492, 1855

Mishra, Čemeljić, Varela & Falanga, 2023, “Auroras on Planets around Pulsars”, ApJL, 959, L13 (SPI choice)

-On-line resources:

Abramowicz & Straub, “Accretion discs”, Scholarpedia article: http://www.scholarpedia.org/article/Accretion_discs

Use Linux. Full stop. The Microsoft Corporation is today the largest user of Linux. I am echoing the Richard (Matthew) Stallman's (rms) vocation:

“THERE IS NO SYSTEM BUT GNU AND LINUX IS ONE OF IT'S KERNELS.”

rms created GNU (Gnu's not Unix) GNU/Linux, a Unix-like operating system made up of different OS components and services that create the Linux OS. He created Emacs, the GNU C Compiler, and the GNU Debugger, and is one of initial initiators of the open source movement for software to be distributed in such a way that its users have the freedom to use, study, distribute, and modify that software. The four fundamental freedoms for free software are, by him:

- ***THE FREEDOM TO RUN THE PROGRAM AS YOU WISH, FOR ANY PURPOSE.***
- ***THE FREEDOM TO STUDY HOW THE PROGRAM WORKS, AND CHANGE IT SO IT DOES YOUR COMPUTING AS YOU WISH.***
- ***THE FREEDOM TO REDISTRIBUTE COPIES SO YOU CAN HELP YOUR NEIGHBOR.***
- ***THE FREEDOM TO DISTRIBUTE COPIES OF YOUR MODIFIED VERSIONS TO OTHERS.***

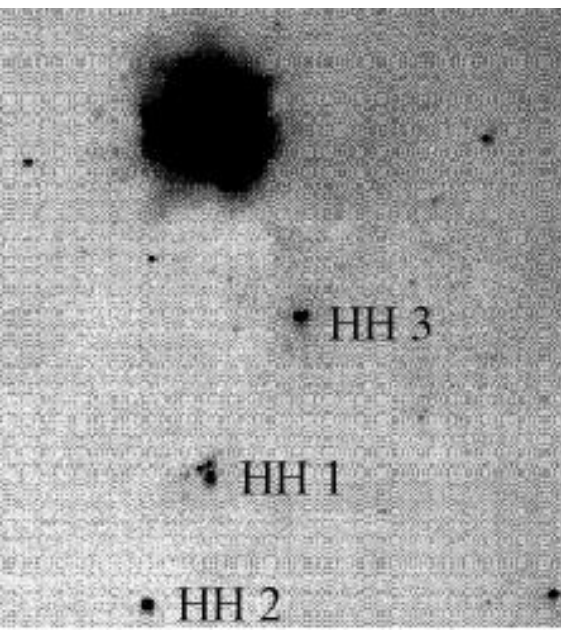
His explanation of the term GNU/Linux: Linux is the kernel: the program in the system that allocates the machine's resources to the other programs that you run. The kernel is an essential part of an operating system, but useless by itself; it can only function in the context of a complete operating system. Linux is normally used in combination with the GNU operating system: the whole system is basically GNU with Linux added, or GNU/Linux. All the so-called “Linux” distributions are really distributions of GNU/Linux.

rms ultimate geek stature in open source community is such that you can find lots of misinformation on him, but also many funny comments like: “Richard Stallman is giving a talk at Microsoft campus. If the world ends today, you know why.”

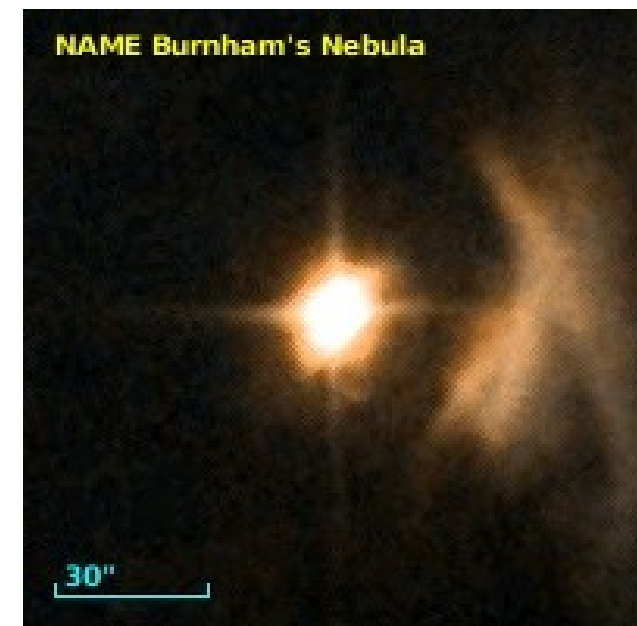
- Numerical simulations are a time-consuming work, requiring hours and hours of sitting in front of the screen. Please take care of appropriate dimensions and position of monitor, desktop settings (not black on white, it is too tiresome for eyes) and seat position, and remember to regularly exercise. You will appreciate it after 20-some years. Remember also to spend enough time with (good) living beings, possibly humans. You will appreciate it immediately.

Historically, accretion was first considered as a relevant process in the close binaries: after collecting a wealth of spectrographic data by Struve and collaborators, it became obvious that simple models of stellar stability are insufficient to explain the spectral features. Theoretical curves were smoothed by the simplifications, and observational curves were not smooth at all! Introducing more physical processes into astrophysics of stars was called “Struve revolution” by Daniel Popper in 1970 (not Karl Popper of the philosophy of Science!).

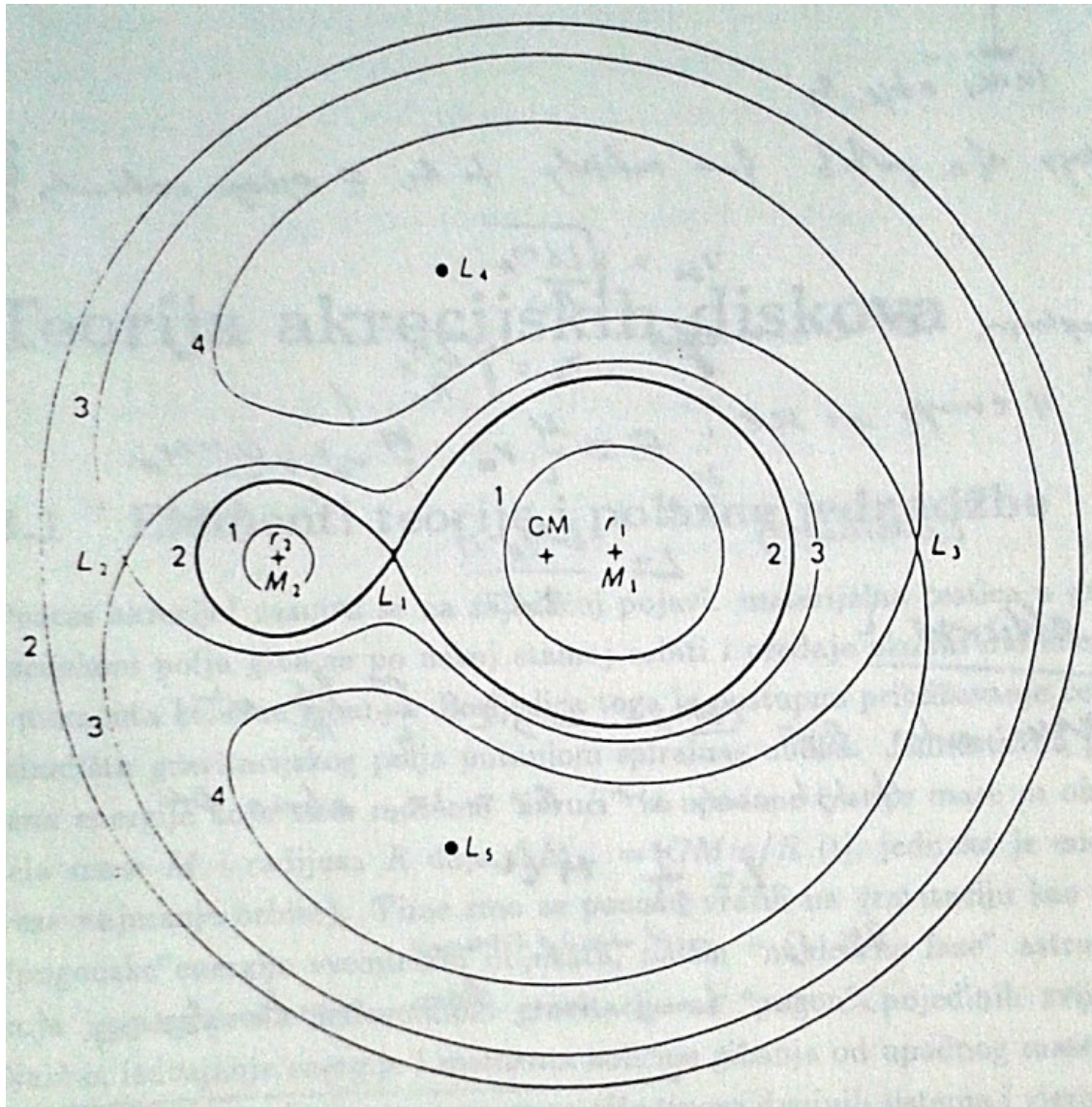
To explain the spectral features and the energy and angular momentum evolution in the “peculiar stars”-which mostly showed to be close binaries, astronomers around the middle of XX century had to include the streams of matter, gas rings, Roche’s equipotential surfaces, and finally Huang (1963) included a thick disk. Gradually, with increase in quality of data, similar concepts were introduced in the objects on other scales, like active galactic nuclei (AGNs), quasars, and centers of clusters of galaxies. Gravity was back, astrophysics of accretion could start!



Herbig-Haro (HH) objects (big one is NGC1999) and young stellar objects (YSOs) envelopes of which T-Tauri with the Burnham’s nebula HH255 were the prototype examples of complicated environment, with streams of matter, gas envelopes and outflows, which show that simple models fail. We needed better theory of star formation to explain such observations.



Roche equipotential surfaces



- Roche surfaces usually emerge when we are dealing with close binaries.
- French mathematician Edouard Albert Roche (1820-1883) discussed the problem of equipotential surfaces in the context of stability of the orbits of small planetary satellites in 1849.
- Physical model is of the small test mass m moving in the gravitational fields of two massive points. There is no gravitational back-reaction from m to M_1 and M_2 .

Roche equipotential surfaces

- Because of tidal forces, with close binaries we usually can work in this approximation.
- Lagrange in 1772 showed the existence of 5 points (Lagrange points L_1 - L_5), where forces from M1 and M2 are balanced.
- If we solve the equations in (x,y,z) put along the line connecting M1 and M2, perpendicular to it in the plane of the paper and vertical out of the paper, we obtain, with μ and $1-\mu$ being the masses expressed in total mass parts $\mu=M1+M2$ and distances r_1 and r_2 in the units of the masses M1 and M2 distance:

$$v^2 = x^2 + y^2 + \frac{2(1-\mu)}{r_1} + \frac{2\mu}{r_2} - C$$

- Constant C is defined by the initial conditions.
- The velocity $v=0$ defines a surface at which velocities are >0 or <0 , real or imaginary, and C defines from which side of this surface the mass m is moving.

Roche equipotential surfaces

- Jacobi found that $v^2=V-C$, where

$$V = \frac{1}{2}(x^2 + y^2) + \frac{1 - \mu}{r_1} + \frac{\mu}{r_2}.$$

- It shows that we can use the same approach for close binaries, even when there are flows between them, or they are filling their respective “Roche lobes”, so that the solution gives us the equipotential surfaces, U is the potential:

$$-U = \frac{1}{2}(x^2 + y^2) + \frac{1 - \mu}{r_1} + \frac{\mu}{r_2}$$

- We have $v^2=-2U-C$

Astronomy packages

- If you need some routine for astrophysical use, it is very probable someone else also needed it. There is a pile of general routines from last decades in Numerical Recipes. Astro routines nowadays you can find in python, and many, many are available in IDL, a quite expensive proprietary software used when TRexes were lingering around. As a Open Source promoter I would not mention it, but:
There is **Open source initiative version of IDL, called GDL**, which has most-but not all, e.g. they lacked contour plots at my last look at it about decade ago - functionality of IDL. For simpler graphics or most of computations it usually works, give it a try. "G" in GDL is from Gnu..., so it is distributed with major linuxen, or can easily be installed. If you inherited someone's IDL routines for data handling, it is very probable they will run as they are in GDL, for plotting, you might need to fiddle a bit.
- If you are lucky, your needed code might be already translated to python, and available in Github or similar. One such library is **PyAstronomy**-currently at 0.23 beta edition, but growing, so best is you browse for it and find the current version, it will for certain grow steadily, and is probably already partially translated to the next "must know" code for the next generations of students (Julia? Or simply "oh Ailadin, could you please plot for me..."?). I show how simple it is:

Roche surfaces in PyAstronomy

```

x - + Terminal - miki@mikic: ~/Pv
File Edit View Terminal Tabs Help
I A rochepot.py (python) from future import print function, division
from __future__ import print function, division
from PyAstronomy import pyasl
import numpy as np
import matplotlib.pyplot as plt

x, y = np.linspace(-1.5, 2, 300), np.linspace(-1.6, 1.6, 300)
xx, yy = np.meshgrid(x, y)
# Coordinates in orbital plain
z = 0

# Mass ratio
q = 0.2

# Get dimensional values of Roche potential
p = pyasl.rochepot_dl(xx, yy, z, q)

# Positions (and potentials) of Lagrange points
l1, l1pot = pyasl.get_lagrange_1(q)
l2, l2pot = pyasl.get_lagrange_2(q)
l3, l3pot = pyasl.get_lagrange_3(q)
l4, l5 = pyasl.get_lagrange_4(), pyasl.get_lagrange_5()
l4pot = pyasl.rochepot_dl(l4[0], l4[1], l4[2], q)
l5pot = pyasl.rochepot_dl(l5[0], l5[1], l5[2], q)

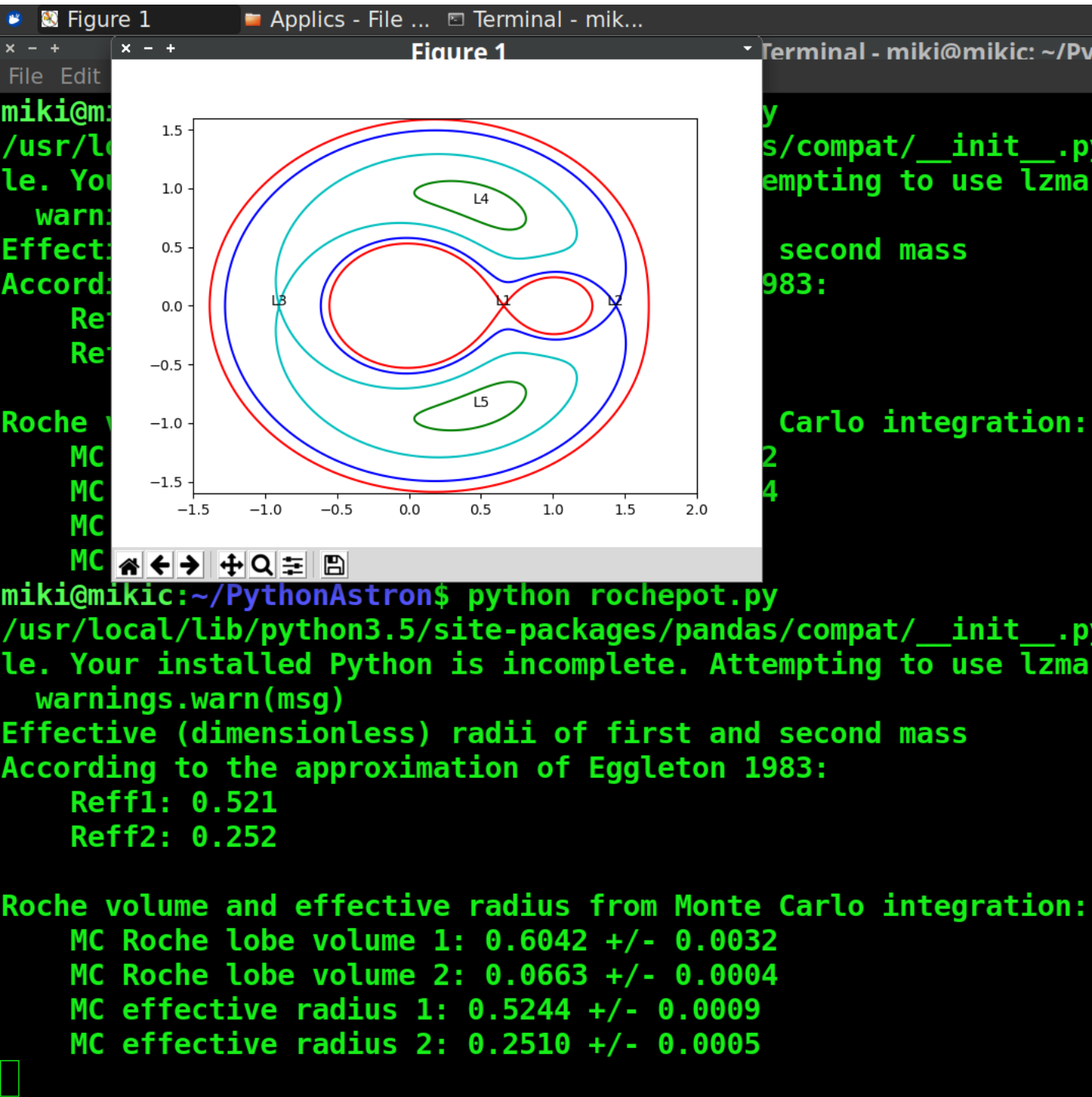
print("Effective (dimensionless) radii of first and second mass")
print("According to the approximation of Eggleton 1983:")
r1eff = pyasl.roche_lobe_radius_eggleton(q, 1)
r2eff = pyasl.roche_lobe_radius_eggleton(q, 2)
print("    Reff1: %5.3f" % r1eff)
print("    Reff2: %5.3f" % r2eff)
print()
print("Roche volume and effective radius from Monte Carlo integration:")
mcvol1 = pyasl.roche_vol_MC(q, 1)
mcvol2 = pyasl.roche_vol_MC(q, 2)
print("    MC Roche lobe volume 1: %6.4f +/- %6.4f" % (mcvol1[0:2]))
print("    MC Roche lobe volume 2: %6.4f +/- %6.4f" % (mcvol2[0:2]))
print("    MC effective radius 1: %6.4f +/- %6.4f" % (mcvol1[2:]))
print("    MC effective radius 2: %6.4f +/- %6.4f" % (mcvol2[2:]))

plt.contour(p, [l5pot*1.02, l3pot, l2pot, l1pot], colors=['g', 'c', 'b', 'r'], extent=[-1.5, 2, -1.6, 1.6])
plt.text(l1, 0, 'L1', horizontalalignment='center')
plt.text(l2, 0, 'L2', horizontalalignment='center')
plt.text(l3, 0, 'L3', horizontalalignment='center')
plt.text(l4[0], l4[1], 'L4', horizontalalignment='center')
plt.text(l5[0], l5[1], 'L5', horizontalalignment='center')
plt.show()

```

This is a complete code for plotting Roche equipotential surfaces in PyAstronomy.

Roche surfaces in PyAstronomy

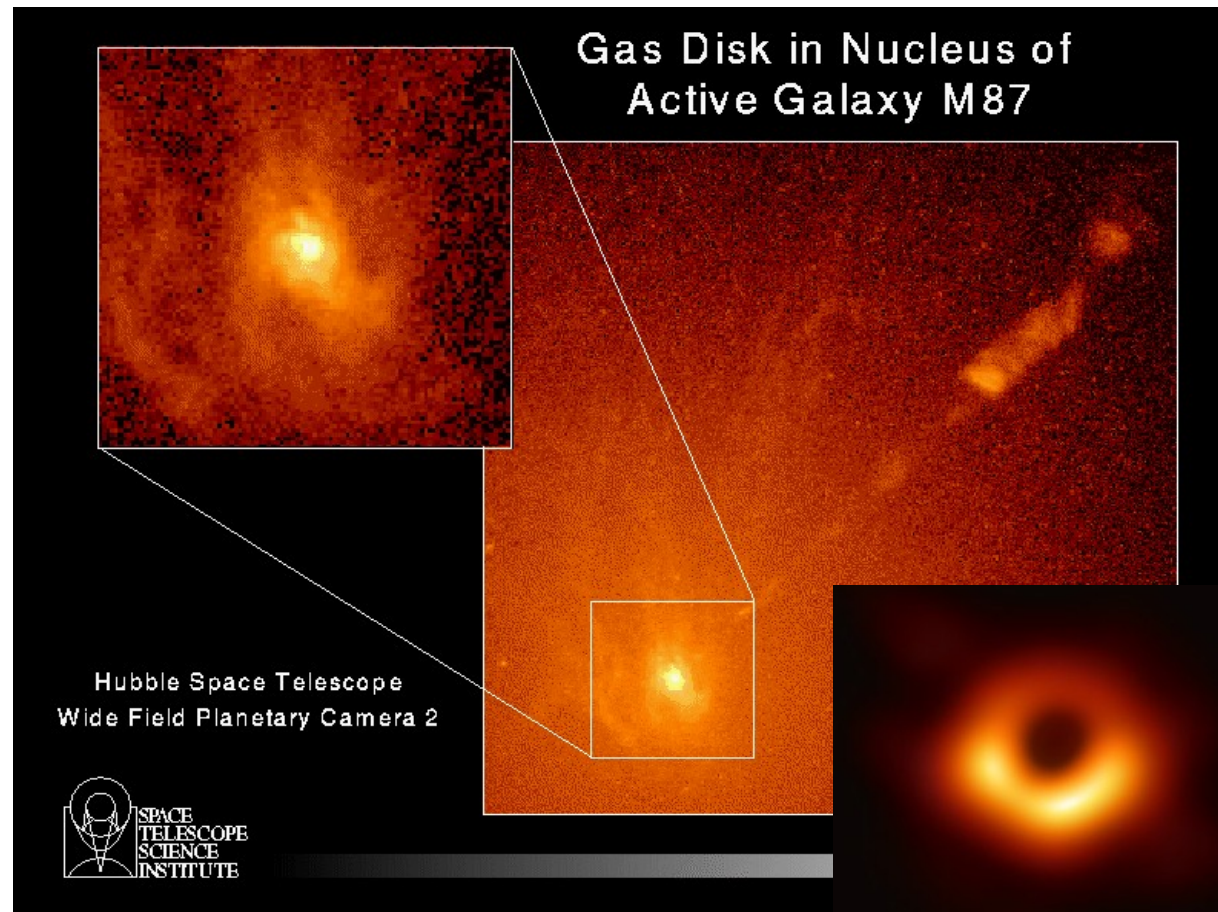


You run it in Python in terminal and get the result in a pop-up window.

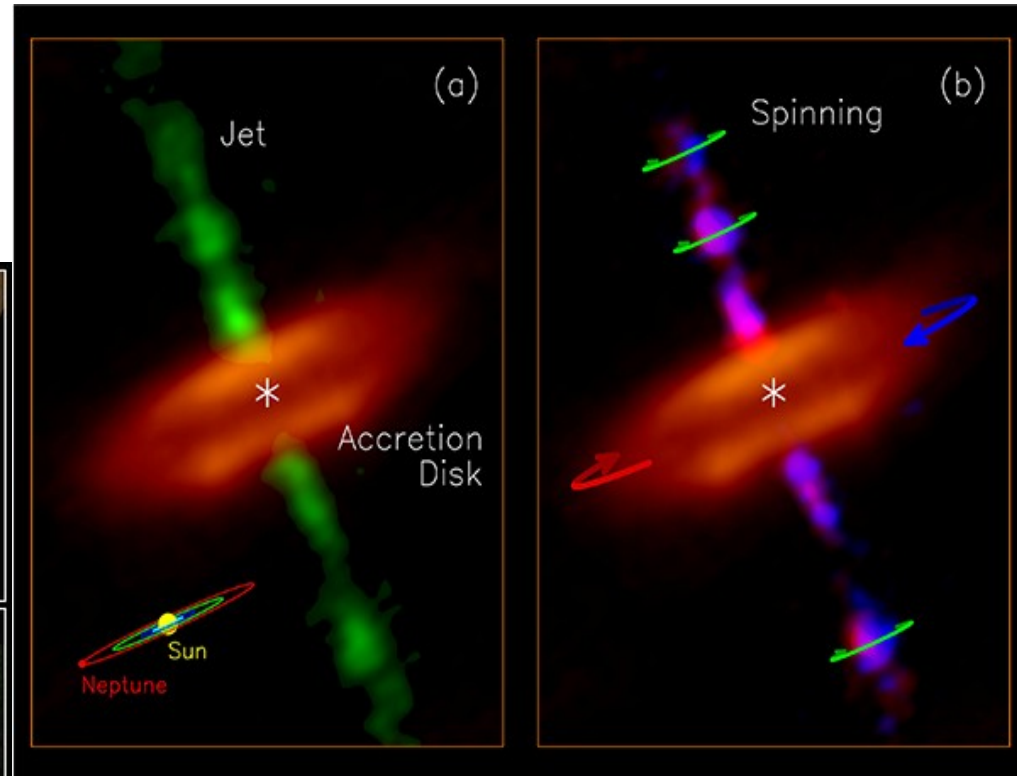
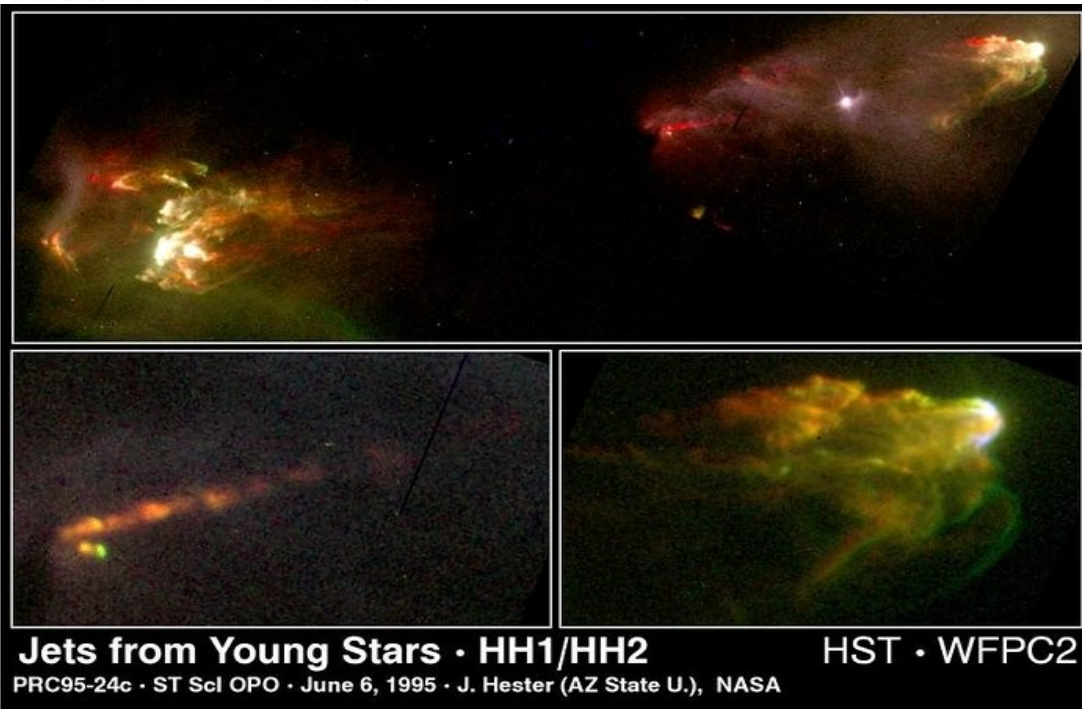
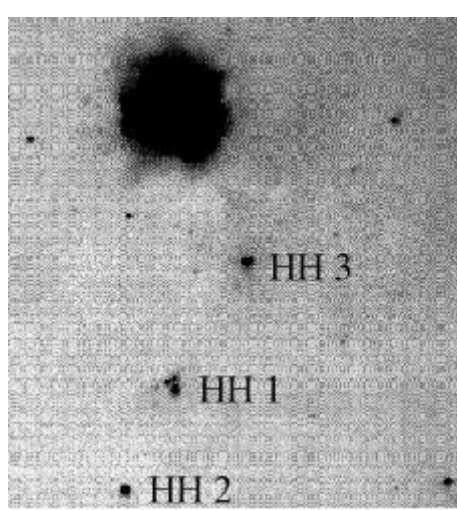
Observations of jets

We did not see accretion disks 100 years ago, but we knew jets. We know about jets for more than 100 years-M87 was the first jet to be observed, by Heber Curtis at Lick Observatory. He first noticed this “curious straight ray” in 1918 on photographic plates. The first visual observation of M87’s 5,000-light-year-long jet was made by Otto Struve through the 100-inch telescope at Mount Wilson. It was thought too dim for amateurs, but Barbara Wilson sighted it during the 1991 Texas Star Party through her 20-inch reflector (*disclaimer, many others saw it before, but not reported. If you ever looked through a 0.6m Dobsonian, you know!). It is a typical elliptical galaxy in Virgo, resembling an unresolved globular cluster or the head of a comet.

M87 (NGC 4486, Virgo A) is a giant galaxy at 55 million light-years from us, measuring 120,000 light-years across, with 100 billions of stars and mass about 2 trillion solar masses. Only in the era of Hubble Space Telescope (HST) we obtained well resolved disk (dust and gas, not accretion disk!) and jet optical observations. In the case of M87, with Event Horizon Telescope (EHT) collaboration we recently got very, very close to the central supermassive black hole (SMBH).

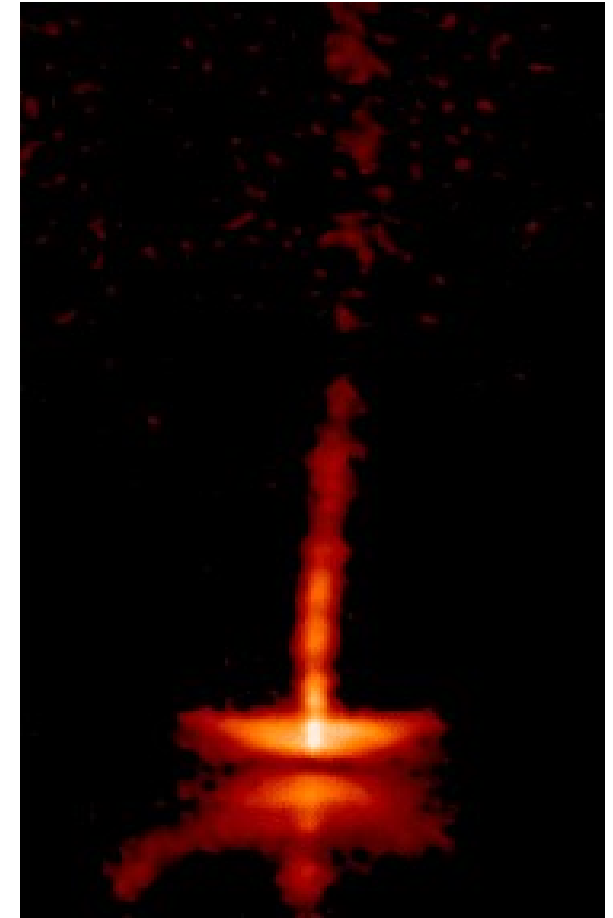
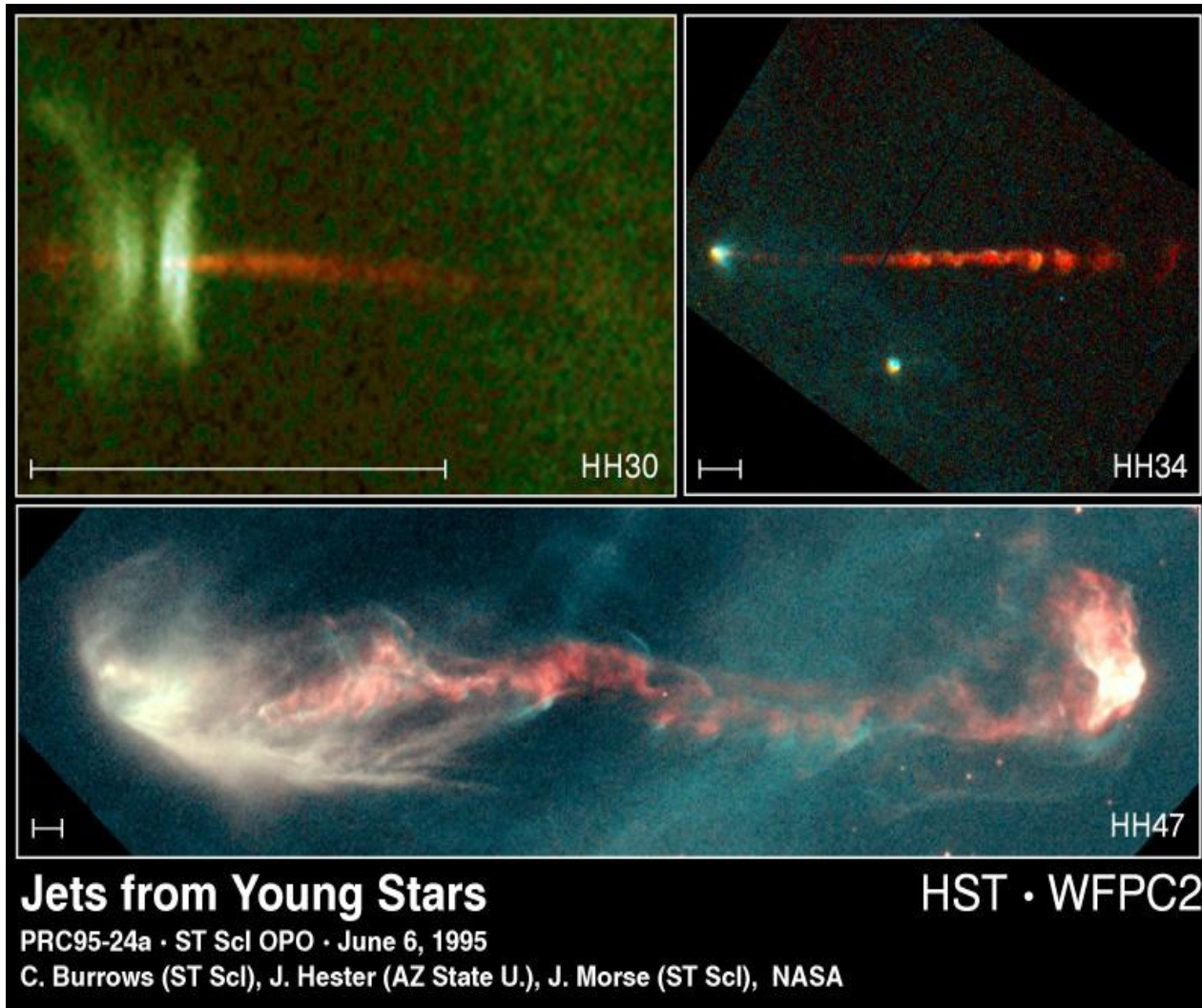


Observations of jets



Stellar jets followed in HH objects in 1950's. Here also only HST provided well resolved disk and jet observations. In the ALMA era, we got even closer-a team from ASIAA, Taiwan recently measured a rotating disk and jet in HH212. Resolution of the observation is down to 8 AU! The angular momentum carried by a jet is so small that it must be launched from the region well inside the disk, about 0.05 AU from the star. This matches with the magnetospheric jet launching.

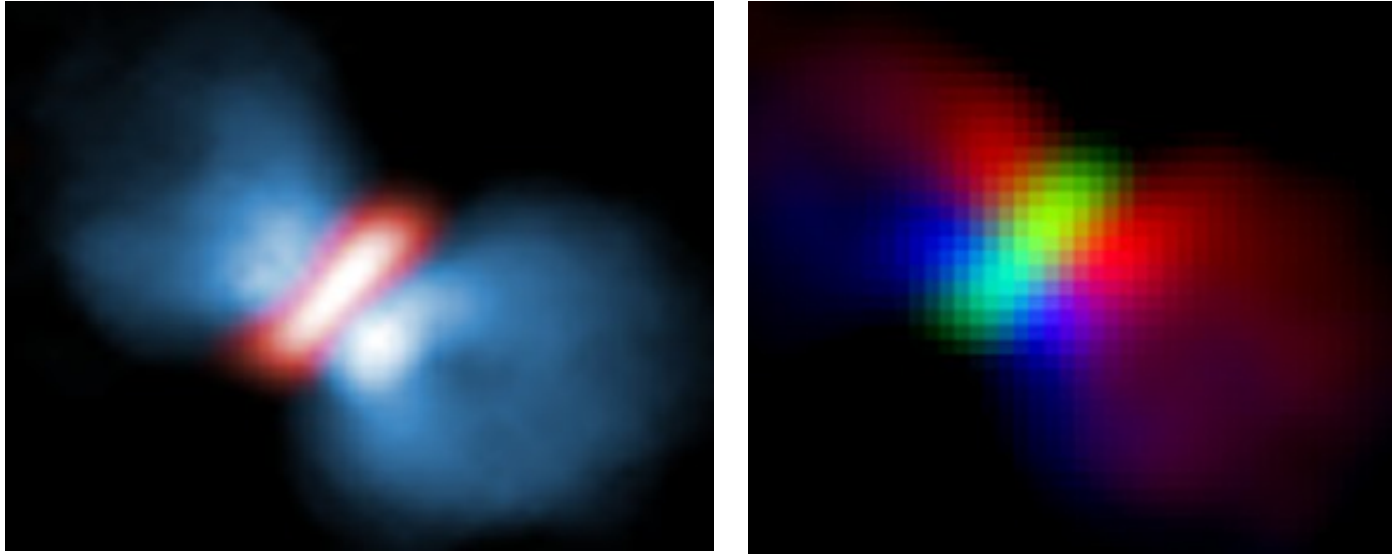
Observations of jet movement



NASA HST/Wide Field and Planetary Camera 2.

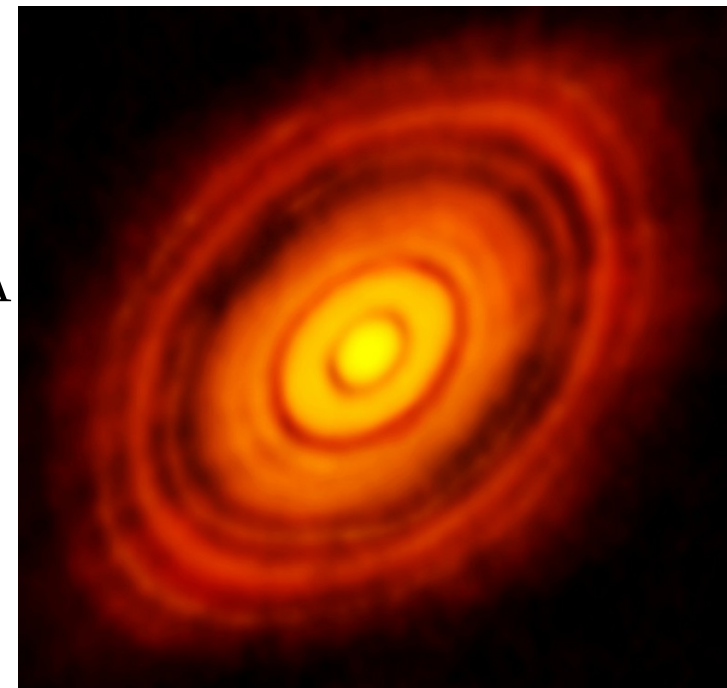
We know well how the jets are moving through space, but we do not yet know how they form. It is obvious that from the disk, but how? How they get collimated, how the knots form?

Detailed observations of jet and disk



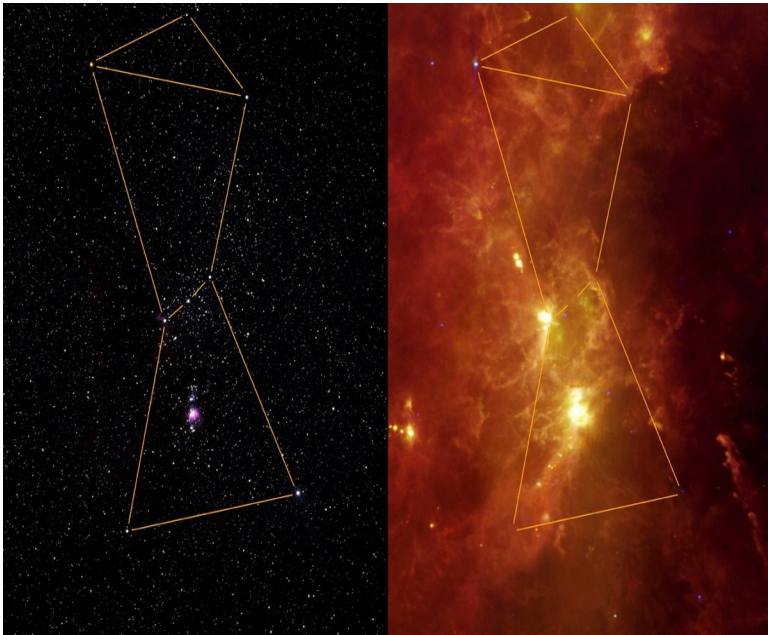
Stellar outflows in the case of massive young stars comply more to the magnetocentrifugal outflow launching, where the outflow is launched from the disk surface. Here is a recent ALMA image for Orion KL Source 1, and measured velocities. In the right panel the color shows the motion of the gas: red shows gas moving away from us, blue shows gas moving toward us. The disk is shown in green (Hirota et al., 2017).

Spectacular ALMA image of the HL Tau protoplanetary disk, with the planet trajectories carved-out, is another example of what we can expect from the new instruments (ALMA, 2014). A million years young star with a disk of more than three Neptune orbits radius, is located at 450 ly from us. It came as a large surprise that such a young star would already show signs of planet formation. Such observations will force numerical simulations to be much more detailed, it is not enough any more to just get a stable disk!

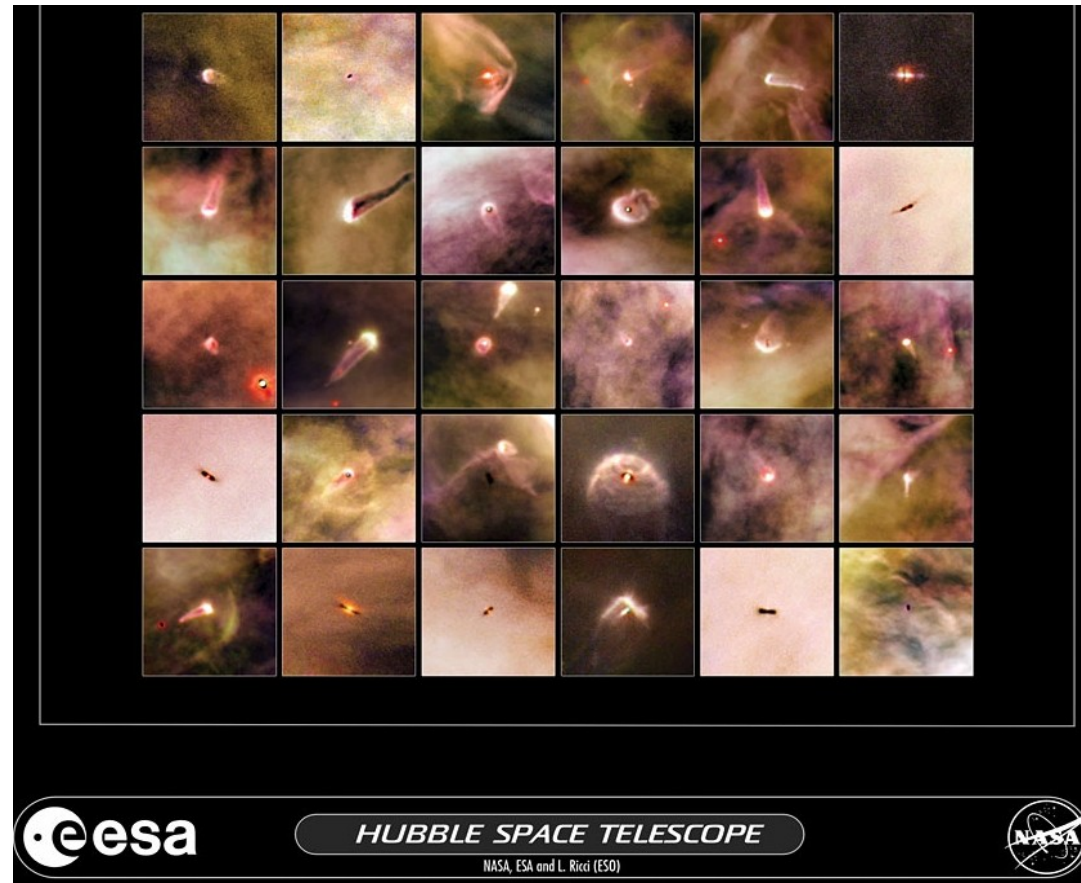


Disks & jets paradigm

It was observed that jets always go in pair with the disk and that the jet speed is always about the escape velocity from the central object.

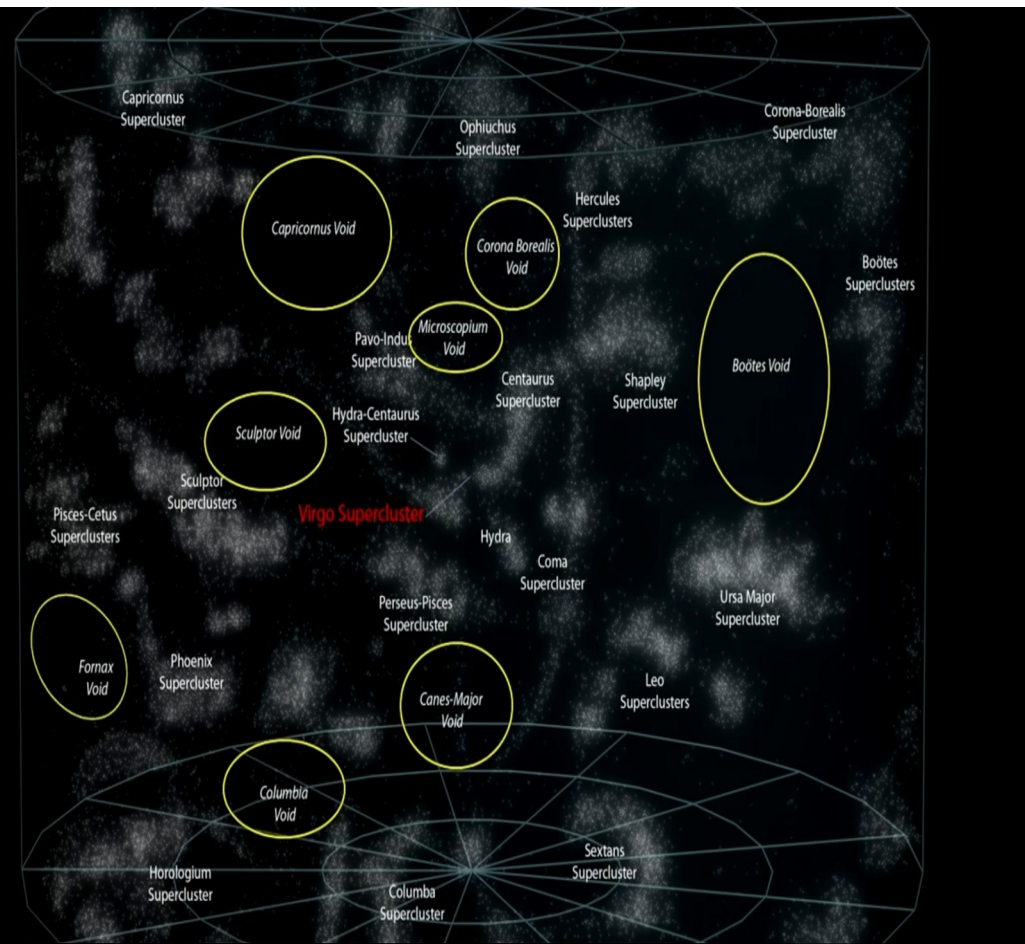
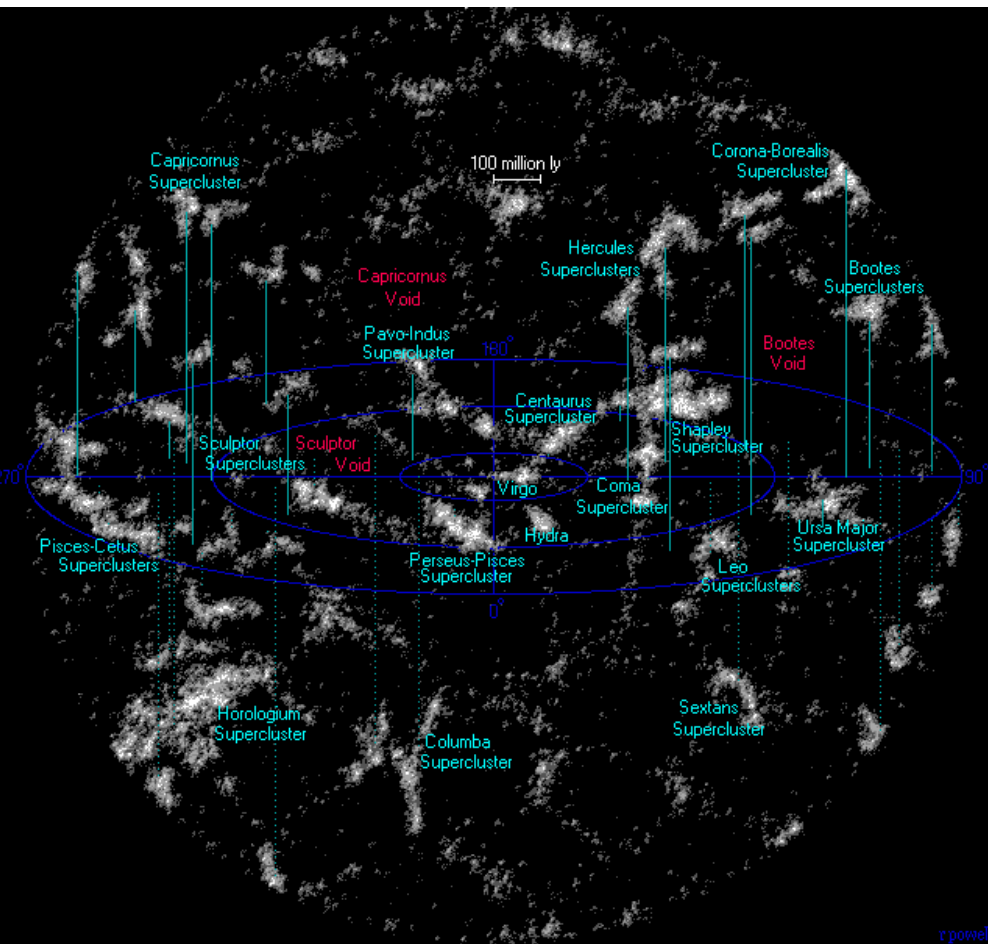


Orion nebula with its disks and jets.

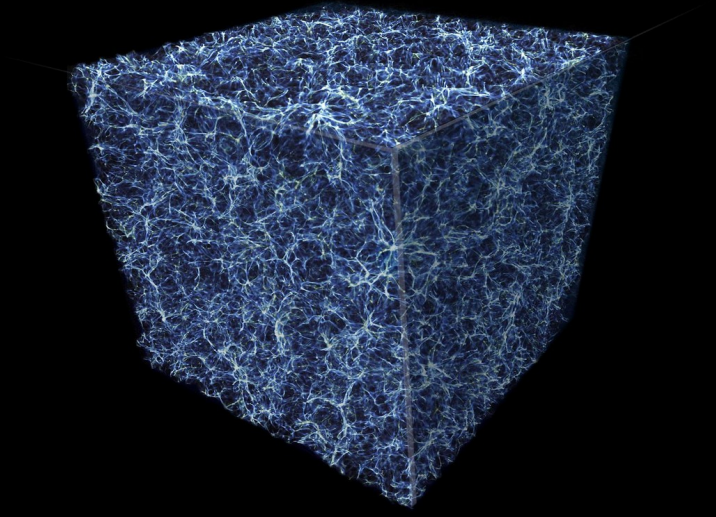


Models of accretion process followed not only the collapse of the material, but also the mechanism of the extraction of the angular momentum from the system. The highly collimated jets can hardly be explained without the action of the magnetic field. Such jets affect the interstellar environment, mixing the material and expelling the magnetic field into it. In the case of active galactic nuclei (AGN) jets, the material and magnetic field are expelled into the intergalactic space.

Magnetic field between galaxis, voids

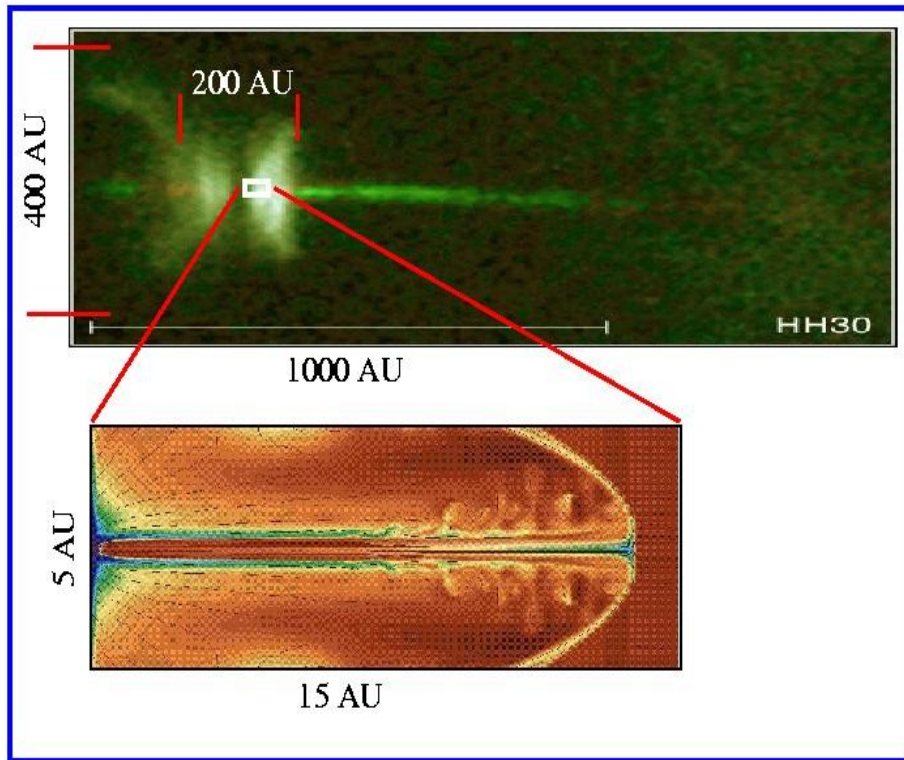


This could be part of the answer to the fact that between the clusters of galaxies we observe voids with less galaxies than average. If there is a magnetic field in the voids, how it formed? Such galaxies do not have enough time from their formation to rotate around their axis to produce a working dynamo.

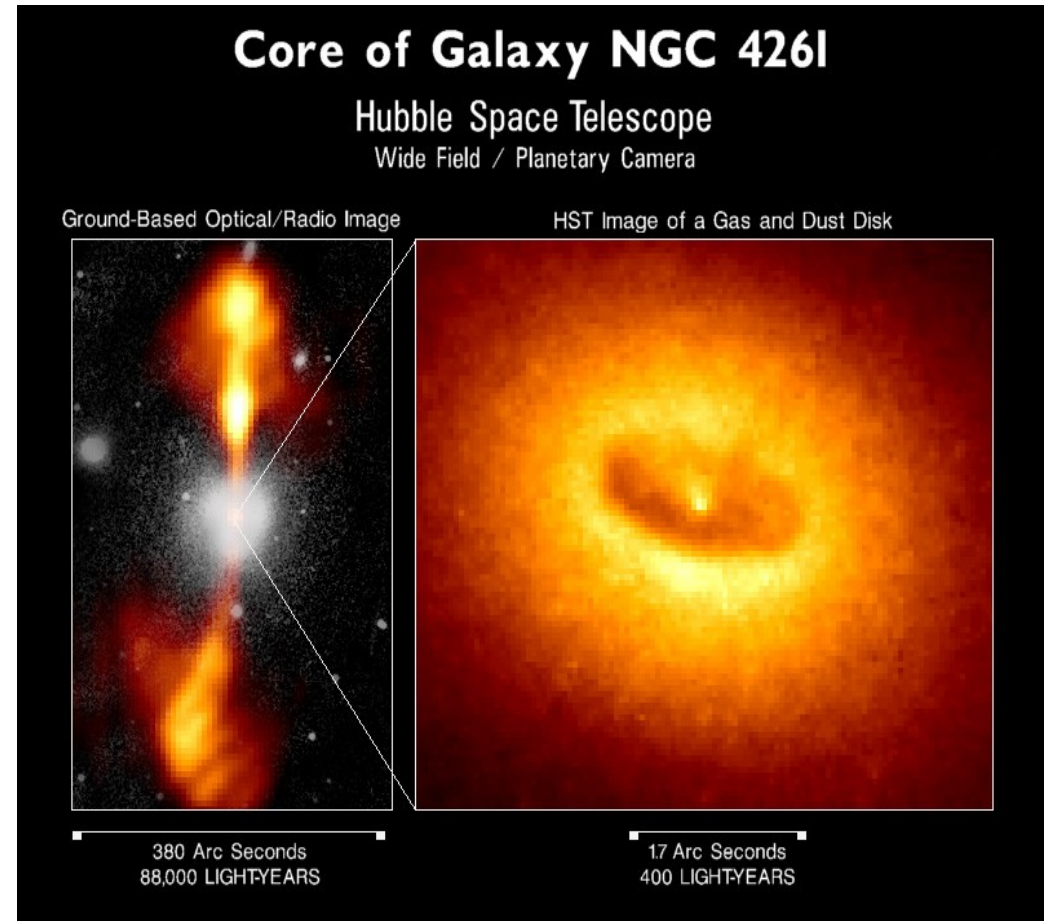


Two different scales

In the cases of YSO and AGN jets we have similar objects at two very different scales, stellar and extragalactic, which are about 100 000 times different. Are the processes also similar? We still do not know, our simulations are not detailed enough to explain the details in observations.

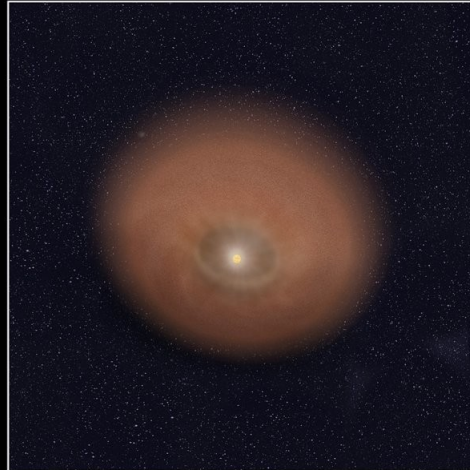
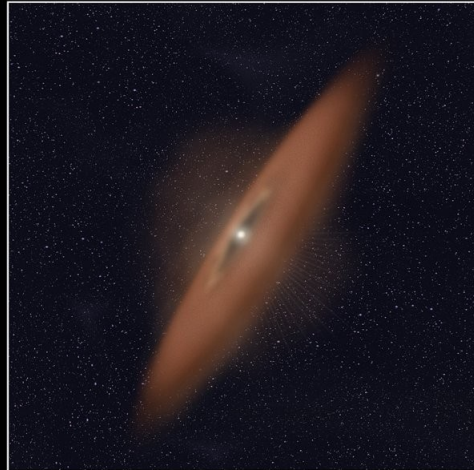
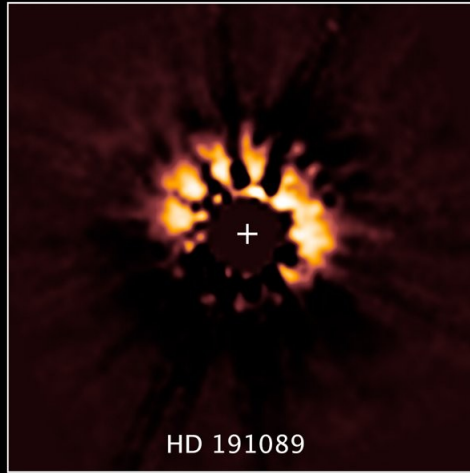
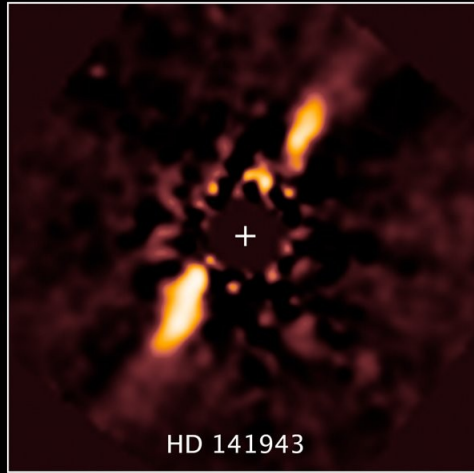


Reality ver. simulations 100 000 AU=1.6 ly



Hercules A, disk and jet in the galaxy with SMBH.

Accretion disk around young stellar objects (YSOs)



Circumstellar Disks
Hubble Space Telescope ■ NICMOS

What is needed for the model of a disk around young star? It is important also because of the planet formation.

In the 1970-ties Shakura & Sunyaev computed the hydrodynamical model, in which dissipation is needed for the transport of angular momentum.

Viscosity causes the angular momentum to be transported outwards during the infall of matter, because of the internal friction in the flow.

Further computations showed that such discs would not be stable. Also, such a mechanism can not explain highly collimated jets.

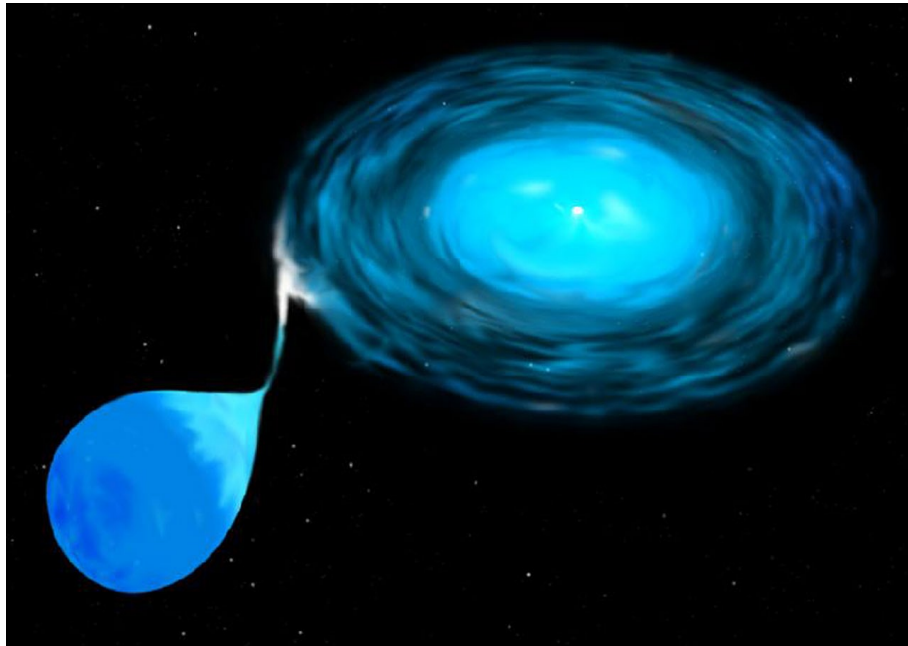
Objects in which we observe disks and jets

In a brief summary, objects in which we observe disks and jets are:

-**Active galactic nuclei (AGN)**, with a supermassive black hole in the center are the largest objects launching jets.

Stellar jets we observe from:

- **Young stellar objects** with accretion disks (protoplanetary disks).
- **Neutron stars** or **black holes** with accretion disk, usually in binary systems with matter from other, larger star.
- **White dwarfs** with accretion disk in double systems of white dwarf with a larger star or a neutron star.



Artistic rendering (credit: STScI) of the cataclysmic variable (CV) star. White dwarf inside the disk of matter infalling from a normal star of slightly sub-solar mass.



Jets from SMBH in the center of Hercules A. Composite of HST and VLA radio telescope.

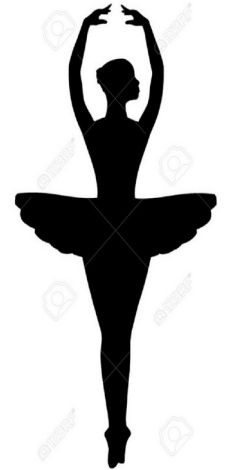
Accretion disks and jets

-Accretion disk forms during the gravitational collapse of matter.

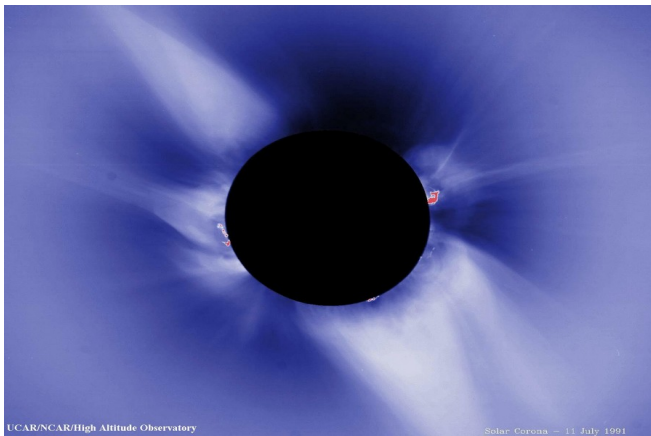
Until the middle of 20th ct. gravity was included in the star formation models only as an attractive force pulling the matter inwards. The problem of decrease of the initial angular momentum was not solved: from $\mathbf{J} = \mathbf{R} \times \mathbf{mv}$ for $\mathbf{R}_1 \gg \mathbf{R}_2$, for $\mathbf{J}, \mathbf{m} = \text{const}$, $\mathbf{v}_2 \gg \mathbf{v}_1$.

We know that Sun-like stars are rotating much slower than it would follow from the angular momentum of the initial protostellar cloud. Without some mechanism enabling the decrease of angular momentum, they would explode! The following facts help to start understanding:

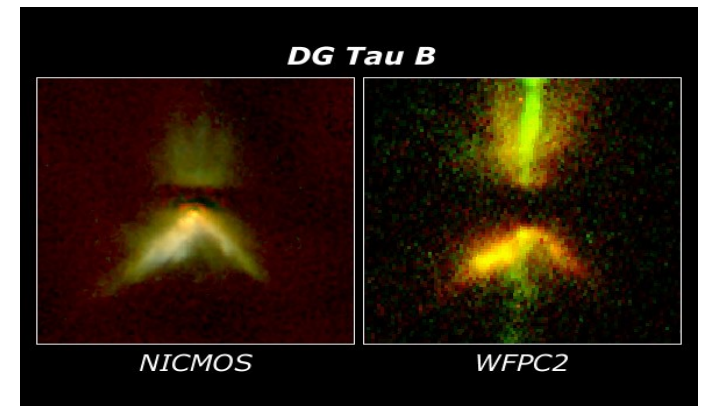
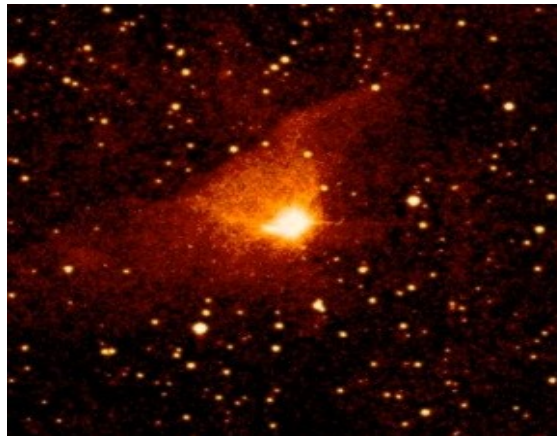
- During the evolution from a pre-stellar core to protostar, the angular momentum decreases for about 4 orders of magnitude. The spin-up of a star is probably prevented by the **magnetic interaction** between the star and the disk.
- The angular momentum can be extracted from the system in different ways:
 - stellar winds, -violent outbursts, -stable outflows/jets, -accretion column onto the star.



Solar corona



FU Ori (ESO)



Magnetic fields in the universe

- We still do not know what is the origin of the magnetic field in the universe. Most of the mechanisms, like magnetic dynamo in galaxies or stars, can only increase the already existing field, but can not create it.
- One of proposed mechanism is Weibel instability, discovered in 1959, which causes magnetic field creation in the homogenous plasma with two oppositely directed particles (e.g. if there are regions of different temperature in the plasma). Because of the movement of particles, generated is the electromagnetic field.
- There are many other models, with phase transitions, quantum effects etc.
- Magnetic fields are observed from the atomic to cosmological scales, with strengths from nano-Gauss (10^{-9}) to 10^{15} Gauss.

Strengths of cosmic magnetic fields

Initially non-existing or very small cosmic magnetic field increased during the evolution of stars and galaxies. Turbulence enables the dynamo effect during the rotation of gases and the field is increased locally.

-At the Earth surface magnetic field strength is about 0.3 Gauss (SI: 0.3×10^{-4} T).

-At the Solar surface it is 1 Gauss, YSOs up to hundreds of Gauss

-White dwarfs 10 000-million Gauss.

-At neutron stars in some close binaries (millisecond pulsars) 100 million (10^8) to 10^{12} Gauss, and 10^{15} Gauss on NSs with extremal magnetic field.

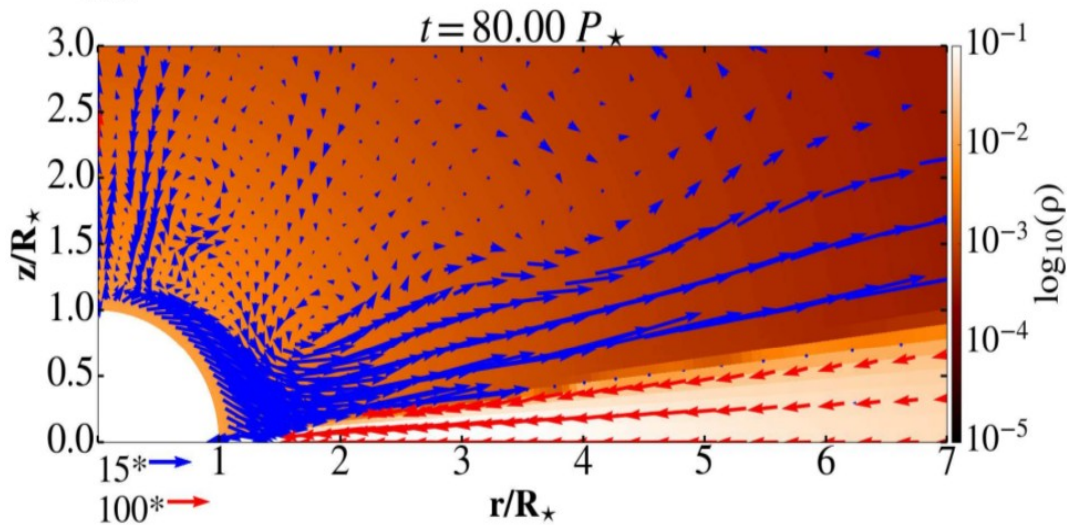
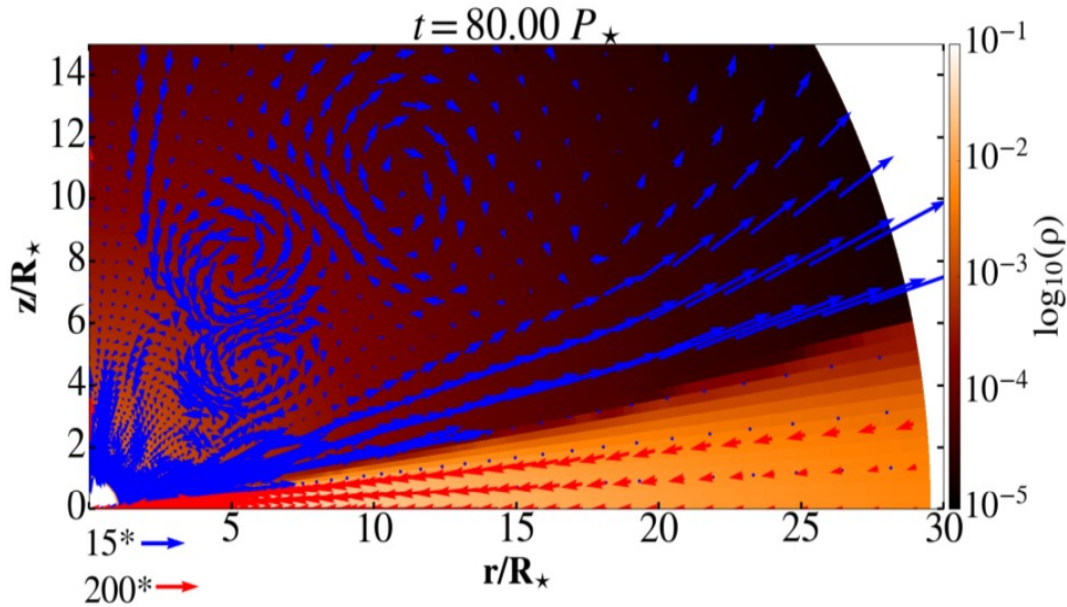
-In the galaxies it is 10μ (10×10^{-6}) Gauss, in the intergalactic space 1μ Gauss.

How do we measure the magnetic field?

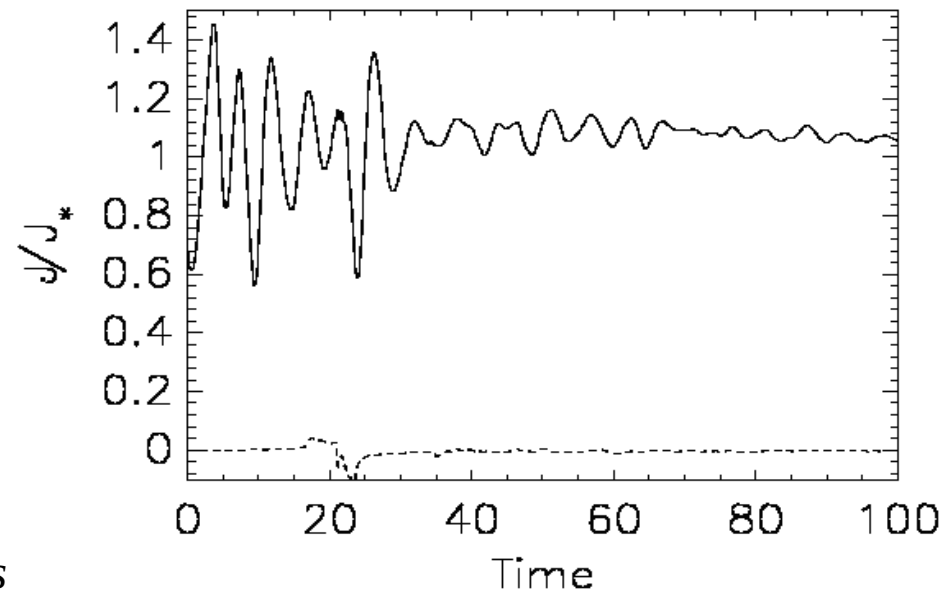
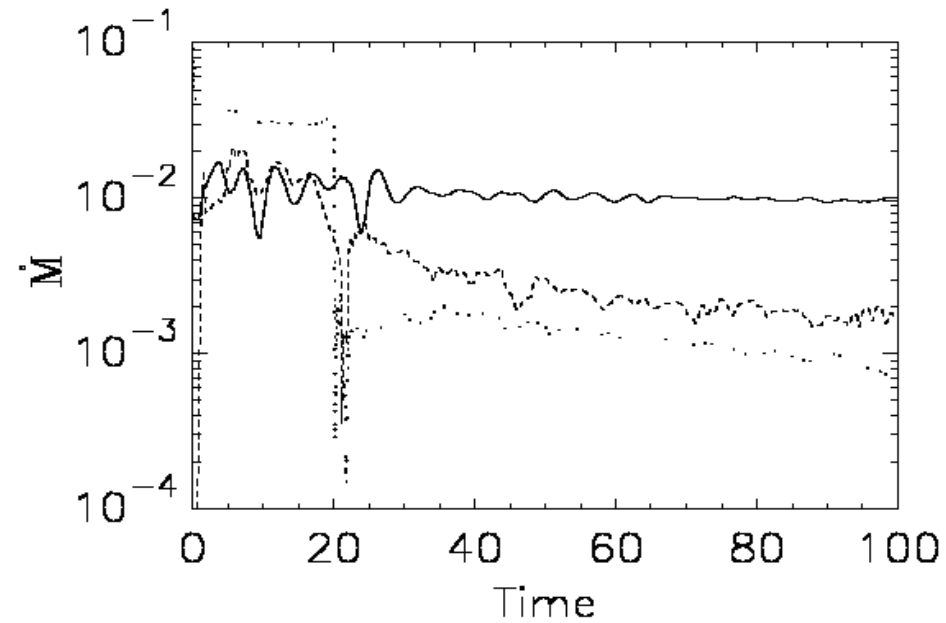
-in the lab: with magnetometer, measuring of the magnetic force.

-in the universe: synchrotron radiation (produced by the electrons moving in the magnetic field); partial polarization of light when it passes through the dust oriented uniformly in the magnetic field; Faraday rotation (1845, first proof of the connection between light and electromagnetism) change of the polarisation plane; Zeeman effect, splitting of the spectral lines in the magnetic field; indirect method-measuring the angle between the direction of the radiation intensity change and the direction of the magnetic field to infer the field strength.

Simulations you will learn to do: Hydro-dynamical (HD) star-disk simulations

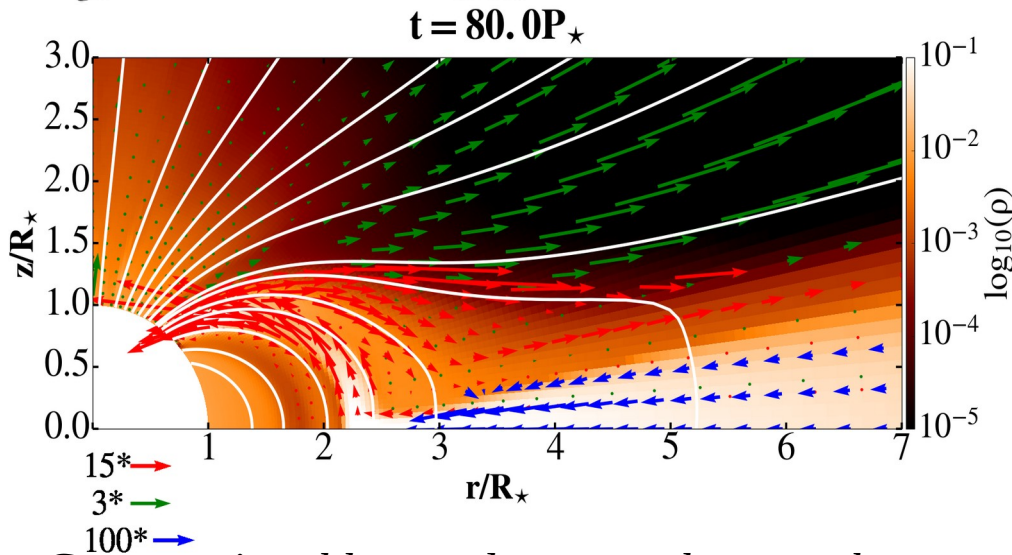
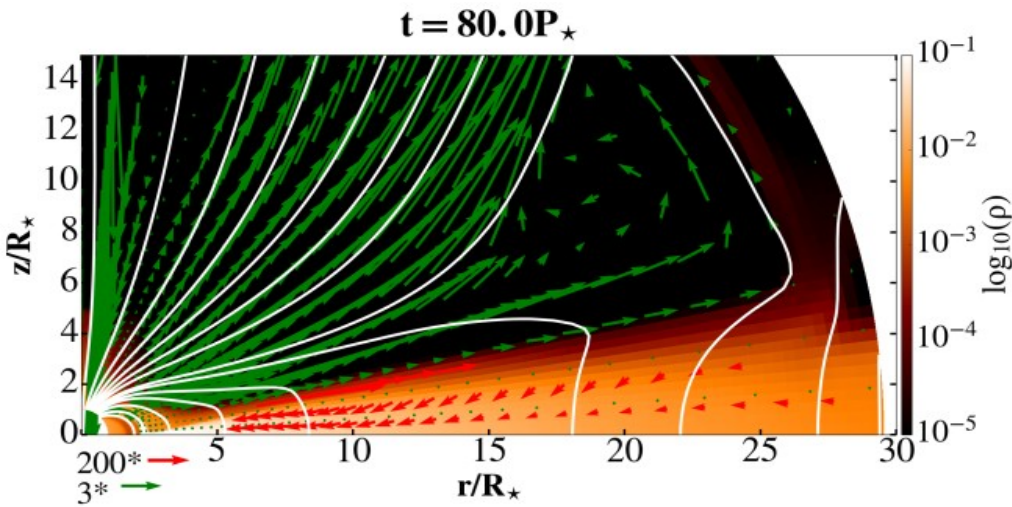


Computational box and a zoom closer to the star after 80 stellar rotations. In color is shown the density, and vectors show velocity, with the different normalization in the disk and stellar wind.

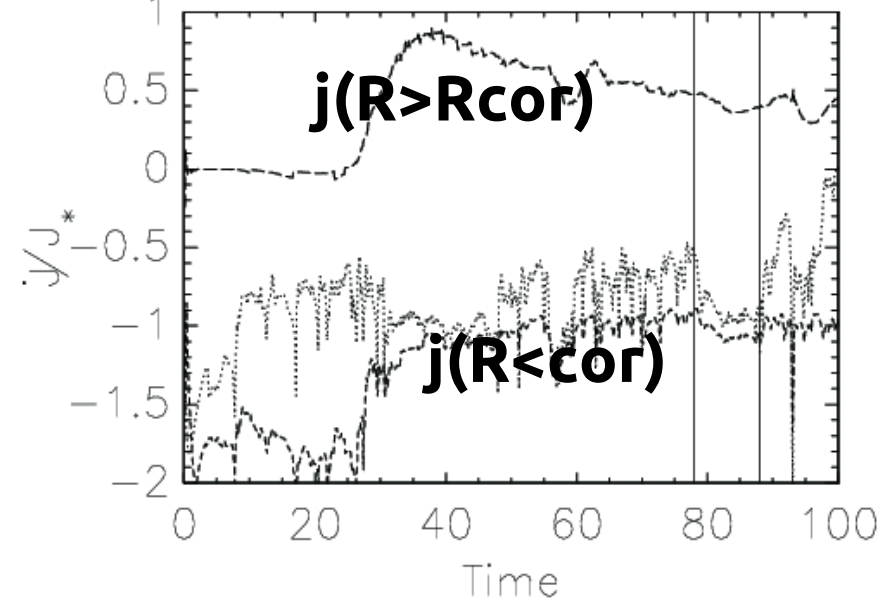
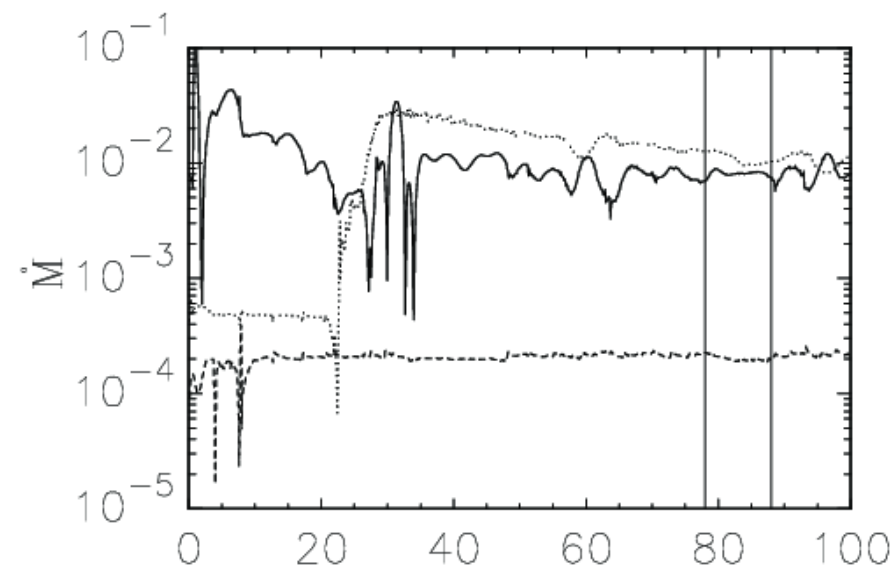


Time dependence of the mass and angular momentum fluxes in the various components in our simulations.

Star-disk magnetospheric interaction (SDMI) simulations



Computational box and a zoom closer to the star after 80 stellar rotations, to visualize the accretion column and the magnetic field lines (white solid lines) connected to the disk beyond the corotation radius $R_{\text{cor}} = 2.92 R_{\star}$. In color is shown the density, and vectors show velocity, with the different normalization in the disk, column and stellar wind.



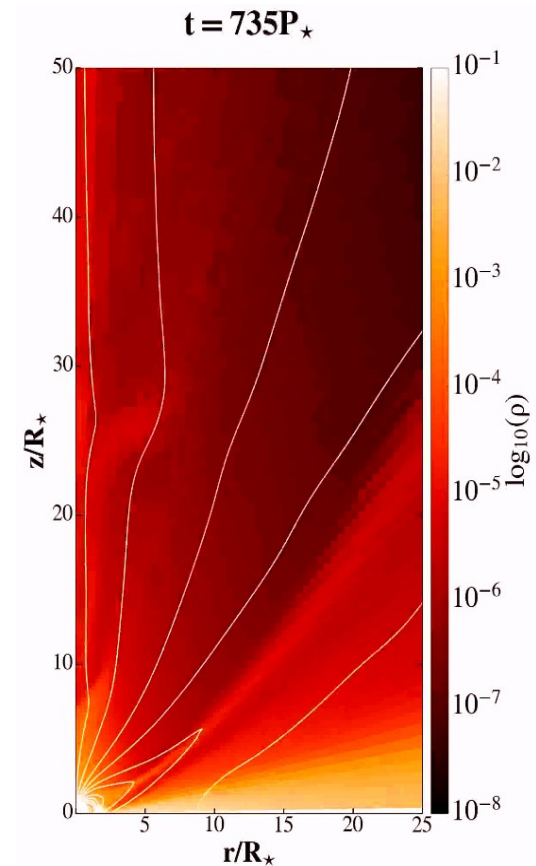
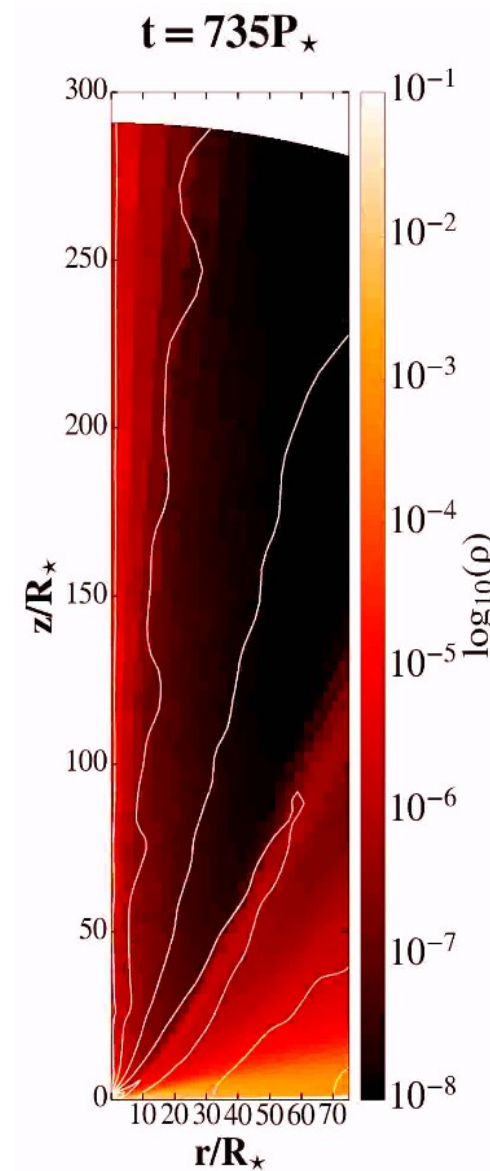
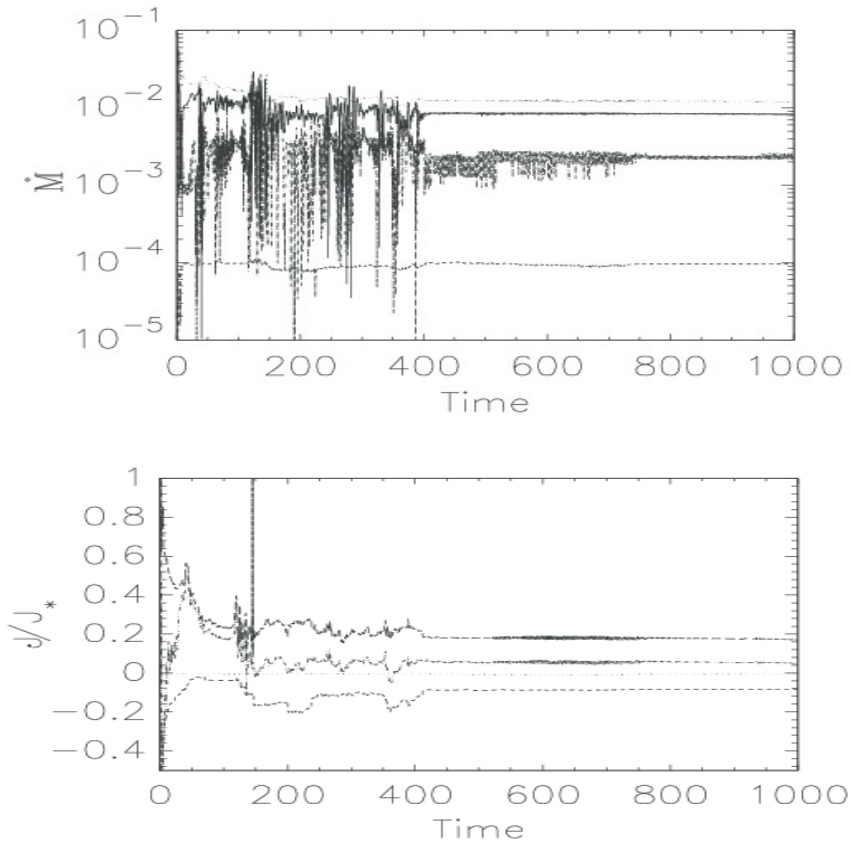
Time dependence of the mass and angular momentum fluxes in the various components in our simulations with marked the time interval in which the average for the quasi-stationarity is computed.

Motivation for such simulations: stellar rotation rates

- Solar mass young stars show a large dispersion of rotation rates. When they reach the main sequence, they rotate with very different rotational velocities: from less than 10 km/s to more than 200 km/s. In a later evolution, after few billion years, most of them rotates with rotational velocity of few km/s; dispersion in rotation drops to only a few percents.
- For solar mass stars, spin-down is thought to be mainly because of a braking effect of magnetically driven winds. As the wind moves away from the star, its angular velocity decreases. The magnetic field of the star interacts with the wind, which slows the stellar rotation. As a result, angular momentum is transferred from the star to the wind, and the star's rate of rotation gradually decreases. **Skumanich's Law** (1972) states that, for a Main Sequence star on time scale of several hundred Myrs, angular velocity of a star decreases as $\Omega \sim 1/\sqrt{t}$.
- To obtain a full picture about torques in the system, both wind braking and star-disk interaction have to be considered. My simulations give an input on star-disk interaction.
- Goal is to find scaling laws for exchange of angular momentum between the star and surrounding.
- Idea is to predict the global stellar torque, which will then be used in stellar evolution models. For this, we need to be able to determine torques of stars of different masses and at different evolutionary stages. We will focus on the early evolutionary phases.
- I also investigated the influence of magnetic field geometry on the transport of angular momentum between the star and the environment. For this, a parameter study was needed, determining the torque in the system:
 - changing the rotation rates from 2-10 days, accretion rates from 10^{-9} to 10^{-6} solar mass/year, with mass outflow of about 1/10 of the accretion rate.
 - all this with various strengths and geometry of magnetic field.

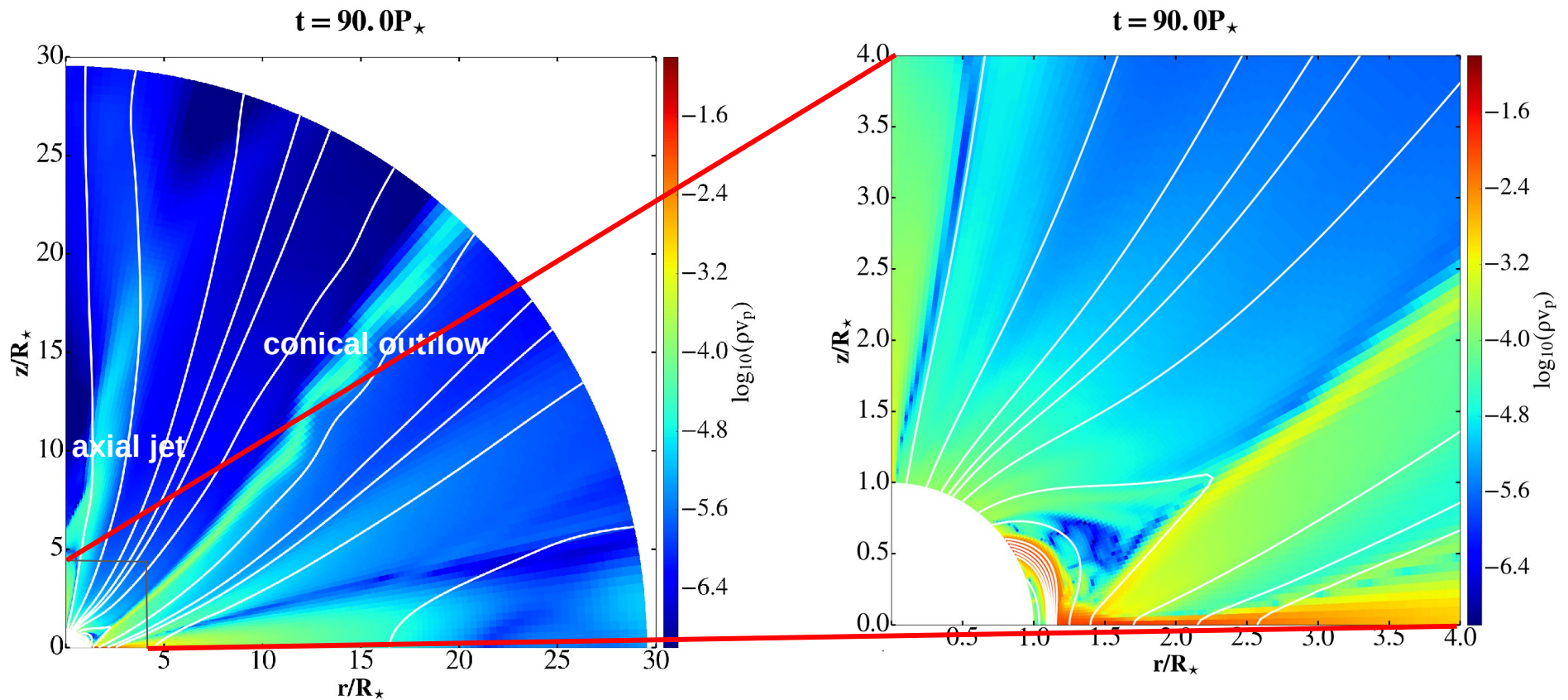
Another important motivation: jet launching mechanism

- In a part of the parameter space, there is a continuous launching of an axial jet from the star-disk magnetosphere. I found that one has to wait until few hundreds of rotations of the star.
- The axial jet and the conical outflow are launched after the relaxation from the initial conditions. They are similar to the results in Romanova et al. (2009) and Zanni & Ferreira (2013).



Zoom into the launching region.

Magnetospheric launching of conical outflow and axial jet

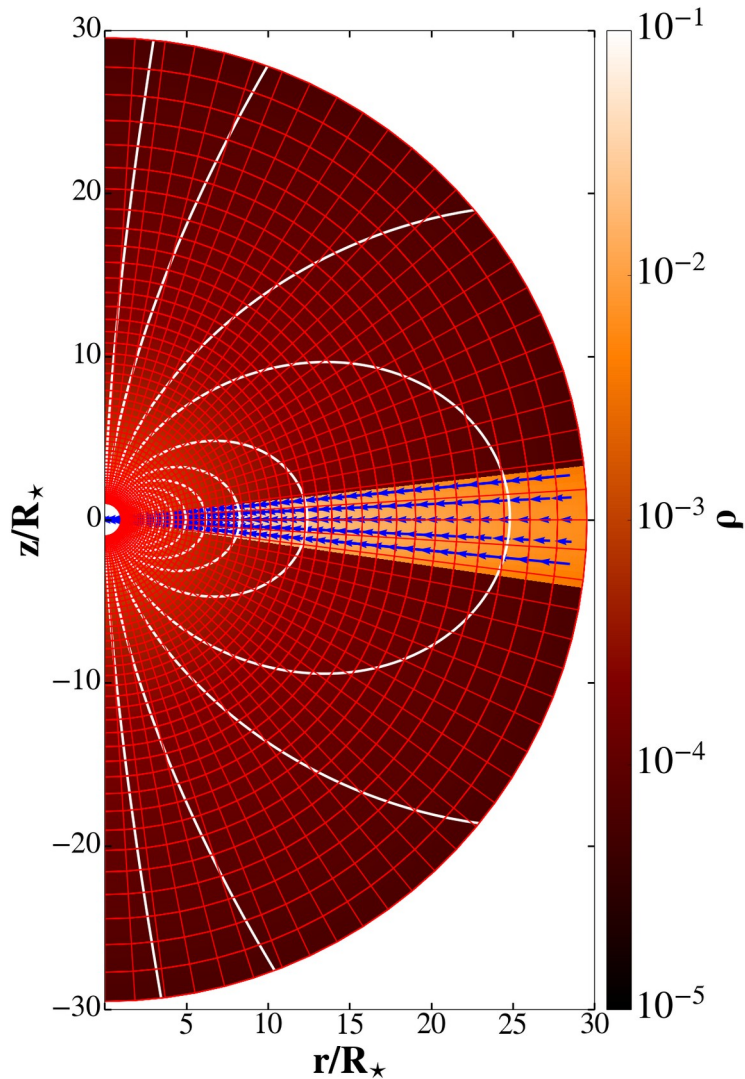


Color shows momentum in the MHD simulation in the young stellar object with conical outflow and axial jet, lines are the magnetic field lines. Right panel is a zoom into the left panel close to the star, to show the closest vicinity of the star.

The asymmetric jet launching (with A. Kotek)

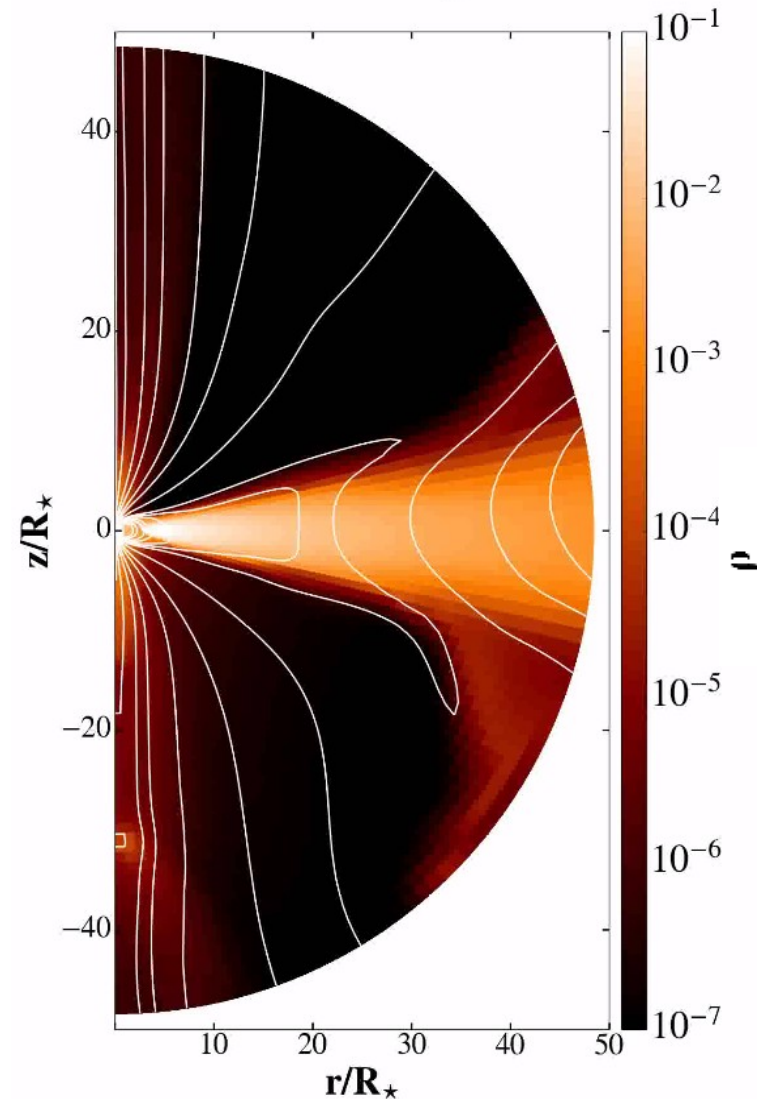
With A. Kotek in her MS Thesis at the Warsaw Uni. we took another look at the solutions with the jet launching in the full meridional plane, with $R \times \theta = [217 \times 200]$ grid cells in $\theta = [0, \pi]$. We obtained the asymmetric jets launched from the star-disk magnetosphere.

$t = 0.0 P_{\star}$



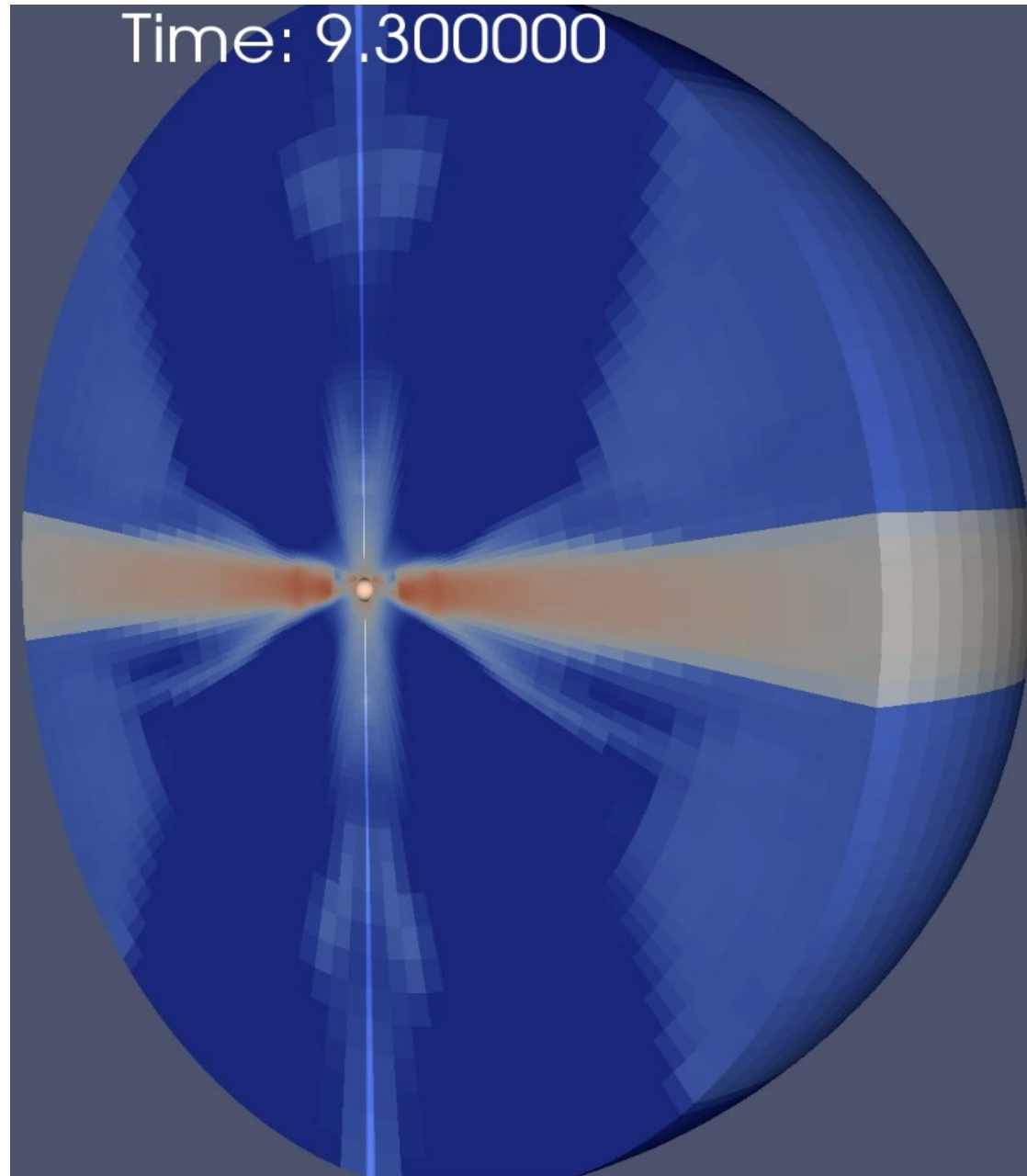
Initial setup in a full meridional plane.

$t = 60.0 P_{\star}$



Asymmetric jet launched from the magnetosphere.

The asymmetric jet launching in 3D simulations



- In the full 3D simulations I also obtain asymmetric jets. To be continued... maybe some of you will do it.

Basic Linux shell commands

man <command> -displays the manual page for a given command.

ls -lists the current working directory

cd -changes the current working directory

pwd -prints the user's current working directory

cp <old> <new> -copies a file <old> to <new>

mkdir <name> -creates a new directory <name>

mv <old> <new> -moves (renames) a file or directory <old> to <new>

rm <name> -removes (deletes) a file <name>, **use with care, it is irreversible**

* (asterisk) -matches characters in a filename, so *.txt matches all files ending in .txt

grep -selects lines in all files that match patterns, **very useful**

Text editors: beware, some editors add metacharacters to text or rearrange the start and end of lines, which can break your code. Use whatever you feel comfortable with for everyday work, but learn some basics of terminal editors, because e.g. on clusters you might not be able to use display remotely

Terminal text editors: “vi”, “vim”, many linuxen come with “nano”, in CAMK we use archaic (but capable enough) “joe”.

Text editors

Text editors: beware, some editors add meta-characters to text or rearrange the start and end of lines, which can break your code. Use whatever you feel comfortable with for everyday work, but learn some basics of terminal editors, because e.g. on clusters you might not be able to use display remotely

Terminal text editors: “vi”, “vim”, many linuxen come with “nano”, in CAMK we use archaic (but capable enough) “joe”.

The image displays two terminal windows side-by-side, both running the nano text editor. The left window shows the start of a Python script named 'setup.py' in the 'PLUTO' directory. The right window shows the same script, but with a status bar at the bottom indicating the current cursor position (Row 1, Col 1). The status bar also shows the current file name and the editor's name (nano).

```

Terminal - miki@mikic: ~
File Edit View Terminal Tabs Help
REGION      GO TO      GO TO      DELETE     EXIT       SEARCH
^Arrow Select ^Z Prev. word  ^U/^V PgUp/PgDn ^D Char.  ^KX Save  ^KF F
^KB Begin     ^X Next word  MISC       ^Y Line   ^C Abort  ^L N
^KK End       ^KU Top of file ^KJ Paragraph ^W >Word  ^KQ All   HELP
^KC Copy      ^KV End of file ^KA Center line ^O Word<  FILE      Esc .
^KM Move      ^A Beg. of line ^K Space Status ^J >Line  ^KE Edit  Esc ,
^KW File      ^E End of line  SPELL      ^[O Line< ^KR Insert ^KH O
^KY Delete    ^KL To line no. Esc N Word  ^_ Undo   ^KD Save  ^T M
^K/ Filter    ^G Matching (  Esc L File  ^~ Redo   ^K` Revert

I A PLUTO/setup.py (python) import os      Row 1 Col 1
import os
import sys
import shutil

try:
    os.environ['PLUTO_DIR']
except KeyError:
    print 'PLUTO_DIR not defined. Setting it to the Current Directory'
    pluto_directory = os.getcwd()
    pass
else:
    pluto_directory = os.environ['PLUTO_DIR']

sys.path.append(pluto_directory + '/Tools/Python/')
import menu
import configure
from make_problem import MakeProblem

def PlutoInterFace(pluto_dir, do_auto_update = True,
                    work_dir = os.getcwd(),
                    interface_optval = '',
                    interface_opts = ['Setup problem', 'Change ma
Terminal - miki@mikic: ~
File Edit View Terminal Tabs Help
^G Get Help  ^O Write Out  ^W Where Is  ^K Cut Text  ^J Justify
^X Exit      ^R Read File  ^_ Replace   ^U Paste Text ^I To Spell
  
```

Ecology of computing

The Ecological Impact of High-performance Computing in Astrophysics

Simon Portegies Zwart

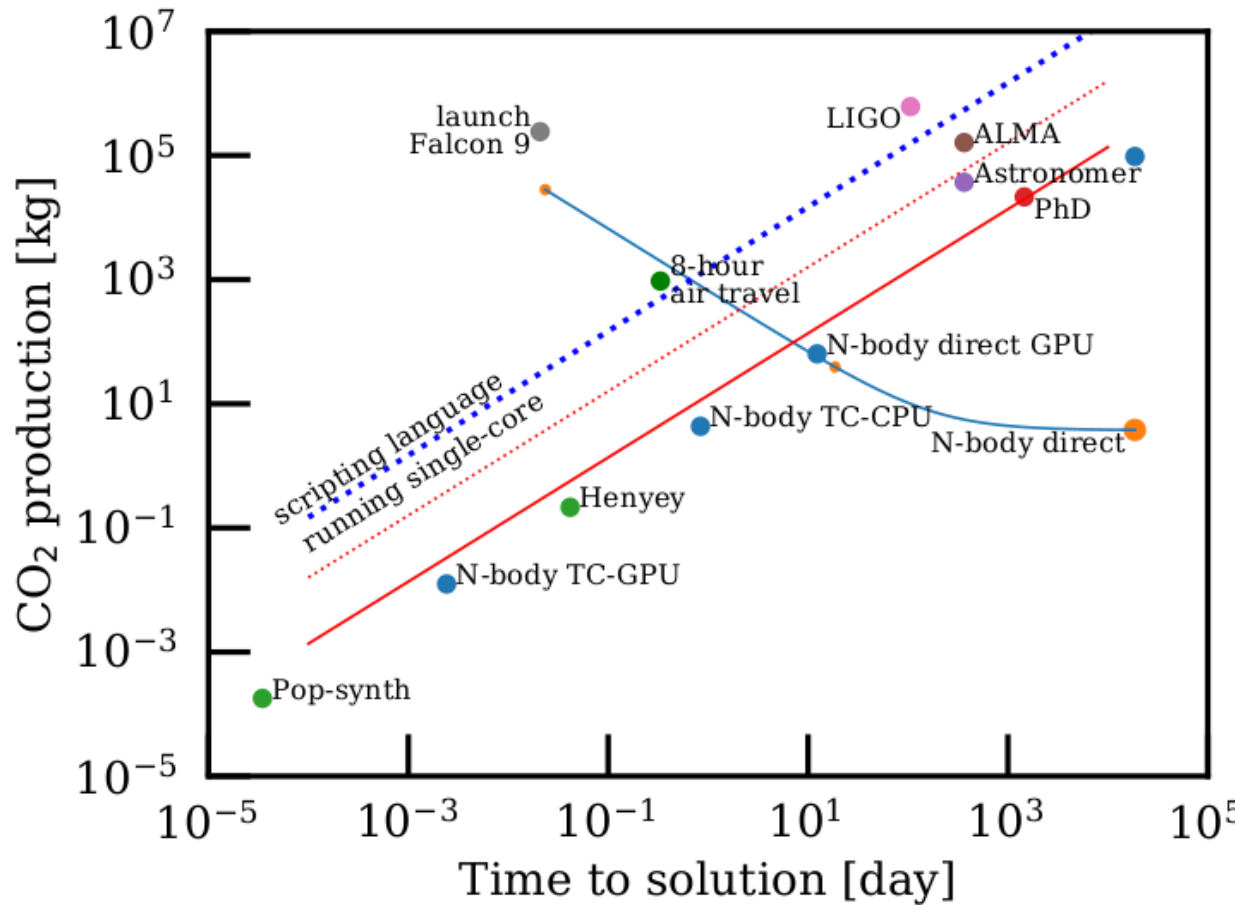
¹*Leiden Observatory, Leiden University, PO Box 9513, 2300 RA, Leiden, The Netherlands*¹

¹Non-anonymous Dutch scientists.

Computer use in astronomy continues to increase, and so also its impact on the environment. To minimize the effects, astronomers should avoid interpreted scripting languages such as Python, and favor the optimal use of energy-efficient workstations.

ArXiv:2009.11295; Nature Astronomy vol.4, 819 (2020)

Carbon footprint of astronomy and computing ³⁵

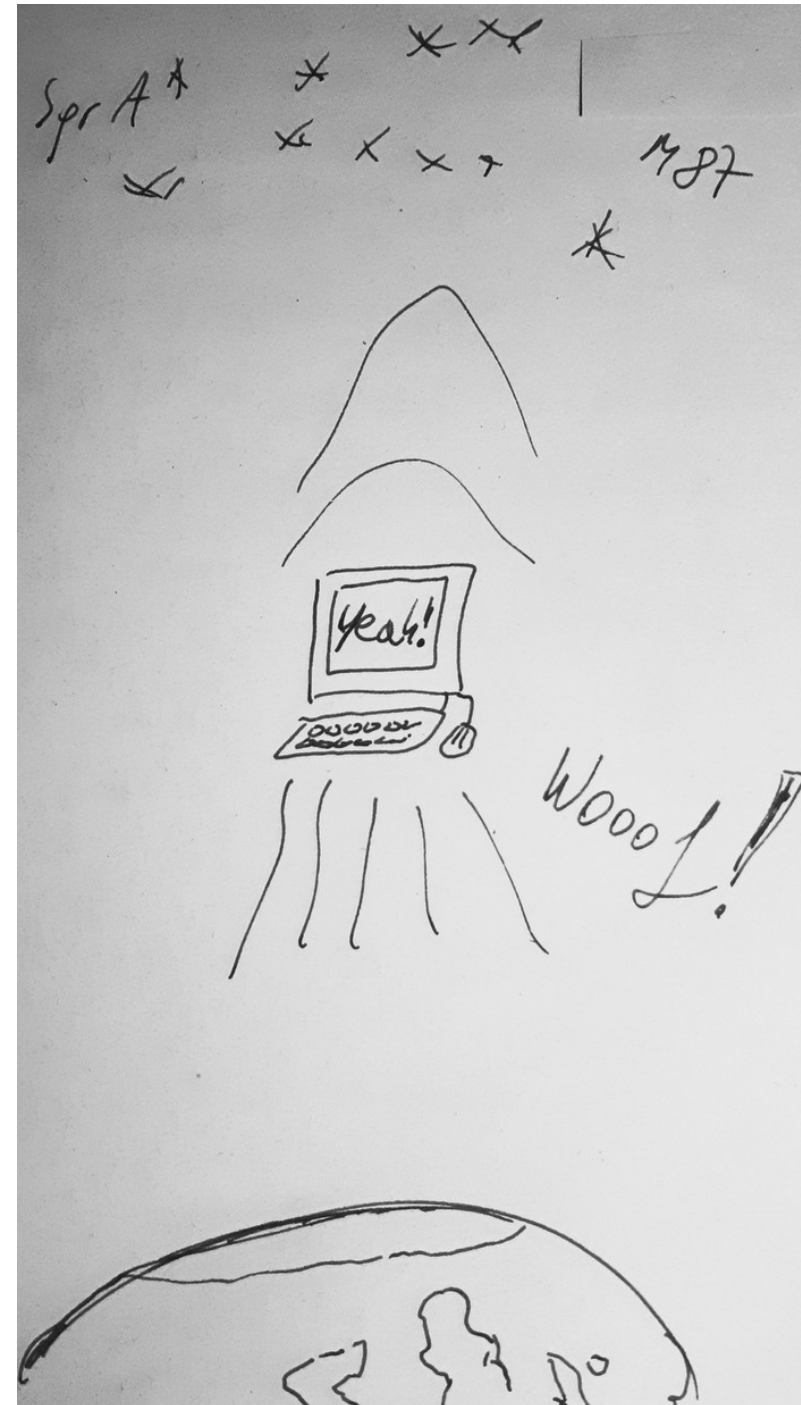


- Comparison of the average Human production of CO₂ (red line) with other activities, such as telescope operation, the emission of an average astronomer, and finishing a (four year) PhD.
- The emission of carbon while running a workstation is comparable to the world's per-capita average.

Figure 1: CO₂ emission (in kg) as a function of the time to solution (in days) for a variety of popular computational techniques employed in astrophysics, and other activities common among astronomers^[3,4]. The solid red curve gives the current individual world-average production, whereas the dotted curves give the maximum country average. The LIGO carbon production is taken over its first 106-day run (using ~ 180 kW)^[5], and for ALMA a 1-year average^[6]. A Falcon 9 launch lasts about 32 minutes during which ~ 110 000 liters of highly refined kerosene is burned. The tree-code running on GPU is performed using $N = 2^{20}$ particles. The direct N-body code on CPU (right-most blue bullet) was run with $N = 2^{13}$ ^[7], and the other codes with $N = 2^{16}$. All performance results were scaled to $N = 2^{20}$ particles. The calculations were performed for 10 N-body time units^[8]. The energy consumption was computed using the scaling relations of^[9] and a conversion of KWh to Co₂ of 0.283 kWh/kg. The blue dotted curve shows the estimated carbon emission when these calculations would have been implemented in Python running on a single core. The solid blue curve to the right, starting with the orange bullet shows how the performance and carbon production changes while increasing the number of compute cores from 1 to 10⁶ (out of a total of 7 299 072, left-most orange point) using the performance model by^[10].

Carbon footprint of computing

- The relation between the time-to-solution and the carbon footprint of the calculations is not linear. When running a single core, a supercomputer-used to capacity-produces less carbon than a workstation. More cores result in better performance, at the cost of producing more carbon.
- Similar **performance as a single GPU is reached when running 1000 cores, but** when the number of cores is further increased, the performance continues to grow at an enormous cost in carbon production.
- When **running a million cores, the emission by supercomputer** by far exceeds air travel and **approaches the carbon footprint of launching a rocket into space.**



Ecological impact of computing language

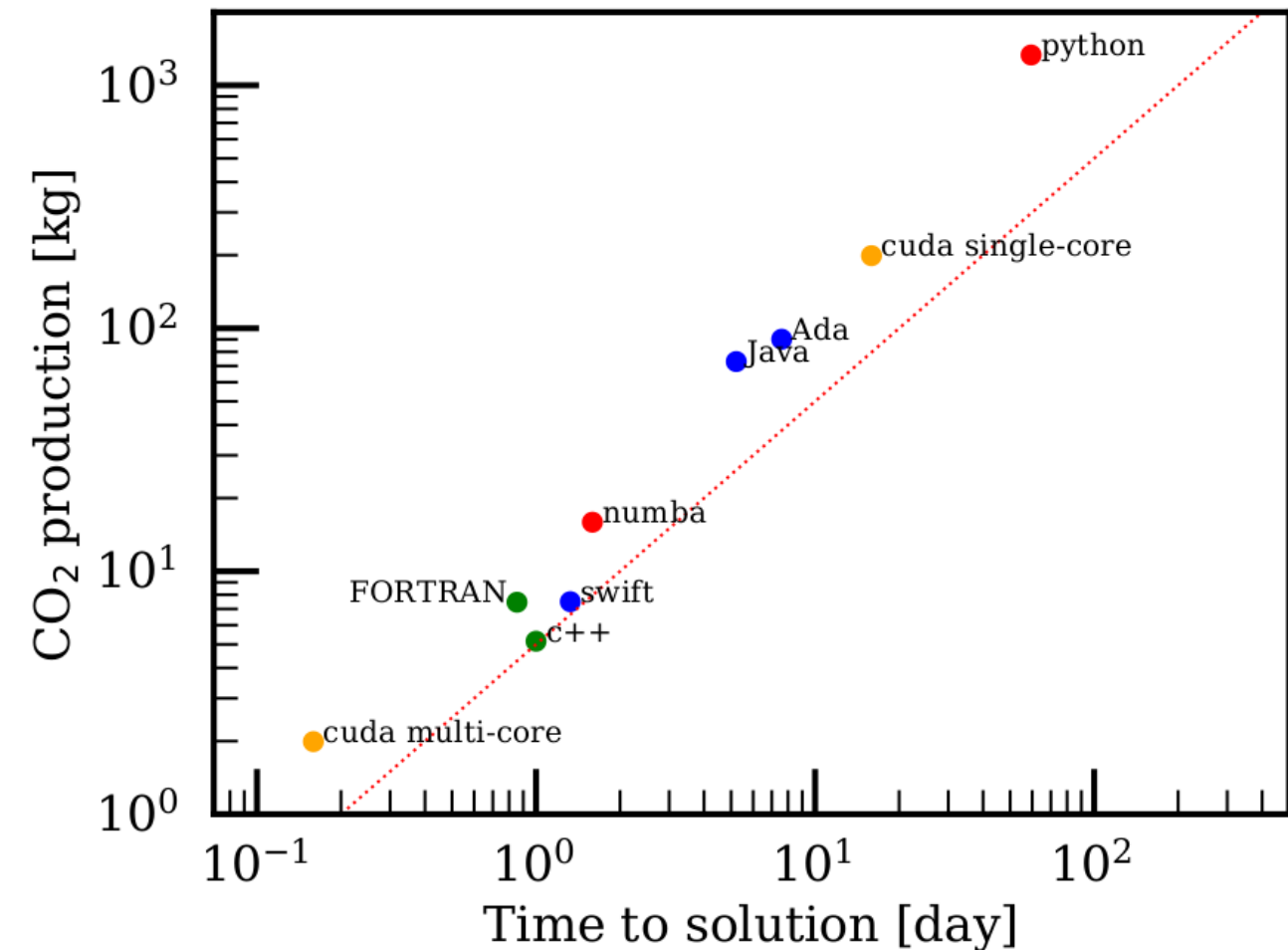


Figure 3: Here we used the direct N -body code from [\[23\]](#) to measure execution speed and the relative energy efficiency for each programming language from table 3 of [\[22\]](#). The dotted red curve gives a linear relation between the time-to-solution and carbon footprint ($\sim 5 \text{ kg CO}_2/\text{day}$). The calculations were performed on a 2.7GHz Intel Xeon E-2176M CPU and NVIDIA Tesla P100 GPU.

- Results were obtained with the assumption that astrophysicists invest in full code optimization that uses the hardware optimally.
- In practice, most effort is generally invested into solving the research question; designing, writing, and running the code is not the primary concern, if the result is obtained reasonably fast. This is why **inefficient** (and **slow**) scripting languages as Python flourish.
- According to the Astronomical Source Code Library, $\sim 43\%$ of the code is written in Python, 7 % Java, IDL and Mathematica. Only 18%, 17% and 16% of codes are written in Fortran, C and C++ respectively.
- Python and Java are also less efficient in terms of energy per operation than compiled languages, which explains the offset away from the dotted curve. Among 27 tested languages, only Perl and Lua are slower than Python-**popularity of Python should be confronted with the ecological consequences.**

How to improve?

- Runtime performance of Python can be improved **using numba or NumPy libraries**, which offer pre-compiled code for common operations-it leads to an enormous increase in speed and reduced carbon emission. However, these libraries are rarely adopted for reducing carbon emission or runtime with more than an order of magnitude.
- NumPy, for example, is mostly used for its advanced array handling and support functions. Using these will reduce runtime and, therefore, also carbon emission, but **optimization** is generally stopped as soon as the calculation runs within an unconsciously determined reasonable amount of time, such as the coffee-refill time-scale or a holiday weekend. We even teach Python to students, but without realizing the ecological impact.
- The carbon footprint of computational astrophysics can be reduced substantially by **running on GPUs**, but the development time of such code still requires major investments in time and expertise.
- As an alternative, one could run concurrently **using multiple cores, rather than a single thread**. It is even better to **port the code to a supercomputer and share the resources**.
- Best for the environment is to **abandon Python** for a more environmentally friendly (compiled) programming language.
- Even better is to **use other interesting strongly-typed languages** with characteristics similar to Python, such as Alice, Julia, Rust, and Swift. They offer the flexibility of Python but with the performance of compiled C++.
- Educators may want to **reconsider teaching Python** to University students. There are plenty environmentally friendly alternatives.

Summary of the Lect. 1

- General introduction to this lectures, Linux
- General intro to accretion history, observations
- Roche equipotential surfaces, PyAstronomy package
- Motivation and examples for accr.disk simulations, cosmic magnetic fields
- Linux shell commands, terminal editors
- Ecology of computing

Outline, Lect. 2: More detailed introduction to accretion

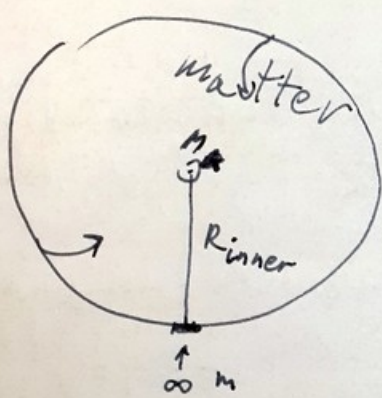
- Energetics of accretion, Eddington limit, spherical (Bondi) accretion
- Thin accretion disc, fluid & (M)HD eqs.
- Viscosity, resistivity, Alfven waves
- Code PLUTO, structure of the code, initial and boundary conditions
- Hands-on installation and testing, visualization with gnuplot,

Energetics of accretion

When I said that with accretion gravity made a comeback, I should say that it made it with a boom! - accretion is by far the most efficient way of extracting energy out of the matter we know: it yields about 10 times more than nuclear fusion!

We can show it in a back-of-the-envelope calculation for the luminosity of the disk acquired by the infall of material from the large distance onto a central object:

$\Delta \bar{E}_{acr} = \frac{6 M v^2}{R}$



Keplerian velocity at R_i orbit

$$v_{ki} = \sqrt{\frac{6 M v^2}{R_i}}$$

is velocity acquired by a particle infalling from $r \rightarrow \infty$, passing from $E_{p\infty}$ to $E_p(R_i)$.

$$v_{\infty} = \sqrt{\frac{26 M v^2}{R_i}}$$

We see the difference in energy:

$$E = \frac{M}{2} v_{\infty}^2 - \frac{M}{2} v_{ki}^2 = \frac{6 M v^2}{2 R_i}$$

Luminosity $L = \frac{dE}{dt} = \frac{6 M v^2 \dot{M}}{2 R_i}$

How efficient is this?

BH with Schwarzschild radius $R_g = \frac{26 M v^2}{c^2} \Rightarrow L = \frac{\dot{M}}{4} \frac{R_g}{R_i} c^2$

If disk ends at $R_i \approx 3 R_g$ above BH

$$L = \frac{1}{12} \dot{M} c^2 \sim 8\% \text{ of rest mass energy}$$

0.0833

In nuclear fusion we obtain typically $\sim 1\%$

\Rightarrow 10 times the energy from nuclear fusion!

Energetics of accretion

- In the literature, one can find various numbers for the efficiency of accretion, I list some below, but what is meant by “efficiency”?
It is the power available at given **mass accretion rate \dot{M}** onto an object of radius R : **$P = \dot{M} GM/R$** . This power is usually dissipated (through radiation) away, otherwise there will be no accretion-e.g. heat would push the matter away.
- Efficiency of pair annihilation: **$\eta = 1$**
- Efficiency of Nuclear (H) fusion: $\eta \sim 10^{-4}$
- Accretion efficiency η : Earth: 10^{-9} , Sun: 10^{-6} ,
White Dwarf: 10^{-4} , Neutron star: 10^{-1}
- Accretion efficiency **$\eta = GM/(Rc^2)$** onto black hole (no hard surface) depends on the details of accretion flow and spin of BH:
- **$0.057 < \eta < 0.42$** for thin accretion disk

Eddington limit

What is the maximum luminosity at which matter still can be accreted?
(This means that gravitational force on a chunk of fluid still just exceeds the radiation pressure)

- Simplest case is radial accretion onto a mass point M . If medium is fully ionised gas of electrons and protons, and we assume Compton scattering with the simplest radiation pressure $F_{rad} = +\frac{\sigma_T}{c} \frac{L}{4\pi r^2}$ and $F_g = -m_p \frac{GM}{r^2}$

from $F_{rad} = F_g$ we get that $L_{Edd} = \frac{4\pi GMm_p c}{\sigma_T}$

- Some Eddington luminosities: solar mass NS $L_{Edd} = 1.3 \times 10^{38} \left(\frac{M}{M_\odot}\right) \text{ erg/s}$
supermassive BH $L_{Edd} = 1.3 \times 10^{46} \left(\frac{M}{10^8 M_\odot}\right) \text{ erg/s}$

- Eddington mass accretion rate: $\dot{m}_{Edd} = \frac{L_{Edd}}{\eta c^2}$

- Usually it is said that the accretion is not possible if $L > L_{Edd}$ but there are cases when it is not true, and they are very interesting cases of supernovae and non-spherical accretion cases in disks and jets.

Spherical (Bondi) accretion-fast forward

H. Bondi (1952): an analytic solution for the spherically symmetric, steady-state accretion flow of an infinite gas cloud onto a point mass, in the Newtonian approach. It is spherical accretion onto a compact object traveling through the interstellar medium. It is generally used in the context of neutron star and black hole accretion.

Such model was later extended, to be applied from the study of star and planet formation to cosmology.

The derivation is not a simple one, Wikipedia answer: a rough estimate goes from the accretion rate $\dot{M} \approx \pi R^2 v \rho$ where ρ is the ambient density, v is the object's velocity, and R is the Bondi radius, which comes from setting escape velocity equal to the sound speed and solving for radius. It represents the boundary between subsonic and supersonic infall, and it is $R = 2GM/c_s^2$. Inserted into \dot{M} it gives $\dot{M} \approx \pi \rho G^2 M^2 / c_s^3$. *More detailed version is below.*

- Bondi considered adiabatic ($p \sim \rho^\gamma$) accretion of gas. Far from central mass, gas elements move in dependence of their thermal energy only, so that with gas temperature T_{inf} with sound speed c_s we can say that at some critical distance from the central mass r_{cr} the escape velocity is equal to the speed velocity: $r_{\text{cr}} = 2GM/c_s^2$

For $r < r_{\text{cr}}$ material falls freely onto the central mass, and for the density above the radius r_{cr} , ρ_{inf} we can write the infalling mass $\dot{M} = 4\pi G^2 M^2 \rho_{\text{inf}} / c_s^2$

Hydrostatic equilibrium gives $\rho \sim r^{-3/2}$ (with $\gamma = 5/3$) and temperature

$T \sim 1/r^{[3(\gamma-1)/2]}$. Infalling gas reaches speed of sound at distance r_s from the center. We find $r_s = GM/c_s^2 (5-3\gamma)/4$. *Even more in details is on the next 6 pages, I give it if you'd ever need it, but here we do not need it, we go for the disk.*

Let us take another view on accretion: material point orbiting around a center of mass interacts with its surrounding, transferring part of its energy and angular momentum.

- Consequence of such scenario is slowly spiral-in of the mass point. Energy which can be extracted is equal to the bonding energy of the smallest orbit: $E_{acr} = GMm/R$, see the back of the envelope calculation.
- The derivation of the basics of accretion process can be given within General Physics terminology, as follows.

-We consider rotating volume of gas with angular momentum \mathbf{L} in cylindrical coordinates (R, φ, z) , with \mathbf{z} parallel to the axis of rotation.

-We further assume that distribution of L between the gas particles is much slower than radiation transfer and rotation= \mathbf{L} of the particle with mass m remains constant, but its kinetic and internal energy are distributed to other particles by collisions, shocks and radiation.

-For the constant \mathbf{L} the minimal energy is for the circular orbit= \Rightarrow we obtain the thin disk in which particles rotate with $v_{\varphi} = R\Omega(R)$, we can write, with potential Φ : $F_g = ma = mv_{\varphi}^2/R = -d\Phi/dR = F_{cf}$.

Accretion disk

- If there is a process counteracting the spread of particles (as viscosity), energy spreads through the system by heat, and escapes from the system by radiation.
- As a consequence, mass particle will orbit at smaller R , we can understand this as transformation of the orbital energy into radiation energy.
- With the gas surface density $S(R,t)$ and radial velocity $v_r(R,t)$, we observe the element of gas with inner radius R and outer $R+\Delta R$. Mass of such ring is $\Delta m=2\pi R\cdot\Delta R\cdot S$, angular momentum $\mathbf{L}=\mathbf{R}\times\mathbf{p}$, where for angle of 90° between \mathbf{R} and \mathbf{p} we can write $L=Rmv_\phi$, and in fact we can write, with $L=mR^2\Omega$, that the angular momentum of such ring is $2\pi R\Delta R S R^2\Omega$. Change of mass of such a ring is equal to the fluxes in and out from the neighboring rings (positive sign is away from the center): $\partial/\partial t(\Delta m)=\text{flux}(R)-\text{flux}(R+\Delta R)=$

$$\begin{aligned}
 &= v_r(R,t) \cdot 2\pi R S(R,t) - v_r(R+\Delta R,t) 2\pi (R+\Delta R) S(R+\Delta R,t) = \\
 &= v_r(R,t) 2\pi R S(R,t) - v_r(R+\Delta R,t) 2\pi R S(R+\Delta R,t) - \\
 &\quad - v_r(R+\Delta R,t) 2\pi \Delta R S(R+\Delta R,t) =
 \end{aligned}$$

$$= [\text{with } \Delta R \rightarrow 0, \text{ 3}^{\text{rd}} \text{ term}=0 \text{ and } f(x+\Delta x)-f(x)=\Delta x \partial f(x)/\partial x] = -\Delta R \partial(2\pi R S v_r)/\partial R$$

Accretion disk

- Now we can write $\partial/\partial t(\Delta m)/\Delta R = -\partial/\partial R(2\pi R S v_r)$ and since $\Delta m/\Delta R = 2\pi R S$, so we stay, after divide by 2π , with $\partial/\partial t(RS) = -\partial/\partial R(RS v_r)$, $\partial R/\partial t = v_r$ and we can write further $v_r S + R \partial S/\partial t = -v_r S - R \partial/\partial R(S v_r)$. Since $\partial/\partial R(RS v_r) = v_r S + R \partial/\partial R(S v_r)$ we can write: $R \partial S/\partial t + \partial/\partial R(RS v_r) = -v_r S = 0$, since we are interested only in the **change** of mass.
- The same we can do for conservation of the angular momentum of such a ring, but adding the term for transfer of angular momentum between the rings, because of viscous torques, $\Delta R \partial G/\partial R$:

$$\begin{aligned}
 \frac{\partial}{\partial t}(2\pi R \Delta R S R^2 \Omega) &= v_r(R, t) 2\pi R S(R, t) R^2 \Omega(R) - \\
 &- v_r(R + \Delta R, t) 2\pi (R + \Delta R) S(R + \Delta R, t) \cdot (R + \Delta R)^2 \Omega(R + \Delta R) + \\
 &+ \frac{\partial G}{\partial R} \Delta R = [(R + \Delta R)^3 = R^3 + 3R^2 \Delta R + 3R(\Delta R)^2 + (\Delta R)^3 = \\
 &= \text{linearna aproksimacija} = R^3 + 3R^2 \Delta R] =
 \end{aligned}$$

Accretion disk

$$= v_r(R, t)2\pi R S(R, t)R^2\Omega(R + \Delta R) - \\ - 3v_r(R + \Delta R, t)2\pi\Delta R S(R + \Delta R, t)R^2\Omega(R + \Delta R) + \frac{\partial G}{\partial R}\Delta R$$

- In the linear approximation, first two terms are $-\Delta R \partial(2\pi v_r R S R^2 \Omega) / \partial R$ and we have:

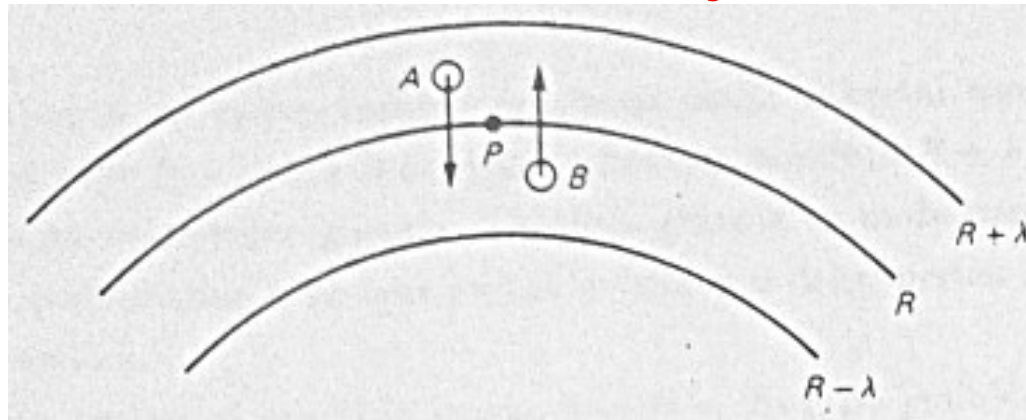
$$2\pi\Delta R \frac{\partial}{\partial t}(R S R^2 \Omega) = -\Delta R \frac{\partial}{\partial R}(2\pi v_r R S R^2 \Omega) - \\ - 3v_r 2\pi\Delta R S R^2 \Omega + \frac{\partial G}{\partial R}\Delta R$$

$$\frac{\partial R}{\partial t} S R^2 \Omega + R^2 \frac{\partial}{\partial R}(S R^2 \Omega) = -\frac{\partial}{\partial R}(v_r R S R^2 \Omega) - 3v_r S R^2 \Omega + \frac{\partial G}{\partial R} \cdot \frac{1}{2\pi}$$

- Again we discard constant 1st l.h.s and 2nd r.h.s. terms and write $\partial R / \partial t = v_r$ to get:

$$R \frac{\partial}{\partial t}(S R^2 \Omega) + \frac{\partial}{\partial R}(R v_r S R^2 \Omega) = \frac{1}{2\pi} \frac{\partial G}{\partial R}$$

Viscosity



Two neighbor rings in the disk.

- Now we will find the torque of two neighbor rings. The speed of chaotic motion in the gas is \bar{u} , and λ is the characteristic scale, which is also the mean free path. After exchange, element A will (in average) have torque from the position $R - \lambda/2$, and element in B from $R + \lambda/2$. Material in chaotic movement does not transfer matter (in average =0), only the steady flow can.
- Transferred mass is $\partial m / \partial t = H \rho \bar{u}$, where H is the disk height in z direction.
- For the accretion process essential is the difference in transported torques, and there is transport of torque because of chaotic motions. This is viscous torque.
- Observer in point P, rotating with $\Omega(R)$ sees fluid in $R - \lambda/2$ moving with speed

$$\left(R - \frac{\lambda}{2}\right) \Omega\left(R - \frac{\lambda}{2}\right) + \Omega(R) \frac{\lambda}{2}$$

Viscosity

- This gives the average flow of angular momentum by the unit angle directed outwards:

$$\rho \bar{v} H R \left[\left(R - \frac{\lambda}{2} \right) \Omega \left(R - \frac{\lambda}{2} \right) + \Omega(R) \frac{\lambda}{2} \right]$$

and inwards:

$$\rho \bar{v} H R \left[R + \frac{\lambda}{2} \Omega \left(R + \frac{\lambda}{2} \right) - \Omega(R) \frac{\lambda}{2} \right].$$

- Torque on the outer ring by the inner ring is equal to total outwards torque. In the first approximation we have:

$$\begin{aligned} & \rho \bar{v} H R \left\{ \left[\left(R - \frac{\lambda}{2} \right) \Omega \left(R - \frac{\lambda}{2} \right) + \Omega(R) \frac{\lambda}{2} \right] - \left[\left(R + \frac{\lambda}{2} \right) \Omega \left(R + \frac{\lambda}{2} \right) - \Omega(R) \frac{\lambda}{2} \right] \right\} = \\ & = \rho \bar{v} H R \left\{ R \Omega \left(R - \frac{\lambda}{2} \right) - R \Omega \left(R + \frac{\lambda}{2} \right) - \frac{\lambda}{2} \Omega \left(R - \frac{\lambda}{2} \right) - \frac{\lambda}{2} \Omega \left(R + \frac{\lambda}{2} \right) + 2 \Omega(R) \frac{\lambda}{2} \right\} = \end{aligned}$$

- = [first two terms in { } give $-R\lambda\partial\Omega/\partial R$, 3rd and 4th after $\lambda/2 \rightarrow 0$ give $-\lambda/2\Omega(R)$] = $-\lambda\rho\bar{v}HR^2\partial\Omega/\partial R$.

Viscosity, and back to the disk

- For the whole ring we multiply the obtained result with $2\pi R$, and with the surface density $\rho H = S$ [from $\rho = m/V$, $S = m/A$ we divide with H , we have $S/H = m/(AH)$, r.h.s. = ρ] we obtain that the torque of the outer to the inner ring
- (- inner torque to the outer ring) is $G(R) = 2\pi R \nu S R^2 \partial\Omega/\partial R$, where $\nu = \lambda \bar{u}$ is the kinematic viscosity coefficient.
- We had $G = G(R, t)$, and with $R \partial\Omega/\partial R = A$ we have $G(R) = 2\pi R \nu S A R$, where $\nu S A$ is a viscous force per unit angle.
- Now we can insert the obtained viscosity in the disk equations. We insert G into the equation we obtained from angular momentum conservation:

$$R \frac{\partial}{\partial t} (S R^2 \Omega) + \frac{\partial}{\partial R} (R v_r S R^2 \Omega) = \frac{1}{2\pi} \frac{\partial G}{\partial R}$$

- We divide with R and together with $R \partial S/\partial t + \partial/\partial R (R S v_r) = 0$ we can eliminate v_r .

Viscosity, and back to the disk

- The first equation, after division with R , we can rewrite as:

$$S \frac{\partial}{\partial t} (R^2 \Omega) + R^2 \Omega \frac{\partial S}{\partial t} + \frac{1}{R} R^2 \Omega \frac{\partial}{\partial R} (S R v_r) +$$

$$+ \frac{1}{R} S R v_r \frac{\partial}{\partial R} (R^2 \Omega) = \frac{1}{R} \frac{\partial}{\partial R} (\nu S R^3 \frac{\partial \Omega}{\partial R}).$$

- We write $R \partial S / \partial t + \partial / \partial R (R S v_r) = 0$ as $\partial (R S v_r) / \partial R = -R \partial S / \partial t$ and we have

$$S \frac{\partial}{\partial t} (R^2 \Omega) + R^2 \Omega \frac{\partial S}{\partial t} - R^2 \Omega \frac{\partial S}{\partial t} + S v_r \frac{\partial}{\partial R} (R^2 \Omega) =$$

$$= \frac{1}{R} \frac{\partial}{\partial R} (\nu S R^3 \frac{\partial \Omega}{\partial R}).$$

- In the first approximation \mathbf{L} is a constant vector, and since $R^2 \Omega$ is proportional to its length, we can discard the 1st term.

Viscosity, and back to the disk eqs.

- We obtain:

$$v_r = \frac{\frac{1}{R} \frac{\partial}{\partial R} (\nu S R^3 \frac{\partial \Omega}{\partial R})}{S \frac{\partial}{\partial R} (R^2 \Omega)}$$

- Inserting it into $R \partial S / \partial t + \partial / \partial R (R S v_r) = 0$ we

have:

$$\begin{aligned} \frac{\partial S}{\partial t} &= -\frac{1}{R} \frac{\partial}{\partial R} \left[R S \frac{\frac{1}{R} \frac{\partial}{\partial R} (\nu S R^3 \frac{\partial \Omega}{\partial R})}{S \frac{\partial}{\partial R} (R^2 \Omega)} \right] = \\ &= \frac{1}{R} \frac{\partial}{\partial R} \left\{ \frac{\frac{\partial}{\partial R} [\nu S R^3 (-\frac{\partial \Omega}{\partial R})^2]}{\frac{\partial}{\partial R} (R^2 \Omega)} \right\}. \end{aligned}$$

- With $F_g = F_{cf}$, potential of point mass M is $mv^2/R = GMm/R^2$ and $v_\phi = \Omega R$, **G=gravity const.**, Keplerian $\Omega = (GM/R^3)^{1/2}$ and $d\Omega/dR = -3/2(GM/R^5)^{1/2}$ and \rightarrow
This is the diffusion equation for the surface density S : mass diffuses inwards, angular momentum outwards.
- Diffusion timescale is $t_{\text{visc}} = R^2/\nu$.

$$\begin{aligned} \frac{\partial}{\partial R} (R^2 \Omega) &= \frac{\partial}{\partial R} (R^2 \sqrt{GM} R^{-3/2}) = \\ &= \frac{\partial}{\partial R} (\sqrt{GM} R^{1/2}) = \frac{1}{2} \sqrt{GM} R^{-1/2} \end{aligned}$$

$$\begin{aligned} \frac{\partial S}{\partial t} &= \frac{1}{R} \frac{\partial}{\partial R} \left\{ \frac{\frac{\partial}{\partial R} [\nu S R^3 \frac{3}{2} \sqrt{GM} R^{1/2}]}{\frac{1}{2} \sqrt{GM} R^{-1/2}} \right\} = \\ &= \frac{1}{R} \frac{\partial}{\partial R} \left\{ \frac{\frac{\partial}{\partial R} [\nu S \frac{3}{2} \sqrt{GM} R^{1/2}]}{\frac{1}{2} \sqrt{GM} R^{-1/2}} \right\} = \\ &= \frac{3}{R} \frac{\partial}{\partial R} \left[\sqrt{R} \frac{\partial}{\partial R} (\nu S \sqrt{R}) \right] \end{aligned}$$

Viscosity, general discussion

- We obtained the solution for S . In general, ν depends on local conditions in the disk, and $\nu = \nu(S, R, t)$ so that we obtained nonlinear diffusion eq. for S .
- If ν depends on R only, eq. is linear in S , even for the power of R (it was clear already in 1920-ies, Jeffreys 1924, Weizsacker in 1948).
- Most of the mass moves towards the center, losing energy and torque. A tail of matter moves towards larger R to conserve the angular momentum. Matter from the initial ring arrives to the center, and total angular momentum is transported to large radii by a very small mass, compared to the disk mass. The disk slowly spreads outwards.
- In 1973 Shakura & Sunyaev gave a solution, parameterizing viscosity as $\nu = \alpha c_s H$, where $\alpha < 1$ is a coefficient describing “turbulent viscosity”. Usually $\nu \sim LV$, where L is characteristic scale, and v characteristic velocity of the turbulent eddies—so we assumed $L \sim H$ of the disk, and $V \sim c_s$ (turbulence is usually assumed to be subsonic).
In astrophysics we are usually dealing with large Reynolds numbers Re , defined through $Re = LV/\nu$, simply because of large L .

Viscosity, general discussion

- Re measures ratio of inertial to viscous forces, so in the disc we usually have proportionality with v_ϕ^2/R
- For $Re \ll 1$ viscous forces are dominating, and with $Re \gg 1$ they are unimportant. In accretion discs usually $Re \gg 10^{11}$ and we can not get much lower.
- Clue of the problem is exactly in so large Re: from experiments we know that fluids have some critical value Re_c , at which the velocity becomes chaotic, so we have turbulence. Typical $Re_c = 10^3$, so we can conclude that disc material is turbulent.
- There were many works on turbulence, but we still do not have the full understanding of the mechanism in accretion disks. Currently accepted paradigm is the one by Balbus & Hawley (1992), where magneto-rotational (MRI) turbulence is invoked.
- Mathematically, viscous process is a diffusion process (of matter and angular momentum), this is the basics for our description. We will see it in the following equations.

Fluid equations

We will now make a general intro to (M)HD equations-for the first read I suggest J.D.Jackson “Classical electrodynamics”, 10th chapter (up to the 3rd edition, later removed, probably as too specialized).

10.2 Magnetohydrodynamic Equations

We first consider the behavior of an electrically neutral, conducting fluid in electromagnetic fields. For simplicity, we assume the fluid to be nonpermeable. It is described by a matter density $\rho(\mathbf{x}, t)$, a velocity $\mathbf{v}(\mathbf{x}, t)$, a pressure $p(\mathbf{x}, t)$ (taken to be a scalar), and a real conductivity σ . The hydrodynamic equations are the continuity equation

$$\frac{\partial \rho}{\partial t} + \nabla \cdot (\rho \mathbf{v}) = 0 \quad (10.1)$$

and the force equation:

$$\rho \frac{d\mathbf{v}}{dt} = -\nabla p + \frac{1}{c} (\mathbf{J} \times \mathbf{B}) + \mathbf{F}_v + \rho \mathbf{g} \quad (10.2)$$

In addition to the pressure and magnetic-force terms we have included viscous and gravitational forces. For an incompressible fluid the viscous force can be written

$$\mathbf{F}_v = \eta \nabla^2 \mathbf{v} \quad (10.3)$$

where η is the coefficient of viscosity. It should be emphasized that the time derivative of the velocity on the left side of (10.2) is the *convective derivative*,

$$\frac{d}{dt} = \frac{\partial}{\partial t} + \mathbf{v} \cdot \nabla \quad (10.4)$$

which gives the total time rate of change of a quantity moving instantaneously with the velocity \mathbf{v} .

With the neglect of the displacement current, the electromagnetic fields in the fluid are described by

$$\left. \begin{aligned} \nabla \times \mathbf{E} + \frac{1}{c} \frac{\partial \mathbf{B}}{\partial t} &= 0 \\ \nabla \times \mathbf{B} &= \frac{4\pi}{c} \mathbf{J} \end{aligned} \right\} \quad (10.5)$$

The condition $\nabla \cdot \mathbf{J} = 0$, equivalent to the neglect of displacement currents, follows from the second equation in (10.5). The two divergence equations have been omitted in (10.5). It follows from Faraday’s law that $(\partial/\partial t) \nabla \cdot \mathbf{B} = 0$, and the requirement $\nabla \cdot \mathbf{B} = 0$ can be imposed as an initial condition. With the neglect of the displacement current, it is appropriate to ignore Coulomb’s law as well. The reason is that the electric field is completely determined by the curl equations and Ohm’s law (see below). If the displacement current is retained in Ampère’s law and $\nabla \cdot \mathbf{E} = 4\pi\rho_e$ is taken into account, corrections of only the order of (v^2/c^2) result. For normal magnetohydrodynamic problems these are completely negligible.

To complete the specification of dynamical equations we must specify the relation between the current density \mathbf{J} and the fields \mathbf{E} and \mathbf{B} . For a simple conducting medium of conductivity σ , Ohm’s law applies, and the current density is

$$\mathbf{J}' = \sigma \mathbf{E}' \quad (10.6)$$

where \mathbf{J}' and \mathbf{E}' are measured in the rest frame of the medium. For a medium moving with velocity \mathbf{v} relative to the laboratory, we must transform both the current density and the electric field appropriately. The transformation of the field is given by equation (6.10). The current density in the laboratory is evidently

$$\mathbf{J} = \mathbf{J}' + \rho_e \mathbf{v} \quad (10.7)$$

where ρ_e is the electrical charge density. For a one-component conducting

Fluid equations

To complete the specification of dynamical equations we must specify the relation between the current density \mathbf{J} and the fields \mathbf{E} and \mathbf{B} . For a simple conducting medium of conductivity σ , Ohm's law applies, and the current density is

$$\mathbf{J}' = \sigma \mathbf{E}' \quad (10.6)$$

where \mathbf{J}' and \mathbf{E}' are measured in the rest frame of the medium. For a medium moving with velocity \mathbf{v} relative to the laboratory, we must transform both the current density and the electric field appropriately. The transformation of the field is given by equation (6.10). The current density in the laboratory is evidently

$$\mathbf{J} = \mathbf{J}' + \rho_e \mathbf{v} \quad (10.7)$$

where ρ_e is the electrical charge density. For a one-component conducting fluid, $\rho_e = 0$. Consequently, Ohm's law assumes the form,

$$\mathbf{J} = \sigma \left(\mathbf{E} + \frac{\mathbf{v}}{c} \times \mathbf{B} \right) \quad (10.8)$$

Sometimes it is possible to assume that the conductivity of the fluid is effectively infinite. Then under the action of fields \mathbf{E} and \mathbf{B} the fluid flows in such a way that

$$\mathbf{E} + \frac{1}{c} (\mathbf{v} \times \mathbf{B}) = 0 \quad (10.9)$$

is satisfied.

10.3 Magnetic Diffusion, Viscosity, and Pressure

The behavior of a fluid in the presence of electromagnetic fields is governed to a large extent by the magnitude of the conductivity. The effects are both electromagnetic and mechanical. We first consider the electromagnetic effects. We will see that, depending on the conductivity, quite different behaviors of the fields occur. The time dependence of the magnetic field can be written, using (10.8) to eliminate \mathbf{E} , in the form:

$$\frac{\partial \mathbf{B}}{\partial t} = \nabla \times (\mathbf{v} \times \mathbf{B}) + \frac{c^2}{4\pi\sigma} \nabla^2 \mathbf{B} \quad (10.10)$$

Here it is assumed that σ is constant in space. For a fluid at rest (10.10) reduces to the diffusion equation

$$\frac{\partial \mathbf{B}}{\partial t} = \frac{c^2}{4\pi\sigma} \nabla^2 \mathbf{B} \quad (10.11)$$

This means that an initial configuration of magnetic field will decay away in a diffusion time

$$\tau = \frac{4\pi\sigma L^2}{c^2} \quad (10.12)$$

where L is a length characteristic of the spatial variation of \mathbf{B} . The time τ is of the order of 1 sec for a copper sphere of 1 cm radius, of the order of 10^4 years for the molten core of the earth, and of the order of 10^{10} years for a typical magnetic field in the sun.

For times short compared to the diffusion time τ (or, in other words, when the conductivity is so large that the second term in (10.10) can be neglected) the temporal behavior of the magnetic field is given by

$$\frac{\partial \mathbf{B}}{\partial t} = \nabla \times (\mathbf{v} \times \mathbf{B}) \quad (10.13)$$

From (6.5) it can be shown that this is equivalent to the statement that the magnetic flux through any loop moving with the local fluid velocity is constant in time. We say that the lines of force are frozen into the fluid and are carried along with it. Since the conductivity is effectively infinite,

Fluid equations

the velocity \mathbf{w} of the lines of force (defined to be perpendicular to \mathbf{B}) is given by (10.9):

$$\mathbf{w} = c \frac{(\mathbf{E} \times \mathbf{B})}{B^2} \quad (10.14)$$

This so-called “ $E \times B$ drift” of both fluid and lines of force can be understood in terms of individual particle orbits of the electrons and ions in crossed electric and magnetic fields (see Section 12.8).

A useful parameter to distinguish between situations in which diffusion of the field lines relative to the fluid occurs and those in which the lines of force are frozen in is the *magnetic Reynolds number* R_M . If V is a velocity typical of the problem and L is a corresponding length, then the magnetic Reynolds number is defined as

$$R_M = \frac{V\tau}{L} \quad (10.15)$$

where τ is the diffusion time (10.12). Transport of the lines of force with the fluid dominates over diffusion if $R_M \gg 1$. For liquids like mercury or sodium in the laboratory $R_M < 1$, except for very high velocities. But in geophysical and astrophysical applications R_M can be very large compared to unity.

The above considerations have shown that if the conductivity is large the lines of force are frozen into the fluid and move along with it. Any departure from that state decays rapidly away. In considering the mechanical or electromagnetic effects we treated the opposite quantities as given, but the equations are, of course, coupled. In the limit of very large conductivity it is convenient to relate the current density \mathbf{J} in the force equation to the magnetic induction \mathbf{B} via Ampère’s law and to use the infinite conductivity expression (10.9) to eliminate \mathbf{E} from Faraday’s law to yield (10.13). The magnetic force term in (10.2) can now be written

$$\frac{1}{c}(\mathbf{J} \times \mathbf{B}) = -\frac{1}{4\pi} \mathbf{B} \times (\nabla \times \mathbf{B}) \quad (10.19)$$

With the vector identity

$$\frac{1}{2} \nabla(\mathbf{B} \cdot \mathbf{B}) = (\mathbf{B} \cdot \nabla)\mathbf{B} + \mathbf{B} \times (\nabla \times \mathbf{B}) \quad (10.20)$$

Equation (10.19) can be transformed into

$$\frac{1}{c}(\mathbf{J} \times \mathbf{B}) = -\nabla \left(\frac{B^2}{8\pi} \right) + \frac{1}{4\pi} (\mathbf{B} \cdot \nabla)\mathbf{B} \quad (10.21)$$

This equation shows that the magnetic force is equivalent to a *magnetic hydrostatic pressure*,

$$p_M = \frac{B^2}{8\pi} \quad (10.22)$$

plus a term which can be thought of as an additional tension along the lines of force. The result (10.21) can also be derived from the Maxwell stress tensor (see Section 6.9).

If we neglect viscous effects and assume that the gravitational force is derivable from a potential $\mathbf{g} = -\nabla\psi$, the force equation (10.2) takes the form

$$\rho \frac{d\mathbf{v}}{dt} = -\nabla(p + p_M + \rho\psi) + \frac{1}{4\pi} (\mathbf{B} \cdot \nabla)\mathbf{B} \quad (10.23)$$

In some simple geometrical situations, such as \mathbf{B} having only one component, the additional tension vanishes. Then the static properties of the fluid are described by

$$p + p_M + \rho\psi = \text{constant} \quad (10.24)$$

This shows that, apart from gravitational effects, any change in mechanical pressure must be balanced by an opposite change in magnetic pressure. If the fluid is to be confined within a certain region so that p falls rapidly to zero outside that region, the magnetic pressure must rise equally rapidly in order to confine the fluid. This is the principle of the pinch effect

Alfven waves

10.8 Magnetohydrodynamic Waves

In ordinary hydrodynamics the only type of small-amplitude wave motion possible is that of longitudinal, compressional (sound) waves. These propagate with a velocity s related to the derivative of pressure with respect to density at constant entropy:

$$s^2 = \left(\frac{\partial p}{\partial \rho} \right)_0 \quad (10.64)$$

If the adiabatic law $p = K\rho^\gamma$ is assumed, $s^2 = \gamma p_0 / \rho_0$, where γ is the ratio of specific heats. In magnetohydrodynamics another type of wave motion is possible. It is associated with the transverse motion of lines of magnetic force. The tension in the lines of force tends to restore them to straight-line form, thereby causing a transverse oscillation. By analogy with ordinary sound waves whose velocity squared is of the order of the hydrostatic pressure divided by the density, we expect that these magnetohydrodynamic waves, called *Alfvén waves*, will have a velocity

$$v_A \sim \left(\frac{B_0^2}{8\pi\rho_0} \right)^{1/2} \quad (10.65)$$

where $B_0^2/8\pi$ is the magnetic pressure.

Alfven is my hero in writing of a short, impactful article!

Existence of Electromagnetic-Hydrodynamic Waves

If a conducting liquid is placed in a constant magnetic field, every motion of the liquid gives rise to an E.M.F. which produces electric currents. Owing to the magnetic field, these currents give mechanical forces which change the state of motion of the liquid.

N A I

406

Thus a kind of combined electromagnetic-hydrodynamic wave is produced which, so far as I know, has as yet attracted no attention.

The phenomenon may be described by the electrodynamic equations

$$\text{rot } H = \frac{4\pi}{c} i$$

$$\text{rot } E = - \frac{1}{c} \frac{dB}{dt}$$

$$B = \mu H$$

$$i = \sigma(E + \frac{v}{c} \times B);$$

together with the hydrodynamic equation

$$\rho \frac{dv}{dt} = \frac{1}{c} (i \times B) - \text{grad } p,$$

where σ is the electric conductivity, μ the permeability, ρ the mass density of the liquid, i the electric current, v the velocity of the liquid, and p the pressure.

Consider the simple case when $\sigma = \infty$, $\mu = 1$ and the imposed constant magnetic field H_0 is homogeneous and parallel to the z -axis. In order to study a plane wave we assume that all variables depend upon the time t and z only. If the velocity v is parallel to the x -axis, the current i is parallel to the y -axis and produces a variable magnetic field H' in the x -direction. By elementary calculation we obtain

$$\frac{d^2 H'}{dz^2} = \frac{4\pi\partial}{H_0^2} \frac{d^2 H'}{dt^2},$$

which means a wave in the direction of the z -axis with the velocity

$$V = \frac{H_0}{\sqrt{4\pi\partial}}$$

Waves of this sort may be of importance in solar physics. As the sun has a general magnetic field, and as solar matter is a good conductor, the conditions for the existence of electromagnetic-hydrodynamic waves are satisfied. If in a region of the sun we have $H_0 = 15$ gauss and $\partial = 0.005$ gm. cm.⁻³, the velocity of the waves amounts to

$$V \sim 60 \text{ cm. sec.}^{-1}.$$

This is about the velocity with which the sunspot zone moves towards the equator during the sunspot cycle. The above values of H_0 and ∂ refer to a distance of about 10^{10} cm. below the solar surface where the original cause of the sunspots may be found. Thus it is possible that the sunspots are associated with a magnetic and mechanical disturbance proceeding as an electromagnetic-hydrodynamic wave.

The matter is further discussed in a paper which will appear in *Arkiv för matematik, astronomi och fysik*.

H. ALFVÉN.

Kgl. Tekniska Högskolan,
Stockholm.

Aug. 24.

Simulation ver. computation

- Computation is actually an evaluation: you plug the numbers in a known algorithm and obtain the result. For this, you need to know the analytical expression. You still can use a (human?) calculator with a slide ruler, or mechanical or electrical or electronic calculator or, today, computer to actually obtain numbers and plot e.g. trajectory of a bullet, but you **do** know the equation for the solution.
- Simulation is needed when you do not know a simple equation for the solution. You set the governing equations, e.g. differential equations, and use a numerical method to find the solutions. This is usually done in time steps, and we obtain the solution to some precision. We do not know the analytical expression for the solution, we just have numbers. We can interpolate some power law and write the equation afterwards, but this will be only an approximation, without physical understanding of the outcome. Then we usually hand-wave the solution. More stirring of the air usually means less of physical understanding.
- Why PLUTO? I used other codes, but PLUTO is constantly evolving (and is used in variety of problems) **and** the development is followed in the manual-which is not so often the case in the coding world. The version 4.4.2. just changed to 4.4.3. in September 2024. PLUTO user manual gives chance to students to go through the-still steep-learning curve of the numerical simulations in the shortest possible time. Check also Doxygen html files in PLUTO/Doc.

PLUTO documentation, templates and test examples

I HOPE YOU MANAGED TO DOWNLOAD THE CODE AND DO THE FIRST TEST. WE WILL BRIEFLY GO THROUGH THE STEPS.

- PLUTO is freely available. Source files of the code are downloadable from <http://plutocode.ph.unito.it/>
- After unpacking, the source code is in PLUTO directory. In PLUTO/Doc is the manual, `userguide.pdf`. Follow the “Quick start” at the beginning of the document to **install and test the code. Produce the gnuplot output specified in the manual, to verify if the setup works.**
- The code comes with templates of subroutines which are usually changed. They are given in the PLUTO/Src/Templates
- Test examples, under /PLUTO/Test_Problems, are basic versions of setups used in previous versions of the code, during the developments of the setups for simulations presented in publications by various groups. It is a good library of examples for faster start of one’s own project.
- I will provide the setup for HD and MHD accretion disk for this lectures.

PLUTO physics modules, equations

6.1 The HD Module

The HD module may be used to solve the Euler or the Navier-Stokes equations of classical fluid dynamics. The relevant source files and definitions for this module can be found in the `Src/HD` directory.

With the HD module, **PLUTO** evolves in time following system of conservation laws:

$$\frac{\partial}{\partial t} \begin{pmatrix} \rho \\ \mathbf{m} \\ E_t + \rho\Phi \end{pmatrix} + \nabla \cdot \begin{pmatrix} \rho\mathbf{v} \\ \mathbf{m}\mathbf{v} + p\mathbf{l} \\ (E_t + p + \rho\Phi)\mathbf{v} \end{pmatrix}^T = \begin{pmatrix} 0 \\ -\rho\nabla\Phi + \rho\mathbf{g} \\ \mathbf{m} \cdot \mathbf{g} \end{pmatrix} \quad (6.1)$$

where ρ is the mass density, $\mathbf{m} = \rho\mathbf{v}$ is the momentum density, \mathbf{v} is the velocity, p is the thermal pressure and E_t is the total energy density:

$$E_t = \rho e + \frac{\mathbf{m}^2}{2\rho}. \quad (6.2)$$

An equation of state provides the closure $\rho e = \rho e(p, \rho)$.

The source term on the right includes contributions from body forces and is written in terms of the (time-independent) gravitational potential Φ and the acceleration vector \mathbf{g} (§5.4).

6.2 The MHD Module

The MHD module is suitable for the solution of ideal or resistive (non-relativistic) magnetohydrodynamical equations. Source and definition files are located inside the Src/MHD directory.

With the MHD module, **PLUTO** solves the following system of conservation laws:

$$\begin{aligned}
 \frac{\partial \rho}{\partial t} + \nabla \cdot (\rho \mathbf{v}) &= 0 \\
 \frac{\partial \mathbf{m}}{\partial t} + \nabla \cdot \left[\mathbf{m} \mathbf{v} - \mathbf{B} \mathbf{B} + \mathbf{l} \left(p + \frac{\mathbf{B}^2}{2} \right) \right]^T &= -\rho \nabla \Phi + \rho \mathbf{g} \\
 \frac{\partial \mathbf{B}}{\partial t} + \nabla \times (c \mathbf{E}) &= 0 \\
 \frac{\partial (E_t + \rho \Phi)}{\partial t} + \nabla \cdot \left[\left(\frac{\rho \mathbf{v}^2}{2} + \rho e + p + \rho \Phi \right) \mathbf{v} + c \mathbf{E} \times \mathbf{B} \right] &= \mathbf{m} \cdot \mathbf{g}
 \end{aligned} \tag{6.4}$$

where ρ is the mass density, $\mathbf{m} = \rho \mathbf{v}$ is the momentum density, \mathbf{v} is the velocity, p is the gas (thermal) pressure, \mathbf{B} is the magnetic field² and E_t is the total energy density:

$$E_t = \rho e + \frac{\mathbf{m}^2}{2\rho} + \frac{\mathbf{B}^2}{2}. \tag{6.5}$$

where an additional equation of state provides the closure $\rho e = \rho e(p, \rho)$ (see Chapter 7). The source term on the right includes contributions from body forces and is written in terms of the (time-independent) gravitational potential Φ and the acceleration vector \mathbf{g} (see §5.4).

In the third of Eq. (6.4), \mathbf{E} is the electric field defined by the expression

$$c \mathbf{E} = -\mathbf{v} \times \mathbf{B} + \frac{\eta}{c} \cdot \mathbf{J} + \frac{\mathbf{J}}{ne} \times \mathbf{B} \quad \left(\mathbf{J} = c \nabla \times \mathbf{B} \right) \tag{6.6}$$

where the first term is the convective term, the second term is the resistive term (η denotes the resistivity tensor. see §8.2) while the third term is the Hall term (§8.1). Note that the speed of light c never enters

PLUTO physics modules, equations

6.3 The RHD Module

The RHD module implements the equations of special relativistic fluid dynamics in 1, 2 or 3 dimensions. Velocities are always assumed to be expressed in units of the speed of light. The special relativistic module comes with 2 different equations of state, and it also works in curvilinear coordinates. Gravity in Newtonian approximation can also be incorporated. The relevant source files and definitions for this module can be found in the Src/RHD directory.

The special relativistic module evolves the conservative set U of state variables

$$U = \left(D, m_1, m_2, m_3, E_t \right)^T$$

where D is the laboratory density, $m_{x1,x2,x3}$ are the momentum components, E_t is the total energy (including contribution from the rest mass). The evolutionary conservative equations are

$$\frac{\partial}{\partial t} \begin{pmatrix} D \\ \mathbf{m} \\ E_t \end{pmatrix} + \nabla \cdot \begin{pmatrix} D\mathbf{v} \\ \mathbf{m}\mathbf{v} + p\mathbf{l} \\ \mathbf{m} \end{pmatrix}^T = \begin{pmatrix} 0 \\ \mathbf{f}_g \\ \mathbf{v} \cdot \mathbf{f}_g \end{pmatrix}$$

where \mathbf{v} is the velocity, p is the thermal pressure. Primitive variables V always include the rest-mass density ρ , three-velocity $\mathbf{v} = (v_{x1}, v_{x2}, v_{x3})$ and pressure p . With PLUTO 4.4, the acceleration term \mathbf{f}_g is treated consistently³ with the formalism of [Tau48]. If \mathbf{a} is the acceleration vector,

$$\mathbf{f}_g = \rho\gamma^2 [\gamma^2 \mathbf{v} (\mathbf{v} \cdot \mathbf{a}) + \mathbf{a}] . \quad (6.12)$$

PLUTO physics modules, equations

6.4 The RMHD Module

The RMHD module implements the equations of (ideal) special relativistic magnetohydrodynamics in 1, 2 or 3 dimensions. Velocities are always assumed to be expressed in units of the speed of light. Source and definition files are located inside the Src/RMHD directory.

The RMHD module solves the following system of conservation laws:

$$\frac{\partial}{\partial t} \begin{pmatrix} D \\ \mathbf{m} \\ E_t \\ \mathbf{B} \end{pmatrix} + \nabla \cdot \begin{pmatrix} D\mathbf{v} \\ w_t\gamma^2\mathbf{v}\mathbf{v} - \mathbf{b}\mathbf{b} + p_t \\ \mathbf{m} \\ \mathbf{v}\mathbf{B} - \mathbf{B}\mathbf{v} \end{pmatrix}^T = \begin{pmatrix} 0 \\ \mathbf{f}_g \\ \mathbf{v} \cdot \mathbf{f}_g \\ 0 \end{pmatrix} \quad (6.13)$$

where D is the laboratory density, \mathbf{m} is the momentum density, E is the total energy (including contribution from the rest mass) while \mathbf{f}_g is an acceleration term (see [6.3](#)).

Primitive variables are similar to the RHD module but they also contain the magnetic field, $\mathbf{V} = (\rho, \mathbf{v}, p, \mathbf{B})$. The relation between \mathbf{V} and \mathbf{U} is

$$\begin{aligned} D &= \gamma\rho \\ \mathbf{m} &= w_t\gamma^2\mathbf{v} - b^0\mathbf{b} \\ E_t &= w_t\gamma^2 - b^0b^0 - p_t \end{aligned} \quad , \quad \begin{cases} b^0 = \gamma\mathbf{v} \cdot \mathbf{B} \\ \mathbf{b} = \mathbf{B}/\gamma + \gamma(\mathbf{v} \cdot \mathbf{B})\mathbf{v} \\ w_t = \rho h + \mathbf{B}^2/\gamma^2 + (\mathbf{v} \cdot \mathbf{B})^2 \\ p_t = p + \frac{\mathbf{B}^2/\gamma^2 + (\mathbf{v} \cdot \mathbf{B})^2}{2} \end{cases}$$

PLUTO physics modules, equations

A note on public vs. non-public modules.

Besides the official code release, a few modules have not yet been made available with the standard public version, as they are still under active development or testing stage. In other circumstances, a private module may have been implemented under specific collaboration policies, which do not grant its public distribution. These non-offical modules include:

- Lagrangian Particle Module
(Developers: B. Vaidya [bvaidya@iiti.ac.in], D. Mukherjee [dipanjan@iucaa.in]);
- Dust Module
(Developers: A. Mignone [mignone@to.infn.it], M. Flock [flock@mpia.de]);
- Relativistic Resistive MHD
(Developers: A. Mignone [mignone@to.infn.it], G. Mattia [mattia@mpia.de]);

Distribution, private sharing and usage of these modules is permitted only in the form of a collaboration between our partner institutions network, requiring co-authorship from at least one of the module developers.

6.5 The Resistive RMHD (*ResRMHD*) Module

Note: This module is not part of the public code release, see “Terms & Conditions of Use” at the beginning of this guide

The ResRMHD module deals with the non-ideal relativistic MHD equations using the approaches discussed in [MMBD19](#). Source and definition files are located inside the Src/ResRMHD directory.

The set of resistive relativistic equations arising from the time and space split of the covariant are, in vectorial form,

$$\begin{aligned}
 \frac{\partial D}{\partial t} + \nabla \cdot (D\mathbf{v}) &= 0, \\
 \frac{\partial \mathbf{m}}{\partial t} + \nabla \cdot (w\mathbf{u}\mathbf{u} + p\mathbf{l} + \mathbb{T}) &= 0, \\
 \frac{\partial \mathcal{E}}{\partial t} + \nabla \cdot \mathbf{m} &= 0, \\
 \frac{\partial \mathbf{B}}{\partial t} + \nabla \times \mathbf{E} &= 0, \\
 \frac{\partial \mathbf{E}}{\partial t} - \nabla \times \mathbf{B} &= -\mathbf{J},
 \end{aligned} \tag{6.14}$$

where \mathbf{l} is the identity matrix and the fluid conserved variables are the density $D = \rho\gamma$ as measured in the laboratory frame, the total momentum density $\mathbf{m} = w\gamma\mathbf{u} + \mathbf{E} \times \mathbf{B}$, and the total energy density

$$\mathcal{E} = w\gamma^2 - p + \mathcal{P}_{\text{EM}}. \tag{6.15}$$

In the expressions above, $w = \varepsilon + p$ is the specific enthalpy and $\mathcal{P}_{\text{EM}} = (E^2 + B^2)/2$ denotes the EM energy density. Finally,

$$\mathbb{T} = -\mathbf{E}\mathbf{E} - \mathbf{B}\mathbf{B} + \frac{1}{5}(E^2 + B^2)\mathbf{l} \tag{6.16}$$

7. Equation of State

In the current implementation, **PLUTO** describes a thermally ideal gas obeying the *thermal* Equation of State (EOS)

$$p = nk_B T = \frac{\rho}{m_u \mu} k_B T \quad (7.1)$$

where p is the pressure, n is the total particle number density, k_B is the Boltzmann constant, T is the temperature, ρ is the density, m_u is the atomic mass unit and μ is the mean molecular weight. The thermal EOS describes the thermodynamic state of a plasma in terms of its pressure p , density ρ , temperature T and chemical composition μ . Eq. (7.1) is written in CGS physical units. Using code units for p and ρ while leaving temperature in Kelvin, the thermal EOS is conveniently re-expressed as

$$p = \frac{\rho T}{\mathcal{K} \mu} \quad \iff \quad T = \frac{p}{\rho} \mathcal{K} \mu \quad \left(\text{where } \mathcal{K} = \frac{m_u v_0^2}{k_B} \right) \quad (7.2)$$

where \mathcal{K} is the **KELVIN** macro which depends explicitly on the value of `UNIT_VELOCITY`.

8. Nonideal Effects

In this chapter we give an overview of the code capabilities for treating dissipative (or diffusion) terms which, at present, include

- Hall MHD (MHD), described in §8.1
- Resistivity (MHD), described in §8.2
- Thermal conduction (HD, MHD), described in §8.3
- Viscosity (HD, MHD), described in §8.4

Each modules can be individually turned on from the physics sub-menus accessible via the Python script.

Shell variable setup, aliases

- We follow the “Quick start” from the beginning of the `PLUTO/Doc/userguide.pdf`
- Instead of every time after login repeating
`export PLUTO_DIR=/home/user/PLUTO` # in bash shell
Create in `.bash_aliases` (or `.bashrc`) a shell variable with path to PLUTO:
`export PLUTO_DIR="/home/miki/PLUTO"`
- Also, it is useful to create an alias (shortcut) for running the `setup.py`, e.g.:
`alias pls='python $PLUTO_DIR/setup.py'`
 - For runs on multiple processors on laptop, useful is alias like:
`alias plutorun6='mpirun -np 6 ./pluto'`

System setup

```
IW .bash_aliases (Modified)
alias sshdisco='ssh -Y miki@disco'
alias sshchuck='ssh miki@chuck'
alias sftpchuck='sftp miki@chuck.camk.edu.pl'
alias kju='squeue -u miki'

alias sshgate='ssh -X -l miki gate.tiara.sinica.edu.tw'
alias sftpgate='sftp miki@gate.tiara.sinica.edu.tw'

#alias pls='python $PLUTO_DIR/setup.py'
alias pls41='python $PLUT041_DIR/setup.py'
alias pls42='python $PLUT042_DIR/setup.py'
alias pls43='python $PLUT043_DIR/setup.py'
alias pls44='python $PLUT044_DIR/setup.py'
alias pls442='python3 $PLUT0442_DIR/setup.py'
alias pls443='python3.12 $PLUT0443_DIR/setup.py'
alias plschombo='python $PLUT044AMR_DIR/setup.py --with-chombo'

alias plutorun2='mpirun -np 2 ./pluto'
alias plutorun4='mpirun -np 4 ./pluto'
alias plutorun6='mpirun -np 6 ./pluto'
alias plutorun8='mpirun -np 8 ./pluto'
alias plutorun24='mpirun -np 24 ./pluto'
alias plutorun42='mpirun -np 42 ./pluto'

alias echopl4='echo "mpirun -np 4 ./pluto" | at now'
alias echopl8='echo "mpirun -np 8 ./pluto" | at now'
alias echopl16='echo "mpirun -np 16 ./pluto" | at now'
alias echopl32='echo "mpirun -np 32 ./pluto" | at now'
```

Hands-on introduction: PLUTO/setup.py

```
I A setup.py (python) import os
import os
import sys
import shutil

try:
    os.environ['PLUTO_DIR']
except KeyError:
    print 'PLUTO_DIR not defined. Setting it to the Current Directory'
    pluto_directory = os.getcwd()
    pass
else:
    pluto_directory = os.environ['PLUTO_DIR']

sys.path.append(pluto_directory + '/Tools/Python/')
import menu
import configure
from make_problem import MakeProblem

def PlutoInterface(pluto_dir, do_auto_update = False):
    work_dir = os.getcwd()
    interface_optval = ''
    interface_opts = ['Setup problem', 'Change makefile',
                     'Auto-update', 'Save Setup', 'Quit']

    if do_auto_update:
        MakeProblem(work_dir, pluto_dir, 1, 1)
```


Hands-on introduction: PLUTO/Config/Linux.mpicc.defs

```
miki@petri: ~/Applics/PLUTO44
IW Config/Linux.mpicc.defs Row 1 Col 1 9:
#####
#
# Configuration file for mpicc (parallel)
#
#####

CC      = mpicc
CFLAGS  = -c -O3 -Wundef
LDFLAGS = -lm

PARALLEL = TRUE
USE_HDF5  = FALSE
USE_PNG   = FALSE

#####
# MPI additional specifications
#####

ifeq ($(strip $(PARALLEL)), TRUE)
endif

#####
# HDF5 library options
#####

ifeq ($(strip $(USE_HDF5)), TRUE)
INCLUDE_DIRS +=/usr/local/lib/HDF5-parallel/include
LDFLAGS +=/usr/local/lib/HDF5-parallel/lib -lz -lm -lhdf5
endif

#####
# PNG library options
#####

** Joe's Own Editor v4.1 ** (utf-8) ** Copyright © 2015 **
```

Test problem: Sod shock tube in 1D

0.2 Running a simple shock-tube problem

PLUTO can be quickly configured to run one of the several test problems provided with the distribution. Assuming that your system satisfies all the requirements described in the next chapter (i.e. C compiler, Python, etc..) you can quickly setup **PLUTO** in the following way:

1. Change directory to any of the test problems under `PLUTO/Test_Problems`, e.g.

```
~> cd $PLUTO_DIR/Test_Problems/HD/Sod
```

2. Copy the header and initialization files from a configuration of our choice (e.g. #01):

```
~/PLUTO/Test_Problems/HD/Sod> cp definitions_01.h definitions.h
~/PLUTO/Test_Problems/HD/Sod> cp pluto_01.ini pluto.ini
```

3. Run the Python script using

```
~/PLUTO/Test_Problems/HD/Sod> python $PLUTO_DIR/setup.py
```

and select “Setup problem” from the main menu, see Fig. [1.2](#) You can choose (by pressing Enter) or modify the default setting using the arrow keys.

4. Once you return to the main menu, select “Change makefile”, choose a suitable makefile (e.g. `Linux.gcc.defs`) and press enter.

All the information relevant to the specific problem should now be stored in the four files `init.c` (assigns initial condition and user-supplied boundary conditions), `pluto.ini` (sets the number of grid zones, Riemann solver, output frequency, etc.), `definitions.h` (specifies the geometry, number of dimensions, reconstruction, time stepping scheme, and so forth) and the makefile.

5. Exit from the main menu (“Quit” or press ‘q’) and type

```
~/PLUTO/Test_Problems/HD/Sod> make
```

to compile the code.

6. You can now run the code by typing

```
~/PLUTO/Test_Problems/HD/Sod> ./pluto
```

At this point, **PLUTO** reads the initialization file `pluto.ini` and starts integrating. The run should take a few seconds (or less) and the integration log should be dumped to screen.

Files for setup and their modifications

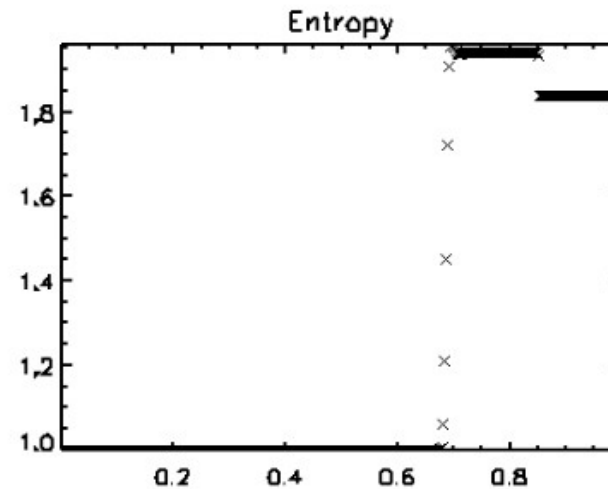
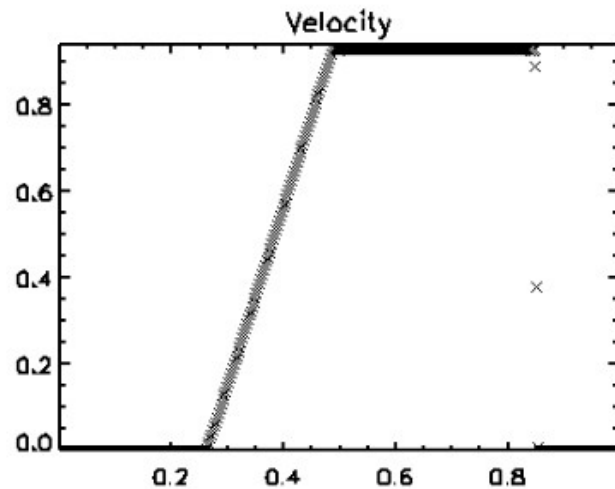
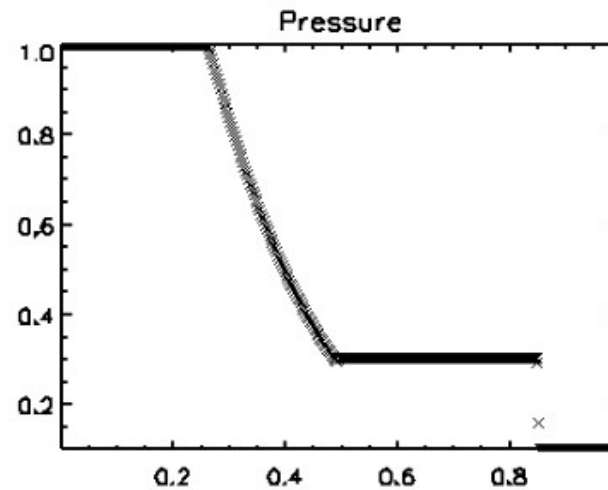
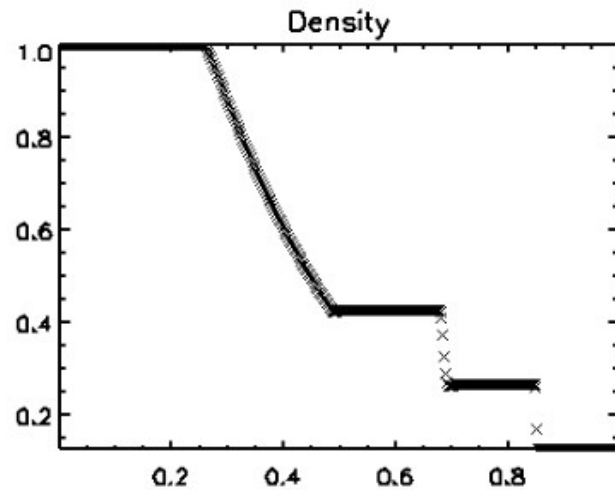
- The PLUTO original source will not be changed, for our simulations we just append to it our version of some files in a pre-compiling step.
- The changed version of a file in the work directory (for which I suggest the name /home/Pluto and plz do it so, that I could easier help you, navigating you to the routines where you should check for errors) has, by default in PLUTO, priority to the original version in PLUTO/Src directory.
- The files to be copied into the work directory from the working version into a new setup are **init.c**, **pluto.ini**, **definitions.h**, (+userdef_output.c, res_eta.c, visc_nu.c for the accretion disk setup).
- The file definitions.h is the only *.h file changed in the work directory. All the other *.h files are to be changed directly in PLUTO/Src directory.
- In the file **pluto.ini** are defined the grid, solvers and run parameters.
- Most of the entries in **definitions.h** are done through the python environment during the setup of the run, but some entries are to be done by hand editing the definitions.h file, prior to compilation.
- In the file **init.c** is defined the physics setup.

Test problem: Sod shock tube in 1D

Detailed Description from **Doxygen file**: The Sod shock tube problem is one of the most used benchmark for shock-capturing schemes. It is a one-dimensional problem with initial condition given by a discontinuity separating two constant states:

$$\begin{aligned} (\rho, v_x, p)_L &= (1, 0, 1) && \text{for } x < 0.5 \\ (\rho, v_x, p)_R &= \left(\frac{1}{8}, 0, \frac{1}{10}\right) && \text{for } x > 0.5 \end{aligned}$$

The evolved structured at $t=0.2$ is shown in the panels below and consists of a left-going rarefaction wave, a right-going contact discontinuity and a right-going shock wave. The results shown here were carried with PARABOLIC interpolation, CHARACTERISIC_TRACING time stepping and the two_shock Riemann solver on 400 zones (**configuration #04**).

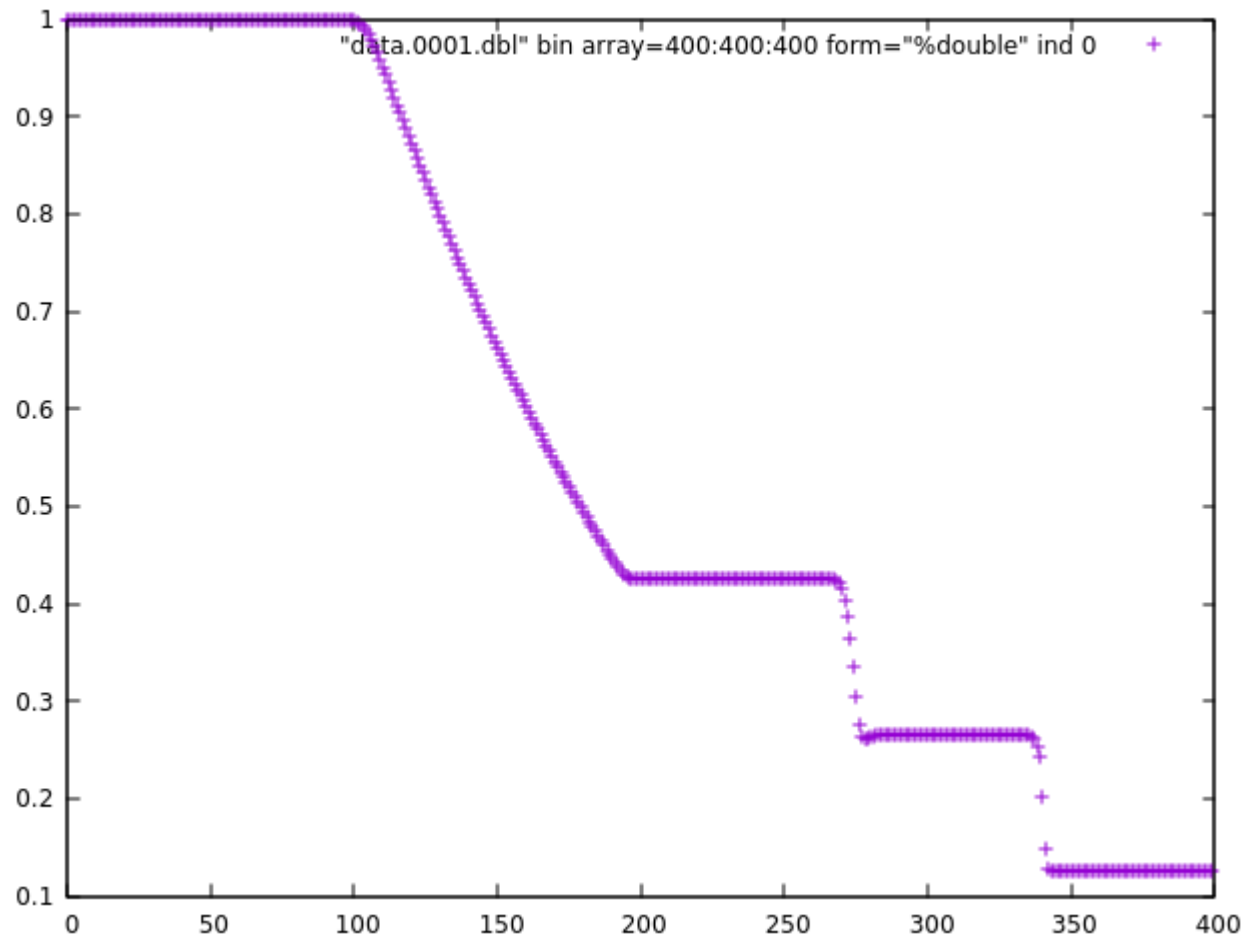


Test problem: Sod shock tube in 1D

Typing in terminal:

```
gnuplot> plot "data.0001.dbl" bin array=400:400:400 form="%double" ind 0
```

You should obtain:



Summary of the Lect. 2

- Energetics of accretion, Eddington limit, spherical (Bondi) accretion
- Thin accretion disc, fluid & (M)HD eqs.
- Viscosity, resistivity, Alfven waves
- Code PLUTO, structure of the code, initial and boundary conditions
- Hands-on installation and testing, visualization with gnuplot,

Outline, Lect.3 : General solutions for thin disk

- Shakura-Sunyaev 1973 disc
- Initial and boundary conditions in PLUTO
- Setup and running of Orszag-Tang problem in 2D and 3D
- Visualization in 2D and 3D with Paraview

General equations

- We will go through (sometimes painful, but nobody said it is to be easy!) detail into the accretion disk equations.
- The obtained solution is still a starting point for explanation of the birth of stars and larger structures.
- Matter which we consider, when undergoing accretion, is gaseous, which means that interaction is by the collisions, not short distance forces. We use, as we did before, λ for the mean free path of the particles, \bar{v} for the mean velocity (velocities are measured in the comoving coordinates, and distributed following a Maxwell-Boltzmann distribution, which is dependent on the temperature, T), ρ for the mass density of gas. When observing the gas at scales $L \gg \lambda$, we can consider it as a continuous fluid, with density, velocity and temperature defined in every point of the flow. The equations to describe such fluid are the equations of conservation of mass, momentum and energy.

- Conservation of mass:
$$\frac{\partial \rho}{\partial t} + \nabla \cdot (\rho \vec{v}) = 0$$

Conservation of momentum follows from the force acting on a fluid element:

$$-\oint_S P d\vec{n} = (\text{Gauss} - \text{Ostrogradski}) = -\int_V \nabla P dV$$

P is pressure, and the direction of ort vector \mathbf{n} is outwards from the volume.

General equations

- Force acting on the unit volume element of the gas is $(-\nabla P)$, and its equation of motion we obtain from the 2nd Newton, multiplying it with the unit volume mass=density ρ and acceleration, so we can write:

$$\rho \frac{d\vec{v}}{dt} = -\nabla P$$

- Acceleration is also with respect to the comoving coordinates, not in the background rest system, so we have two parts in the velocity change in this equation: one is the change of velocity in the given point of space at a time interval dt : $\partial\mathbf{v}/\partial t dt$ and another is the difference in velocities at two points of space, distanced \mathbf{r} , through which the fluid flows during dt , what we can write as $d\mathbf{r}\nabla\mathbf{v}$, so we can write all together:

$$d\vec{v} = \frac{\partial\vec{v}}{\partial t}dt + d\mathbf{r}\nabla \cdot \vec{v} / \frac{1}{dt}$$

$$\frac{d\vec{v}}{dt} = \frac{\partial\vec{v}}{\partial t} + \vec{v}\nabla \cdot \vec{v}$$

- When we insert it to the above equation of motion, we obtain

$$\rho \frac{\partial\vec{v}}{\partial t} + \rho\vec{v}\nabla \cdot \vec{v} = -\nabla P$$

- General equation of motion should add the source term for the external forces acting on the system, we obtain the Euler equation:
- If we insert $\mathbf{f}=\rho\mathbf{g}$ for a gas in gravity field (\mathbf{g} is the gravity acceleration), \mathbf{f} could contain contributions from viscosity, external magnetic field etc.

$$\rho \frac{\partial\vec{v}}{\partial t} + \rho\vec{v}\nabla \cdot \vec{v} = -\nabla P + \vec{f} \quad (\text{E})$$

General equations

- Momentum of the fluid element is $\rho \mathbf{v}$, conservation of the momentum is:

$$\frac{\partial}{\partial t} \rho \vec{v} = 0 = \frac{\partial \rho}{\partial t} \vec{v} + \rho \frac{\partial \vec{v}}{\partial t}$$

- For a stationary flow $\partial \rho / \partial t = 0$, so also the last derivative equals zero, so with E we have:

$$\rho \vec{v} \nabla \cdot \vec{v} + \nabla P - \rho \vec{g} = 0 \quad (\text{A})$$

- From $m \vec{g} = -GmM \vec{r}_0 / r^2$ **is** $\vec{g} = -GM \vec{r}_0 / r^2$.

- For the accretion onto spherical object of mass M, we choose spherical coordinates (r, θ, φ) , radial component of the equation (A) is (G=grav. const)

$$\rho v_r \frac{1}{r^2} \left[\frac{\partial}{\partial r} (r^2 v_r) \right] + \frac{\partial P}{\partial r} + \rho \frac{GM}{r^2} = 0 \quad / \frac{1}{\rho}$$

- where $[\] = 2rv_r + r^2 \partial v_r / \partial r$ so we have

$$\frac{2v_r^2}{r} + v_r \frac{\partial v_r}{\partial r} + \frac{1}{\rho} \frac{\partial P}{\partial r} + \frac{GM}{r^2} = 0 \quad (\text{B})$$

General equations

- From the continuity equation we have, for the stationary case with $\partial P/\partial t=0$ that $\partial\rho/\partial t+\nabla(\rho v_r)=0$. For any vector A radial part is $\nabla \cdot \vec{A} = \frac{1}{r^2} \left[\frac{d}{dr} (r^2 A_r) \right]$, so we have $\rho \frac{1}{r^2} \frac{d}{dr} (r^2 v_r) = 0 / \int$ which means that $r^2 v_r = \text{const}$.

Since $(-\rho v_r)$ is inflow mass flux, this const must be related to mass flux,

- i.e. the accretion rate $\dot{M}=4\pi r\rho(-v_r)$, since $r^2 \cdot (\text{inflow flux}) = \text{const} = \dot{M}/4\pi$, for the whole sphere is $4\pi r^2 \dot{M} \cdot (\text{inflow flux})$.

Now we insert $r^2 v_r = -\dot{M}/4\pi\rho$ into eq.(B) from the previous slide to obtain

$v_r = -\dot{M}/4\pi\rho r^2$, which in the limit $r \rightarrow 0$ gives $v_r = 0$ and for the stationary spherical accretion we stay with

$$v_r \frac{dv_r}{dr} + \frac{1}{\rho} \frac{dP}{dr} + \frac{GM}{r^2} = 0$$

General equations

- Energy conservation:

The gas element energy is a sum of kinetic term $\frac{1}{2}\rho v^2$ (by unit volume) and internal (thermal) energy $\epsilon\rho$ (ϵ is specific energy-by mass unit, dependent on temperature T). From the equipartition of energy we know that each degree of freedom has average energy of $\frac{1}{2}kT$, so for mono-atomic gas we have only 3 translational directions and we can write $\epsilon = \frac{3}{2}kT$.

- Energy conservation equation we write similar to mass conservation, plus adding source terms, depending on physics we include in our model, now instead of ρ we conserve the kinetic and internal energy, and in the spatial derivative we will have work done by the pressure, $P\mathbf{v}$:

$$\frac{\partial}{\partial t}(\frac{1}{2}\rho v^2 + \rho\epsilon) + \nabla \cdot [(\frac{1}{2}\rho v^2 + \rho\epsilon + P)\vec{v}] - \vec{f}\vec{v} = 0 \quad \text{and for a stationary case:}$$

$$\nabla \cdot [(\frac{1}{2}\rho v^2 + \rho\epsilon + P)\vec{v}] = \vec{f}\vec{v}.$$

On the r.h.s. we can add the losses (so, - sign!) by radiation, heat etc. as the source terms inside $-\nabla()$.

Perturbative solutions for the disk

- Now we move to the perturbation method-we will compute the perturbation in relation to the hydrostatic balance. We had

$$\begin{aligned}\nabla \cdot (\rho \vec{v}) &= 0 \\ \rho(\vec{v} \cdot \nabla)\vec{v} &= -\nabla P + \vec{f} \\ \nabla \cdot \left[\left(\frac{1}{2} \rho v^2 + \rho \epsilon + P \right) \vec{v} \right] &= \vec{f} \cdot \vec{v}.\end{aligned}$$

and with $\mathbf{v}=0$ in the hydrostatic case we stay only with

$$\nabla P = \mathbf{f}$$

- For the ideal gas, which we can assume everywhere except degenerate gas in some dense objects or near the centres of the normal stars, we have

$$P = \frac{\rho k T}{\mu m_H}$$

- with $m_H \sim m_{\text{proton}}$ is the hydrogen atom mass, and μ is the average molecular mass in units of m_H , so that for completely ionized hydrogen it is $\mu=0.5$ and for neutral hydrogen $\mu=1$.

Perturbative solutions for the disk

- Now we assume a **small** shift in the density and pressure (ρ' , P') from the initial balance values (ρ_0 , P_0): $\rho = \rho_0 + \rho'$, $P = P_0 + P'$, $\mathbf{v} = \mathbf{v}'$
- Depending on the processes, perturbations can be isothermal or adiabatic.
- For adiabatic changes with $\gamma = 5/3$ and isothermal with $\gamma = 1$ we can write $P/\rho^\gamma = \text{const} = k$, so we can write $P_0 + P' = k(\rho_0 + \rho')^\gamma$ [**set $\gamma = 1.05$ in simuls!**]

- Linearizing the mass continuity eq.:
- with $\nabla(\rho')\mathbf{v} \rightarrow 0$ in the first approx.

$$\begin{aligned} \frac{\partial \rho}{\partial t} + \nabla \cdot (\rho \mathbf{v}) &= \frac{\partial}{\partial t}(\rho_0 + \rho') + \nabla \cdot [(\rho_0 + \rho') \cdot \mathbf{v}'] = \\ &= \frac{\partial \rho'}{\partial t} + \rho_0 \nabla \cdot \mathbf{v}' = 0 \end{aligned}$$

- We do the same with Euler eq. to obtain:

$$\begin{aligned} (\rho_0 + \rho') \frac{\partial \mathbf{v}'}{\partial t} + (\rho_0 + \rho') \mathbf{v}' \cdot \nabla \cdot \mathbf{v}' &= -\nabla(P_0 + P') + \vec{f} \\ \rho_0 \frac{\partial \mathbf{v}'}{\partial t} + \rho_0 \mathbf{v}' \cdot \nabla \cdot \mathbf{v}' &= -\nabla P_0 - \nabla P' + \vec{f} \end{aligned}$$

- Since $\nabla P_0 = \mathbf{f}$, and products of second and higher orders are neglected, we obtain $\rho_0 \partial \mathbf{v}' / \partial t = -\nabla P'$.

- We obtained two eqs.:

$$\frac{\partial \rho'}{\partial t} + \rho_0 \nabla \cdot \mathbf{v}' = 0 \quad (\text{C})$$

$$\frac{\partial \mathbf{v}'}{\partial t} + \frac{1}{\rho_0} \nabla P' = 0$$

Perturbative solutions for the disk

- From $P_0 + P' = k(\rho_0 + \rho')^{\gamma}$ we see that P is a function of ρ only, so that we can write $\nabla P' = (\partial P / \partial \rho)_0 \nabla \rho'$, to the first order, where with a subscript $_0$ we assigned that we evaluate the derivation for the equilibrium state.

- The second of the eqs. (C) we can write now as:

$$\frac{\partial \vec{v}'}{\partial t} + \frac{1}{\rho_0} (\partial P / \partial \rho)_0 \nabla \rho' = 0$$

- We act on it with $\nabla \cdot$:

$$\nabla \cdot \frac{\partial \vec{v}'}{\partial t} + \left[\frac{1}{\rho_0} (\partial P / \partial \rho)_0 \nabla^2 \rho' \right] = 0.$$

- We act on the 1st eq.in (C) with $\partial / \partial t$:

$$\frac{\partial^2 \rho'}{\partial t^2} + (\rho_0 \nabla \cdot \frac{\partial \vec{v}'}{\partial t}) = 0$$

- We subtract the two eqs.to obtain:

$$\frac{\partial^2 \rho'}{\partial t^2} = (\partial P / \partial \rho)_0 \nabla^2 \rho'$$

the wave equation! With \uparrow as the sound speed, c_s^2 , we can write

$$\frac{\partial^2 \rho'}{\partial t^2} = c_s^2 \nabla^2 \rho'$$

Perturbative solutions for the disk

- For P' and \mathbf{v}' we obtain the equivalent equations, so we conclude that small perturbations around the *hydrostatic equilibrium positions spread with the speed of sound*.
- Depending on the kind of perturbation, we have two possibilities,

adiabatic

$$c_s^{ad} = \sqrt{\frac{5P}{3\rho}} = \sqrt{\frac{5kT}{3\mu m_H}} \propto \rho^{\frac{1}{3}}$$

or isothermal:

$$c_s^{izot} = \sqrt{\frac{P}{\rho}} = \sqrt{\frac{kT}{\mu m_H}}$$

Stationary thin disk

- Back in “Viscosity, and back to the disk eqs”, slide 25, we obtained the equation: (G is gravity const. here!)

$$\begin{aligned} \frac{\partial S}{\partial t} &= \frac{1}{R} \frac{\partial}{\partial R} \left\{ \frac{\frac{\partial}{\partial R} [\nu S R^{3\frac{3}{2}} \sqrt{GM} R^{\frac{5}{2}}]}{\frac{1}{2} \sqrt{GM} R^{-\frac{1}{2}}} \right\} = \\ &= \frac{1}{R} \frac{\partial}{\partial R} \left\{ \frac{\frac{\partial}{\partial R} [\nu S^{\frac{3}{2}} \sqrt{GM} R^{\frac{1}{2}}]}{\frac{1}{2} \sqrt{GM} R^{-\frac{1}{2}}} \right\} = \\ &= \frac{3}{R} \frac{\partial}{\partial R} \left[\sqrt{R} \frac{\partial}{\partial R} (\nu S \sqrt{R}) \right] \end{aligned}$$

- To continue, we need the viscosity. That the disk would be “stationary” and that viscosity would work, we need that the mass accretion rate \dot{M} would be slow enough. Then we can set $\partial/\partial t=0$ and from the mass conservation we can write $\dot{M}=2\pi R S (-v_r)$ and from the angular momentum conservation we have $R S v_r R^2 \Omega = (G(R,t) + C)/(2\pi)$, with $C = \text{const.}$ related to the angular momentum rate of the accreted matter. Star must rotate slower than the breakup rotation at the equator, so when approaching closer to the star, there is a region in the disk where the disk corotates with the star. Even closer to the star, our approximation breaks-here starts the discussion and departure from the simple estimates.

Stationary thin disk

- We had $G=G(R,t)$, and with $R\partial\Omega/\partial R=A$ it was $G(R)=2\pi R\nu SAR$, where νSA is a viscous force per unit angle. After integration we have $-\nu S\partial\Omega/\partial R=S(-v_r\Omega)+C/(2\pi R^3)$ (D), where C is a constant.
- Inside a ring at R_A+b , the rotation of the disk approaches Keplerian, reaches $\partial\Omega/\partial R=0$, and increases until it reaches $R\sim R_A$. We can write $\Omega(R_A+b)=\sqrt{\frac{GM}{R_A^3}}[1+\mathcal{O}(\frac{b}{R_A})]$ (**G is gravity constant now!**).
- Closer than R_A The thin disk approx. is not valid anymore. To find C we insert $R=R_A+b$ and evaluate $C=2\pi R_A^3 S v_r \Omega(R_A+b)|_{R_A+b}$ (now $\Omega()$, not multiplying!), which gives, after inserting mass accretion rate \dot{M} and $\Omega(R_A+b)$, $C=-\dot{M}(GM R_A)^{1/2}$ that $\nu S = \frac{\dot{M}}{3\pi} [1 - \sqrt{\frac{R_A}{R}}]$, exact to order $\mathcal{O}(b/R_A)$. We insert it to eq. D to obtain $D(R) = \frac{g}{4\pi} \frac{\partial\Omega}{\partial R} = \frac{1}{2} (\nu S) (R \frac{\partial\Omega}{\partial R})^2$ which is
- Loss of energy because of viscosity is $D(R)=g/(4\pi)\partial\Omega/\partial R$ per unit disk surface. Inserted back to (D) it gives that $D(R)$ is independent of viscosity: $D(R) = \frac{3GM\dot{M}}{8\pi R^3} [1 - \sqrt{\frac{R_A}{R}}]$

Stationary thin disk

- Now we can estimate the luminosity of a disk between R_1 and R_2 (2 is for 2 disk sides):

$$L(R_1, R_2) = 2 \int_{R_1}^{R_2} D(R) 2\pi R dR$$

$$L(R_1, R_2) = \frac{3GM\dot{M}}{2} \int_{R_1}^{R_2} \left[1 - \sqrt{\frac{R_A}{R}} \right] \frac{dR}{R^2}$$

- If we substitute $x=R/R_A$, we obtain
- For $R=R_1$ and $R_2 \rightarrow \infty$ we obtain the complete disk luminosity (**G is gravity const**):

$$L(R_1, R_2) = \frac{3GM\dot{M}}{2} \left\{ \frac{1}{R_1} \left[1 - \frac{2}{3} \sqrt{\frac{R_A}{R_1}} \right] - \frac{1}{R_2} \left[1 - \frac{2}{3} \sqrt{\frac{R_A}{R_2}} \right] \right\}$$

$$L_{\text{disk}} = \frac{GM\dot{M}}{2R_A} = \frac{1}{2} L_{\text{akrecije}}$$

- where we defined

$$L_{\text{akrecije}} = \frac{\Delta E_{\text{akr}}}{\Delta t} = \frac{GM\dot{M}}{R_A}$$

- This means that half of the energy is radiated from the disk, and half is released very close to the central star, which takes the same amount like the whole disk! (which has a much, much larger surface).

Stationary thin disk

- This was for radial direction, is it all consistent with the vertical direction? In the vertical, z direction, there is mainly no flow, we have the hydrostatic equilibrium: $\frac{1}{\rho} \frac{\partial P}{\partial z} = \frac{\partial}{\partial z} \left[\frac{GM}{\sqrt{R^2 + z^2}} \right]$ which we get from the vertical component of

Euler eq. (E), neglecting all the terms with velocities.

For the thin disk $z \ll R$ we have $\frac{1}{\rho} \frac{\partial P}{\partial z} = -\frac{GMz}{R^3}$

- Since $H \ll z$ we can write $\partial P / \partial z \sim P/H$ and $z \sim H$, and condition for a thin disk becomes $H \ll R$. For $P \propto \rho c_s^2$ we have

which means that it has to be

$$H \simeq c_s \sqrt{\frac{R}{GM}} R^2$$

$c_s \ll (GM/R)^{1/2}$; additional condition for a thin disk: local Keplerian speed must be highly supersonic. Only with this satisfied, the approximation of thin disk can be used. - This is a strong condition for the inner workings of a disk, and tells us that the local orbiting speed will be close to the Keplerian speed.

Stationary thin disk

- The radial component of the Euler eq. is:
$$v_r \frac{\partial v_r}{\partial R} - \frac{v_\phi^2}{R} + \frac{1}{\rho} \frac{\partial P}{\partial R} + \frac{GM}{R^2} = 0$$
- If we neglect the pressure term, because of $c_s \ll (GM/R)^{1/2}$, we have $\rho^{-1} \partial P / \partial R \sim c_s^2 / R$ in comparison to a larger gravitational term GM/R^2 , with $\dot{M} = 4\pi r \rho (-v_r)$ and we have
$$\nu S = \frac{\dot{M}}{3\pi} \left[1 - \sqrt{\frac{R_A}{R}} \right]$$
- $$v_r = -\frac{3\nu}{2R} \left(1 - \sqrt{\frac{R_A}{R}} \right)^{-1}$$
- Now we are slowly shifting to the Shakura & Sunyaev (1973) main assumption: for any reasonable viscosity, the radial velocity v_r is highly **subsonic**, while orbital velocity is highly **supersonic** and approximately Keplerian: with $\nu \propto c_s H$ we have $v_r \propto \nu / R \sim c_s H / R \ll c_s$
- NOW WE HAVE ALL THE EQUATIONS FOR THE DISK STRUCTURE.*

Lynden-Bell on steady model disk

Now we are in a better position to discuss the SS73 paper, which is one of the most cited papers on accretion disks (10657 at noon Sunday 27th 02 2022, 12244 on 11.10.2024)

Galactic Nuclei as Collapsed Old Quasars

by

D. LYNDEN-BELL

Royal Greenwich Observatory,
Herstmonceux Castle, Sussex

Powerful emissions from the centres of nearby galaxies may represent dead quasars.

RYLE gives good evidence¹ that quasars evolve into powerful radio sources with two well separated radio components, one on each side of the dead or dying quasar. The energies involved in the total radio outbursts are calculated to be of the order of 10^{61} erg, and the optical variability of some quasars indicates that the outbursts probably originate in a volume no larger than the solar system. Now 10^{61} erg have a mass of 10^{40} g or nearly 10^7 Suns. If this were to come from the conversion of hydrogen into helium, it can only represent the nuclear binding energy, which is $3/400$ of the mass of hydrogen involved. Hence 10^9 solar masses would be needed within a volume the size of the solar system, which we take to be 10^{15} cm (10 light h). But the gravitational binding energy of 10^9 solar masses within 10^{15} cm is GM^2/r which is 10^{62} erg. Thus we are wrong to neglect gravity as an equal if not a dominant source of energy. This was suggested by Fowler and Hoyle², who at once asked whether the red-shifts can also have a gravitational origin. Greenstein and Schmidt³, however, earlier showed that this is unlikely because the differential red-shift would wash out the lines. Attempts to avoid this difficulty have looked unconvincing, so I shall adopt the cosmological origin for quasar red-shifts. Even with this hypothesis the numbers of quasar-like objects are very large, or rather they were so in the past. I shall assume that the quasars were common for an initial epoch lasting 10^9 yr, but that each one only remained bright for 10^6 yr, and take Sandage's estimate (quoted in

which we shall call the Schwarzschild throat. We would be wrong to conclude that such massive objects in space-time should be unobservable, however. It is my thesis that we have been observing them indirectly for many years.

Effects of Collapsed Masses

As Schwarzschild throats are considerable centres of gravitation, we expect to find matter concentrated toward them. We therefore expect that the throats are to be found at the centres of massive aggregates of stars, and the centres of the nuclei of galaxies are the obvious choice. My first prediction is that when the light from the nucleus of a galaxy is predominantly starlight, the mass-to-light ratio of the nucleus should be anomalously large.

We may expect the collapsed bodies to have a broad spectrum of masses. True dead quasars may have 10^{10} or $10^{11} M_{\odot}$ while normal galaxies like ours may have only 10^7 – $10^8 M_{\odot}$ down their throats. A simple calculation shows that the last stable circular orbit has a diameter of $12 GM/c^2 = 12m$ so we shall call the sphere of this diameter the Schwarzschild mouth. Simple calculations on circular orbits yield the following results, where M_* is the mass of the collapsed body in units of $10^7 M_{\odot}$, so that M_* ranges from 1 to 10^4 .

Circular velocity

$$V_c = [GM/(r - 2m)]^{1/2} \text{ where } r > 3m \quad (1)$$

Usually cited before Shakura & Sunyaev disk is Lynden-Bell (1969) discussion of the origin of emission from galactic nuclei—"old quasars", **Schwarzschild mouth** was still the term for the event horizon.

It got a reprint in A&A in 2009, and a review by Andrew King, which best describes its importance and why it was needed – it stems from observational evidence, new X-ray astronomy was pending: The mere requirement that an object should produce X-rays at all was already challenging. It showed unambiguously that the accretion flow must itself be luminous, and so quite different from the cool protosolar disks studied in detail in the past.

In addition, tight constraints on sizes, geometry, and timescales flowed from the identification of many of the early sources as close binaries. This opened the possibility of showing that accretion on to a black hole or a neutron star was the only reasonable way of explaining a mass of data. The challenge for theorists was to supply a robust theory of these accretion flows that was easy to apply to observations.

A&A 500, 53–54 (2009)
DOI: [10.1051/0004-6361/200912147](https://doi.org/10.1051/0004-6361/200912147)
© ESO 2009

**Astronomy
&
Astrophysics**
Special issue

COMMENTARY ON: [SHAKURA N. I. AND SUNYAEV R. A., 1973, A&A, 24, 337](#)

Accretion: the gold mine opens

A. King

Theoretical Astrophysics Group, University of Leicester, Leicester LE1 7RH, UK
e-mail: ark@astro.le.ac.uk

In the early 1970s, Yakov Zeldovich suggested that two young Moscow astronomers, Nikolai Shakura and Rashid Sunyaev, should combine their efforts to understand how accretion could power bright X-ray sources.

The result was a paper now amongst the most cited in all astronomy. Another highly influential paper on accretion disks (Pringle 1981) calls it “seminal”, and so it is. Yet it is not by any means the first paper on disks. The references in the paper make it clear that the authors knew of a large literature on the subject going back to the early 1960s. Indeed Pringle (1981) shows that knowledge of the principles and even the equations of disk theory dates back still earlier (to the 1920s and 1940s, respectively).

The reason for the paper’s vast and deserved success lies partly in its approach to the problem it attacked, and partly in a technical innovation. Shakura and Sunyaev’s title: “Black Holes in Binary Systems. Observational Appearance” makes their aim

momentum and so drives accretion, thus tapping the gravitational energy of infall. There is a direct connection between viscosity and accretion rate, and in a steady disk one can infer the surface dissipation rate purely in terms of the latter. Observations made it clear that none of the obvious candidate mechanisms – certainly not the standard “molecular” viscosity for example – was adequate to drive accretion at the rates required.

Authors therefore resorted to various parametrizations of the unknown process, usually thought of as some kind of turbulent effect. Shakura and Sunyaev adopted the now famous alpha-prescription, in modern notation usually written

$$\nu = \alpha c_s H.$$

Here ν is the kinematic viscosity, c_s the sound speed, and H the local disk scaleheight, i.e. the disk semithickness.

Shakura & Sunyaev viscous alpha disk

- With the thin disk approximation, we can compute the structure of the disk. In practice, we are solving the 1D with only a radial dependence, as we decoupled it from the vertical, z-dependence, which is essentially written as a hydrostatic equilibrium and energy transport.
- In the radial direction, the disk structure enters only in the local energy dissipation rate $D(R)$.
- From the hydrostatic eq. $\frac{1}{\rho} \frac{\partial P}{\partial z} = -\frac{GMz}{R^3}$ for isothermal structure we obtain the solution $\rho(R, z) = \rho_c(R) e^{-\frac{z^2}{2H^2}}$ where ρ_c stands for the density at $z=0$.
- The central density of the disk we can approximate as $\rho = S/H$, $H = \rho c_s / v_\phi$. $c_s^2 = P/\rho$, where P is a sum of gas and radiation pressure $P = \frac{\rho k T_c}{\mu m_p} + \frac{4\sigma}{3c} T_c^4$ with an assumption $T(T, z) \sim T_c(R, 0)$. The central temperature T_c is determined by the relation between the vertical energy flux and the energy dissipation because of viscosity.
- Locally, using the thin disk approximation, we now have the vertical temperature gradient, so that for $z = \text{const}$ surface we have radiated energy flux (κ_R is the Rosseland mean opacity):
$$F(z) = -\frac{16\sigma T^3}{3\kappa_R \rho} \frac{\partial T}{\partial z}$$

Shakura & Sunyaev viscous alpha disk

- We assumed the optically thick disk: $\tau = \rho H \kappa_R = S \kappa_R \gg 1$, so that the radiation is locally very close to the black body radiation. In the case with $\tau \leq 1$ radiation could directly exit the disk, and the equation for $F(z)$ from the bottom of previous slide would not be valid any more.
- For the energetic balance must be $F(H) - F(0) = D(R)$, so that $F(z) \sim \frac{4\sigma}{3\tau} T^4(z)$ which, with $T_c^4 \gg T^4(H)$ gives $\frac{4\sigma}{3\tau} T_c^4 = D(R)$.
- For the full set of eqs. we need the $\kappa_R = \kappa_R(\rho, T_c)$ relation, and expression for ν and its relation to S and \dot{M} . This all amounts to 8 equations for **$\rho, S, H, T_c, c_s, P, \tau, \nu$** in dependence of R, M and \dot{M} , with some parameter in the viscosity, which are describing the thin disk model:

$$\begin{aligned}
 (1) \quad \rho &= \frac{S}{H} \\
 (2) \quad H &= \frac{c_s R^{3/2}}{\sqrt{GM}} \\
 (3) \quad c_s^2 &= \frac{P}{\rho} \\
 (4) \quad P &= \frac{\rho k T_c}{\mu m_p} + \frac{4\sigma}{3c} T_c^4
 \end{aligned}$$

$$\begin{aligned}
 (5) \quad \frac{4\sigma T_c^4}{3\tau} &= \frac{3GM\dot{M}}{8\pi R^3} \left[1 - \sqrt{\frac{R_A}{R}}\right] \\
 (6) \quad \tau &= S \kappa_R(\rho, T_c) = \tau(S, \rho, T_c) \\
 (7) \quad \nu S &= \frac{\dot{M}}{3\pi} \left[1 - \sqrt{\frac{R_A}{R}}\right] \\
 (8) \quad \nu &= \nu(\rho, T_c, S, \alpha, \dots)
 \end{aligned}$$

Shakura & Sunyaev viscous alpha disk

- With “alpha viscosity” parameterization $\nu = \alpha c_s H$ Shakura & Sunyaev ('73) gave the first solution. They used the Kramers' law ($6.6 \cdot 10^{22}$ wrongly sometimes!!) $\kappa_R = 5 \cdot 10^{24} \rho T_c^{-7/2} \text{cm}^2/\text{g}$ and neglected the radiation pressure in eq.(4). Now the system of 8 eqs. can be solved. I give steps (from “Accretion power...”):
- First we simplify $f^4 = 1 - (R_A/R)^{1/2}$ and write whole r.h.s. of eq.5 as equal to D. Now with eq.6, κ_R and eq.2 we can write eq.5 as

$$4\sigma T^4 / (3\tau) = D = 4\sigma T^{15/2} / (3 \cdot 5 \cdot 10^{24} \rho S) = [\rho = S/H] = 4\sigma H T^{15/2} / (15 \cdot 10^{24} S^2) =$$

$$= \{ H = c_s R^{3/2} / (GM)^{1/2} \text{ and from eqs. 3 and 4 (without rad pressure term) write}$$

$$H = R^{3/2} T^{1/2} [k_B / (GM \mu m_p)]^{1/2} \} = 4\sigma R^{3/2} T^8 [k_B / (GM \mu m_p)]^{1/2} / (15 \cdot 10^{24} S^2),$$
 and from that obtain $T^8 = 15 \cdot 10^{24} S^2 D [k_B / (GM \mu m_p)]^{1/2} / (4\sigma R^{3/2})$. We insert D back as the r.h.s of eq.5 and use eqs.7 and 8 (where finally $\nu = \alpha c_s H$ comes into game), to write the solution-I give the detailed derivation of solutions on the next slide, this is usually not shown in literature so I leave for you to type it down in Latex; then we can write v_r

Shakura & Sunyaev viscous alpha disk

5) with 6, $\alpha_R = 5 \cdot 10^{-4} \rho T^{-7/2}$ and 2) give

$$\frac{40 T^4}{3 \cdot 5 \cdot 10^4 \rho T^{-7/2}} = \frac{36 M \dot{M}}{8 \pi R^3} \left(1 - \sqrt{\frac{R_A}{R}}\right)$$

$$\frac{S}{H} = \frac{S}{c_s} \sqrt{\frac{GM}{R^3}} = S \sqrt{\frac{GM}{R^3} \frac{M M_H}{k T}}$$

$$\frac{40 T^4}{3 \cdot 5 \cdot 10^4 S \sqrt{\frac{GM}{R^3} \frac{M M_H}{k T}} T^{-7/2}} = \frac{36 M \dot{M}}{8 \pi R^3} \left(1 - \sqrt{\frac{R_A}{R}}\right)$$

$$T^8 = \frac{45 \cdot 10^4}{32 \pi \sigma} S^2 \left(\frac{GM}{R^3}\right)^{3/2} \dot{M} \sqrt{\frac{M M_H}{k}} \left(1 - \sqrt{\frac{R_A}{R}}\right)$$

8) in 7) $\alpha c_s H S = \frac{\dot{M}}{3\pi} \left(1 - \sqrt{\frac{R_A}{R}}\right)$, since $\alpha c_s^2 S = \frac{\dot{M}}{3\pi} \left(1 - \sqrt{\frac{R_A}{R}}\right)$

and $c_s^2 = \frac{p}{\rho} = \frac{kT}{M M_H}$, give $\alpha \frac{kT}{M M_H} \frac{S}{\sqrt{\frac{GM}{R^3}}} = \frac{\dot{M}}{3\pi} \left(1 - \sqrt{\frac{R_A}{R}}\right)$

Now we put it into T8:

$$\left[\frac{M M_H}{k S \alpha} \frac{\dot{M}}{3\pi} \left(1 - \sqrt{\frac{R_A}{R}}\right) \right]^8 = \frac{45 \cdot 10^4}{32 \pi \sigma} S^2 \left(\frac{GM}{R^3}\right)^{3/2} \dot{M} \sqrt{\frac{M M_H}{k}} \left(1 - \sqrt{\frac{R_A}{R}}\right)$$

$$S^{10} \left(\frac{M M_H}{k}\right)^{15/2} \frac{\dot{M}^7 32 \pi \sigma}{45 \cdot 10^4} \frac{1}{(3\pi \alpha)^8} \left(1 - \sqrt{\frac{R_A}{R}}\right)^{-7} \left(\frac{R^3}{GM}\right)^{3/2}$$

$$S = \left(\frac{M M_H}{k}\right)^{3/4} \left(\frac{32 \pi \sigma}{45 \cdot 10^4}\right)^{1/10} \frac{\alpha^{-7/10} \dot{M}^{7/10}}{(3\pi)^{7/5}} \left(\frac{GM}{R^3}\right)^{-3/20} \left(1 - \sqrt{\frac{R_A}{R}}\right)^{7/10}$$

$$H = c_s \sqrt{\frac{R^3}{GM}} = \sqrt{\frac{p}{\rho} \frac{R^3}{GM}} = \sqrt{\frac{kT}{M M_H} \frac{R^3}{GM}}$$

$$H^6 = \left(\frac{k}{M M_H} \frac{R^3}{GM}\right)^3 T^3 = \left(\frac{k}{M M_H} \frac{R^3}{GM}\right)^3 \frac{45 \cdot 10^4}{32 \pi \sigma} S^2 \left(\frac{GM}{R^3}\right)^{3/2} \dot{M} \sqrt{\frac{M M_H}{k}} \left(1 - \sqrt{\frac{R_A}{R}}\right)^8$$

$$H^8 = \left(\frac{k}{M M_H} \frac{R^3}{GM}\right)^4 \left(\frac{45 \cdot 10^4}{32 \pi \sigma}\right)^{4/3} \left(\frac{GM}{R^3}\right)^{2} \dot{M}^{4/3} \left(\frac{M M_H}{k}\right)^{1/3} \left(1 - \sqrt{\frac{R_A}{R}}\right)^{8/3}$$

$$= \left(\frac{k}{M M_H}\right)^{17/3} \left(\frac{R^3}{GM}\right)^{16/3} \dot{M}^{4/3} \left(\frac{45 \cdot 10^4}{32 \pi \sigma}\right)^{4/3} \left(\frac{GM}{R^3}\right)^2 \left(1 - \sqrt{\frac{R_A}{R}}\right)^{8/3}$$

$$= \left(\frac{k}{M M_H}\right)^{17/3} \left(\frac{R^3}{GM}\right)^{10/3} \dot{M}^{4/3} \left(\frac{45 \cdot 10^4}{32 \pi \sigma}\right)^{4/3} \left(\frac{GM}{R^3}\right)^{2/3} \left(1 - \sqrt{\frac{R_A}{R}}\right)^{8/3}$$

$$= \left(\frac{k}{M M_H}\right)^{17/3} \left(\frac{R^3}{GM}\right)^{31/10} \dot{M}^{4/3} \left(\frac{32 \pi \sigma}{45 \cdot 10^4}\right)^{4/3} \left(1 - \sqrt{\frac{R_A}{R}}\right)^{6/5} \frac{\alpha^{-4/5}}{(3\pi)^{4/5}} \sqrt{\frac{M M_H}{k}}$$

$$H = \left(\frac{k}{M M_H}\right)^{3/10} \left(\frac{R^3}{GM}\right)^{31/20} \dot{M}^{2/3} \left(\frac{32 \pi \sigma}{45 \cdot 10^4}\right)^{2/3} \left(1 - \sqrt{\frac{R_A}{R}}\right)^{3/10} \frac{\alpha^{-2/5}}{(3\pi)^{2/5}}$$

$$\rho = \frac{S}{H} = \frac{\left(\frac{M M_H}{k}\right)^{3/4} \left(\frac{32 \pi \sigma}{45 \cdot 10^4}\right)^{1/10} \dot{M}^{7/10} \alpha^{-7/10} \left(\frac{GM}{R^3}\right)^{-3/20} \left(1 - \sqrt{\frac{R_A}{R}}\right)^{7/10}}{\left(\frac{k}{M M_H}\right)^{3/10} \left(\frac{R^3}{GM}\right)^{31/20} \dot{M}^{2/3} \left(\frac{32 \pi \sigma}{45 \cdot 10^4}\right)^{2/3} \left(1 - \sqrt{\frac{R_A}{R}}\right)^{3/10} \frac{\alpha^{-2/5}}{(3\pi)^{2/5}}}$$

$$= \left(\frac{M M_H}{k}\right)^{3/8} \left(\frac{32 \pi \sigma}{45 \cdot 10^4}\right)^{1/20} \dot{M}^{1/10} \frac{\alpha^{-1/10}}{(3\pi)^{1/10}} \left(\frac{GM}{R^3}\right)^{-1/20} \left(1 - \sqrt{\frac{R_A}{R}}\right)^{2/10}$$

$$T = \left(\frac{45 \cdot 10^4}{32 \pi \sigma}\right)^{1/8} S^{1/4} \left(\frac{GM}{R^3}\right)^{3/8} \dot{M}^{1/8} \left(\frac{M M_H}{k}\right)^{1/8} \left(1 - \sqrt{\frac{R_A}{R}}\right)^{1/8} =$$

$$= \left(\frac{45 \cdot 10^4}{32 \pi \sigma}\right)^{1/8} \left(\frac{GM}{R^3}\right)^{3/8} \dot{M}^{1/8} \left(\frac{M M_H}{k}\right)^{1/8} \left(1 - \sqrt{\frac{R_A}{R}}\right)^{1/8}$$

$$\cdot \left(\frac{M M_H}{k}\right)^{3/8} \left(\frac{32 \pi \sigma}{45 \cdot 10^4}\right)^{1/8} \frac{\alpha^{-3/8}}{(3\pi)^{1/8}} \left(\frac{GM}{R^3}\right)^{-3/8} \left(1 - \sqrt{\frac{R_A}{R}}\right)^{7/8} \dot{M}^{7/8} =$$

$$= \left(\frac{45 \cdot 10^4}{32 \pi \sigma}\right)^{1/10} \left(\frac{GM}{R^3}\right)^{3/10} \left(\frac{M M_H}{k}\right)^{1/2} \dot{M}^{3/10} \frac{\alpha^{-1/5}}{(3\pi)^{1/5}} \left(1 - \sqrt{\frac{R_A}{R}}\right)^{3/10}$$

$$\tau = 5 \cdot 10^4 S \rho T^{-7/2} = 5 \cdot 10^4 \left(\frac{M M_H}{k}\right)^{3/4} \left(\frac{32 \pi \sigma}{45 \cdot 10^4}\right)^{1/10} \dot{M}^{7/10} \alpha^{-7/10} \left(\frac{GM}{R^3}\right)^{-3/20} \left(1 - \sqrt{\frac{R_A}{R}}\right)^{7/10}$$

$$\nu = \alpha c_s H = \alpha H^2 \sqrt{\frac{GM}{R^3}} = \frac{\alpha^{1/2} (GM)^{-1/40} \left(\frac{k}{M M_H}\right)^{3/4} \dot{M}^{3/10} \left(\frac{32 \pi \sigma}{45 \cdot 10^4}\right)^{1/10} \left(1 - \sqrt{\frac{R_A}{R}}\right)^{3/10}}{(3\pi)^{1/5} R^2}$$

$$\nu_R = -\frac{3\nu}{2R} \left(1 - \sqrt{\frac{R_A}{R}}\right)^{-1} = -\frac{3}{2R} \frac{\alpha^{1/2}}{(3\pi)^{1/5}} \left(\frac{GM}{R^3}\right)^{-1/40} \left(\frac{k}{M M_H}\right)^{3/4} \dot{M}^{3/10} \left(\frac{32 \pi \sigma}{45 \cdot 10^4}\right)^{1/10} \left(1 - \sqrt{\frac{R_A}{R}}\right)^{-7/10}$$

Shakura & Sunyaev viscous alpha disk

We usually find in the literature:

$$R_{10} = R/(10^{10} \text{ cm}), M_1 = M/M_\odot \text{ i } \dot{M}_{16} = \dot{M}/(10^{16} \text{ g s}^{-1}), \mu = 0.615, f = [1 - (R_A/R)^{0.5}]^{1/4};$$

$$S = 5.2 \alpha^{-4/5} \dot{M}_{16}^{7/10} M_1^{1/4} R_{10}^{-3/4} f^{11/5} \text{ g cm}^{-2},$$

$$H = 1.7 \cdot 10^8 \alpha^{-1/10} \dot{M}_{16}^{3/20} M_1^{-3/8} R_{10}^{9/8} f^{3/5} \text{ cm},$$

$$\rho = 3.1 \cdot 10^{-8} \alpha^{-7/10} \dot{M}_{16}^{11/20} M_1^{5/8} R_{10}^{-15/8} f^{11/5} \text{ g cm}^{-3}$$

$$T_c = 1.4 \cdot 10^4 \alpha^{-1/5} \dot{M}_{16}^{3/10} M_1^{1/4} R_{10}^{-3/4} f^{6/5} \text{ K} \quad (3.39)$$

$$\tau = 190 \alpha^{-4/5} \dot{M}_{16}^{1/5} f^{4/5},$$

$$\nu = 1.8 \cdot 10^{14} \alpha^{4/5} \dot{M}_{16}^{3/10} M_1^{-1/4} R_{10}^{3/4} f^{6/5} \text{ cm}^2 \text{ s}^{-1},$$

$$v_\tau = 2.7 \cdot 10^4 \alpha^{4/5} \dot{M}_{16}^{3/10} M_1^{-1/4} R_{10}^{-1/4} f^{-14/5} \text{ cm s}^{-1}.$$

- It is important that α is nowhere coming with large power, so that any error because of our not knowing it, is less.

Shakura & Sunyaev viscous alpha disk

- The Kramers' law for κ_R is critical, because when it is not holding any more, our approximation breaks down, but until it holds, disk can extend far in R, of the order of Roche boundary for a more massive star.

- Mass in the disk is $M_{disk} = 2\pi \int_{R_A}^{R_{vanjski}} S R dR \lesssim (10^{-10} M_\odot) \alpha^{-4/5} \dot{M}_{16}^{7/10}$, which is even in the

very large disks negligible in comparison with the central object. This justifies the neglect of self-gravity of a disk, which is valid until $\rho \ll M/R^3$. Only for a very small α , of the order of 10^{-10} , this would not be fulfilled.

- The disk thickness in z-direction means that each element of the disc surface radiates as a blackbody with a temperature T (R) given by equating the dissipation rate D(R) per unit face area to the blackbody flux: $\sigma T^4 = D(R)$

- If we insert D from the bottom of slide 47:
- For $R \gg R_*$,

$$T(R) = \left\{ \frac{3GM\dot{M}}{8\pi R^3 \sigma} \left[1 - \left(\frac{R_*}{R} \right)^{1/2} \right] \right\}^{1/4}$$

$$T = T_* (R/R_*)^{-3/4}$$

where

$$\left. \begin{aligned} T_* &= \left(\frac{3GM\dot{M}}{8\pi R_*^3 \sigma} \right)^{1/4} \\ &= 4.1 \times 10^4 \dot{M}_{16}^{1/4} m_1^{1/4} R_9^{-3/4} \text{ K} \\ &= 1.3 \times 10^7 \dot{M}_{17}^{1/4} m_1^{1/4} R_6^{-3/4} \text{ K.} \end{aligned} \right\}$$

$\dot{M}_{16} = \dot{M} / 10^{16} \text{ g s}^{-1}$, $m_1 = M/M_\odot$, $R_9 = R_*/10^9 \text{ cm}$ etc. for disk around WD (R_9) & NS (R_6). **Note $R_A = R_*$ now!**

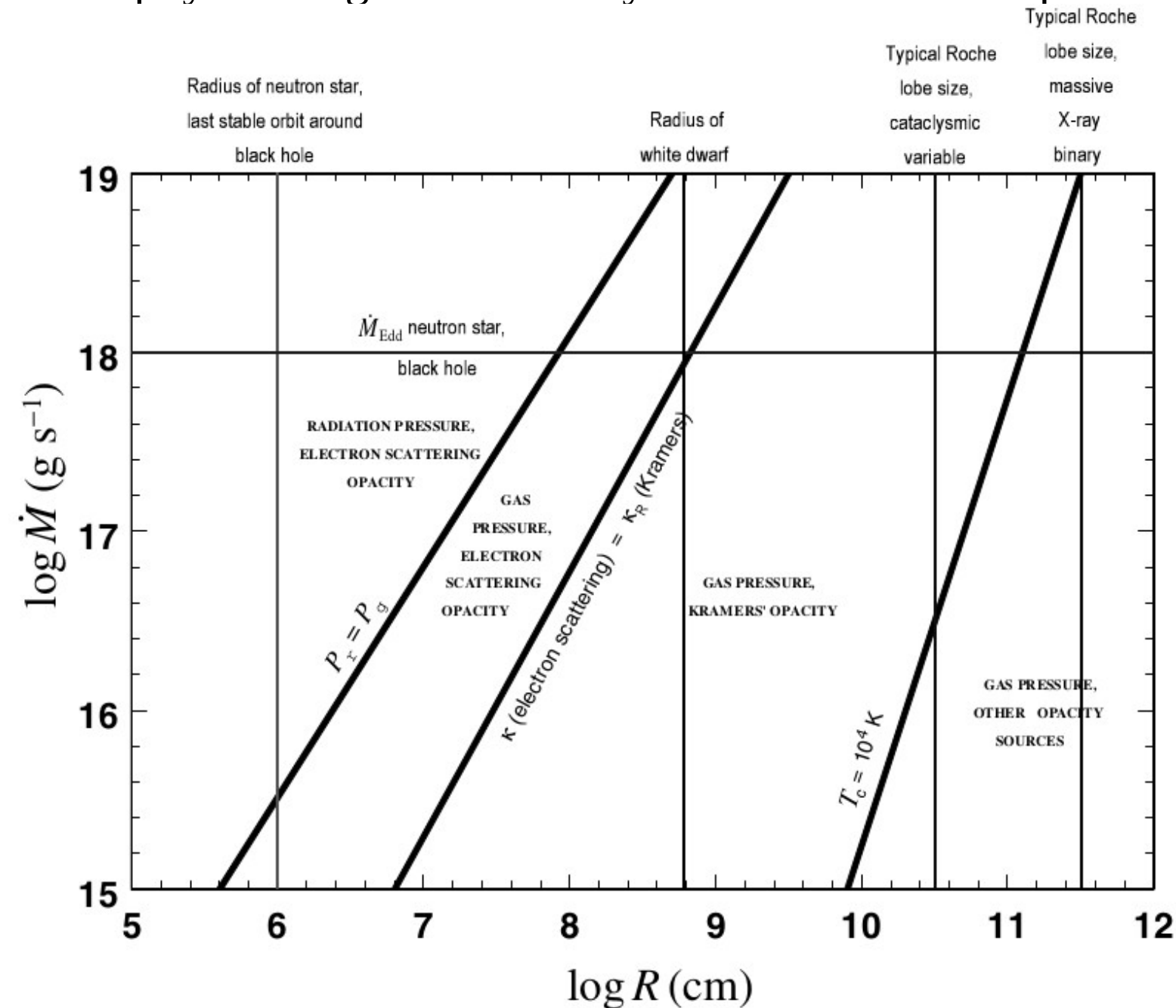
Shakura & Sunyaev viscous alpha disk

- The low power of α in the equations is good for usefulness of α as a parameter, but it also means we cannot expect to learn the typical size of α by direct comparison of steady-state disc theory with observations. This is something what is troubling disk astrophysics until today. No free lunch!
- A good thing is that for $\alpha \leq 1$ we obtained believable solutions, which are not too much off the models from observational data.

Where we expect the assumptions (Kramers' opacity and the neglect of radiation pressure) to break down? We had $\kappa_R = \tau/S = 36 \dot{M}_{16}^{-1/2} m_1^{1/4} R_{10}^{3/4} f^{-2}$ independent of α . We compare with other opacity sources-the major competitive opacity is electron scattering where $\kappa_R = \sigma_T/m_p \sim 0.4 \text{ cm}^2/\text{g}$ with Kramers' opacity dominating for $R > 2.5 \times 10^7 \dot{M}_{16}^{2/3} m_1^{1/3} f^{8/3} \text{ cm}$. This is smaller than the radius of a white dwarf for any reasonable \dot{M} , so for the accretion discs in cataclysmic variables we expect Kramers' opacity to dominate in most of the disc.

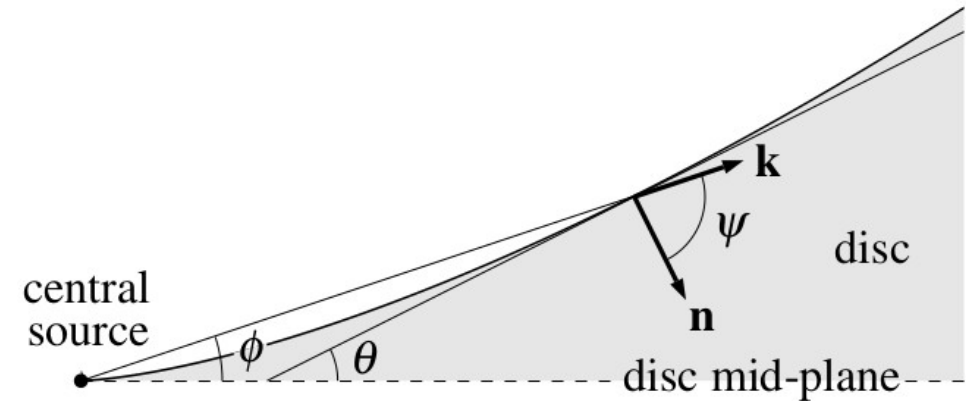
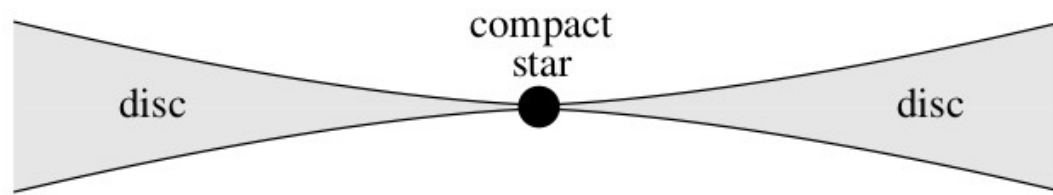
Shakura & Sunyaev viscous alpha disk

- In reasonable range we can rely on the results shown in the figure below for the physical regimes in steady α -discs around compact objects:



SS73 concave disc

- If the disk is concave, then the central, hot regions, could irradiate the more distant, colder parts of the disk with hard radiation, and the picture complicates-this would show in observations.



\mathbf{k} indicates the direction of propagation of the radiation incident on the disc and \mathbf{n} is the local inward-directed normal vector.

- In low-mass X-ray binaries the disk is probably heated by irradiation by the central accretion source. If the accretor is a luminous star, we can have a similar effect.
- If the central source can be regarded as a point, its total radiative flux at disc radius R is $L_{\text{pt}}/(4\pi R^2)$, source with L_{pt} total luminosity. The flux crossing the disc surface at this point is $F = \frac{L_{\text{pt}}}{4\pi R^2} (1 - \beta) \cos \psi$
 β is the albedo, the effective fraction of incident radiation scattered from the surface without absorption, and ψ is the angle between the local inward-directed disc normal and the direction of the incident radiation.

We can write:

$$\psi = \frac{\pi}{2} - \theta + \phi,$$

where

$$\tan \theta = \frac{dH}{dR},$$

and

$$\tan \phi = \frac{H}{R},$$

SS73 concave disc

- Since dH/dR , H/R are both $\ll 1$ for a thin disc

$$\cos \psi = \sin(\theta - \phi) = \cos \theta \cos \phi [\tan \theta - \tan \phi] \simeq \frac{dH}{dR} - \frac{H}{R}$$

- With effective temperature T_{pt} resulting from irradiation by the point source and F from the previous slide,

$$T_{\text{pt}}^4 = \frac{L_{\text{pt}}}{4\pi R^2 \sigma} \left(\frac{H}{R} \right) \left[\frac{d \ln H}{d \ln R} - 1 \right] (1 - \beta),$$

or

$$\left(\frac{T_{\text{pt}}}{T_e} \right)^4 = \frac{H}{R} \left(\frac{R_*}{R} \right)^2 \left[\frac{d \ln H}{d \ln R} - 1 \right] (1 - \beta)$$

T_e is the effective temperature of the central source, defined by $L_{\text{pt}} = 4\pi R_*^2 \sigma T_e^4$,

with the characteristic source dimension R_* . With H varying as $R^{9/8}$, for the non-irradiated disk in the solutions for the disk, in a disc deriving **all** its luminosity from irradiation by a point source, one can show that $H \propto R^{9/7}$, and the factor in square brackets in solution lies between $1/8$ and $2/7$, which we name g , (to add another g). The ratio H/R is roughly constant in a disc, so T_{pt} falls off as $R^{-1/2}$. For a large enough disc T_{pt} dominates the disk effective temperature, which goes as $R^{-3/4}$. We obtain:

- If the central luminosity L_{pt} results from accretion, as in low-mass X-ray binaries, we have $L_{\text{pt}} = GM \dot{M} / R_*$ where $R_* = 10$ km for a neutron star, and a similar value for a black hole. Then
$$\left(\frac{T_{\text{pt}}}{T_{\text{eff}}} \right)^4 = \frac{2}{3} \frac{R L_{\text{pt}}}{GM \dot{M}} \frac{H}{R} g (1 - \beta).$$

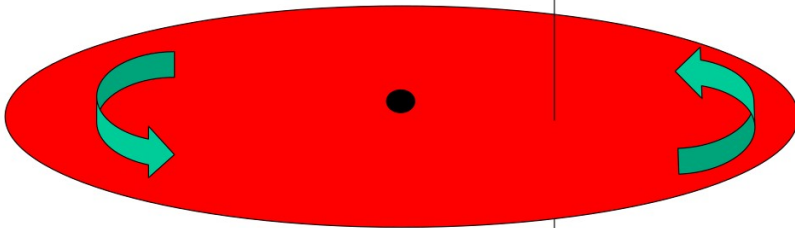
- This means that even if the combination $(H/R)g(1 - \beta)$ can be $< 10^{-3}$, the central source will dominate for a disc with a large enough ratio R/R_* . In low-mass X-ray binaries $R \sim 10^6$ cm and outer disk radius is $\sim 10^{10}$ cm, so $R/R_* \sim 10^4$ and there will be a large range of surface temperatures in the disk.

Working of MRI in a disk

- Alpha viscosity does not give us predictive power.
- Since $\partial/\partial R(R^2\Omega)=0$ [Rayleigh criterion, stability against axisymmetric perturbations] and $\partial\Omega/\partial R < 0$. Most potential mechanisms are sensitive to the angular momentum gradient, so they work in such a way that they are bringing angular momentum INWARDS. We need a mechanism sensitive to Ω .
- If not alpha viscosity, then what? Currently Balbus-Hawley (magnetorotational, MRI) instability (1992), how it works?

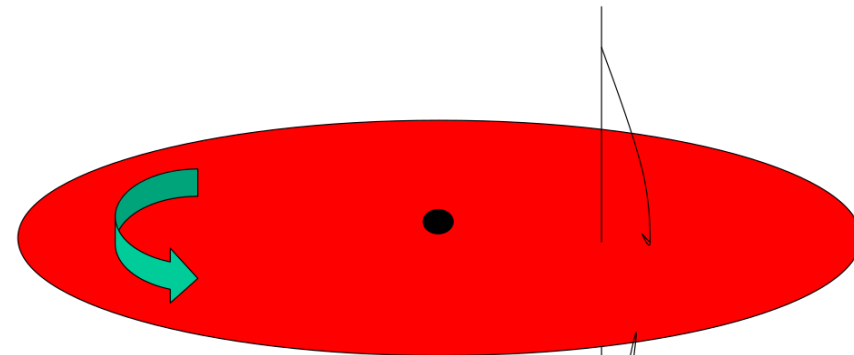
If we imagine a straight magnetic field B line threading a rotating disc, magnetic tension tries to straighten line, there is imbalance between gravity and rotation which bends the line (**figures in this and next 2 slides are from A. King's lecture I found online**).

magnetic field B threading disc →



magnetic tension tries to *straighten* line
imbalance between gravity and rotation *bends* line

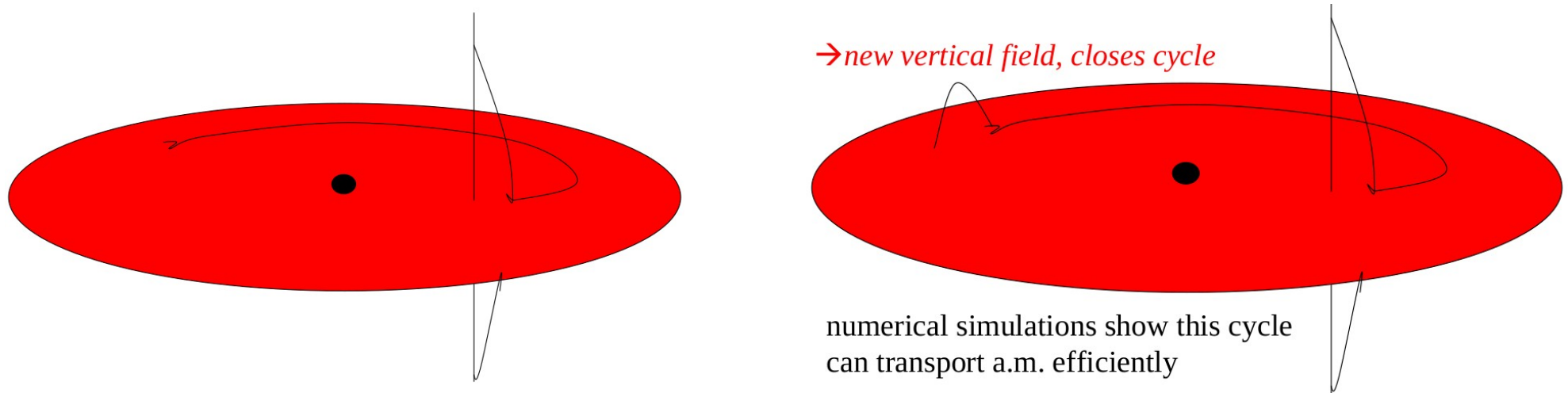
Vertical fieldline perturbed outwards, rotates faster than surroundings, so centrifugal force > gravity → *kink increases*
Line connects fast-moving (inner) matter with slower (outer) matter, and speeds latter up: *outward a.m. transport*



if field too strong instability suppressed
(shortest growing mode has $\lambda > H$)

Working of MRI in a disk

- Vertical fieldline perturbed outwards, rotates faster than surroundings, so centrifugal force $>$ gravity, so that kink increases. Line connects fast-moving (inner) matter with slower (outer) matter, and speeds latter up: outwards a.m. transport!

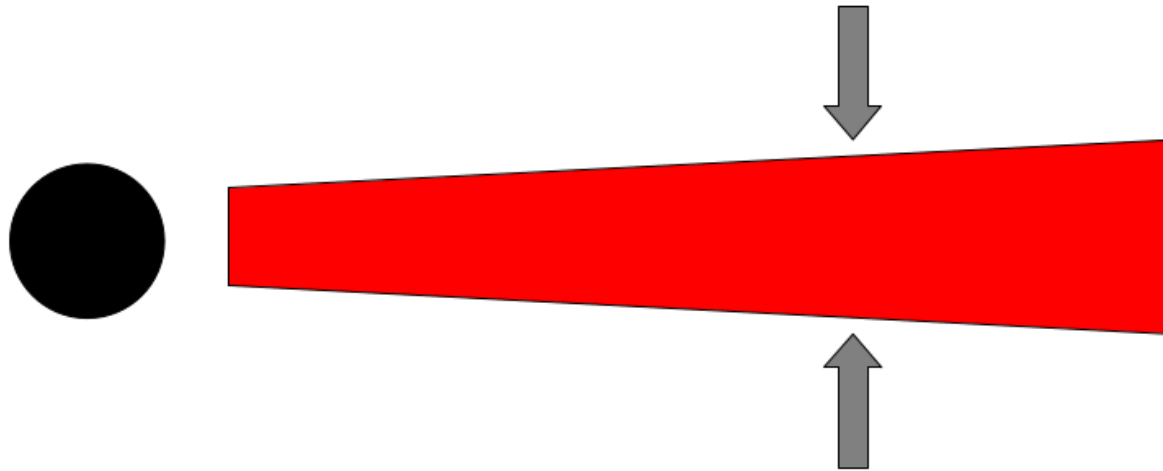


- For a too large mag. field, instability is suppressed. Distorted fieldline stretched azimuthally by differential rotation, strength grows, pressure balance between flux tube and surroundings requires $B^2/8\pi + P_{\text{gas,in}} = P_{\text{gas,out}}$, so that gas pressure (and density) are lower inside tube; buoyant (Parker) instability works, and Flux tube rises above the disk, creating another vertical field, which closes the cycle, which can transport the angular momentum – this was shown to work in numerical simulations.

Self-gravity of disk

- Another effect which will change the picture is when the disk becomes larger:

main difference: *size of AGN disc set by self-gravity*



vertical component of gravity from central mass is $\sim GMH / R^3$

cf that from self-gravity of disc $\sim G\rho H^3 / H^2 \sim G\rho H$

Thus self-gravity takes over where $\rho \sim M / R^3$, or

$$M_{disc} \sim R^2 H \rho \sim \frac{H}{R} M$$

disc breaks up into stars outside this

2D test problem: Orszag-Tang

0.3 Running the Orszag-Tang MHD vortex test

1. Change directory to PLUTO/Test_Problems/MHD/Orszag_Tang.
2. Choose a configuration (e.g. #02) and copy the corresponding configuration files, i.e.,

```
~/PLUTO/Test_Problems/MHD/Orszag_Tang> cp definitions_02.h definitions.h
~/PLUTO/Test_Problems/MHD/Orszag_Tang> cp pluto_02.ini pluto.ini
```

3. Run the Python script:

```
~/PLUTO/Test_Problems/MHD/Orszag_Tang> python $PLUTO_DIR/setup.py
```

select "Setup problem" and choose the default setting by pressing enter;

4. Once you return to the main menu, select "Change makefile" and choose a suitable makefile (e.g. Linux.gcc.defs) and press enter.
5. Exit from the main menu ("Quit" or press 'q'). Edit pluto.ini and, under the *[Grid]* block, lower the resolution from 512 to 200 in both directions (X1-grid and X2-grid). Change *single_file*, in the "dbl" output under the *[Static Grid Output]* block, to *multiple_files*. Finally, edit *definitions.h* and change *PRINT_TO_FILE* from *YES* to *NO*.

6. Compile the code:

```
~/PLUTO/Test_Problems/MHD/Orszag_Tang> make
```

7. If compilation was successful, you can now run the code by typing

```
~/PLUTO/Test_Problems/MHD/Orszag_Tang> ./pluto
```

At this point, **PLUTO** reads the initialization file *pluto.ini* and starts integrating. The run should take a few minutes (depending on the machine you're running on) and the integration log should be dumped to screen.

Orszag-Tang I.C. & B.C.

For each simulation we need to define **initial** and **boundary** conditions.

I introduce some numerical simulations terminology here in **bold**:

We set velocity and magnetic field in a 2D Cartesian coordinates, in a **computational box** with $(x,y,0)=(256 \times 256 \times 0)$ grid cells and a **physical domain** $x,y=[0,2\pi]$

Velocity components: $v = (-\sin y, \sin x, 0)$

Magnetic field: $B = (-\sin y, \sin 2x, 0)$

Density: $\rho = 25/9$

Pressure: $p = 5/3$

Orszag-Tang I.C. & B.C.

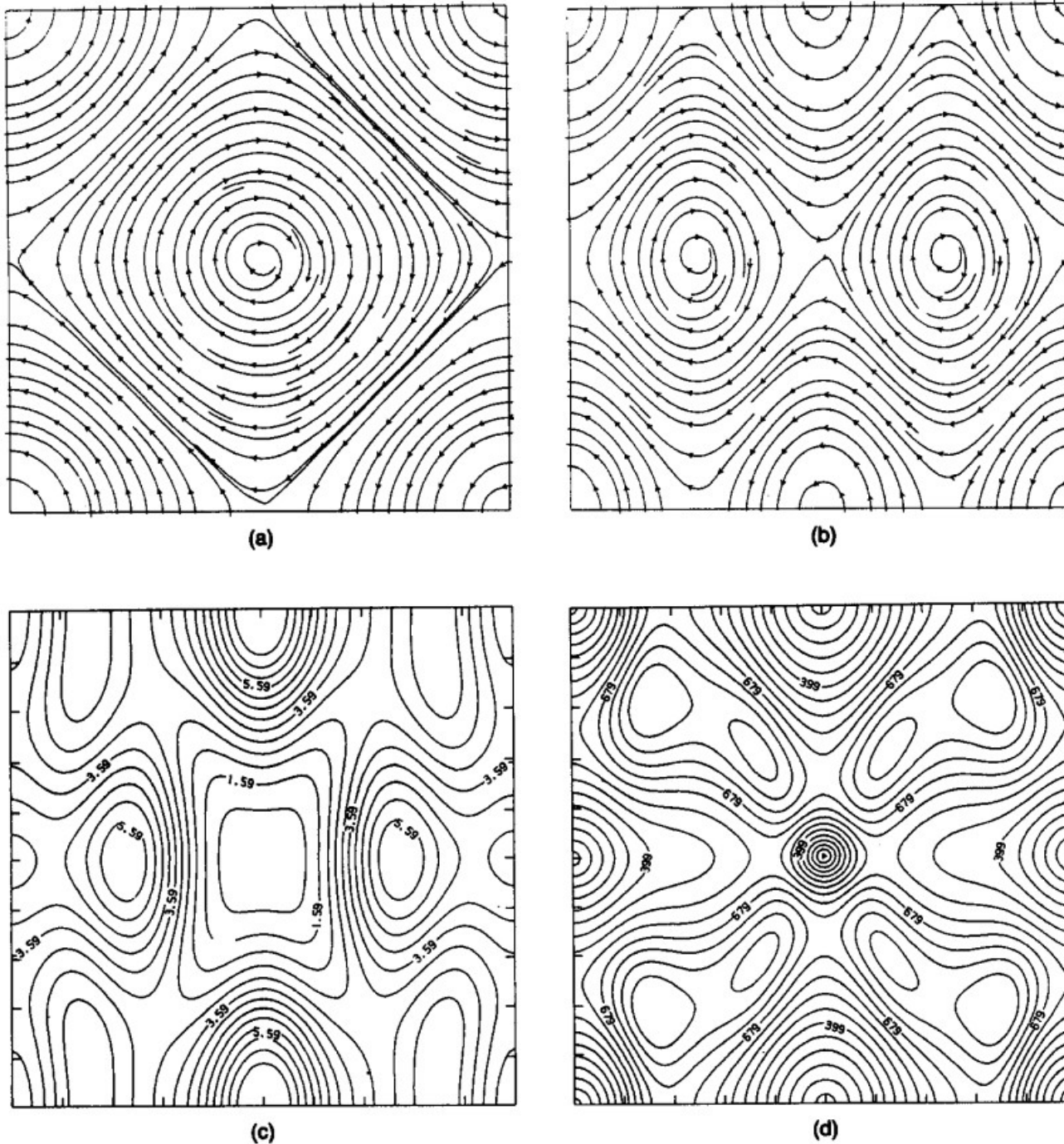
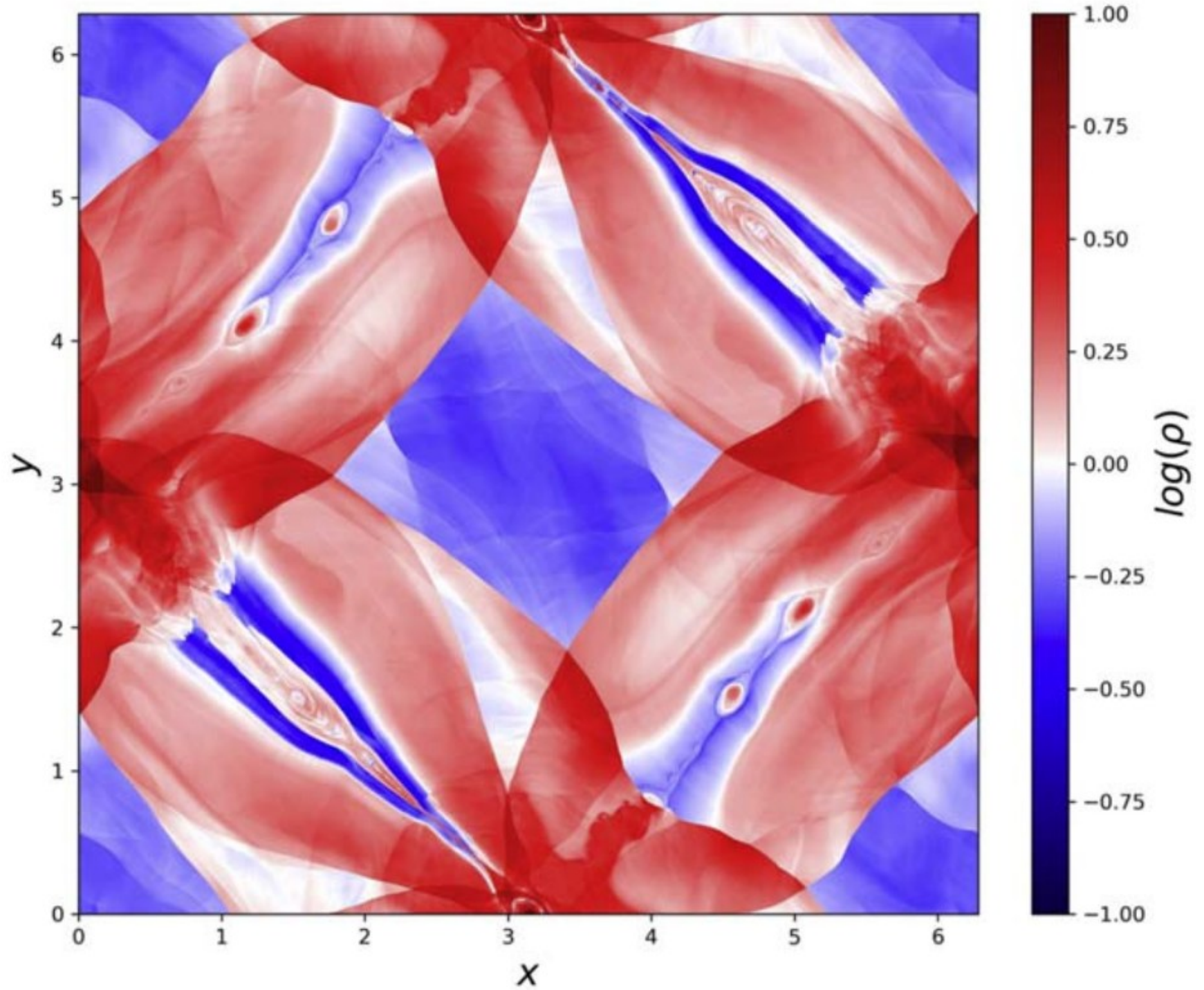


FIG. 1. Initial conditions: (a) velocity field; (b) magnetic field; initial conditions specific to the $M = 0.6$ case: (c) thermal pressure field; (d) local Mach number. Minimum and maximum values are 0.73 and 7.9 for thermal pressure and 0.0 and 0.97 for local Mach number.

OT, standard test but not so standard results



OT, standard test but not so standard results

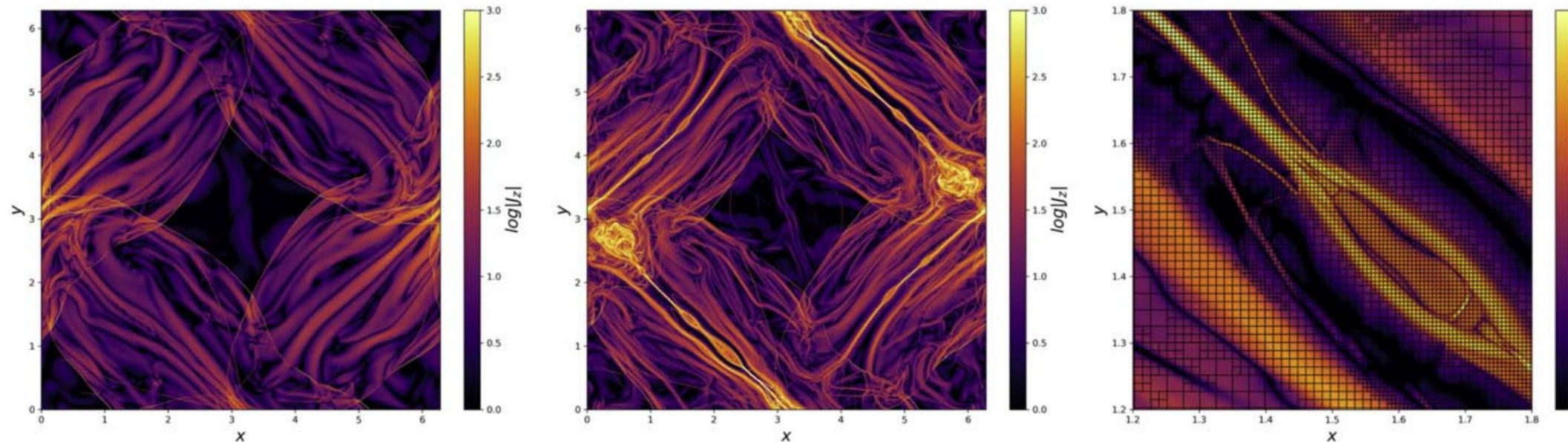


Figure 2. Logarithm of the out-of-plane current density magnitude $|J_z|$ at $t = 10t_c$ for $S = 2 \times 10^3$ (left), $S = 2 \times 10^4$ (middle), and a zoom into the current sheet $S = 2 \times 10^4$ showing the AMR grid blocks (right), each consisting of 8×8 cells, in black. Both cases have an effective resolution of 8192^2 cells in the domain. The plasmoid-unstable current sheet on the right is captured by more than 10 cells over its width.

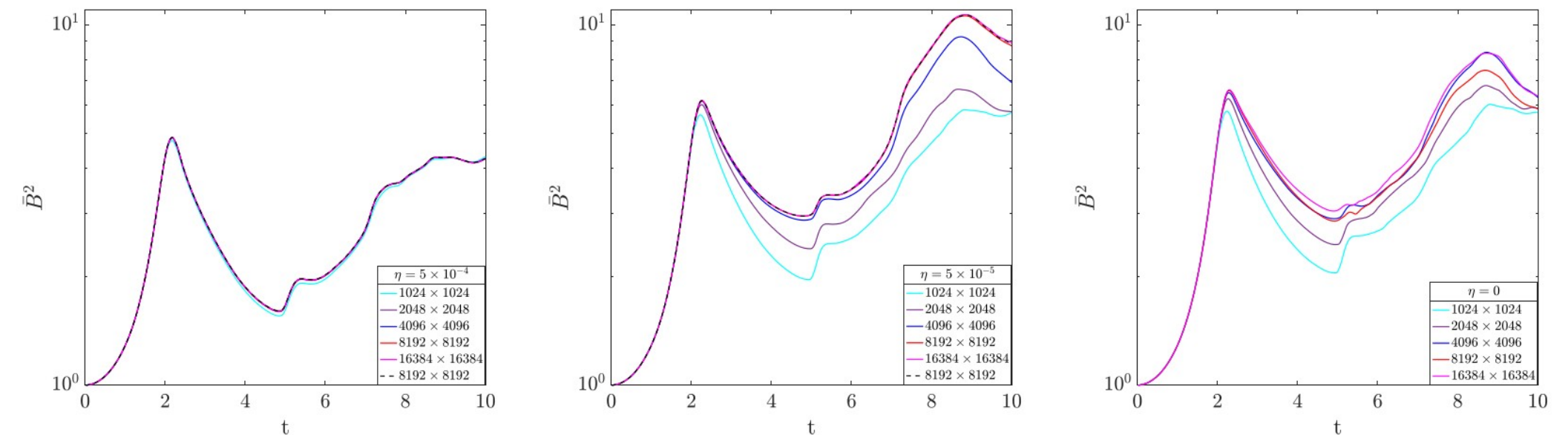


Figure 3. Evolution of the domain-averaged magnetic energy density \bar{B}^2 for $S = 2 \times 10^3$ (left), $S = 2 \times 10^4$ (middle), and the ideal case $\eta = 0$ (right) for all resolutions considered.

Hands-on introduction to setup files of PLUTO

- Guided tour through the source files:
 - pluto.ini contains definition of:
grid, solver, choice of boundary conditions, output steps, parameters.
 - Definition of output formats.
 - Output files, files to save for later analysis and eventual restart.
 - definitions.h: macros setting.
 - init.c: physical setup, equations for **initial** and **boundary** conditions.

Hands-on introduction: pluto.ini

```
miki@petri: ~/Pluto44/OTang2D
I pluto.ini (ini)
[Grid]
X1-grid 1 0.0 200 u 6.28318530717959
X2-grid 1 0.0 200 u 6.28318530717959
X3-grid 1 0.0 1 u 1.0

[Chombo Refinement]
Levels 4
Ref_ratio 2 2 2 2
Regrid_interval 2 2 2 2
Refine_thresh 0.3
Tag_buffer_size 3
Block_factor 4
Max_grid_size 32
Fill_ratio 0.75

[Time]
CFL 0.8
CFL_max_var 1.1
tstop 3.1
first_dt 1.e-4

[Solver]
Solver hll

[Boundary]
```

```
miki@petri: ~/Pluto44/OTang2D
I pluto.ini (ini)
[Boundary]
X1-beg periodic
X1-end periodic
X2-beg periodic
X2-end periodic
X3-beg periodic
X3-end periodic

[Static Grid Output]
uservar 0
dbl 10.31 -1 single_file
flt -1.0 -1 single_file
vtk 0.31 -1 single_file
tab -1.0 -1
ppm -1.0 -1
png -1.0 -1
log 1
analysis -1.0 -1

[Chombo HDF5 output]
Checkpoint_interval -1.0 0
Plot_interval 1.0 0

[Parameters]
SCRH 0
```

Output formats & files to save

- In pluto.ini we defined which output
- data.xxxx.dbl files – viewing, processing with Python, idl etc. packages.
-also, for restart, together with restart.out.
- Data.xxxxdbl.h5 - hdf5 files-need to set the flag in /PLUTO/Config/*.defs file
- data.xxxx.vtk files – for viewing with Paraview, VisIt.
- Together with data.xxxx.dbl and .vtk files, always save also, in the same directory with the results, pluto.ini, definitions.h. init.c, grid.out, dbl.out, restart.out, to know which setup produced the files, and also for some analysis and plotting packages, which might need them.
- grid.out files defines the geometry, dbl.out lists the output variables

```
miki@petri: ~/Pluto44/O_Tang2D
I A definitions.h (c) Row
#define PHYSICS MHD
#define DIMENSIONS 2
#define GEOMETRY CARTESIAN
#define BODY_FORCE NO
#define COOLING NO
#define RECONSTRUCTION LINEAR
#define TIME_STEPPING HANCOCK
#define NTRACER 0
#define PARTICLES NO
#define USER_DEF_PARAMETERS 1

/* -- physics dependent declarations -- */

#define EOS IDEAL
#define ENTROPY_SWITCH NO
#define DIVB_CONTROL EIGHT_WAVES
#define BACKGROUND_FIELD NO
#define AMBIPOLAR_DIFFUSION NO
#define RESISTIVITY NO
#define HALL_MHD NO
#define THERMAL_CONDUCTION NO
#define VISCOSITY NO
#define ROTATING_FRAME NO

/* -- user-defined parameters (labels) -- */

#define SCRH 0

/* [Beg] user-defined constants (do not change this line) */

#define LIMITER MC_LIM
```

Hands-on: definitions.h

```

I      pluto.ini (ini)
[Grid]
X1-grid  1  0.0  2048  u  6.28318530717959
X2-grid  1  0.0  2048  u  6.28318530717959
X3-grid  1  0.0  1    u  1.0
[Chombo Refinement]
Levels      4
Ref_ratio   2 2 2 2 2
Regrid_interval 2 2 2 2
Refine_thresh 0.3
Tag_buffer_size 3
Block_factor 4
Max_grid_size 32
Fill_ratio  0.75
[Time]
CFL          0.45
CFL_max_var  1.1
tstop        3.1
first_dt     1.e-4
[Solver]
Solver        roe
[Boundary]
X1-beg        periodic
X1-end        periodic
X2-beg        periodic
X2-end        periodic
X3-beg        periodic
X3-end        periodic
[Static Grid Output]
uservar       0
dbl           90.1 -1  single_file
flt           -1.0 -1  single_file
vtk           0.310 -1  single_file
tab           -1.0 -1
ppm           -1.0 -1
png           -1.0 -1
log           1
analysis      -1.0 -1

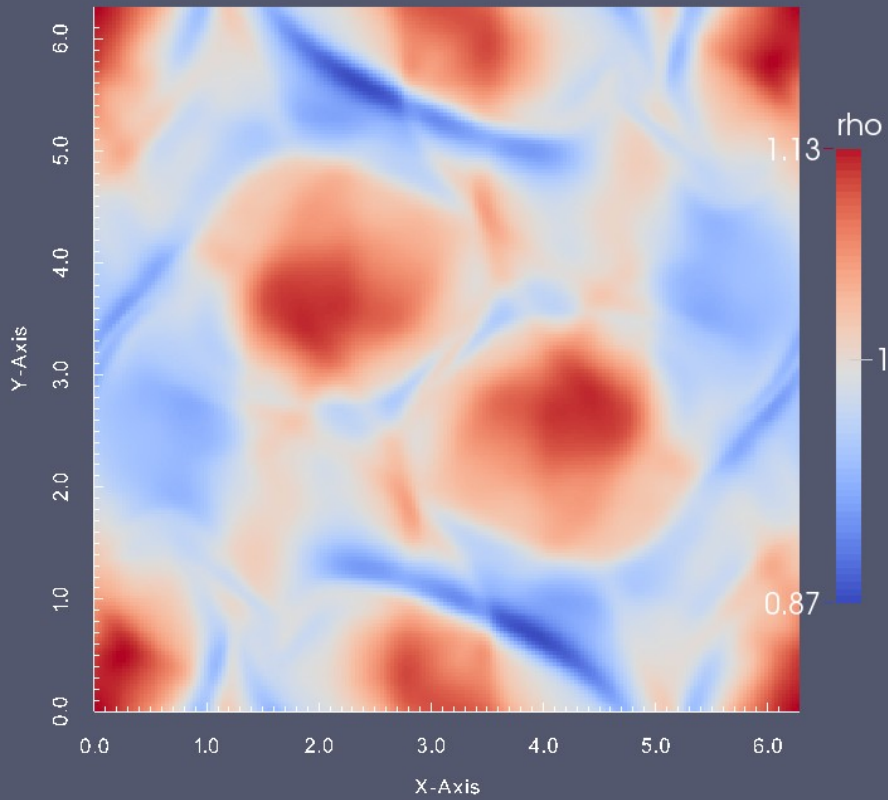
```

Hands-on: pluto.ini

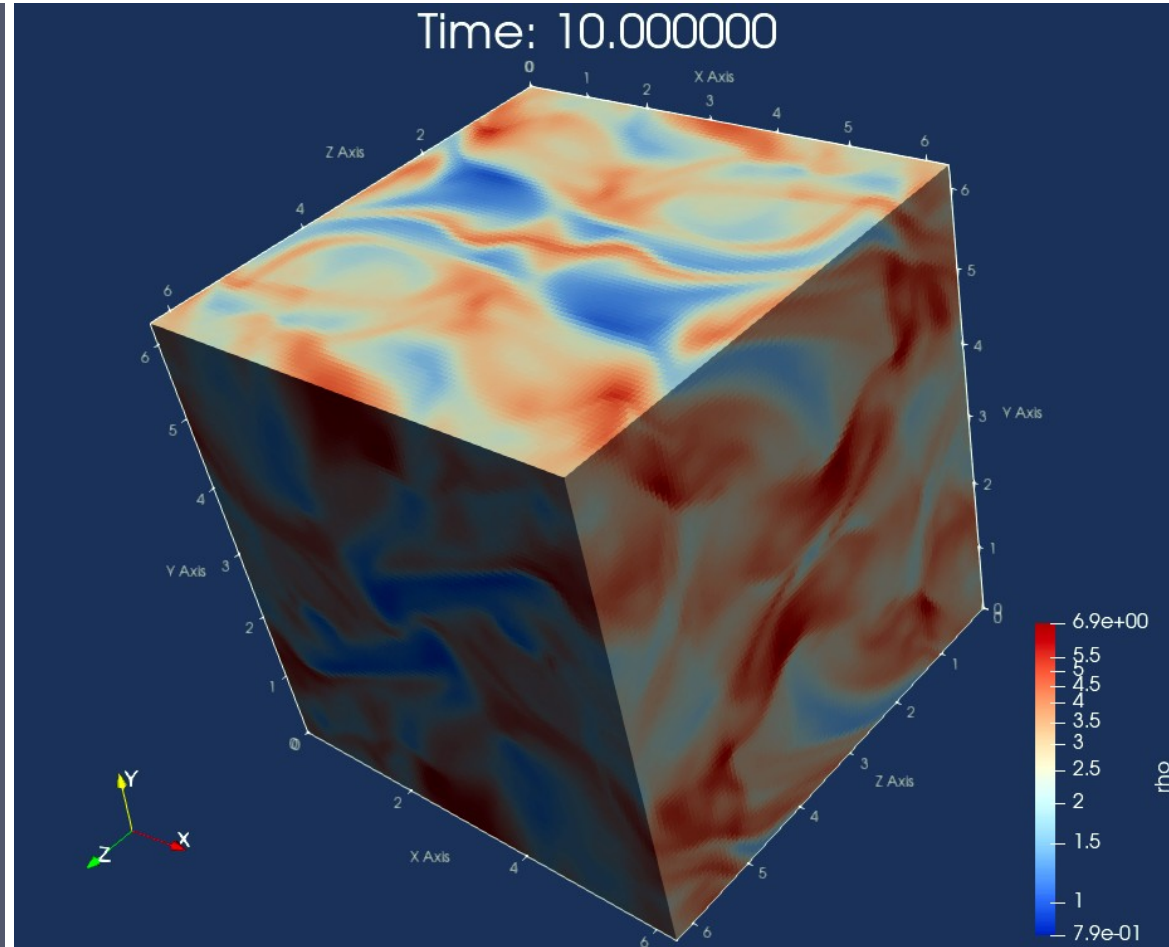
In PLUTO/Test_Problems/MHD/Orszag_Tang copy ***_06*** to pluto.ini (set vtk to + and e.g. change the output frequency in vtk output, so you would get 10 outputs, to see the evolution of run.) and definitions.h and try runs with different resolutions. It was 256x256, try 64x64 and 1024x1024 and 2048x2048, and check the results. You will see the emergence of plasmoids in the vortex, for which the setup is different only in resolution. This is an example of qualitative difference in the results. No help of better algorithms here, the simulation has to be done with better resolution.

Visualization with Paraview

Time: 10.000000



Time: 10.000000



Summary of the Lect. 3

Shakura-Sunyaev 1973 disc

Initial and boundary conditions in PLUTO

2D and 3D Orszag-Tang problem

Visualization in 2D and 3D with Paraview.

Outline, Lect.4 : Kluźniak-Kita solutions for thin disk

- KK 3D solution for thin disc in HD
- Vertically averaged solutions for thin disc
- Setup and running of 2.5D HD KK disc in PLUTO
- Analysis of the results from 2.5D runs with Paraview and Python

Hydrodynamic flows in accretion disks

V. A. Urpin

Ioffe Physics and Technology Institute, USSR Academy of Sciences, Leningrad

(Submitted December 14, 1982)

Astron. Zh. **61**, 84–90 (January–February 1984)

Calculations of the velocity field in an accretion disk show that matter may flow in the disk not only toward but also away from the central object. The rates of flow are determined, and the geometry of hydrodynamic motions in nonstationary disks is discussed.

I was mentioning before the z-averaged solutions. Assumptions by Urpin are ($\hat{\mathfrak{H}} = \eta_v$):

We shall adopt the turbulent-viscosity model.⁶ According to this model the influence of small-scale turbulent motions upon the regular motions is tantamount simply to a renormalization of the viscosity coefficient. The equation of motion will then take the form

$$\rho \frac{\partial \mathbf{V}}{\partial t} + \rho (\mathbf{V} \cdot \nabla) \mathbf{V} = -\nabla p + \rho \nabla \psi + \nabla \hat{\pi},$$

$$(\hat{\pi})_{ik} = \rho \mathfrak{H} \left(\frac{\partial V_i}{\partial x_k} + \frac{\partial V_k}{\partial x_i} - \frac{2}{3} \delta_{ik} \nabla \mathbf{V} \right).$$
(1)

I noticed here we forgot to discuss on viscous tensor, of which the above eq. is a component: The viscosity was defined by the

$$\tau = \eta_v \left[(\nabla \mathbf{v}) + (\nabla \mathbf{v})^T - \frac{2}{3} (\nabla \cdot \mathbf{v}) \mathbf{I} \right],$$

with the dynamic viscosity $\eta_v = \rho \nu_v$

$$\frac{\partial \rho}{\partial t} + \nabla (\rho \mathbf{V}) = 0. \quad (2)$$

It has been suggested that the motions along the r, z directions may take place at subsonic velocities, while the rotational velocity V_ϕ may exceed the sound speed c_s . Estimates indicate (Refs. 1, 2) that these conditions will often be satisfied in real objects. Moreover, we shall consider only objects in which the accretion rate varies so slowly that the inequality

$$t_a > P_{\text{rot}} = 2\pi r / V_\phi \quad (3)$$

holds for all r; here t_a is the time scale for change in the accretion rate. In this event the disk will be axisymmetric.

With these assumptions the z component of Eq. (1) reduces to the simple hydrostatic-equilibrium condition

$$\frac{1}{\rho} \frac{\partial p}{\partial z} = -\frac{GM_z}{r^3},$$

where M is the mass of the central object (we neglect the self-gravitation of the disk). The radial component of Eq. (1) will take the form

$$V_r \frac{\partial V_r}{\partial r} + V_z \frac{\partial V_r}{\partial z} - \frac{V_\phi^2}{r} = -\frac{1}{\rho} \frac{\partial p}{\partial r} + \frac{\partial \psi}{\partial r} + \frac{1}{\rho} (\nabla \hat{\pi})_r.$$

Since $V_r \sim \mathfrak{G}/r$ and $V_z \sim (z_0/r)V_r$ (z_0 is the characteristic disk thickness; see, for example, Shakura and Syun-yaev⁴), one can readily show that the first two terms on the left are much smaller than $(z_0/r)^4 V_\varphi^2 / r$. We may therefore neglect them. The last term on the right is easily estimated:

$$\begin{aligned} \frac{1}{\rho} (\nabla \hat{\pi})_r &\ll \frac{\mathfrak{G} V_\varphi}{r} \sim \left(\frac{v_t}{c_s} \right) \left(\frac{l_t}{z_0} \right) \frac{V_\varphi^2 z_0^2}{r^2 r} \sim \\ &\sim \left(\frac{v_t}{c_s} \right) \left(\frac{l_t}{z_0} \right) \left(\frac{z_0}{r} \right)^2 \frac{V_\varphi^2}{r} \ll \left(\frac{z_0}{r} \right)^2 \frac{V_\varphi^2}{r}; \end{aligned}$$

it too may be neglected. Then

$$\frac{V_\varphi^2}{r} \approx -\frac{\partial \psi}{\partial r} + \frac{1}{\rho} \frac{\partial p}{\partial r}.$$

Later we will need an expression for V_φ accurate to terms of order $(z/r)^2$. Since $\psi = GM/R$, where $R = (r^2 + z^2)^{1/2}$ is the distance from the compact object, we readily find

$$V_\varphi \approx \left(\frac{GM}{r} \right)^{1/2} \left\{ 1 - \frac{3}{4} \frac{z^2}{r^2} + \frac{r^2}{2GM\rho} \frac{\partial p}{\partial r} \right\}. \quad (4)$$

If the condition (3) holds, the φ component of the equation of motion will become

$$\frac{V_r}{r} \frac{\partial}{\partial r} (r V_\varphi) + V_z \frac{\partial V_\varphi}{\partial z} = \frac{1}{\rho} (\nabla \hat{\pi})_\varphi.$$

In the disk $V_z \sim (z_0/r)V_r$, and furthermore $\partial V_\varphi / \partial r \sim (z/r) \partial V_\varphi / \partial z$. We may therefore neglect the second term on the left. Then

$$V_r = \frac{2r}{\rho} \left(\frac{r}{GM} \right)^{1/2} (\nabla \hat{\pi})_\varphi. \quad (5)$$

According to the definition of the tensor $\hat{\pi}$ we may write

$$\begin{aligned} \nabla \hat{\pi} = & [\nabla (\rho \mathfrak{G}) \nabla] \mathbf{V} + \rho \mathfrak{G} \nabla^2 \mathbf{V} + \rho \mathfrak{G} \nabla (\nabla \mathbf{V}) + \nabla [\mathbf{V} \nabla (\rho \mathfrak{G})] \\ & - (\mathbf{V} \nabla) \nabla (\rho \mathfrak{G}) - \frac{2}{3} \nabla (\rho \mathfrak{G} \nabla \mathbf{V}). \end{aligned}$$

Since we have assumed the disk to be axisymmetric with $\partial/\partial\varphi = 0$,

$$(\nabla\hat{\pi})_{\varphi} = \frac{\partial V_{\varphi}}{\partial z} \frac{\partial(\rho\mathfrak{S})}{\partial z} + \frac{\partial(\rho\mathfrak{S})}{\partial r} \left(\frac{\partial V_{\varphi}}{\partial r} - \frac{V_{\varphi}}{r} \right) + \rho\mathfrak{S} \left[\frac{\partial^2 V_{\varphi}}{\partial z^2} + \frac{\partial}{\partial r} \left(\frac{\partial V_{\varphi}}{\partial r} + \frac{V_{\varphi}}{r} \right) \right].$$

Substituting this expression into Eq. (5), we obtain

$$V_r \approx \frac{2r}{\rho} \left(\frac{r}{GM} \right)^{1/2} \left\{ \frac{\partial V_{\varphi}}{\partial z} \frac{\partial(\rho\mathfrak{S})}{\partial z} + \frac{\partial(\rho\mathfrak{S})}{\partial r} \left[\frac{\partial V_{\varphi}}{\partial r} - \frac{V_{\varphi}}{r} \right] + \rho\mathfrak{S} \left[\frac{\partial^2 V_{\varphi}}{\partial z^2} + \frac{\partial}{\partial r} \left(\frac{\partial V_{\varphi}}{\partial r} + \frac{V_{\varphi}}{r} \right) \right] \right\} \\ \approx \frac{2r}{\rho} \left\{ \left(\frac{r}{GM} \right)^{1/2} \left[\frac{\partial V_{\varphi}}{\partial z} \frac{\partial(\rho\mathfrak{S})}{\partial z} + \rho\mathfrak{S} \frac{\partial^2 V_{\varphi}}{\partial z^2} \right] - \frac{3}{2r} \frac{\partial(\rho\mathfrak{S})}{\partial r} - \frac{3}{4r^2} \rho\mathfrak{S} \right\}.$$

It is evident from Eq. (6) that to determine the radial component of the velocity correctly we must know V_{φ} to term of order $(z/r)^2$, since $\partial^2 V_{\varphi} / \partial z^2 \sim \partial^2 V_{\varphi} / \partial r^2 \sim V_{\varphi} / r^2$. Our expression (4) provides this accuracy.

The vertical velocity component V_z can be determined from the equation of continuity:

$$\frac{\partial}{\partial z}(\rho V_z) = -\frac{1}{r} \frac{\partial}{\partial r}(r\rho V_r) - \frac{\partial\rho}{\partial t}.$$

$$(7) \quad \dot{M} \approx \text{const} = - \int_{-\infty}^{+\infty} 2\pi r \rho V_r dz = 3\pi \sqrt{\pi} \rho_c \mathfrak{S} z_0, \quad (10)$$

Next he discusses the three zones of the disk, neglecting the closest one to the star:

firm that the law (8) holds for zones B, C. In zone A, Shakura and Syunyaev¹ found that ρ is independent of height, but if one allows for turbulent heat transfer, this conclusion will no longer be valid.⁷ The density variation in zone A then can also be described to fair accuracy by Eq. (8). However, in the accretion disks around neutron stars and white dwarfs zone A evidently is often absent; we therefore shall consider in detail only the flows in zones B, C.

I have obtained the following expressions for the scale z_0 in these two zones⁷:

$$\begin{aligned} \text{zone C: } z_0 &= 10^4 \alpha^{-1/10} m^{9/10} \dot{m}^{3/20} \mathfrak{R}^{9/5} \text{ cm,} \\ \text{zone B: } z_0 &= 2.1 \cdot 10^4 \alpha^{-1/10} m^{9/10} \dot{m}^{1/5} \mathfrak{R}^{21/20} \text{ cm.} \end{aligned} \quad (9)$$

(6) Here $m = M/M_{\odot}$; $\dot{m} = \dot{M}/(1.9 \cdot 10^{18} \text{ m} \cdot \text{g}/\text{sec})$, with \dot{M} the accretion rate; $\mathfrak{R} = rc^2/6GM = r/(8.89 \cdot 10^5 \text{ m} \cdot \text{cm})$; and the parameter $\alpha = \mathfrak{S}/z_0 c_s$ measures the level to which turbulence has developed in the disk [$c_s = (kT_C/m_p)^{1/2}$].

Along with these expressions we shall also need the condition that the mass flux be conserved. We can obtain it from the equation of continuity, together with Eqs. (6), (8):

where ρ_c is the density in the central disk plane.

Now we compute v_r : we have from eq.4, because of vertical hydrostatic equilibrium

$$\frac{\partial V_\varphi}{\partial z} = \frac{1}{2} \left(\frac{GM}{r^3} \right)^{1/2} \left(-\frac{z}{\rho} \frac{\partial \rho}{\partial r} - \frac{r^3}{CM\rho^2} \frac{\partial p}{\partial r} \frac{\partial \rho}{\partial z} \right). \quad (11)$$

We introduce the convenient dimensionless parameters $\xi = z/z_0$, $f = T/T_c$, $\Psi = \rho/\rho_c$. With these definitions we obtain

$$\begin{aligned} \frac{\partial \ln \rho}{\partial r} &= \frac{\partial \ln \rho_c}{\partial r} - \xi \frac{\dot{\Psi}}{\Psi} \frac{\partial \ln z_0}{\partial r}, \\ \frac{1}{\rho} \frac{\partial p}{\partial r} &= \frac{2kT_c}{m_p} f \left\{ \frac{\partial \ln \rho_c T_c}{\partial r} - \xi \left(\frac{\dot{\Psi}}{\Psi} + \frac{f}{f} \right) \frac{\partial \ln z_0}{\partial r} \right\}. \end{aligned} \quad (12)$$

(the dot signifies differentiation with respect to ξ).

The r -dependence of the parameters ρ_c , T_c , z_0 , ξ has been investigated by Shakura and Syunyaev (Ref. 1) and the author.⁷ For these parameters the following relations hold:

$$\begin{aligned} \text{zone C: } \frac{\partial \ln \rho_c}{\partial \ln r} &= -\frac{15}{8}, & \frac{\partial \ln T_c}{\partial \ln r} &= -\frac{3}{4}, \\ \frac{\partial \ln z_0}{\partial \ln r} &= \frac{9}{8}, & \frac{\partial \ln \xi}{\partial \ln r} &= \frac{3}{4}; \\ \text{zone B: } \frac{\partial \ln \rho_c}{\partial \ln r} &= -\frac{33}{20}, & \frac{\partial \ln T_c}{\partial \ln r} &= -\frac{9}{10}, \\ \frac{\partial \ln z_0}{\partial \ln r} &= \frac{21}{20}, & \frac{\partial \ln \xi}{\partial \ln r} &= \frac{3}{5}. \end{aligned} \quad (13)$$

As mentioned above, $\Psi \sim \exp(-\xi^2)$ in zones B, C. Substituting the expressions (12), (13) into Eq. (11) and noting that $\dot{\Psi}/\Psi \approx -2\xi$, we obtain

$$\begin{aligned} \text{zone C: } \frac{\partial V_\varphi}{\partial z} &= \frac{3z_0}{16r^2} \left(\frac{GM}{r} \right)^{1/2} \xi (5-7f-6\xi^2+6f\xi^2-3\xi f), \\ \text{zone B: } \frac{\partial V_\varphi}{\partial z} &= \frac{3z_0}{40r^2} \left(\frac{GM}{r} \right)^{1/2} \xi (11-17f-14\xi^2+14f\xi^2-7\xi f). \end{aligned}$$

Using these expressions, it is not hard to evaluate V_r . In zone C,

$$\begin{aligned} V_r &= \frac{3\zeta}{r} \left\{ \frac{5}{4} - \frac{7}{8} f - \frac{23}{4} \xi^2 + 4f\xi^2 + \frac{3}{2} \xi^4 \right. \\ &\quad \left. - \frac{3}{2} f\xi^4 - \frac{13}{8} \xi f + \frac{3}{2} \xi^3 f - \frac{3}{8} \xi^2 f \right\}, \end{aligned} \quad (14)$$

while in zone B,

$$V_r = \frac{3\zeta}{20r} \{ 22 - 17f - 106\xi^2 + 76f\xi^2 + 28\xi^4 - 28f\xi^4 - 31\xi f + 28\xi^3 f - 7\xi^2 f \}. \quad (15)$$

Notice that when $\xi = 0$ the radial component of the velocity is positive, and equal to $9\zeta/8r$ in zone C and $3\zeta/4r$ in zone B. Thus in the vicinity of the central plane, matter is flowing away from the compact object.

If ξ is not too large, we may use for the function f the asymptotic expressions⁷:

$$\text{zone C: } f \approx 1 - 0.25\xi^2 + 0.0048\xi^4 - \dots,$$

$$\text{zone B: } f \approx 1 - 0.28\xi^2 + 0.0054\xi^4 - \dots$$

With these we can easily obtain analytic expressions for V_r at reasonably small heights ξ :

$$\text{zone C: } V_r = \frac{9\mathfrak{G}}{8r} (1 - 1.4\xi^2 - 4.8\xi^4 - \dots),$$

$$\text{zone B: } V_r = \frac{3\mathfrak{G}}{4r} (1 - 0.8\xi^2 - 7.6\xi^4 - \dots).$$

Comparison with a numerical calculation of V_r from Eqs. (14), (15) indicates that the asymptotic expressions (16) reproduce the V_r profile almost exactly if $\xi \leq 0.6$; they work quite well for $0.6 \leq \xi \leq 1$ [accurate to $\approx (20-30)\%$], and are qualitatively valid for $1 < \xi < 1.5$.

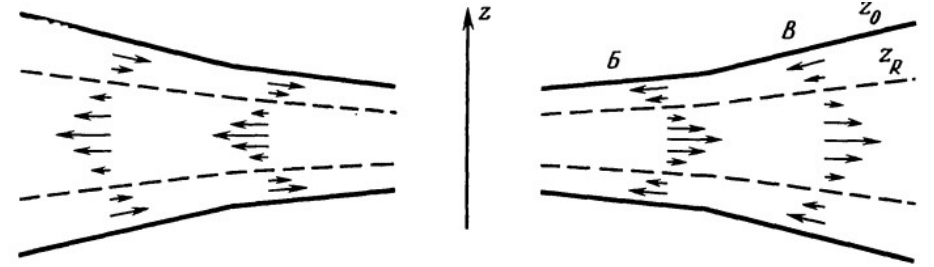
Having V_r , it is not hard to compute from Eq. (7) the vertical velocity component:

$$\text{zone C: } V_z = \frac{9\mathfrak{G}}{8r} \frac{\partial z_0}{\partial r} \xi (1 - 1.4\xi^2 - 4.8\xi^4 - \dots), \quad (17)$$

$$\text{zone B: } V_z = \frac{3\mathfrak{G}}{4r} \frac{\partial z_0}{\partial r} \xi (1 - 0.8\xi^2 - 7.6\xi^4 - \dots);$$

V_z changes sign at the same height z_{cr} as V_r . When $z < z_{cr}$, V_z is directed away from the central plane; when $z > z_{cr}$, towards.

Next he discusses the three zones of the disk, neglecting the closest one to the star:



On substituting into Eqs. (16), (17) the appropriate values⁷ of \mathfrak{G} , we obtain the following expressions for the velocity components in the two zones:

$$\text{zone C: } V_r \approx 9 \cdot 10^5 \alpha^{4/3} m^{-1/3} \dot{m}^{2/3} \mathfrak{R}^{-1/3} (1 - 1.4\xi^2 - 4.8\xi^4 - \dots),$$

$$V_z \approx 1.1 \cdot 10^4 \alpha^{7/10} m^{-3/10} \dot{m}^{9/10} \mathfrak{R}^{-1/5} \xi (1 - 1.4\xi^2 - 4.8\xi^4 - \dots),$$

$$\text{zone B: } V_r \approx 2.6 \cdot 10^6 \alpha^{4/3} m^{-1/3} \dot{m}^{2/3} \mathfrak{R}^{-2/3} (1 - 0.8\xi^2 - 7.6\xi^4 - \dots),$$

$$V_z \approx 6.4 \cdot 10^4 \alpha^{7/10} m^{-3/10} \dot{m}^{9/10} \mathfrak{R}^{-7/10} \xi (1 - 0.8\xi^2 - 7.6\xi^4 - \dots).$$

Figure 2 schematically illustrates the geometry of the regular motions in the disk.

Now let us estimate the rates at which mass flows in different directions in the disk. Denoting by \dot{M}_+ , \dot{M}_- the flux toward and away from the compact object, we will have $\dot{M}_+ - \dot{M}_- = \dot{M} \equiv \text{const}(r)$. Equations (8), (10), (16) then readily yield

$$\dot{M}_- = \int_0^{z_{cr}} 4\pi r \rho V_r dz \approx \begin{cases} 0.35\dot{M} & \text{in zone C,} \\ 0.25\dot{M} & \text{in zone B.} \end{cases}$$

Thus the mass flow toward the center exceeds the opposite flow by a factor of ≈ 4 in zone C and 5 in zone B.

Some of the matter flowing into the disk will change direction immediately adjacent to the compact object; that is where most of the outward flow will originate. Our similarity solution is not valid in this region.

Regev solution

The disk-star boundary layer and its effect on the accretion disk structure

O. Regev

Department of Physics, Technion – Israel Institute of Technology, Haifa 32000, Israel

Received March 15, accepted May 2, 1983

Summary. The method of matched asymptotic expansions is proposed for a self consistent calculation of an accretion disk and the disk-accreting star boundary layer. A model of a thin, optically thick, region (c) accretion disk and boundary layer is calculated with the help of the method. The disk in this model is hotter and denser than in the corresponding Shakura and Sunyaev (1973) model.

The significance of the model is discussed and the method is proposed for other cases of interest.

soft X-rays, emerging from the top and bottom Pringle and Savonije (1979) propose strong shock thin emitting region in the boundary layer to emission of dwarf novae. Finally, Tytenda (possibility of hard X-ray emission in an optically boundary layer without strong shocks. In a recent al. (1982) point out that observations show that is significantly smaller than predicted by a theoretical model.

- In Regev's solution by expansion on a small parameter of H/R is proposed. On this, later similar solutions are developed.
- We will contrast his solution with the later ones, to better understand the development.

Regev solution

- Boundary layer between the inner disk radius and stellar surface is important-there Ω_K of the infalling material changes to Ω_* in a very thin layer, compared to the disk extension in radius.
- As we obtained at slide 48, up to a half of the accretion luminosity is generated in this thin layer.
- In SS73, Pringle '81 and similar, $d\Omega/dr=0$ is used at $r=r_*$ boundary.
- Solutions by Regev, applied to a disk around a white dwarf relate to region (c) in SS73.
- He searches for steady, axisymmetric solutions, with $\partial/\partial t = \partial/\partial \phi = 0$, viscosity is present (only $r-\phi$ component of the viscous stress tensor is present, the rest is neglected), the disk is optically thick, with radiation transfer treated in the diffusion approximation.

Regev solution

$$u \frac{\partial u}{\partial r} + v \frac{\partial u}{\partial z} - \Omega^2 r = -\frac{1}{\rho} \frac{\partial p}{\partial r} - \frac{GM_*}{r^2} \left(1 + \frac{z^2}{r^2}\right)^{-3/2},$$

$$u \frac{\partial v}{\partial r} + v \frac{\partial v}{\partial z} = -\frac{1}{\rho} \frac{\partial P}{\partial z} - \frac{GM_* z}{r^3} \left(1 + \frac{z^2}{r^2}\right)^{-3/2},$$

$$\frac{u}{r^2} \frac{\partial}{\partial r} (r^2 \Omega) + v \frac{\partial \Omega}{\partial z} = \frac{1}{\rho r^3} \frac{\partial}{\partial r} \left(v \rho r^3 \frac{\partial \Omega}{\partial r} \right),$$

$$\frac{1}{r} \frac{\partial}{\partial r} (r \rho u) + \frac{\partial}{\partial z} (\rho v) = 0,$$

$$\rho C_v \left(u \frac{\partial T}{\partial r} + v \frac{\partial T}{\partial z} \right) = -\chi P \left[\frac{1}{r} \frac{\partial}{\partial r} (r u) + \frac{\partial v}{\partial z} \right] \\ + v \rho r^2 \left(\frac{\partial \Omega}{\partial r} \right)^2 - \frac{1}{r} \frac{\partial}{\partial r} (r F^r) - \frac{\partial}{\partial z} F^z.$$

We are already familiar with the equations: momentum eq. in r and z directions (cylindrical coords), angular momentum (in r), mass continuity and energy eqs. Radiative energy fluxes in r and z directions are, with the assumptions from the bottom of previous slide:

$$F^r = -\frac{4ac}{3} \frac{T^3}{\kappa \rho} \frac{\partial T}{\partial r}, \quad F^z = -\frac{4ac}{3} \frac{T^3}{\kappa \rho} \frac{\partial T}{\partial z}.$$

We need to supply the equation of state for P and opacity χ_R .

The constant mass flux through the disk is another requirement, which is a constraint for the solution:

$$-2\pi r \int_{-\infty}^{\infty} \rho u dz = \dot{M} \text{ (constant)}$$

We will not follow Regev solution in detail but just outline it, because we will repeat it related to KK solution:

In order to proceed it is imperative to write the equations in a non-dimensional form. To this end various quantities are scaled by their typical values (denoted by a tilde \sim). Thus ϱ , T , v , κ are in units of $\tilde{\varrho}$, \tilde{T} , \tilde{v} , $\tilde{\kappa}$, respectively. Velocities are expressed in the units of a typical sound velocity \tilde{v}_s , pressure in units of $\tilde{\varrho}\tilde{v}_s^2$ and Ω in units of the Keplerian angular velocity at the surface $\Omega_{k*} \equiv (GM_*/R_*^3)^{1/2}$. Two length scales are introduced – r is scaled by R_* and z by \tilde{H} , a typical value for the disk half-thickness.

Before writing down the non-dimensional equations it is advantageous to state the next two assumptions (in the framework of which this entire work is done).

(v) The circular flow is highly supersonic or, equivalently, the disk is (geometrically) thin – $z/r \ll 1$ in the disk.

(vi) The viscosity in the bulk of the disk is given by an ‘‘alpha model’’, i.e. $\nu = \alpha v_s H$.

The above assumptions are customary and are used by SS (see also Pringle, 1981). Assumption (v) introduces a small parameter into the problem $\varepsilon \equiv (\tilde{v}_s/\Omega_{k*}R_*) \ll 1$, with the help of which a typical vertical scale of the disk \tilde{H} is expressed – $\tilde{H} = \varepsilon R_*$.

The scaled non-dimensional equations are:

$$\varepsilon^2 u \frac{\partial u}{\partial r} + \varepsilon v \frac{\partial u}{\partial z} - \Omega^2 r = -\varepsilon^2 \frac{1}{\varrho} \frac{\partial P}{\partial r} - \frac{1}{r^2} + \varepsilon^2 \frac{3}{2} \frac{z^2}{r^4}, \quad (7)$$

$$\varepsilon u \frac{\partial v}{\partial r} + v \frac{\partial v}{\partial z} = -\frac{1}{\varrho} \frac{\partial P}{\partial z} - \frac{z}{r^3} + \varepsilon^2 \frac{3}{2} \frac{z^3}{r^5}, \quad (8)$$

$$\varepsilon \frac{1}{r} \frac{\partial}{\partial r} (r \varrho u) + \frac{\partial}{\partial z} (\varrho v) = 0, \quad (9)$$

$$\varepsilon \frac{u}{r^2} \frac{\partial}{\partial r} (r^2 \Omega) + v \frac{\partial \Omega}{\partial z} = \varepsilon^2 \alpha \frac{1}{\varrho r^3} \frac{\partial}{\partial r} \left(v \varrho r^3 \frac{\partial \Omega}{\partial r} \right), \quad (10)$$

$$\beta_g \left(\varepsilon u \frac{\partial T}{\partial r} + v \frac{\partial T}{\partial z} \right) \varrho C_v = -\chi P \left[\varepsilon \frac{1}{r} \frac{\partial}{\partial r} (ru) + \frac{\partial v}{\partial z} \right] + \alpha v \varrho r^2 \left(\frac{\partial \Omega}{\partial r} \right)^2 - \eta \left[\varepsilon^2 \frac{1}{r} \frac{\partial}{\partial r} (r F^r) + \frac{\partial}{\partial z} F^z \right]. \quad (11)$$

C_v is expressed in units of \mathcal{R}/μ_A with \mathcal{R} the gas constant and μ_A the mean molecular weight. The new nondimensional constants here are:

$$\beta_g \equiv \frac{\tilde{P}_{\text{gas}}}{\tilde{\varrho}\tilde{v}_s^2}; \quad \eta \equiv \beta_r \lambda,$$

where

$$\beta_r \equiv \frac{\tilde{P}_{\text{rad}}}{\tilde{\varrho}\tilde{v}_s^2} \quad \text{and} \quad \lambda \equiv \frac{4c}{\tilde{v}_s} \frac{1}{\tilde{\tau}_z}.$$

\tilde{P}_{gas} and \tilde{P}_{rad} are the gas and radiation pressure respectively for typical conditions, c is the velocity of light and $\tilde{\tau}_z$ is the optical depth in the vertical direction in a typical point of the disk $\tilde{\tau}_z \equiv \tilde{\kappa} \tilde{H}$. The physical meaning of these constants is self evident and their numerical value depends on the scaling quantities which reflect a particular regime of interest.

The scaled form of Eq. (6) is:

$$r \int_{-\infty}^{\infty} \varrho u dz = -\varepsilon \mu \dot{M}, \quad (12)$$

where \dot{M} is in units of \tilde{M} and $\mu \equiv \dot{M}/(2\pi \tilde{H}^2 \tilde{\varrho} \tilde{v}_s)$. The fluxes F^r and F^z are given as in Eq. (5), but with the constant term $(4ac/3)$ now missing.

Regev solution

Equations 7-12 depend on the small parameter ϵ and other nondimensional constants, order of which is important for finding an approximate solution. The “method of matched asymptotic expansions” is used [Regev refers to it as “Bender & Orszag (1978, chapter 9) solution for differential eqs. which exhibit a boundary layer structure”, I usually refer to it as doing Taylor expansion in a small parameter ϵ , as this is to what we resort at the end.]. Scaling is done to the typical values as in the table:

Scaling variables	Non-dimensional constants
$R_* = 9 \cdot 10^8 \text{ cm}$	$\epsilon = \frac{\tilde{H}}{R_*} = 1.37 \cdot 10^{-2}$
$M_* = 1 M_\odot$	
$\Omega_{*k} = \left(\frac{GM_*}{R_*^3} \right)^{1/2} = 0.427 \text{ rad s}^{-1}$	$\beta_g = \frac{\tilde{P}_{\text{gas}}}{\tilde{\rho} \tilde{v}_s^2} = \frac{1}{\gamma} = \frac{3}{5}$
$\tilde{T} = 10^5 \text{ }^\circ\text{K}$	
$\tilde{V}_s = \left(\frac{5}{3} \frac{\mathcal{R}}{\mu_A} \tilde{T} \right)^{1/2} = 5.265 \cdot 10^6 \text{ cm s}^{-1}$	$\beta_r = \frac{\frac{1}{3} a \tilde{T}^4}{\tilde{\rho} \tilde{v}_s^2} = 1.819 \cdot 10^{-3}$
$\tilde{H} = \frac{\tilde{v}_s}{\Omega_{*k}} = 1.233 \cdot 10^7 \text{ cm}$	$\lambda = \frac{4c}{\tilde{v}_s} \cdot \frac{1}{\tilde{\kappa} \tilde{\rho} \tilde{H}} = 3.525 \cdot 10^2$
$\tilde{\rho} = 5 \cdot 10^{-6} \text{ g cm}^{-3}$	$\eta = \beta_r \lambda = 0.641$
$\tilde{P} = \tilde{\rho} \tilde{v}_s^2 = 1.386 \cdot 10^8 \text{ dyne cm}^{-2}$	$\alpha = 1$
$\tilde{\kappa} = 0.11 \tilde{n} \tilde{T}^{-3.5} = 1.048 \text{ cm}^2 \text{ g}^{-1}$	$\chi = \left(\frac{\partial \ln P}{\partial \ln T} \right)_e = 1$
$\tilde{M} = 2 \cdot 10^{16} \text{ g s}^{-1} = 3.15 \cdot 10^{-10} M_\odot \text{ yr}^{-1}$	$C_v = \frac{3}{2}$
	$\mu = \frac{\tilde{M}}{2\pi \tilde{H}^2 \tilde{\rho} \tilde{v}_s} = 0.795$

The ideal gas eq. is assumed, the radiative term neglected, opacity for free-free transitions is assumed, in the main solution and also in the boundary layer. Viscosity in the boundary layer is assumed as $\nu_{\text{BL}} = K v_{\text{turb}} \Lambda$, with

K and v_{turb} constant and Λ being a characteristic length scale in the boundary layer. In the nondimensional units it is

$$\nu_{\text{BL}} = \frac{K}{\alpha} \frac{v_{\text{turb}}}{\tilde{v}_s} \frac{\Lambda}{\tilde{H}}$$

Now comes the “matched” part: solution of eq. 7 in previous slide in the leading order is proportional with $r^{-3/2}$, this can not be valid at the boundary. An “outer” expansion at $r \neq 1$, $\epsilon \rightarrow 0$ is constructed and matched to the **inner expansion, valid in the disk.**

1. The outer solution

Let $\Omega = \Omega_0 + \varepsilon\Omega_1 + \dots$; $u = u_0 + \varepsilon u_1 + \dots$; $v = v_0 + \varepsilon v_1 + \dots$ with the other variables expanded in ε in a similar way. In lowest order we obtain from Eq. (7) $\Omega_0^2 = \frac{1}{r^3}$, and thus:

$$\Omega_0 = r^{-3/2} \quad (\text{Keplerian}). \quad (14)$$

Equation (8) gives

$$\frac{1}{\varrho_0} \frac{\partial P_0}{\partial z} = -\frac{z}{r^3}. \quad (15)$$

v_0 has been set to be equal to zero for the following reason. From Eq. (9) it follows that $(\partial/\partial z)(\varrho_0 v_0) = 0$ and thus $\varrho_0 v_0 = f(r)$. At $z = 0$ $v_0 = 0$ (symmetry), thus $f(r) = 0$ and since $\varrho_0 \neq 0$, $v_0 = 0$ everywhere.

The lowest order term in Eq. (10) is trivial $v_0(\partial\Omega_0/\partial z) = 0$, and from Eq. (11) we get

$$\alpha v_0 \varrho_0 r^2 \left(\frac{\partial \Omega_0}{\partial r} \right)^2 = \eta \frac{\partial}{\partial z} F_0^z. \quad (16)$$

Order ε of Eq. (10) gives: $u_0(\partial/\partial r)(r^2\Omega_0) = 0$, which implies $u_0 = 0$. Using this in the order ε of Eq. (9) gives $(\partial/\partial z)(\varrho_0 v_1) = 0$ and thus also $v_1 = 0$. Thus, the ε^2 order of Eq. (10) implies

$$r u_1 \varrho_0 \frac{\partial}{\partial r} (r^2 \Omega_0) = \alpha \frac{\partial}{\partial r} \left(v_0 \varrho_0 r^3 \frac{\partial \Omega_0}{\partial r} \right). \quad (17)$$

$$\Sigma_0(r) = \int_{-\infty}^{\infty} \varrho_0(r, z) dz = 2\bar{\varrho}_0(r)H(r) \quad (18)$$

with $H(r)$, the half thickness of the disk to be given from (15) by

$$H(r) = \frac{v_{s0}}{\Omega_0} = T_0^{1/2} r^{3/2}. \quad (19)$$

Also

$$v_0 = v_{s0}H(r) = T_0 r^{3/2}. \quad (20)$$

Integrating now Eqs. (16) and (17) over z

$$\alpha v_0 \Sigma_0 r^2 \left(\frac{\partial \Omega_0}{\partial r} \right)^2 = 2\eta F_0^z, \quad (21)$$

$$-\mu \dot{M} \frac{\partial}{\partial r} (r^2 \Omega_0) = \alpha \frac{\partial}{\partial r} \left(v_0 \Sigma_0 r^3 \frac{\partial \Omega_0}{\partial r} \right), \quad (22)$$

where condition (13) has been used in (21).

Proceeding as in SS we put $F_0^z = \frac{1}{2} T_0^4 / (\kappa_0 \Sigma_0)$ with $\kappa_0 = \bar{\varrho}_0 T_0^{-3.5}$ and thus $F_0^z = T_0^{7.5} H(r) / \Sigma_0^2 = T_0^8 \Sigma_0^{-2} r^{3/2}$. Using (14) and (20) Eq. (21) takes the form:

$$T_0^7 = \left(\frac{9\alpha}{8\eta} \right) \Sigma_0^3 r^{-3}. \quad (23)$$

Integration of (22) gives

$$r^2 \Omega_0 - C = - \left(\frac{\alpha}{\mu \dot{M}} \right) T_0 \Sigma_0 r^{9/2} \frac{\partial \Omega_0}{\partial r}, \quad (24)$$

where C is a constant to be determined by the inner boundary condition. SS (and others—see Pringle, 1981) put $C = 1$ arguing that $(\partial\Omega_0/\partial r) = 0$ at approximately $r = 1$ where $\Omega_0 = 1$. This is entirely inconsistent with (14). In the framework of our treatment C is left undetermined at this stage and will be found from the matching with the inner solution. This is the important difference between this and the SS solution, giving rise to a significant correction (as will be seen below). Substituting Ω_0 and v_0 in (24) solving it together with (23) for T_0 and Σ_0 one gets

$$T_0 = A \alpha^{-1/5} \dot{M}^{3/10} r^{-3/4} (1 - Cr^{-1/2})^{3/10}, \quad (25)$$

$$\Sigma_0 = B \alpha^{-4/5} \dot{M}^{7/10} r^{-3/4} (1 - Cr^{-1/2})^{7/10}, \quad (26)$$

where A and B are known constants:

$$A \equiv (\mu^3/3\eta)^{1/10}; \quad B \equiv A(8\eta/9)^{1/3}.$$

Equations (25) and (26) are equivalent to the SS formulae for region (c) of the disk except for the constant C . Other variables can be found also; for instance the inflow velocity:

$$u_1 = -\mu \dot{M} r^{-1} \Sigma_0^{-1} \quad \text{etc.} \quad (27)$$

- Similar is done for the inner region, in the case when star is fast rotating, near the breakup velocity, he assumes

$\Omega_* = \varepsilon^{1/2} \Omega_{K*}$. This is different from our solution later,

when we will relax this constraint, so we do not follow it further in detail here, just an outline:

Regev solution

It is convenient to use here P_0 as a variable. In our units $P_0 = 1/\gamma \varrho_0 T_0$ (γ is the adiabatic exponent = 5/3 in our case) and thus $\varrho_0 = \gamma P_0 / T_0$.

From the thin disk approximation $H = T_0^{1/2} / \Omega_0$ and $\Sigma_0 = 2\varrho_0 H = 2\gamma P_0 T_0^{-1/2} \Omega_0^{-1}$. Using these relations the following set of equations is obtained:

$$\frac{\partial P_0}{\partial R} = \gamma \frac{P_0}{T_0} (\Omega_0^2 - 1), \quad (34)$$

$$\frac{\partial \Omega_0}{\partial R} = \left(\frac{\mu}{2\gamma} \right) \dot{M} \Omega_0 (1 - \Omega_0) T_0^{1/2} P_0^{-1}, \quad (35)$$

$$\frac{\partial Q_0}{\partial R} = \frac{\mu^2}{4\eta\gamma} \dot{M}^2 \Omega_0^2 (1 - \Omega_0)^2 P_0^{-1}, \quad (36)$$

$$\frac{\partial T_0}{\partial R} = -\gamma \kappa_0 \frac{P_0}{T_0^4} Q_0 \quad (37)$$

with $\kappa_0 = P_0 T_0^{-4.5}$ for free-free opacity. It should be pointed out that various quantities like P_0 , ϱ_0 etc. are in fact z -average here (like

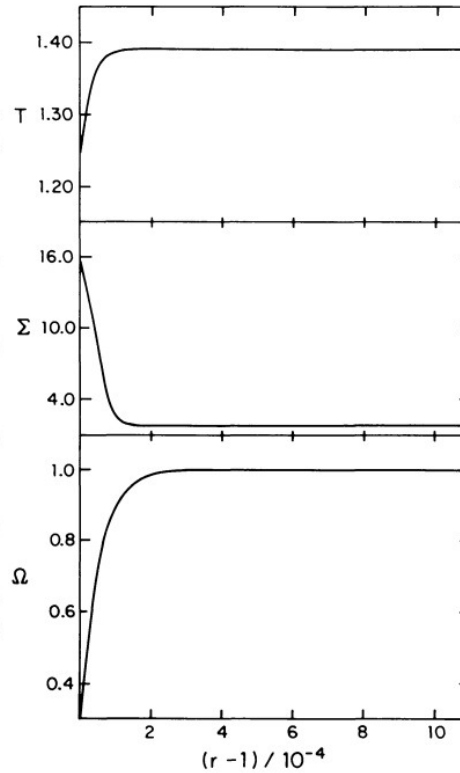


Fig. 1. The structure of the boundary layer for the model example. T – the temperature, Σ – the surface density and Ω – the angular velocity are given as a function of radius very near the star's surface. The quantities are in units used in the text (see Table)

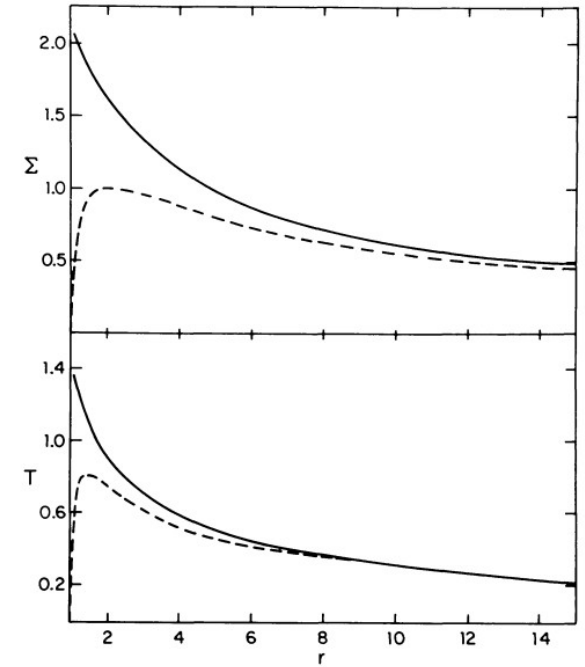


Fig. 2. The structure of the disk as obtained from the matched solution for the model example (solid curves). The dashed curves correspond to a solution with $C=1$ like that of SS (see text)

This is another z -averaged solution, only more involved than Urpin's. Those equations need to be solved numerically, in difference to KK solution, which we will derive analytically. Regev obtains curves from Figs. 1&2 for the disk structure. Since KK obtained a general solution, all this became obsolete.

Kluźniak-Kita solution

THREE-DIMENSIONAL STRUCTURE OF AN ALPHA ACCRETION DISK

Włodzimierz Kluźniak and David Kita

Physics Department, University of Wisconsin, Madison, WI 53706, USA

ABSTRACT

An analytic solution is presented to the three-dimensional problem of steady axisymmetric fluid flow through an accretion disk. The solution has been obtained through a systematic expansion in the small parameter $\epsilon = \bar{H}/\bar{R}$ (the ratio of disk thickness to its radial dimension) of the equations of viscous hydrodynamics. The equation of state was assumed to be polytropic. For all values $\alpha < 0.685$ of the viscosity parameter, we find significant backflow in the midplane of the disk occurring at all radii larger than a certain value; however, in the inner regions of the disk the fluid always flows toward the accreting object. The region of backflow is separated from the region of inflow by a surface flaring outwards from a circular locus of stagnation points situated in the midplane of the disk.

The work in KK00 paper, which exists only in arXiv version, is actually a PhD thesis of David Kita from 1995 at Madison University, USA. It is a general solution obtained similarly to Regev's, but without assumptions he used at the inner disk radius. It is a 3D, axisymmetric, purely HD solution.

- David Kita's Thesis is not available online, it is only in hard copy in the library in USA and an example in CAMK, Warsaw-but arXiv paper is actually very similar to the Thesis, all the formalism is copied in the paper.
- Paper in arXiv is with figures given at the end, I rearranged it and made a more handy version with figures positioned in their places in the text. You can download it from my orange webpage:

<http://web.tiara.sinica.edu.tw/~miki/PostPrez/KK00mikiversion.pdf>

Kluźniak-Kita solution

- We will go through the process of deriving asymptotic matched solutions in, again sometimes painful, detail. It is a very instructive example, and it could be of use for other similar work.
- Motivation of KK00 paper is to find the solutions which would show that the backflow, which appeared also in other solutions except Urpin and Regev, is not of a thermal origin. Urpin included thermal effects but made the simplification of zero net angular momentum flow in the disk (equivalently, his self-similar solution is valid asymptotically for large radii). KK chose the opposite route—neglect thermal effects, but include the inner boundary condition. They were able to find a global solution. They show how the backflow is fed by the inflowing fluid.
- An interesting note: Narayan & Yi (1995) went beyond the one-dimensional solutions by numerically constructing axisymmetric ADF solutions which factorize the three-dimensional equations, i.e., solutions of the type $f(r, \theta) = R(r)\Theta(\theta)$. Solutions in KK00 are **not** factorizable.

Magnetic Kluźniak-Kita disk solution (MKK)

- Not to repeat the lengthy derivations twice, we will do the magnetic version, and outline the HD solutions by setting $\mathbf{B}=0$. *It is interesting that both are non-published work, present only in arXiv, referees did not appreciate the contributions, yet. KK00 paper has a decent following and garnered 60-some citations until now...more than many “published” papers, so it will stay in arXiv domain. The more recent magnetic generalization is still in push for publication. **DISCLAIMER:** in 2023 we finally got the part of the magnetic version published (and within it, the non-magnetic) in A&A! The complete one I present here is a rewrite of rejected version, not yet published. Referee did not appreciate our effort. (S)he thought it useless. True? Envy? I see our solution as maths: nobody did it yet, so it should be published, someone might improve on it, not wasting time on rederiving it-it took us quite some time to get it cleaned, more than less, of errors. It is 75 equations in 16 pages, beat that!*
- HD solutions can be obtained since the set of HD equations is closed. For the magnetic case it is not the case, and only some general conditions can be obtained. I verify, with help of numerical simulations both the HD and non-ideal MHD solutions.

Magnetic Kluźniak-Kita disk solution (MKK)

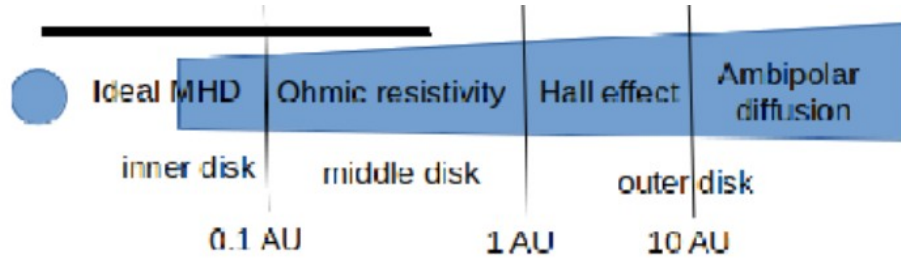


Fig. 1. Illustration of the reach of the inner, middle and outer disk regions in the case of Young Stellar Objects. In the innermost disk region the disk is in the ideal MHD regime. Further away from the star, in the middle disk region, the Ohmic resistivity adds to the viscous dissipation. In the outer disk, which we do not analyze here, other resistive terms prevail in the induction equation. Radial extension of the physical domain in our simulations is indicated with the horizontal thick black solid line.

We search for the quasi-stationary state solutions, assuming that all the heating is radiated away from the disk. This is why the dissipative viscous and resistive terms are not present in the energy equation, nor are the cooling terms. We still solve the equations in the non-ideal MHD regime, because of the viscous terms in the momentum equation, and the Ohmic resistive term in the induction equation. We are solving viscous and resistive MHD equations (in the cgs units):

$$\nabla \cdot \mathbf{B} = 0, \quad (1)$$

$$\frac{\partial \rho}{\partial t} + \nabla \cdot (\rho \mathbf{v}) = 0, \quad (2)$$

$$\frac{\partial \mathbf{B}}{\partial t} + \nabla \times (\mathbf{B} \times \mathbf{v} + \eta_m \mathbf{J}) = 0, \quad (3)$$

$$\frac{\partial \rho \mathbf{v}}{\partial t} + \nabla \cdot \left[\rho \mathbf{v} \mathbf{v} + \left(P + \frac{\mathbf{B} \cdot \mathbf{B}}{8\pi} \right) \mathbf{I} - \frac{\mathbf{B} \mathbf{B}}{4\pi} - \boldsymbol{\tau} \right] = \rho \mathbf{g}, \quad (4)$$

$$\frac{\partial E}{\partial t} + \nabla \cdot \left[\left(E + P + \frac{\mathbf{B} \cdot \mathbf{B}}{8\pi} \right) \mathbf{v} - \frac{(\mathbf{v} \cdot \mathbf{B}) \mathbf{B}}{4\pi} \right] = \rho \mathbf{g} \cdot \mathbf{v}, \quad (5)$$

where ρ , P , \mathbf{v} and \mathbf{B} are the density, pressure, velocity and magnetic field, respectively. The symbols η_m and $\boldsymbol{\tau}$ represent the Ohmic resistivity and the viscous stress tensor, respectively, with $\boldsymbol{\tau} = \eta \mathbf{T}$, where η is the dynamic viscosity and \mathbf{T} is the strain tensor.

The gravity acceleration is $\mathbf{g} = -\nabla \Phi_g$, with the gravitational potential of the star with mass M_\star equal to $\Phi_g = -GM_\star/R$. The total energy density $E = P/(\gamma - 1) + \rho(\mathbf{v} \cdot \mathbf{v})/2$, and the electric current is given by the Ampere's law $\mathbf{J} = \nabla \times \mathbf{B}/4\pi$. We assume the ideal gas with an adiabatic index $\gamma = 5/3$ and polytropic index $n = 3/2$, ($\gamma = 1 + 1/n$).

Magnetic Kluźniak-Kita disk solution (MKK)

- To compare the magnitude of the different terms in the equations, they have to be written in normalized units. We will repeat what was done in Regev (1983): all the variables are written in the Taylor expansion, with the coefficient of expansion given by the characteristic ratio of disk height to the radius, $\epsilon = H/R \ll 1$. For a variable X we have then $X = X_0 + \epsilon X_1 + \epsilon^2 X_2 + \epsilon^3 X_3 + \dots$ and we can compare the terms of the same order in ϵ for each variable.
- In the case of a viscous HD disk ($\mathbf{B} = 0$), the equations can be solved inside the disk (KK00). One can assume that the disk density decreases smoothly to zero towards the disk surface, which greatly simplifies the solution. In the case with a stellar magnetic field, the disk solution is connected with the magnetosphere of a star-disk system, through the coronal magnetic field. Reconnection and outflows complicate the solution in the magnetosphere, together with a back-reaction from the disk.
- In a magnetic case, we can obtain only the most general conditions for the disk magnetic field from the equations.
- We will be searching for the rotationally invariant stationary solutions, so that stationarity, $\partial/\partial t = 0$, and axial symmetry $\partial/\partial \phi = 0$ both hold. [In some cases we write $\partial/\partial \mathbf{x} = \partial_x$ for simplification.]
- Another assumption is that the structure of the disk is symmetric under reflection about the $z=0$ midplane. From this follows that physical quantities such as Ω , ρ , P , η , $u=v_r$, and c_s are even functions of z , while $v=v_z$ is odd under reflections through the equatorial plane. When we expand an even/odd function (e.g. Ω) in powers of $\epsilon \ll 1$, we require each term in the expansion (e.g. Ω_i ; $i = 0, 1, 2, \dots$) to be independently even/odd. **This means that e.g. for $\Omega = \Omega_0 + \epsilon \Omega_1 + \epsilon^2 \Omega_2 + \epsilon^3 \Omega_3 + \dots$, when we have $\Omega = \text{even}$, all the terms [including ϵ in $(\epsilon \Omega_n)$] should be even $\Rightarrow \epsilon \Omega_1 = 0 = \Omega_1 = 0$ and so on for all the odd terms. This is generalized in Rebusco et al. (2009).**

Magnetic Kluźniak-Kita disk solution (MKK)

- We work in the cylindrical coordinates (r, φ, z) . The normalization is defined with the following equations: $\varepsilon = \tilde{c}_s / (\tilde{R}\tilde{\Omega}) = \tilde{H} / \tilde{R} \ll 1$, so that $\tilde{c}_s = \varepsilon\tilde{R}\tilde{\Omega}$, and then $c'_s = c_s / \tilde{c}_s = c_s / (\varepsilon\tilde{R}\tilde{\Omega})$. Twiddles denote characteristic values of the variables, and primes the scaled variables. Further, $\Omega' = \Omega / \tilde{\Omega}$, $\tilde{\Omega} = \Omega_K = \sqrt{GM_\star / \tilde{R}^3}$, $r' = r / \tilde{R}$, $z' = z / (\varepsilon\tilde{R})$, $v'_r = v_r / \tilde{c}_s = v_r / (\varepsilon\tilde{R}\tilde{\Omega})$, $v'_z = v_z / \tilde{c}_s = v_z / (\varepsilon\tilde{R}\tilde{\Omega})$, $v'_\varphi = v_\varphi / (\tilde{R}\tilde{\Omega})$. The magnetic field we normalize with the Alfvén speed $\tilde{v}_A = \tilde{B} / \sqrt{4\pi\tilde{\rho}}$ as a characteristic speed, and $\rho' = \rho / \tilde{\rho}$. Then we have $B' = B / \tilde{B} = B / (\tilde{v}_A^2 \sqrt{4\pi\tilde{\rho}})$, and \tilde{B} is the normalization for all the magnetic field components: $B'_r = B_r / \tilde{B}$, $B'_z = B_z / \tilde{B}$, $B'_\varphi = B_\varphi / \tilde{B}$.

The beta plasma parameter $\beta = P_{\text{gas}} / P_{\text{mag}} = 8\pi P_{\text{gas}} / B^2$. With $P = P_{\text{gas}}$ we can write $c_s^2 = \gamma P / \rho = \gamma\beta B^2 / (8\pi\rho) = \gamma\beta v_A^2 / 2$, so that $\tilde{v}_A^2 / \tilde{c}_s^2 = 2 / (\gamma\tilde{\beta})$.

The viscosity scales with the sound speed as a characteristic velocity and the height of the disk H , so that the normalization for the kinetic viscosity is $\tilde{\nu}_v = \tilde{c}_s \tilde{H} = \varepsilon^2 \tilde{R}^2 \tilde{\Omega}$, and then $\tilde{\eta} = \tilde{\rho} \tilde{\nu}_v = \tilde{\rho} \varepsilon^2 \tilde{R}^2 \tilde{\Omega}$. Then $\eta' = \eta / \tilde{\eta} = \eta / (\tilde{\rho} \varepsilon^2 \tilde{R}^2 \tilde{\Omega})$. For the resistivity we choose the normalization with the Alfvén speed as a characteristic speed, so that $\tilde{\eta}_m = \tilde{v}_A \tilde{H} = \varepsilon \tilde{R} \tilde{v}_A$. Then $\eta'_m = \eta_m / \tilde{\eta}_m = \eta_m / (\varepsilon \tilde{R} \tilde{v}_A) = \eta_m \sqrt{\gamma\tilde{\beta}/2} / (\tilde{c}_s \varepsilon \tilde{R}) = \eta_m \sqrt{\gamma\tilde{\beta}/2} / (\varepsilon^2 \tilde{R}^2 \tilde{\Omega})$.

We illustrate the asymptotic approximation method in detail by deriving all the terms through the second order in the continuity equation. Other equations are derived by following the same method.

The continuity equation is:

$$\frac{\partial \rho}{\partial t} + \nabla \cdot (\rho \mathbf{v}) = 0. \quad (7)$$

In the stationary case $\partial_t \rho = 0$. With the condition of axial symmetry $\partial_\varphi(\rho \mathbf{v}) = 0$:

$$\frac{1}{r} \partial_r (r \rho v_r) + \partial_z (\rho v_z) = 0. \quad (8)$$

The normalized equation, with the terms in the order of a small parameter ϵ :

$$\frac{1}{\tilde{R} r'} \frac{1}{\tilde{R}} \partial_{r'} (r' \tilde{R} \tilde{\rho} \rho' \epsilon \tilde{\Omega} \tilde{R} v'_r) + \frac{1}{\epsilon \tilde{R}} \partial_{z'} (\rho \tilde{\rho} \epsilon \tilde{\Omega} \tilde{R} v'_z) = 0. \quad (9)$$

Dividing through $\tilde{\rho} \tilde{\Omega}$ and removing the primes, we can write:

$$\frac{\epsilon}{r} \partial_r (r \rho v_r) + \partial_z (\rho v_z) = 0. \quad (10)$$

With the expansion in ϵ in each quantity:

$$\begin{aligned} & \frac{\epsilon}{r} \partial_r [r(\rho_0 + \epsilon \rho_1 + \epsilon^2 \rho_2 + \dots)(v_{r0} + \epsilon v_{r1} + \epsilon^2 v_{r2} + \dots)] \\ & + \partial_z [(\rho_0 + \epsilon \rho_1 + \epsilon^2 \rho_2 + \dots)(v_{z0} + \epsilon v_{z1} + \epsilon^2 v_{z2} + \dots)] = 0. \end{aligned} \quad (11)$$

Now we can write the terms in the different orders in ϵ .

Order ϵ^0 :

$$\frac{\partial}{\partial z} (\rho_0 v_{z0}) = 0 \Rightarrow v_{z0} \equiv 0. \quad (12)$$

Since ρ_0 is an even function, and v_z is odd with respect to z , at the disk equatorial plane this product is $\rho_0 v_{z0} = 0$. Since it does not depend on z , and $\rho_0 \neq 0$, we conclude that $v_{z0} = 0$ throughout the disk.

Order ϵ^1 :

In the first order in ϵ it is:

$$\frac{1}{r} \frac{\partial}{\partial r} (r \rho_0 v_{r0}) + \frac{\partial}{\partial z} (\rho_0 v_{z1}) = 0 \Rightarrow v_{z1} \equiv 0. \quad (13)$$

See the next slide for this.

Since $v_{r0} \equiv 0$ (KK00), we have $\partial_z (\rho_0 v_{z1}) = 0 \Rightarrow \rho_0 v_{z1} = \text{const}$ along z . Since v_z is odd with respect to z , following the same argumentation as above in the zeroth order term in ϵ , we conclude that $v_{z1} = 0$ everywhere.

Order ϵ^2 :

In the second order in ϵ :

$$\frac{1}{r} \frac{\partial}{\partial r} (r \rho_0 v_{r1}) + \frac{\partial}{\partial z} (\rho_0 v_{z2}) = 0. \quad (14)$$

Finding the solution for v_{r1} will give us the vertical dependence of v_{z2} .

The same procedure is carried in each of the following equations.

MKK-radial momentum

Radial momentum:

$$\begin{aligned}
 \epsilon^2 v_r \frac{\partial v_r}{\partial r} + \epsilon v_z \frac{\partial v_r}{\partial z} - \Omega^2 r &= -\frac{1}{r^2} \left[1 + \epsilon^2 \left(\frac{z}{r} \right)^2 \right]^{-3/2} \\
 -\epsilon^2 n \frac{\partial c_s^2}{\partial r} + \frac{2}{\gamma \tilde{\beta}} \frac{1}{\rho} \left(\epsilon^2 B_r \frac{\partial B_r}{\partial r} + \epsilon B_z \frac{\partial B_r}{\partial z} - \epsilon^2 \frac{B_\varphi^2}{r} \right) \\
 -\frac{\epsilon^2}{\gamma \tilde{\beta}} \frac{1}{\rho} \frac{\partial B^2}{\partial r} + \frac{\epsilon^3}{\rho r} \frac{\partial}{\partial r} \left(2\eta r \frac{\partial v_r}{\partial r} \right) + \frac{\epsilon}{\rho} \frac{\partial}{\partial z} \left(\eta \frac{\partial v_r}{\partial z} \right) \\
 + \frac{\epsilon^2}{\rho} \frac{\partial}{\partial z} \left(\eta \frac{\partial v_z}{\partial r} \right) - \epsilon^3 \frac{2\eta v_r}{\rho r^2} - \frac{2\epsilon^3}{3\rho} \frac{\partial}{\partial r} \left[\eta \frac{1}{r} \frac{\partial}{\partial r} (r v_r) \right] \\
 - \frac{2}{3} \frac{\epsilon^2}{\rho} \frac{\partial}{\partial r} \left(\eta \frac{\partial v_z}{\partial z} \right).
 \end{aligned} \tag{19}$$

For an ideal gas with the polytropic index n , if adiabatic index $\gamma = 5/3$, we have $n = 3/2$.

Order ϵ^0 :

$$\Omega_0 = r^{-3/2}$$

Order ϵ^1 :

$$-2r\Omega_0\Omega_1 = \frac{2}{\gamma \tilde{\beta}} \frac{1}{\rho_0} B_{z0} \frac{\partial B_{r0}}{\partial z} + \frac{1}{\rho_0} \frac{\partial}{\partial z} \left(\eta_0 \frac{\partial v_{r0}}{\partial z} \right) \tag{21}$$

In HD case, from vertical symmetry and also parity consideration, $\Omega_1 = 0$, and here we obtain $\mathbf{u}_0 = \mathbf{v}_{r0} = 0$. Since $v_{r0} \equiv 0$, from the vertical symmetry $\Omega_1 = 0$ follows, as shown in KK00 for the HD disk, see also Appendix A in Rebusco et al. (2009) for a more formal derivation. ***If this is maintained in the MHD case, we can write, with $v_{r0} = 0$:

$$B_{z0} \frac{\partial B_{r0}}{\partial z} = 0. \tag{22}$$

Order ϵ^2 :

$$\begin{aligned}
 2r\rho_0\Omega_0\Omega_2 &= \frac{3\rho_0}{2} \frac{z^2}{r^4} + n\rho_0 \frac{\partial c_{s0}^2}{\partial r} - \frac{\partial}{\partial z} \left(\eta_0 \frac{\partial v_{r1}}{\partial z} \right) \\
 -\frac{2}{\gamma \tilde{\beta}} \left(B_{r0} \frac{\partial B_{r0}}{\partial r} + B_{z0} \frac{\partial B_{r1}}{\partial z} + B_{z1} \frac{\partial B_{r0}}{\partial z} - \frac{B_{\varphi 0}^2}{r} \right) \\
 + \frac{1}{\gamma \tilde{\beta}} \frac{\partial B_0^2}{\partial r}.
 \end{aligned} \tag{20} \tag{23}$$

***In Rebusco et al. (2009) is given a non-axisymmetric solution. It is obtained with help of Gegenbauer (or hyper-spherical) equation and its solutions are known in terms of combinations of the associated Legendre functions (also known as Gegenbauer polynomials), with use of Wolfram Mathematica 6 software. As mentioned above, there is also given a general discussion of eqs. for the first order in angular velocity, I copy it in the next slide:

In the previous order the explicit form of the viscosity η was not needed, but now the situation is not as comfortable. Following Shakura and Sunyaev (9), we posit the following form of the (ϕ, r) viscous stress tensor component

$$|\tau_{\phi r}| = \alpha P_0, \quad (25)$$

where α is an adimensional parameter. This gives

$$\eta r \left| \frac{d\Omega_0}{dr} \right| = \alpha P_0 \quad \rightarrow \quad \eta = \frac{2}{3} \alpha r^{3/2} \rho_0^{5/3} \quad (26)$$

tion is vertically dependent, i.e., the vertical distribution of stress is assumed to follow We now substitute this η together with the polytropic relation, $\Omega_0 = r^{-3/2}$ and use ion (12) in equations (17,18), which become, after some straightforward algebra

$$\frac{2\alpha}{3} \rho_0^{2/3} r^3 \frac{\partial^2 u_0}{\partial z^2} - \frac{2\alpha}{3} z \frac{\partial u_0}{\partial z} + (2r\Omega_1) = 0 \quad (27)$$

$$\frac{2\alpha}{3} \rho_0^{2/3} r^3 \frac{\partial^2 (2r\Omega_1)}{\partial z^2} - \frac{2\alpha}{3} z \frac{\partial (2r\Omega_1)}{\partial z} - u_0 = 0 \quad (28)$$

APPENDIX A: THE VANISHING OF Ω_1 AND u_0

Rewriting the first order equations (27) and (28) with the definitions $U \equiv u_0$ and $V \equiv 2r\Omega_1$ gives

$$\left[\left(\frac{2\alpha}{3} \right) r^3 \rho_0^{2/3} \right] \frac{\partial^2 U}{\partial z^2} - \left(\frac{2\alpha}{3} \right) z \frac{\partial U}{\partial z} + V = 0 \quad (A1)$$

$$\left[\left(\frac{2\alpha}{3} \right) r^3 \rho_0^{2/3} \right] \frac{\partial^2 V}{\partial z^2} - \left(\frac{2\alpha}{3} \right) z \frac{\partial V}{\partial z} - U = 0. \quad (A2)$$

Substituting now the zeroth order solution $\rho_0^{2/3} = (h^2 - z^2)/(5r^3)$ and rearranging leads to

$$U_{zz} - \frac{5z}{h^2 - z^2} U_z + \frac{a}{h^2 - z^2} V = 0 \quad (A3)$$

$$V_{zz} - \frac{5z}{h^2 - z^2} V_z - \frac{a}{h^2 - z^2} U = 0, \quad (A4)$$

where the subscripts z denote here the differentiation with respect to z and $a \equiv 15/(2\alpha)$ is a constant. Using now $Q(z) \equiv (h^2 - z^2)^{5/2}$ as an integrating factor for the first two terms in both of the above equations, we see that

$$\frac{\partial}{\partial z} \left(Q \frac{\partial U}{\partial z} \right) = -a(h^2 - z^2)^{3/2} V \quad (A5)$$

$$\frac{\partial}{\partial z} \left(Q \frac{\partial V}{\partial z} \right) = a(h^2 - z^2)^{3/2} U. \quad (A6)$$

Multiplying the first equation by U , the second by V , adding and integrating over the domain $[-h, h]$, gives, after dropping the integrated parts,

$$\int_{-h}^h \left[\left(\frac{\partial U}{\partial z} \right)^2 + \left(\frac{\partial V}{\partial z} \right)^2 \right] Q(z) dz = 0. \quad (A7)$$

Because $Q(z) \neq 0$, except at $z = \pm h$ and the functions U, V are bound, they must be equal to *constants*. Thus, it follows from equations (A3, A4), that $U = V = 0$, except perhaps at $z = \pm h$. However, since they are bound and constant in all the domain, they (and hence u_0 and Ω_1) must be zero identically.

MKK-azimuthal momentum

Azimuthal momentum:

$$\begin{aligned} \epsilon \frac{\rho v_r}{r^2} \frac{\partial}{\partial r} (r^2 \Omega) + \rho v_z \frac{\partial \Omega}{\partial z} &= \frac{\epsilon^2}{r^3} \frac{\partial}{\partial r} \left(r^3 \eta \frac{\partial \Omega}{\partial r} \right) + \frac{\partial}{\partial z} \left(\eta \frac{\partial \Omega}{\partial z} \right) \\ &+ \frac{2}{\gamma \tilde{\beta}} \frac{1}{r} \left(\epsilon^2 B_r \frac{\partial B_\varphi}{\partial r} + \epsilon B_z \frac{\partial B_\varphi}{\partial z} + \epsilon^2 \frac{B_\varphi B_r}{r} \right) \end{aligned} \quad (24)$$

Order ϵ^0 :

$$0 = \frac{\partial}{\partial z} \left(\eta_0 \frac{\partial \Omega_0}{\partial z} \right), \quad (25)$$

consistent with Eq. (20).

Order ϵ^1 :

$$\frac{\rho_0 v_{r0}}{r^2} \frac{\partial}{\partial r} (r^2 \Omega_0) = \frac{\partial}{\partial z} \left(\eta_0 \frac{\partial \Omega_1}{\partial z} \right) + \frac{2}{\gamma \tilde{\beta}} \frac{1}{r} B_{z0} \frac{\partial B_{\varphi 0}}{\partial z} \quad (26)$$

Since $v_{r0} = \Omega_1 = 0$, we obtain that:

$$B_{z0} \frac{\partial B_{\varphi 0}}{\partial z} = 0. \quad (27)$$

Order ϵ^2 :

$$\begin{aligned} \frac{\rho_0 v_{r1}}{r} \frac{\partial}{\partial r} (r^2 \Omega_0) &= \frac{2}{\gamma \tilde{\beta}} \left(B_{r0} \frac{\partial B_{\varphi 0}}{\partial r} + B_{z0} \frac{\partial B_{\varphi 1}}{\partial z} + \frac{B_{r0} B_{\varphi 0}}{r} \right) \\ &+ \frac{1}{r^2} \frac{\partial}{\partial r} \left(r^3 \eta_0 \frac{\partial \Omega_0}{\partial r} \right) + \frac{\partial}{\partial z} \left(\eta_0 \frac{\partial \Omega_2}{\partial z} \right). \end{aligned}$$

Vertical momentum:

$$\begin{aligned} \epsilon v_r \frac{\partial v_z}{\partial r} + v_z \frac{\partial v_z}{\partial z} &= -\frac{z}{r^3} \left[1 + \epsilon^2 \left(\frac{z}{r} \right)^2 \right]^{-3/2} \\ -n \frac{\partial c_s^2}{\partial z} + \frac{2}{\gamma \tilde{\beta}} \frac{1}{\rho} \left(\epsilon B_r \frac{\partial B_z}{\partial r} + B_z \frac{\partial B_z}{\partial z} \right) &- \frac{1}{\gamma \tilde{\beta}} \frac{1}{\rho} \frac{\partial B^2}{\partial z} \\ &+ \frac{2}{\rho} \frac{\partial}{\partial z} \left(\eta \frac{\partial v_z}{\partial z} \right) + \frac{\epsilon^2}{\rho r} \frac{\partial}{\partial r} \left(r \eta \frac{\partial v_z}{\partial r} \right) \\ -\frac{2}{3} \frac{\epsilon}{\rho} \frac{\partial}{\partial z} \left[\frac{\eta}{r} \frac{\partial}{\partial r} (r v_r) \right] &- \frac{2}{3\rho} \frac{\partial}{\partial z} \left(\eta \frac{\partial v_z}{\partial z} \right) \\ &+ \frac{\epsilon}{\rho r} \frac{\partial}{\partial r} \left(\eta r \frac{\partial v_r}{\partial z} \right) \end{aligned} \quad (29)$$

Order ϵ^0 :

$$0 = -\frac{z}{r^3} - n \frac{\partial c_{s0}^2}{\partial z} - \frac{1}{\gamma \tilde{\beta}} \frac{1}{\rho_0} \frac{\partial B_0^2}{\partial z}. \quad (30)$$

From Eqs. (16), (22) and (27), with $B_{z0} = f(r)$ it follows that $B_{r0} = f(r)$ and $B_{\varphi 0} = f(r)$. With $B_0^2 = B_{r0}^2 + B_{z0}^2 + B_{\varphi 0}^2$ it gives $\partial_z B_0^2 = 0 = \partial_z B_0$. For a disk in the vertical equilibrium, components of the magnetic field do not contribute in the zeroth order in ϵ to the vertical gradient of the magnetic field.

We remain with the vertical hydrostatic equilibrium equation identical to the purely HD case:

$$\frac{z}{r^3} = -n \frac{\partial c_{s0}^2}{\partial z}. \quad (31)$$

This is consistent with the demand that, for a quasi-stationary disk, the lowest order in ϵ of the magnetic field components does not contribute to the solution:

$$B_{r0} = B_{z0} = B_{\varphi 0} = 0 \Rightarrow B_0 = 0. \quad (32)$$

MKK-HD solutions

Order ϵ^1 :

$$\frac{2}{\gamma\tilde{\beta}} \left[B_{z0} \frac{\partial B_{z1}}{\partial z} - \frac{\partial}{\partial z} (B_0 B_1) \right] - \frac{2}{3r} \frac{\partial}{\partial z} \left[\eta_0 \frac{\partial}{\partial r} (rv_{r1}) \right] + \frac{1}{r} \frac{\partial}{\partial r} \left(\eta_0 r \frac{\partial v_{r1}}{\partial z} \right) = 0. \quad (33)$$

With $B_{z0} = B_0 = 0$ we obtain:

$$\frac{\partial}{\partial z} \left[\eta_0 \frac{\partial}{\partial r} (rv_{r1}) \right] = \frac{3}{2} \frac{\partial}{\partial r} \left(\eta_0 r \frac{\partial v_{r1}}{\partial z} \right). \quad (34)$$

Order ϵ^2 :

$$0 = B_{r0} \frac{\partial B_{z1}}{\partial r} + B_{r1} \frac{\partial B_{z0}}{\partial r} + B_{z0} \frac{\partial B_{z2}}{\partial z} + B_{z1} \frac{\partial B_{z1}}{\partial z} + \frac{1}{\gamma\tilde{\beta}} \frac{\partial}{\partial z} (B_1^2 + 2B_0 B_2) + \frac{2}{3} \frac{\partial}{\partial z} \left[\frac{\eta_1}{r} \frac{\partial}{\partial r} (rv_{r1}) \right] - 2 \frac{\partial}{\partial z} (\eta_0 v_{z2}) + \frac{2}{3} \frac{\partial}{\partial z} \left(\eta_0 \frac{\partial v_{z2}}{\partial z} \right) - \frac{1}{r} \frac{\partial}{\partial r} \left(\eta_0 r \frac{\partial v_{r1}}{\partial z} \right). \quad (35)$$

If now we use Eq. (17) with $B_{r0} = 0$, giving

$$\frac{\partial B_{z1}}{\partial z} = 0, \quad (36)$$

we obtain:

$$\frac{3\rho_0 z^3}{2 r^7} = 2n\rho_0 \frac{\partial}{\partial z} (c_{s0} c_{s2}) + n\rho_2 \frac{\partial c_{s0}^2}{\partial z} + \frac{1}{\gamma\tilde{\beta}} \frac{\partial B_1^2}{\partial z} - 2 \frac{\partial}{\partial z} (\eta_0 v_{z2}) + \frac{2}{3} \frac{\partial}{\partial z} \left[\frac{\eta_1}{r} \frac{\partial}{\partial r} (rv_{r1}) \right] + \frac{2}{3} \frac{\partial}{\partial z} \left(\eta_0 \frac{\partial v_{z2}}{\partial z} \right) - \frac{1}{r} \frac{\partial}{\partial r} \left(\eta_0 r \frac{\partial v_{r1}}{\partial z} \right). \quad (37)$$

We review already obtained results with the vanishing components of B_0 , when magnetic field influences the solution only in the higher orders in ϵ . Then Eqs. (14), (23) and (28) become the same as in a HD case:

$$\begin{aligned} \frac{1}{r} \frac{\partial}{\partial r} (r\rho_0 v_{r1}) + \frac{\partial}{\partial z} (\rho_0 v_{z2}) &= 0, \\ 2r\rho_0 \Omega_0 \Omega_2 &= \frac{3\rho_0 z^2}{2 r^4} + n\rho_0 \frac{\partial c_{s0}^2}{\partial r} - \frac{\partial}{\partial z} \left(\eta_0 \frac{\partial v_{r1}}{\partial z} \right) \\ \frac{\rho_0 v_{r1}}{r} \frac{\partial}{\partial r} (r^2 \Omega_0) &= \frac{1}{r^2} \frac{\partial}{\partial r} \left(r^3 \eta_0 \frac{\partial \Omega_0}{\partial r} \right) + \frac{\partial}{\partial z} \left(\eta_0 \frac{\partial \Omega_2}{\partial z} \right). \end{aligned} \quad (38)$$

In the disk solution in Hōshi (1977) and KK00, those equations were solved by assuming that the disk density decreases towards the surface, $\rho_0 \rightarrow 0$. If, instead, we supply at the disk surface a value at the boundary with the coronal density ρ_{cd} , we obtain:

$$\rho_0 = \left(\rho_{cd}^{2/3} + \frac{h^2 - z^2}{5r^3} \right)^{3/2}, \quad \text{It was my addition to this derivation, nobody needed it before. Feels good!} \quad (39)$$

where h is the disk semi-thickness. The pressure and sound speed now become:

$$P_0 = \left(\rho_{cd}^{2/3} + \frac{h^2 - z^2}{5r^3} \right)^{5/2}, \quad c_{s0} = \sqrt{\frac{5}{3} \left(\rho_{cd}^{2/3} + \frac{h^2 - z^2}{5r^3} \right)}. \quad (40)$$

MKK-HD and MHD solutions

The Hōshi (1977) solution is recovered by setting $\rho_{cd} = 0$, for the boundary at the disk maximal height.

In our case, since $h \propto r$, we can write, with the proportionality constant h' , $h = h'r$. Assuming the corona at the surface of the disk to be in the hydrostatic equilibrium, with $\rho_{cd} \propto (\rho_{c0}/r)^{3/2}$ we can write:

$$\begin{aligned} c_{s0}^2 &= \frac{5}{3} \left(\rho_{cd}^{2/3} + \frac{h'^2 r^2 - z^2}{5r^3} \right) = \frac{5}{3} \left(\frac{k_\rho \rho_{c0}}{r} + \frac{h'^2}{5r} - \frac{z^2}{5r^3} \right) \\ &= \frac{5k_\rho \rho_{c0} + h'^2}{3r} \left[1 - \left(\zeta \frac{z}{r} \right)^2 \right] \propto \frac{1}{r} \left[1 - \left(\zeta \frac{z}{r} \right)^2 \right], \end{aligned} \quad (41)$$

with $\zeta^2 = 1/(5k_\rho \rho_{c0} + h'^2)$, where k_ρ is the proportionality constant, and $\rho_{c0} \sim 0.01$ is the ratio between the initial corona and disk density.

Now we can continue with the rest of equations.

Magnetic field solenoidality ($\nabla \cdot \mathbf{B} = 0$):

$$\frac{\epsilon}{r} \frac{\partial}{\partial r} (rB_r) + \frac{\partial B_z}{\partial z} = 0$$

Order ϵ^0 :

$$\frac{\partial B_{z0}}{\partial z} = 0 \Rightarrow B_{z0} = f(r) \text{ or } B_{z0} = 0.$$

Order ϵ^1 :

$$\frac{1}{r} \frac{\partial}{\partial r} (rB_{r0}) + \frac{\partial B_{z1}}{\partial z} = 0.$$

Order ϵ^2 :

$$\frac{1}{r} \frac{\partial}{\partial r} (rB_{r1}) + \frac{\partial B_{z2}}{\partial z} = 0$$

MKK-MHD solutions

Radial induction equation:

$$0 = B_z \frac{\partial v_r}{\partial z} + v_r \frac{\partial B_z}{\partial z} - B_r \frac{\partial v_z}{\partial z} - v_z \frac{\partial B_r}{\partial z} + \sqrt{\frac{2}{\gamma\tilde{\beta}}} \left(\frac{\partial \eta_m}{\partial z} \frac{\partial B_r}{\partial z} - \epsilon \frac{\partial \eta_m}{\partial z} \frac{\partial B_z}{\partial r} \right) + \eta_m \sqrt{\frac{2}{\gamma\tilde{\beta}}} \left(\frac{\partial^2 B_r}{\partial z^2} - \epsilon \frac{\partial^2 B_z}{\partial r \partial z} \right). \quad (42)$$

Order ϵ^0 :

$$\frac{\partial \eta_{m0}}{\partial z} \frac{\partial B_{r0}}{\partial z} + \eta_{m0} \frac{\partial^2 B_{r0}}{\partial z^2} = 0. \quad (43)$$

If we multiply this with B_{z0} , the first term equals zero because of Eq. (22), and we remain with the second term:

$$\eta_{m0} B_{z0} \frac{\partial^2 B_{r0}}{\partial z^2} = 0. \quad (44)$$

If all the zeroth-order magnetic field components are zero, $B_{r0} = 0$ and we remain with

$$0 = 0. \quad (45)$$

Order ϵ^1 :

$$B_{z0} \frac{\partial v_{r1}}{\partial z} + \sqrt{\frac{2}{\gamma\tilde{\beta}}} \left(\frac{\partial \eta_{m0}}{\partial z} \frac{\partial B_{r1}}{\partial z} + \frac{\partial \eta_{m1}}{\partial z} \frac{\partial B_{r0}}{\partial z} - \frac{\partial \eta_{m0}}{\partial z} \frac{\partial B_{z0}}{\partial r} \right) + \sqrt{\frac{2}{\gamma\tilde{\beta}}} \left(\eta_{m0} \frac{\partial^2 B_{r1}}{\partial z^2} + \eta_{m1} \frac{\partial^2 B_{r0}}{\partial z^2} - \eta_{m0} \frac{\partial^2 B_{z0}}{\partial r \partial z} \right) = 0. \quad (46)$$

With the components of B_0 vanishing, we remain with:

$$\frac{\partial}{\partial z} \left(\eta_{m0} \frac{\partial B_{r1}}{\partial z} \right) = 0. \quad (47)$$

Order ϵ^2 :

$$0 = B_{z0} \frac{\partial v_{r2}}{\partial z} + B_{z1} \frac{\partial v_{r1}}{\partial z} + v_{r1} \frac{\partial B_{z1}}{\partial z} - B_{r0} \frac{\partial v_{z2}}{\partial z} - v_{z2} \frac{\partial B_{r0}}{\partial z} + \sqrt{\frac{2}{\gamma\tilde{\beta}}} \left(\frac{\partial \eta_{m0}}{\partial z} \frac{\partial B_{r2}}{\partial z} + \frac{\partial \eta_{m1}}{\partial z} \frac{\partial B_{r1}}{\partial z} + \frac{\partial \eta_{m2}}{\partial z} \frac{\partial B_{r0}}{\partial z} - \frac{\partial \eta_{m1}}{\partial r} \frac{\partial B_{z0}}{\partial r} - \frac{\partial \eta_{m0}}{\partial z} \frac{\partial B_{z1}}{\partial r} \right) + \sqrt{\frac{2}{\gamma\tilde{\beta}}} \left(\eta_{m0} \frac{\partial^2 B_{r2}}{\partial z^2} + \eta_{m1} \frac{\partial^2 B_{r1}}{\partial z^2} - \eta_{m0} \frac{\partial^2 B_{z1}}{\partial r \partial z} - \eta_{m1} \frac{\partial^2 B_{z0}}{\partial r \partial z} \right). \quad (48)$$

Without the components of B_0 , we remain with:

$$0 = B_{z1} \frac{\partial v_{r1}}{\partial z} + \sqrt{\frac{2}{\gamma\tilde{\beta}}} \left(\frac{\partial \eta_{m0}}{\partial z} \frac{\partial B_{r2}}{\partial z} + \frac{\partial \eta_{m1}}{\partial z} \frac{\partial B_{r1}}{\partial z} - \frac{\partial \eta_{m0}}{\partial z} \frac{\partial B_{z1}}{\partial r} + \eta_{m0} \frac{\partial^2 B_{r2}}{\partial z^2} + \eta_{m1} \frac{\partial^2 B_{r1}}{\partial r^2} - \eta_{m0} \frac{\partial B_{z2}}{\partial r \partial z} \right).$$

MKK-MHD solutions

Azimuthal induction equation:

$$\begin{aligned}
 0 = & \epsilon r B_r \frac{\partial \Omega}{\partial r} + \epsilon r \Omega \frac{\partial B_r}{\partial r} + \epsilon \Omega B_r + r B_z \frac{\partial \Omega}{\partial z} + r \Omega \frac{\partial B_z}{\partial z} \\
 & - \epsilon^2 v_r \frac{\partial B_\varphi}{\partial r} - \epsilon v_z \frac{\partial B_\varphi}{\partial z} - \epsilon^2 B_\varphi \frac{\partial v_r}{\partial r} - \epsilon B_\varphi \frac{\partial v_z}{\partial z} \\
 & + \sqrt{\frac{2}{\gamma \tilde{\beta}}} \left(\frac{\epsilon^3 B_\varphi}{r} \frac{\partial \eta_m}{\partial r} + \epsilon^3 \frac{\partial \eta_m}{\partial r} \frac{\partial B_\varphi}{\partial r} + \epsilon \frac{\partial \eta_m}{\partial z} \frac{\partial B_\varphi}{\partial z} \right) \\
 & + \eta_m \sqrt{\frac{2}{\gamma \tilde{\beta}}} \left(\frac{\epsilon^3}{r} \frac{\partial B_\varphi}{\partial r} - \frac{\epsilon^3 B_\varphi}{r^2} + \epsilon^3 \frac{\partial^2 B_\varphi}{\partial r^2} + \epsilon \frac{\partial^2 B_\varphi}{\partial z^2} \right).
 \end{aligned} \tag{50}$$

Order ϵ^0 :

$$r \Omega_0 \frac{\partial B_{z0}}{\partial z} = 0 \Rightarrow \frac{\partial B_{z0}}{\partial z} = 0,$$

in agreement with Eq. (16).

Order ϵ^1 :

$$\begin{aligned}
 & r B_{r0} \frac{\partial \Omega_0}{\partial r} + r \Omega_0 \frac{\partial B_{r0}}{\partial r} + r \Omega_0 \frac{\partial B_{z1}}{\partial z} \\
 & + \sqrt{\frac{2}{\gamma \tilde{\beta}}} \left(\frac{\partial \eta_{m0}}{\partial z} \frac{\partial B_{\varphi 0}}{\partial z} + \eta_{m0} \frac{\partial^2 B_{\varphi 0}}{\partial z^2} \right) = 0,
 \end{aligned} \tag{52}$$

which, with vanishing components of B_0 , becomes:

$$r \Omega_0 \frac{\partial B_{z1}}{\partial z} = 0.$$

This confirms Eq. (36).

Order ϵ^2 :

$$\begin{aligned}
 0 = & r \frac{\partial B_{r1}}{\partial r} \frac{\partial \Omega_0}{\partial r} + r \Omega_0 \frac{\partial B_{r1}}{\partial r} + r B_{z0} \frac{\partial \Omega_2}{\partial z} + r \Omega_0 \frac{\partial B_{z2}}{\partial z} \\
 & + \sqrt{\frac{2}{\gamma \tilde{\beta}}} \left(\frac{\partial \eta_{m1}}{\partial z} \frac{\partial B_{\varphi 0}}{\partial z} + \frac{\partial \eta_{m0}}{\partial z} \frac{\partial B_{\varphi 1}}{\partial z} + \eta_{m0} \frac{\partial^2 B_{\varphi 1}}{\partial z^2} \right. \\
 & \left. + \eta_{m1} \frac{\partial^2 B_{\varphi 0}}{\partial z^2} \right).
 \end{aligned} \tag{54}$$

Without the vanishing components of B_0 it becomes:

$$\begin{aligned}
 & r \frac{\partial B_{r1}}{\partial r} \frac{\partial \Omega_0}{\partial r} + r \Omega_0 \frac{\partial B_{r1}}{\partial r} + r \Omega_0 \frac{\partial B_{z2}}{\partial z} \\
 & + \sqrt{\frac{2}{\gamma \tilde{\beta}}} \left(\frac{\partial \eta_{m0}}{\partial z} \frac{\partial B_{\varphi 1}}{\partial z} + \eta_{m0} \frac{\partial^2 B_{\varphi 1}}{\partial z^2} \right) = 0.
 \end{aligned} \tag{55}$$

Vertical induction equation:

$$\begin{aligned}
 0 = & \frac{v_z B_r}{r} - \frac{v_r B_z}{r} + B_r \frac{\partial v_z}{\partial r} - v_r \frac{\partial B_z}{\partial r} + v_z \frac{\partial B_r}{\partial r} \\
 & - B_z \frac{\partial v_r}{\partial r} + \sqrt{\frac{2}{\gamma \tilde{\beta}}} \left(\epsilon \frac{\partial \eta_m}{\partial r} \frac{\partial B_z}{\partial r} - \frac{\partial \eta_m}{\partial r} \frac{\partial B_r}{\partial z} \right) \\
 & + \eta_m \sqrt{\frac{2}{\gamma \tilde{\beta}}} \left(\frac{\epsilon}{r} \frac{\partial B_z}{\partial r} - \frac{1}{r} \frac{\partial B_r}{\partial r} - \frac{\partial^2 B_r}{\partial r \partial z} + \epsilon \frac{\partial^2 B_z}{\partial r^2} \right).
 \end{aligned} \tag{56}$$

MKK-MHD solutions

Order ϵ^0 :

$$\eta_{m0} \left(\frac{1}{r} \frac{\partial B_{r0}}{\partial r} + \frac{\partial^2 B_{r0}}{\partial r \partial z} \right) + \frac{\partial \eta_{m0}}{\partial r} \frac{\partial B_{r0}}{\partial z} = 0, \quad (57)$$

giving, with $B_{r0} = 0$:

$$0 = 0. \quad (58)$$

Order ϵ^1 :

$$\begin{aligned} & v_{r1} \left(\frac{B_{z0}}{r} + \frac{\partial B_{z0}}{\partial r} \right) + B_{z0} \frac{v_{r1}}{\partial r} \\ &= \sqrt{\frac{2}{\gamma \tilde{\beta}}} \left[\frac{\partial \eta_{m0}}{\partial r} \left(\frac{\partial B_{z0}}{\partial r} - \frac{\partial B_{r1}}{\partial z} \right) - \frac{\partial \eta_{m1}}{\partial r} \frac{\partial B_{r0}}{\partial z} \right. \\ & \quad \left. + \frac{\eta_{m0}}{r} \left(\frac{\partial B_{z0}}{\partial r} - \frac{\partial B_{r1}}{\partial r} \right) - \eta_{m0} \frac{\partial^2 B_{r1}}{\partial r \partial z} \right. \\ & \quad \left. - \eta_{m1} \left(\frac{1}{r} \frac{\partial B_{r0}}{\partial r} + \frac{\partial^2 B_{r0}}{\partial r \partial z} \right) \right]. \end{aligned} \quad (59)$$

With vanishing components of B_0 :

$$\frac{\partial}{\partial r} \left(\eta_{m0} \frac{\partial B_{r1}}{\partial z} \right) + \frac{\eta_{m0}}{r} \frac{\partial B_{r1}}{\partial r} = 0. \quad (60)$$

Order ϵ^2 :

$$\begin{aligned} & \frac{1}{r} \left(v_{z2} B_{r0} - v_{r1} B_{z1} - v_{r2} B_{z0} \right) + B_{r0} \frac{\partial v_{z2}}{\partial r} + v_{z2} \frac{\partial B_{r0}}{\partial r} \\ & - \left(B_{z0} \frac{\partial v_{r2}}{\partial r} + v_{r2} \frac{\partial B_{z0}}{\partial r} \right) - \left(B_{z1} \frac{\partial v_{r1}}{\partial r} + v_{r1} \frac{\partial B_{z1}}{\partial r} \right) \\ & = \sqrt{\frac{2}{\gamma \tilde{\beta}}} \left[\frac{\partial \eta_{m0}}{\partial r} \left(\frac{\partial B_{r2}}{\partial z} - \frac{\partial B_{z1}}{\partial r} \right) + \frac{\partial \eta_{m1}}{\partial r} \left(\frac{\partial B_{r1}}{\partial z} \right. \right. \\ & \quad \left. \left. - \frac{\partial B_{z0}}{\partial r} \right) + \frac{\partial \eta_{m2}}{\partial r} \frac{\partial B_{r0}}{\partial z} + \frac{\eta_{m0}}{r} \left(\frac{\partial B_{r2}}{\partial r} - \frac{\partial B_{z1}}{\partial r} \right) \right. \\ & \quad \left. + \frac{\eta_{m1}}{r} \left(\frac{\partial B_{r1}}{\partial r} - \frac{\partial B_{z0}}{\partial r} \right) + \frac{\eta_{m2}}{r} \frac{\partial B_{r0}}{\partial r} + \eta_{m0} \frac{\partial^2 B_{r2}}{\partial r \partial z} \right. \\ & \quad \left. + \eta_{m1} \frac{\partial^2 B_{r1}}{\partial r \partial z} + \eta_{m2} \frac{\partial^2 B_{r0}}{\partial r \partial z} - \eta_{m0} \frac{\partial^2 B_{z1}}{\partial r^2} - \eta_{m1} \frac{\partial^2 B_{z0}}{\partial r^2} \right], \end{aligned} \quad (61)$$

which with vanishing components of B_0 becomes:

$$\begin{aligned} 0 &= -\frac{1}{r} v_{r1} B_{z1} - B_{zr1} \frac{\partial v_{r1}}{\partial r} - v_{r2} \frac{\partial B_{z2}}{\partial r} \\ &= \sqrt{\frac{2}{\gamma \tilde{\beta}}} \left[\frac{\partial \eta_{m0}}{\partial r} \left(\frac{\partial B_{r2}}{\partial z} - \frac{\partial B_{z1}}{\partial r} \right) \right. \\ & \quad \left. + \frac{\eta_{m0}}{r} \left(\frac{\partial B_{r2}}{\partial r} - \frac{\partial B_{z1}}{\partial r} \right) + \frac{\partial \eta_{m1}}{\partial r} \frac{\partial B_{r1}}{\partial z} \right. \\ & \quad \left. + \frac{\eta_{m1}}{r} \frac{\partial B_{r1}}{\partial r} + \eta_{m0} \frac{\partial^2 B_{r2}}{\partial r \partial z} + \eta_{m1} \frac{\partial^2 B_{r1}}{\partial r \partial z} - \eta_{m0} \frac{\partial^2 B_{z1}}{\partial r^2} \right]. \end{aligned} \quad (62)$$

MKK-MHD solutions

Energy equation:

$$\begin{aligned}
 & \epsilon^4 \tilde{R}^2 \tilde{\Omega}^2 n \rho v_r \frac{\partial c_s^2}{\partial r} + \epsilon^3 \tilde{R}^2 \tilde{\Omega}^2 n \rho v_z \frac{\partial c_s^2}{\partial z} + \epsilon \rho \tilde{v}^2 v_z \frac{\partial v^2/2}{\partial z} \\
 & + \epsilon^2 \rho \tilde{v}_A^2 v_r \frac{\partial v_A}{\partial r} + \epsilon \rho \tilde{v}_A^2 v_z \frac{\partial v_A^2}{\partial z} + \epsilon^2 \rho \tilde{v}^2 v_r \frac{\partial v/2}{\partial r} \\
 & + \left[\epsilon^2 \rho \tilde{\Omega}^2 \tilde{R}^2 \frac{v_r}{r^2} + \epsilon^3 \rho \tilde{\Omega}^2 \tilde{R}^2 \frac{v_z z}{r^3} \right] \left[1 + \epsilon^2 \left(\frac{z}{r} \right)^2 \right]^{-3/2} \\
 & = \frac{\tilde{v}_A^2 B_r}{r} (\epsilon^2 v_r B_r + \epsilon \Omega r B_\varphi) \\
 & + \tilde{v}_A^2 \frac{\partial}{\partial r} (\epsilon^2 v_r B_r^2 + \epsilon^2 v_z B_z B_r + \epsilon \Omega r B_\varphi B_r) \\
 & + \tilde{v}_A^2 \frac{\partial}{\partial z} (\epsilon v_r B_r B_z + \epsilon v_z B_z^2 + \Omega r B_\varphi B_z).
 \end{aligned} \tag{63}$$

Order ϵ^0 :

$$0 = \tilde{v}_A^2 \frac{\partial}{\partial z} (\Omega_0 r B_{\varphi 0} B_{z 0}) \Rightarrow B_{\varphi 0} \frac{\partial B_{z 0}}{\partial z} + B_{z 0} \frac{\partial B_{\varphi 0}}{\partial z} = 0,$$

which, with the first term vanishing by Eq. (16), confirms the Eq. (27).

Order ϵ^1 :

$$\begin{aligned}
 & B_{\varphi 0} \left(\frac{B_{r 0}}{2r} + \frac{\partial B_{r 0}}{\partial r} + \frac{\partial B_{z 1}}{\partial z} \right) + B_{z 0} \frac{\partial B_{\varphi 1}}{\partial z} \\
 & + B_{r 0} \frac{\partial B_{\varphi 0}}{\partial r} + B_{z 1} \frac{\partial B_{\varphi 0}}{\partial z} = 0.
 \end{aligned} \tag{64}$$

With Eq. 17, we can write:

$$B_{r 0} \left(\frac{\partial B_{\varphi 0}}{\partial r} - \frac{B_{\varphi 0}}{2r} \right) + B_{z 0} \frac{\partial B_{\varphi 1}}{\partial z} + B_{z 1} \frac{\partial B_{\varphi 0}}{\partial z} = 0. \tag{65}$$

Order ϵ^2 :

$$\begin{aligned}
 & \Omega_0 B_{r 0} B_{\varphi 1} + \frac{\partial}{\partial r} \left[r \Omega_0 (B_{r 0} B_{\varphi 1} + B_{r 1} B_{\varphi 0}) \right] \\
 & + \frac{\partial}{\partial z} \left[v_{r 1} B_{r 0} B_{z 0} + r \Omega_0 (B_{z 2} B_{\varphi 0} + B_{z 1} B_{\varphi 1} \right. \\
 & \quad \left. + B_{z 0} B_{\varphi 2}) + r \Omega_2 B_{z 0} B_{\varphi 0} \right] = 0,
 \end{aligned} \tag{66}$$

which with $\partial_z B_{z 0} = 0$ can be recast into:

$$\begin{aligned}
 & \Omega_0 B_{r 0} B_{\varphi 1} + \frac{\partial}{\partial r} \left[r \Omega_0 (B_{r 0} B_{\varphi 1} + B_{r 1} B_{\varphi 0}) \right] \\
 & + B_{z 0} \frac{\partial}{\partial z} \left[v_{r 1} B_{r 0} + r (\Omega_0 B_{\varphi 2} + \Omega_2 B_{\varphi 0}) \right] = 0,
 \end{aligned} \tag{67}$$

In all three orders in ϵ , with $B_{i 0} = 0$ with $i = (r, \varphi, z)$ we obtain identities $0=0$, confirming that our assumptions and results are in agreement with the energy equation.

MKK-MHD solutions

- We list now the solutions. Far away from the star, where we expect a small effect of the magnetic field, solutions in the simulations should not differ much from the HD solutions. Closer to the star, the magnetic field influence increases and the change in results will be larger. Higher order terms in the MHD solution may differ from those in KK00.

- $v_{r0} = v_{z0} = v_{z1} = \Omega_1 = c_{s1} = \rho_1 = 0$, as found in HD case.

we readily obtain $\Omega_0 = r^{-3/2}$. This solution is valid equally in the HD and MHD cases.

- $B_0 = 0$ and also $B_{i0} = 0$, with $i = (r, \varphi, z)$. Magnetic field influences the disk only in the higher orders in a small parameter ϵ .
- $\partial_z B_{z1} = 0$, vertical dependence of the leading component of the magnetic field in the vertical direction is $f(r)$ only.
- Vertical hydrostatic equilibrium condition gives the same solutions for the lowest order in ϵ for the density (see Eq. 39), pressure and the sound speed as in the HD solution. The difference from KK00 is that now the disk surface boundary condition is not vacuum, but a corona with the density $\rho_{cd}(r)$ at the disk interface. The zeroth order profile of density, pressure, and the sound speed are:

$$\begin{aligned} \rho_0(r, z) &= \left[\rho_{cd}^{2/3}(r) + \frac{h^2 - z^2}{5r^3} \right]^{3/2}, \\ P_0(r, z) &= \left[\rho_{cd}^{2/3}(r) + \frac{h^2 - z^2}{5r^3} \right]^{5/2}, \\ c_{s0}(r, z) &= \sqrt{\frac{5}{3} \left[\rho_{cd}^{2/3}(r) + \frac{h^2 - z^2}{5r^3} \right]}. \end{aligned} \quad (68)$$

Clearly, $\rho_0(r, h) = \rho_{cd}(r)$.

MKK-HD and MHD numerical solutions

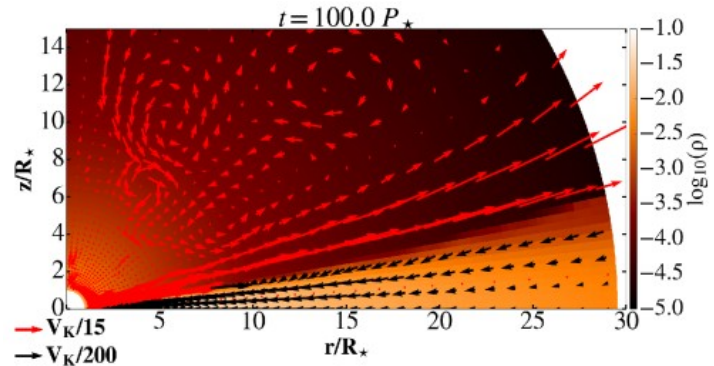


Fig. 2. Capture of our hydrodynamic simulation after $t=100$

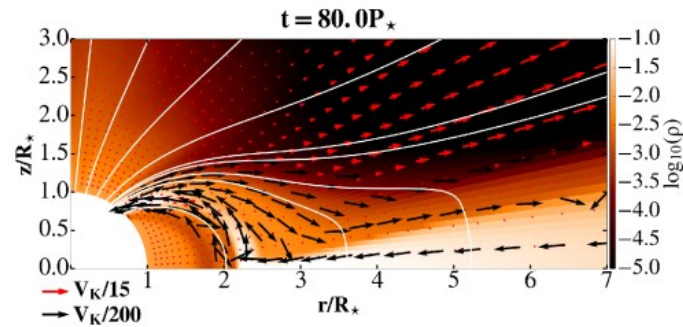
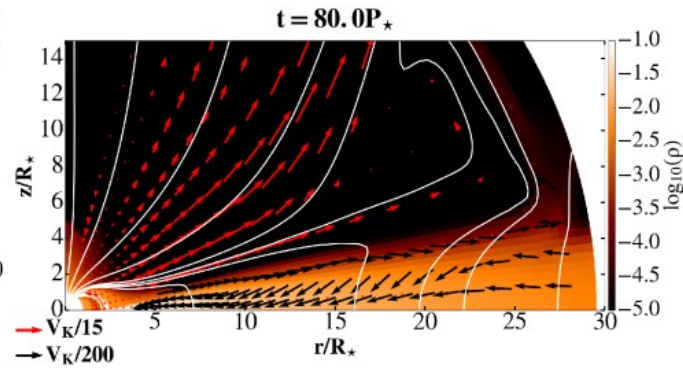


Fig. 4. Captures of our magnetic simulation after $t=80$ stellar rotations (top panel), and a zoom closer to the star (bottom panel) to better show the accretion column. Colors and vectors have the same meaning as in Fig. 2. Note the different scale of the poloidal velocity (arrows below the panels). A sample of the poloidal magnetic field lines is shown with the solid lines.

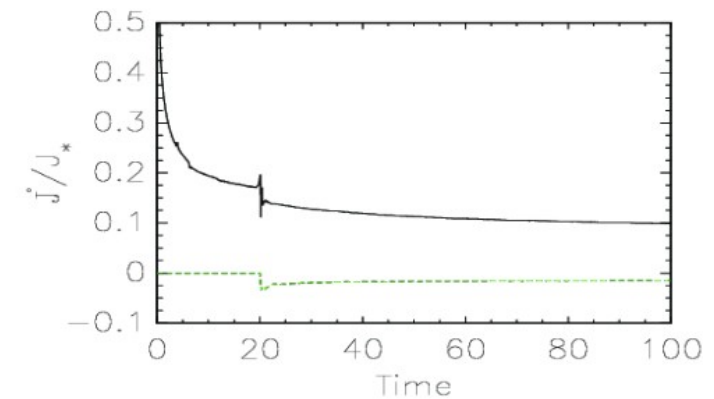
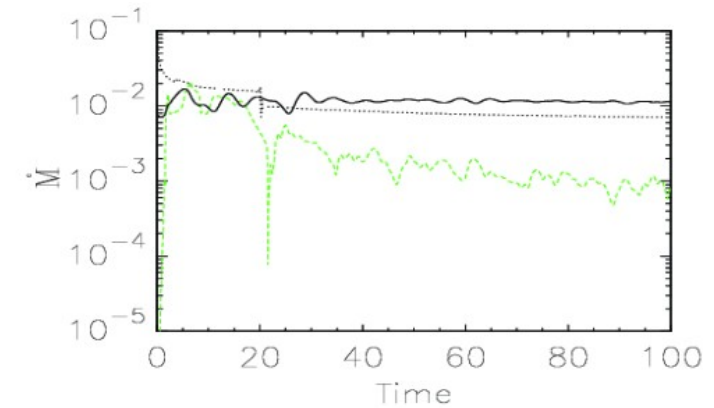


Fig. 3. Illustration of the quasi-stationarity of our solution in

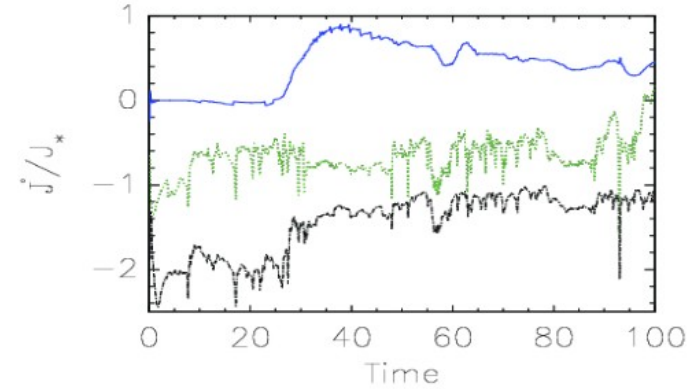
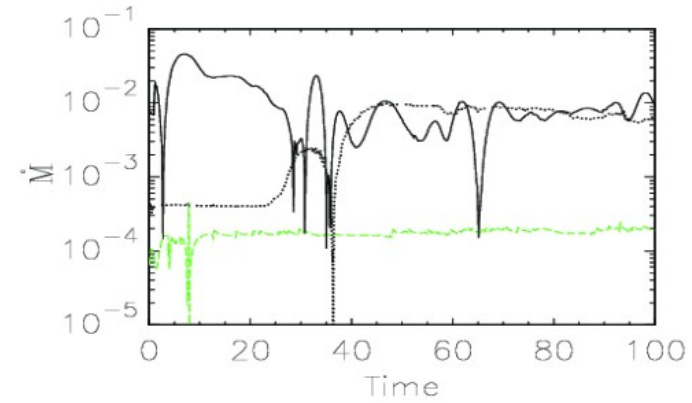


Fig. 5. Illustration of the quasi-stationarity in our magnetic case solutions, in the same units as in Fig. 3. *Top panel:* the

We can write the results in our simulations as simple functions obtained in KK00, with coefficients of proportionality we find from our simulations:

$$\rho(r, z) = \frac{k_1}{r^{3/2}} \left[1 - \left(\zeta_1 \frac{z}{r} \right)^2 \right]^{3/2}, \quad (69)$$

$$v_r(r, z) = \frac{k_2}{r^{1/2}} \left[1 + (\zeta_2 z)^2 \right], \quad (70)$$

$$v_z(r, z) \approx \frac{z}{r} v_r(r, z) = k_3 \frac{z}{r^{3/2}} \left[1 + (\zeta_3 z)^2 \right],$$

$$v_\varphi(r, z) = \frac{k_4}{\sqrt{r}}, \quad \Omega = \frac{v_\varphi}{r} = \frac{k_4}{r^{3/2}}.$$

Magnetic field components are proportional to r^{-3} , as expected for the dipole stellar field, and depend linearly on height above the disk midplane:

$$B_r(r, z) = \frac{k_5}{r^3} z, \quad B_z(r, z) = \frac{k_6}{r^3} z, \quad B_\varphi(r, z) = \frac{k_7}{r^3} z, \quad (71)$$

In the case of B_r , the linear dependence is a consequence of the boundary condition at the disk equatorial plane, where the magnetic field components are reflected, with the change in sign of the component tangential to the boundary. This means that the radial magnetic field component $B_r \rightarrow 0$ at the equatorial plane, and is slowly increasing above (and below) that plane, in the densest parts of the disk.

$$\eta(r, z) = \frac{k_8}{r} \left[1 - \left(\zeta_8 \frac{z}{r} \right)^2 \right]^2, \quad (72)$$

$$\eta_m(r, z) = k_9 \sqrt{r} \left[1 - \left(\zeta_9 \frac{z}{r} \right)^2 \right]^{1/2}.$$

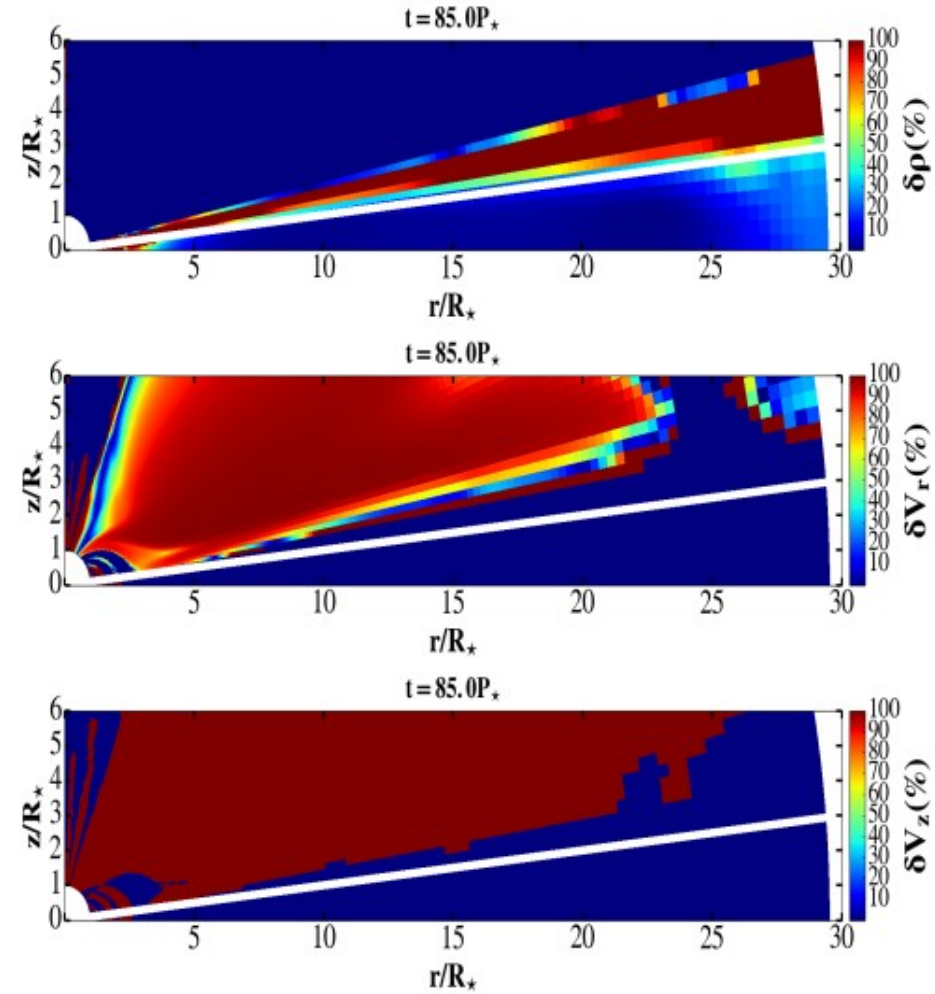


Fig. A.1. Difference between our numerical solutions and analytical expressions, in percentage of the value in the simulations. Our analytical solution is mostly inside the 10% margin everywhere inside the thin disk region, below the thick white solid line demarcating $h = 0.1r$ dependence, where h is the disk height. Close to the star and accretion column footpoint, our simulations are in the ideal MHD regime, so the analytical expressions fail there. It is also failing close to the outer boundary, where the material is fed into the disk by the amount based on the analytical solution in purely HD approach.

MKK- analytical expressions from the numerical solutions

Table 1. The proportionality coefficients in our simulations with $B_\star=0.5$ kG and 1 kG.

B(kG)	0.5		1	
coef.	R=6	R=15	R=6	R=15
$k_{1i} k_{1o}$	0.9		1.2	0.29
$k_{2i} k_{2o}$	-0.01	-0.006	$+1.2 \times 10^{-4}$	-2.9×10^{-3}
k_3	-2.65×10^{-4}		-4.4×10^{-3}	-3.6×10^{-5}
k_4	0.255		0.255	
$k_{5i} k_{5o}$	-0.69	-0.41	-1.25	
$k_{6i} k_{6o}$	-0.35	-0.15	-0.29	-0.19
$k_{7i} k_{7o}$	-2.8	-1.1	-8.2	-1.18
k_8	5.8×10^{-3}		$8. \times 10^{-3}$	
k_9	0.01		0.01	
ζ_1	5.		5.	
ζ_2	0.5		0.5	
ζ_8	5.		6.8	
ζ_9	6.		4.5	

Using this table, we can “prescribe” the disk-it will fairly well describe the disk, as we saw in the previous slide.

- We could plug in any other disk model and compare with simulations or other computation result
- We write such a script, for comparison of solutions.
- I supply a template in `mc_razlikaANnum.py`, it can easily be modified. We test it with one of the results from simulations.

Accretion disk simulations

- First numerical solution of (HD) accretion disk was by Prendergast & Burbidge (1968) (no pics!)
- Analytical solution was given by Shakura & Sunyaev (1973), with alpha-viscosity prescription.
- From that time to the 1990-ies many developments and models, with different approximations.
- In Kluźniak & Kita (2000) was given a solution of the HD disk in the full 3D. It was obtained by the method of asymptotic approximation (Taylor expansion).
- In 2009, numerical simulations of star-disk magnetospheric interaction were done in 2D-axisymmetric simulations, by Romanova et al. (2009, 2013, with non-public code), Zanni & Ferreira (2009, 2013, with modification of a publicly available code PLUTO v. 3.0).
- Development of disk simulations in the direction of MRI in the disk (Flock et al.), but nothing much in star-disk magnetospheric simulations for a decade.
- In Čemeljić et al. (2017) and Čemeljić (2019, “Atlas” paper), the first repeating of Zanni et al. (2009, 2013) axi-symmetric viscous & resistive MHD simulations in 2D with PLUTO code, v.4.1. The results are similar to Romanova et al., obtained with their (non-public) code with entropy conservation, not energy.
- In “Atlas” paper I performed a parameter study to investigate the influence of different parameters. This publication, especially its Appendix, is used here as a guide through setup and numerical methods.

Normalization in the code

Code works in the normalized units. For translating into other units, one needs to multiply with the corresponding scaling factors. When using Cooling, one needs to define units in definitions.h subroutine.

Table A.1. Typical values and scaling for different central objects.

	YSOs	WDs	NSs
$M_{\star}(M_{\odot})$	0.5	1	1.4
R_{\star}	$2R_{\odot}$	5000 km	10 km
P_{\star}	4.6 d	6.1 s	0.46 ms
B_{\star} (G)	500	5×10^5	10^8
ρ_{d0} (g cm^{-3})	1.2×10^{-10}	9.4×10^{-9}	4.6×10^{-6}
v_0 (km s^{-1})	218	5150	136 000
$\dot{M}_0(M_{\odot} \text{ yr}^{-1})$	5.7×10^{-7}	1.9×10^{-9}	10^{-9}
B_0 (G)	200	5×10^4	2.93×10^7

Equations solved by the code

- Code I used in “Atlas” is PLUTO (v.4.1) by Mignone et al. (2007, 2012). We will do it in v.4.4.3(=4.4.patch3)
- If the disk is to reach the quasi-stationary state, the Ohmic and viscous heating in the energy equation should be balanced with the source term. In such a case, we effectively neglect the dissipative terms in the energy equation-this is equal to the assumption that all the heat is radiated away from the disk.
- Viscosity and resistivity are still affecting the solution, in the equation of motion and in the induction equation.

$$\frac{\partial \rho}{\partial t} + \nabla \cdot (\rho \mathbf{v}) = 0$$

$$\frac{\partial \rho \mathbf{v}}{\partial t} + \nabla \cdot \left[\rho \mathbf{v} \mathbf{v} + \left(P + \frac{\mathbf{B} \cdot \mathbf{B}}{8\pi} \right) \mathbf{I} - \frac{\mathbf{B} \mathbf{B}}{4\pi} - \boldsymbol{\tau} \right] = \rho \mathbf{g}$$

$$\frac{\partial E}{\partial t} + \nabla \cdot \left[\left(E + P + \frac{\mathbf{B} \cdot \mathbf{B}}{8\pi} \right) \mathbf{v} - \frac{(\mathbf{v} \cdot \mathbf{B}) \mathbf{B}}{4\pi} \right] + \nabla \cdot \left[\underbrace{\eta_m \mathbf{J} \times \mathbf{B} / 4\pi - \mathbf{v} \cdot \boldsymbol{\tau}}_{\text{heating terms}} \right] = \rho \mathbf{g} \cdot \mathbf{v} - \underbrace{\Lambda}_{\text{cooling}}$$

$$\frac{\partial \mathbf{B}}{\partial t} + \nabla \times (\mathbf{B} \times \mathbf{v} + \eta_m \mathbf{J}) = 0$$

the gravity acceleration is $\mathbf{g} = -\nabla \Phi_g$, where the gravitational potential of the star with mass M_\star is equal to $\Phi_g = -GM_\star/R$. Then $g_R = -1.0/R^2$ in the code units.

$$\frac{\partial E}{\partial t} + \nabla \cdot \left[\left(E + P + \frac{\mathbf{B} \cdot \mathbf{B}}{8\pi} \right) \mathbf{u} - \frac{(\mathbf{u} \cdot \mathbf{B}) \mathbf{B}}{4\pi} \right] + \nabla \cdot \left[\eta_m \mathbf{J} \times \mathbf{B} / 4\pi - \mathbf{u} \cdot \boldsymbol{\tau} \right] = \rho \mathbf{g} \cdot \mathbf{u} - \Lambda_{\text{cool}}$$

Practical part: init.c file, Hydro-dynamical star-disk setup

The initial disk was set with the initial density ρ a self-similar profile and the aspect ratio ϵ :

$$\begin{aligned}\rho_d &= \rho_{d0} \left\{ \frac{\gamma - 1}{\gamma \epsilon^2} \left[\frac{R_\star}{R} - \left(1 - \frac{\gamma \epsilon^2}{\gamma - 1} \right) \frac{R_\star}{R \sin \theta} \right] \right\}^{1/(\gamma-1)} \\ &= \rho_{d0} \left\{ \frac{2}{5 \epsilon^2} \left[\frac{R_\star}{R} - \left(1 - \frac{5}{2} \epsilon^2 \right) \frac{R_\star}{R \sin \theta} \right] \right\}^{3/2}.\end{aligned}$$

The pressure was

$$\begin{aligned}P_d &= \epsilon^2 \rho_{d0} v_{K\star}^2 \left(\frac{\rho_d}{\rho_{d0}} \right)^\gamma = \\ &= \frac{\rho_{d0} v_{K\star}^2}{\epsilon^3} \left\{ \frac{2}{5} \left[\frac{R_\star}{R} - \left(1 - \frac{5 \epsilon^2}{2} \right) \frac{R_\star}{R \sin \theta} \right] \right\}^{5/2}\end{aligned}$$

The initial disk velocity profile is, following KK00:

$$\begin{aligned}v_{Rd} &= -\alpha_v \epsilon^2 \left[10 - \frac{32}{3} \Lambda \alpha_v^2 - \Lambda \left(5 - \frac{1}{\epsilon^2 \tan^2 \theta} \right) \right] \sqrt{\frac{GM_\star}{R \sin^3 \theta}}, \\ v_{R\phi} &= \left[\sqrt{1 - \frac{5 \epsilon^2}{2}} + \frac{2}{3} \epsilon^2 \alpha_v^2 \Lambda \left(1 - \frac{6}{5 \epsilon^2 \tan^2 \theta} \right) \right] \sqrt{\frac{GM_\star}{R \sin \theta}}\end{aligned}\quad (\text{A.10})$$

where

$$\Lambda = \frac{11}{5} / \left(1 + \frac{64}{25} \alpha_v^2 \right).\quad (\text{A.11})$$

In the corona, density and pressure are:

$$\begin{aligned}\rho_c &= \rho_{c0} (R_\star / R)^{1/(\gamma-1)}, \\ P_c &= \rho_{c0} \frac{\gamma - 1}{\gamma} \frac{GM_\star}{R_\star} \left(\frac{R_\star}{R} \right)^{\gamma/(\gamma-1)}\end{aligned}$$

Viscosity tensor is given by Landau-Lifshitz def:

$$\tau = \eta_v \left[(\nabla \mathbf{v}) + (\nabla \mathbf{v})^T - \frac{2}{3} (\nabla \cdot \mathbf{v}) \mathbf{I} \right],\quad (\text{A.7})$$

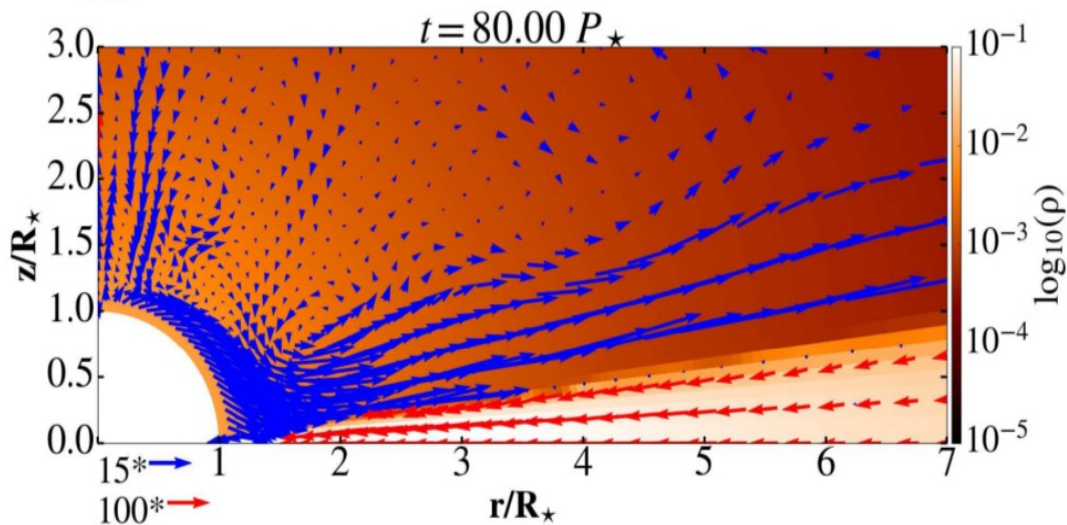
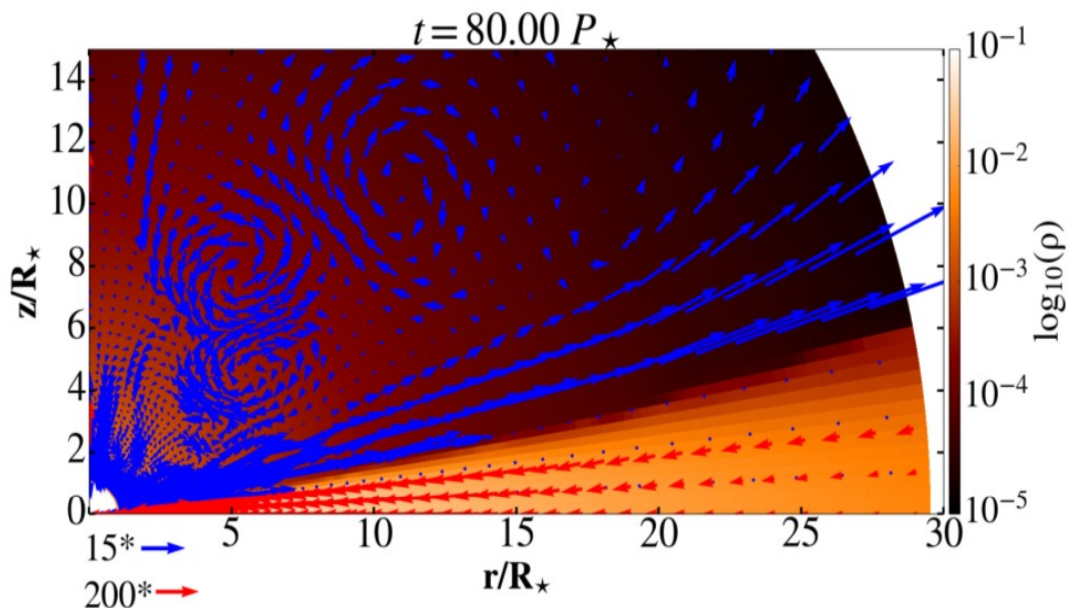
with the dynamic viscosity $\eta_v = \rho \nu_v$ given with

$$\eta_v = \frac{2}{3} \rho \alpha_v \left[c_s^2(r)|_{z=0} + \frac{2}{5} \left(\frac{GM_\star}{R} - \frac{GM_\star}{r} \right) \right] \sqrt{\frac{r^3}{GM_\star}},\quad (\text{A.8})$$

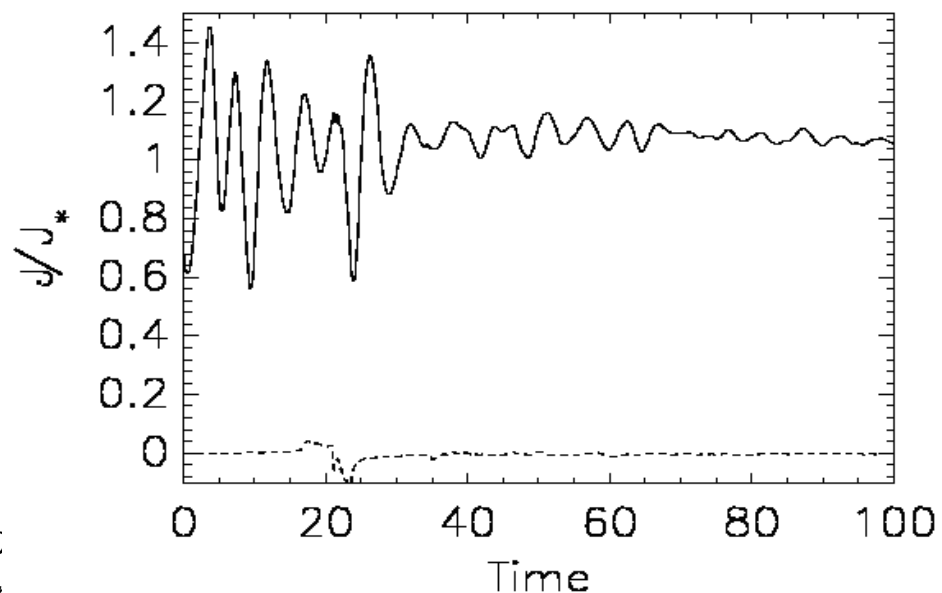
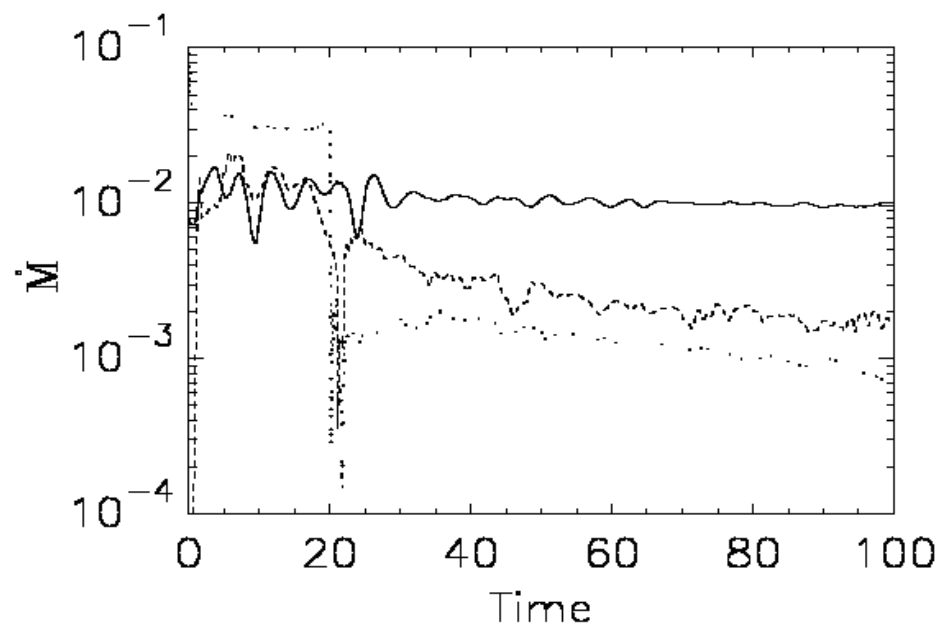
where ν_v is the kinematic viscosity. The magnetic diffusivity was assumed proportional to the viscosity, with the free parameter

$$\nu_m = \frac{3}{2} \alpha_m \frac{\nu_v}{\alpha_v},$$

Practical part: results in Hydro-dynamical star-disk simulations



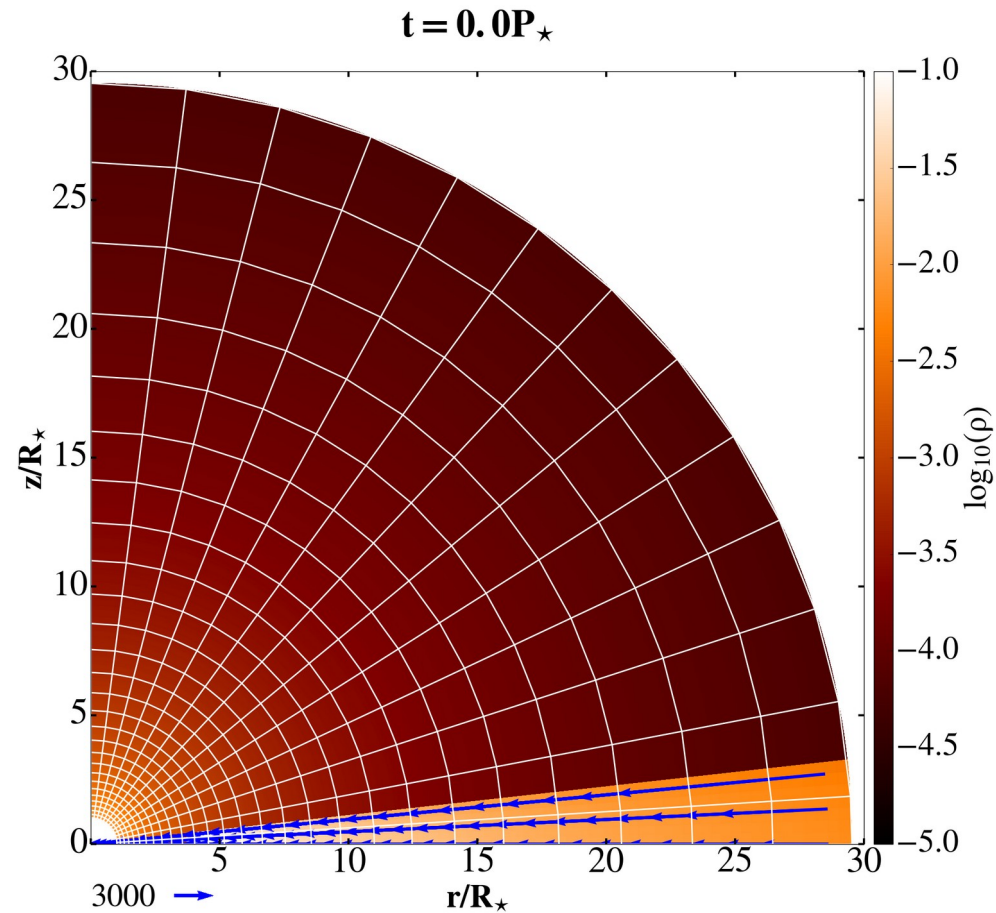
Ideally, this is what we wish to obtain. Computational bc and a zoom closer to the star after 80 stellar rotations. In color is shown the density, and vectors show velocity, with the different normalization in the disk and stellar wind.



Time dependence of the mass and angular momentum fluxes in the various components in our simulations.

Star-disk simulations setup

- The Kluźniak-Kita (2000) analytical solution is purely HD.
- We will start with the HD disk, and then add the magnetic field.
- Stellar surface is a rotating boundary around the origin of the spherical computational domain. In the non-magnetic setup, it is just a simple setup with “absorption” of the flow atop the stellar surface—we assume the star to be a (differentially) rotating magnetized rotator.
- The initial corona is a non-rotating corona in a hydrostatic balance with the 100 times denser disk below it. After short relaxation, lasting for the few stellar rotations, corona starts rotating, following the disk.



Logarithmic grid in a star-disk simulations setup

The image shows a PDF viewer window titled "Pluto44usgui.pdf". The page number is 31 (32 of 151). The table of contents on the left lists various sections, with "The [Grid] block" highlighted at page 30. The main text on the page discusses logarithmic grids in star-disk simulations.

In practice, the mesh spacing in the $l+$ grid is obtained by reversing the spacing in the $l-$ grid.

Note: The interval should not include the origin when using a logarithmic grid.

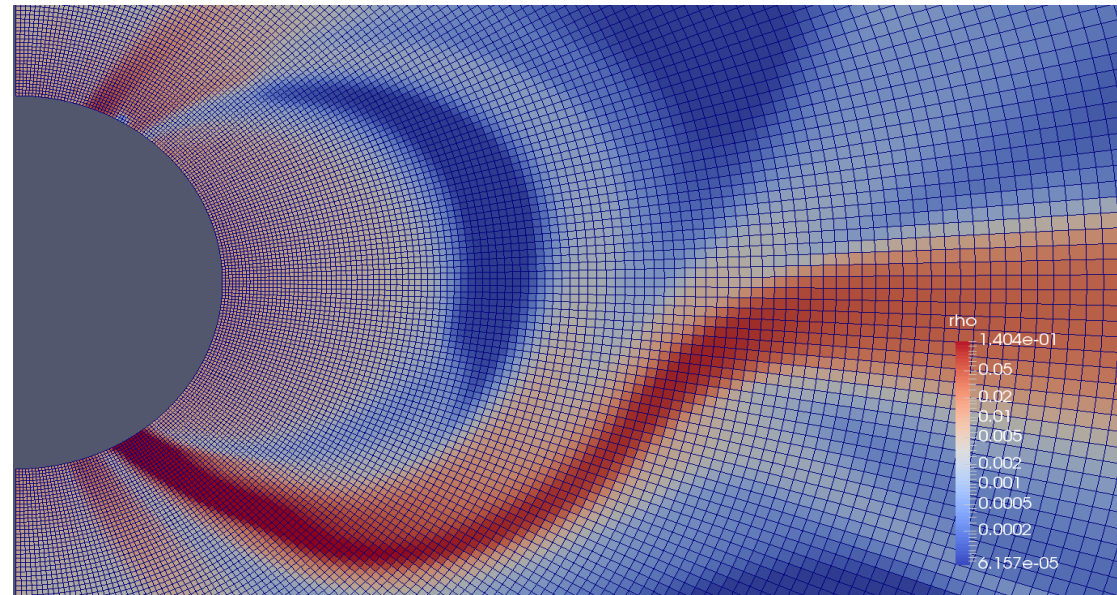
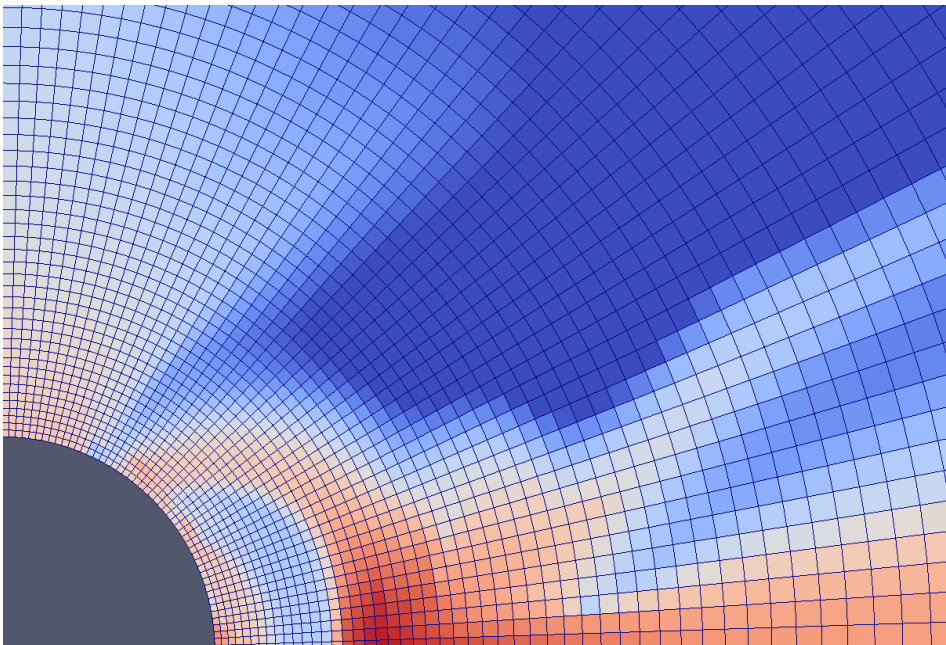
In *CYLINDRICAL* or *SPHERICAL* coordinates, a radial logarithmic grid has the advantage of preserving the cell aspect ratio at any distance from the origin. In addition, the condition to obtain approximately squared cells (aspect ratio ≈ 1) is $\Delta r_1 \approx r_1 \Delta \phi$ where $\Delta r_1 = r_L (e^{\Delta \xi} - 1)$ is the radial spacing of the first active computational zone. This condition can be used to determine either the number of points in the radial direction or the endpoint:

$$\log_{10} \frac{r_R}{r_L} = N_r \log_{10} \frac{2 + \Delta \phi}{2 - \Delta \phi}.$$

Beware that non-uniform grids may introduce extra dissipation in the algorithm. Changes in the grid spacing are correctly accounted for when RECONSTRUCTION is set to either *LINEAR*, *PARABOLIC* or *WENO3*.

Resolution needed in a setup

- Resolution in my production runs is $R \times \theta = [217 \times 100]$ grid cells in $\theta = [0, \pi/2]$, with a logarithmic grid spacing in the radial direction. For testing I also use $R \times \theta = [109 \times 50]$ grid cells, which gives qualitatively correct results.
- The accretion column is well resolved **if a rule of thumb is satisfied that there is at least that many grid cells how many there is independent variables** (5 in HD case, 8 in MHD case in our setups: density, pressure, 3 components of \mathbf{v} and \mathbf{B}).
- Star rotates at about 1/10 of the breakup rotational velocity.
- I did also $\theta = [0, \pi]$ cases in $R \times \theta = [217 \times 200]$ grid cells, as well as $R \times \theta = [109 \times 100]$ grid cells. Now there is no need to define the equatorial boundary condition, the simulation self-consistently computes across the domain. This case usually leads to an asymmetry with respect to the equatorial plane-I will show more on this in the last lecture.



```

I      pluto.ini (ini)
[[Grid]]
X1-grid  1      1.0      109      l+      30.
X2-grid  1      0.0      50       u       1.570796
X3-grid  1      0.0      1        u       1.0

[[Chombo Refinement]]

Levels           4
Ref_ratio        2 2 2 2 2
Regrid_interval  2 2 2 2
Refine_thresh    0.3
Tag_buffer_size  3
Block_factor     8
Max_grid_size    64
Fill_ratio       0.75

[[Time]]

CFL              0.4
CFL_max_var      1.2
tstop            628.3185
first_dt         1.e-6

[[Solver]]

Solver           hll

```

Star-disk: pluto.ini

```

I      pluto.ini (Modified)(ini)
[[Boundary]]
X1-beg      userdef
X1-end      userdef
X2-beg      axisymmetric
X2-end      eqtsymmetric
X3-beg      outflow
X3-end      outflow

[[Static Grid Output]]
uservar     3 nu num Te
dbl         6.283185 -1  single_file
flt         -1.0 -1  single_file
vtk         6.283185 -1  single_file
tab         -1.0 -1
dbl.h5      -6.279 -1
ppm         -1.0 -1
png         -1.0 -1
log         100
analysis    -1.0 -1

[[Parameters]]

ALPHAM      0.4
MU          0.07
TEMPF      800.0
RHOC       0.01
RD         3.7
EPS        0.1
OMG        0.1
ALPHAV     1.0
DFLOOR     5.e-7

```

Star-disk: definitions.h

```
I A definitions.h (c)
#define PHYSICS MHD
#define DIMENSIONS 2
#define GEOMETRY SPHERICAL
#define BODY_FORCE VECTOR
#define COOLING NO
#define RECONSTRUCTION LINEAR
#define TIME_STEPPING RK2
#define NTRACER 1
#define PARTICLES NO
#define USER_DEF_PARAMETERS 9

/* -- physics dependent declarations -- */

#define EOS IDEAL
#define ENTROPY_SWITCH NO
#define DIVB_CONTROL CONSTRAINED_TRANSPORT
#define BACKGROUND_FIELD YES
#define AMBIPOLAR_DIFFUSION NO
#define RESISTIVITY EXPLICIT
#define HALL_MHD NO
#define THERMAL_CONDUCTION NO
#define VISCOSITY EXPLICIT
#define RADIATION NO
#define ROTATING_FRAME NO

/* -- user-defined parameters (labels) -- */
```

```
I A definitions.h (c)
/* -- user-defined parameters (labels) -- */
#define ALPHAM 0
#define MU 1
#define TEMPF 2
#define RHOC 3
#define RD 4
#define EPS 5
#define OMG 6
#define ALPHAV 7
#define DFLOOR 8

/* [Beg] user-defined constants (do not change this line) */
#define WARNING_MESSAGES NO
#define INTERNAL_BOUNDARY YES
#define SHOCK_FLATTENING MULTID
#define CT_EN_CORRECTION YES
#define UNIT_DENSITY 8.5e-11
#define UNIT_LENGTH 1.392e11
#define UNIT_VELOCITY 2.1839e7
#define VTK_VECTOR_DUMP YES
#define CT_EMF_AVERAGE ARITHMETIC
#define LIMITER VANLEER_LIM

/* [End] user-defined constants (do not change this line) */
```

Star-disk: init.c

```
I A init.c (c) Row 1 Col 1 2:55 Ctrl-K H for help
/* //////////////////////////////////////////////////////////////////// */
/*
 \file
 \brief Contains basic functions for problem initialization.

The init.c file collects most of the user-supplied functions useful
for problem configuration.
It is automatically searched for by the makefile.

 \author A. Mignone (mignone@ph.unito.it)
 \date Sep 10, 2012

 \modified by M. Cemeljic (miki@camk.edu.pl)
 \date July 2020
Below is given Miki's stripped, minimal version of the setup in ideal MHD,
for teaching purpose in SHA0. It is not meant to produce quasi-stationary
or any publication-worthy result, but to provide a platform for teaching.
It is based on the setup described in Appendix of "Atlas" paper,
Cemeljic, 2019, A&A, 624, A31.
*/
/* //////////////////////////////////////////////////////////////////// */
#include "pluto.h"

/* ***** */
void Init (double *v, double x1, double x2, double x3)
/*
***** */
{
double coeff, eps2, pc, rcyl;
double br, bth;
double lambda;
double xhi2, Rco;

I A init.c (c) void Init (double *v, double x1, double x2, double x3) Row 36 Col 1 2:56 Ctrl-K H for help
rcyl=x1*sin(x2);
eps2=g_inputParam[EPS]*g_inputParam[EPS];
coeff=2./5./eps2*(1./x1-(1.-5./2.*eps2)/rcyl);
lambda=11./5./(1.+64./25.*g_inputParam[ALPHAV]*g_inputParam[ALPHAV]);

/* initial non-rotating adiabatic corona in hydrostatic equilibrium */
v[RHO] = g_inputParam[RHOC]*pow(x1,-3./2.);
v[PRS] = 2./5.*g_inputParam[RHOC]*pow(x1,-5./2.);

pc=v[PRS];

v[VX1] = 0.0;
v[VX2] = 0.0;
v[VX3] = 0.0;

/* Keplerian adiabatic disk in vertical pressure equilibrium with the
adiabatic corona, as given by Kluzniak & Kita (2000) */

v[PRS]=eps2*pow(coeff,5./2.);

if (v[PRS] >= pc && rcyl > g_inputParam[RD])
{v[RHO] = pow(coeff,3./2.);
v[VX1] = -g_inputParam[ALPHAV]/sin(x2)*eps2*(10.-32./3.
*lambda*g_inputParam[ALPHAV]*g_inputParam[ALPHAV]
-lambda*(5.-1./(eps2*tan(x2)*tan(x2)))/sqrt(rcyl);
v[VX3] = (sqrt(1.-5./2.*eps2)+2./3.*eps2
*g_inputParam[ALPHAV]*g_inputParam[ALPHAV]
*lambda*(1.-6./(5.*eps2*tan(x2)*tan(x2)))/sqrt(rcyl);
v[TRC] = 1.0; /* Track the disc material */
}
else
{
v[PRS]=2./5.*g_inputParam[RHOC]*pow(x1,-5./2.);
v[TRC] = 0.0; /* Track the corona */
}
}
```

Star-disk: paraview

ParaView 5.7.0

File Edit View Sources Filters Tools Catalyst Macros Help

Time: 0 0 (max is 9)

Representa

NS_current.pvsm

Output Messages Pipeline Browser

Pipeline Browser

- builtin:
- data.000*
- AnnotateTimeFilter1
- PlotOverLine1

Properties Information

Properties

Apply Reset Delete ?

Search ... (use Esc to clear text)

Center on Bounds

Resolution 1000

Display (XYChartRepreser)

Attribute Type Point Data

X Axis Parameters

Use Index For XAxis

Layout #1 +

RenderView1

Time: 0.000000

LineChartView1

Color Map Editor

Search ... (use Esc to cl...)

Array Name: <none>

Render Views

Selection Display Inspector

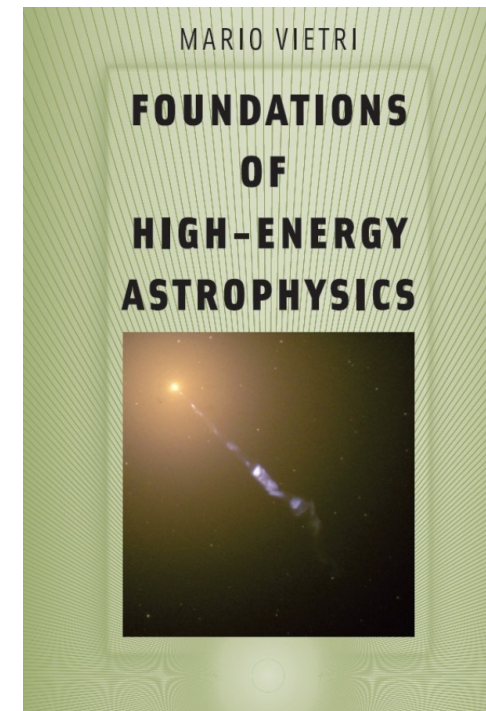
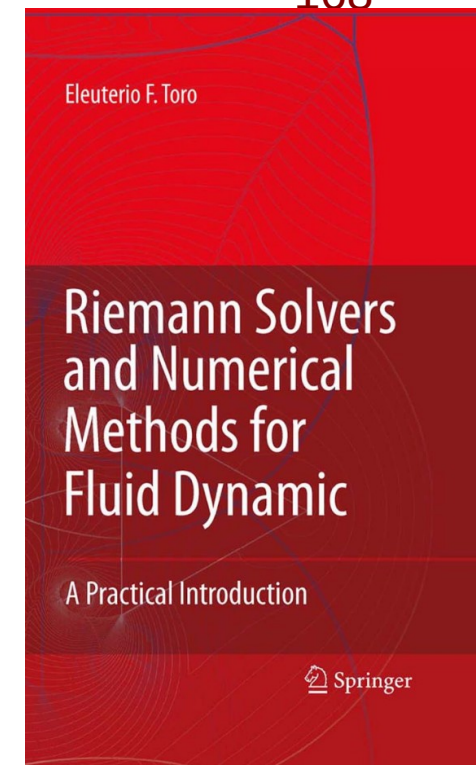
- Cell Labels
- Point Labels
- Selection Color
- Interactive Selection Color

Summary of the Lect. 4

- Approximate, vertically averaged solutions for thin disc
- Kluźniak-Kita 3D solution for thin disc
- Setup of 2.5D HD KK disc in PLUTO
- Analysis of the results with Paraview

Outline, Lect.5 : Numerics essentials and magnetic KK disc

- Riemann problem, Finite difference, Godunov's method, volume and elements methods, CFL condition, RK2, RK3, ...
- Setup and running of 2.5D MHD KK disc in PLUTO
- Analysis of the results from 2.5D magnetic runs with Paraview and Python



Primitive and conservative variables

In the computational fluid dynamics (CFD) we speak about primitive and conservative variables and approximate Riemann solvers all the time, what is it about? I follow the Eleuterio Toro book here: *E.F. Toro. Riemann Solvers and Numerical Methods for Fluid Dynamics. 2009*

- We consider the time–dependent Euler equations: a system of non–linear hyperbolic conservation laws that govern the dynamics of a compressible material, such as gases or liquids at high pressures, for which the effects of body forces, viscous stresses and heat flux are neglected.
- We have a freedom in choosing a set of variables to describe the flow. Usual choice are
 - a) *primitive* variables: $\rho(x, y, z, t)$ = density or mass density, $p(x, y, z, t)$ = pressure, the velocity vector $V = (u, v, w)$ where $u, v, w(x, y, z, t)$ are x, y, z –components of velocity, respectively
 - b) *conserved* variables: the mass density ρ , the momentum components $\rho(u, v, w)$, where u, v, w are the x, y, z momentum components, respectively, and the total energy per unit mass E . The conserved quantities result naturally from the application of the fundamental laws of conservation of mass, Newton’s Second Law and the law of conservation of energy. Computationally, there are some advantages in expressing the governing equations in terms of the conserved variables. This gives rise to a large class of numerical methods called conservative methods.
- We next state the equations in terms of the conserved variables under the assumption that the quantities involved are sufficiently smooth to allow for the operation of differentiation to be defined. Later we remove this smoothness constraint to allow for solutions containing discontinuities, such as shock waves.

Euler equations

The five governing conservation laws are

$$\rho_t + (\rho u)_x + (\rho v)_y + (\rho w)_z = 0 , \quad (1.1)$$

$$(\rho u)_t + (\rho u^2 + p)_x + (\rho uv)_y + (\rho uw)_z = 0 , \quad (1.2)$$

$$(\rho v)_t + (\rho uv)_x + (\rho v^2 + p)_y + (\rho vw)_z = 0 , \quad (1.3)$$

$$(\rho w)_t + (\rho uw)_x + (\rho vw)_y + (\rho w^2 + p)_z = 0 , \quad (1.4)$$

$$E_t + [u(E + p)]_x + [v(E + p)]_y + [w(E + p)]_z = 0 . \quad (1.5)$$

Here E is the total energy per unit volume

$$E = \rho \left(\frac{1}{2} \mathbf{V}^2 + e \right) , \quad (1.6)$$

where

$$\frac{1}{2} \mathbf{V}^2 = \frac{1}{2} \mathbf{V} \cdot \mathbf{V} = \frac{1}{2} (u^2 + v^2 + w^2)$$

is the *specific kinetic energy* and e is the *specific internal energy*. One generally refers to the full system (1.1)–(1.5) as the Euler equations, although strictly speaking the Euler equations are just (1.2)–(1.4).

The conservation laws (1.1)–(1.5) can be written more compact by defining a column vector \mathbf{U} of conserved variables and flux vectors $\mathbf{F}(\mathbf{U})$, $\mathbf{G}(\mathbf{U})$, $\mathbf{H}(\mathbf{U})$ in the x , y and z directions, respectively.

Euler equations

We have now

$$\mathbf{U}_t + \mathbf{F}(\mathbf{U})_x + \mathbf{G}(\mathbf{U})_y + \mathbf{H}(\mathbf{U})_z = \mathbf{0}, \quad (1.7)$$

with

$$\left. \begin{aligned} \mathbf{U} &= \begin{bmatrix} \rho \\ \rho u \\ \rho v \\ \rho w \\ E \end{bmatrix}, \quad \mathbf{F} = \begin{bmatrix} \rho u \\ \rho u^2 + p \\ \rho uv \\ \rho uw \\ u(E + p) \end{bmatrix}, \\ \mathbf{G} &= \begin{bmatrix} \rho v \\ \rho uv \\ \rho v^2 + p \\ \rho vw \\ v(E + p) \end{bmatrix}, \quad \mathbf{H} = \begin{bmatrix} \rho w \\ \rho uw \\ \rho vw \\ \rho w^2 + p \\ w(E + p) \end{bmatrix}. \end{aligned} \right\} \quad (1.8)$$

The flux vectors $\mathbf{F} = \mathbf{F}(\mathbf{U})$, $\mathbf{G} = \mathbf{G}(\mathbf{U})$, $\mathbf{H} = \mathbf{H}(\mathbf{U})$ are functions of the conserved variable vector \mathbf{U} . Any system of the PDE's written like eq. 1.7 is called a system of conservation laws. The differential formulation assumes smooth solutions, that is, partial derivatives are assumed to exist. There are other ways of expressing conservation laws in which the smoothness assumption is relaxed to include discontinuous solutions.

Euler equations

In eqs. 1.1-1.5 we have more unknowns than equations. Relation (1.6) defines the total energy E in terms of the velocity vector \mathbf{V} from equations (1.1)–(1.5) and a new variable e , the specific internal energy. We need relation defining e in terms of other quantities, like pressure and density, as a closure condition. If we add more physical effects to the basic equations (1.1)–(1.5), other variables, e.g. temperature, might enter the equations. Here we are only interested in p – v – T systems, where we can relate the variables by the thermal equation of state $T = T(p, v)$.

We could also have $p = p(T, v)$ or $v = v(T, p)$.

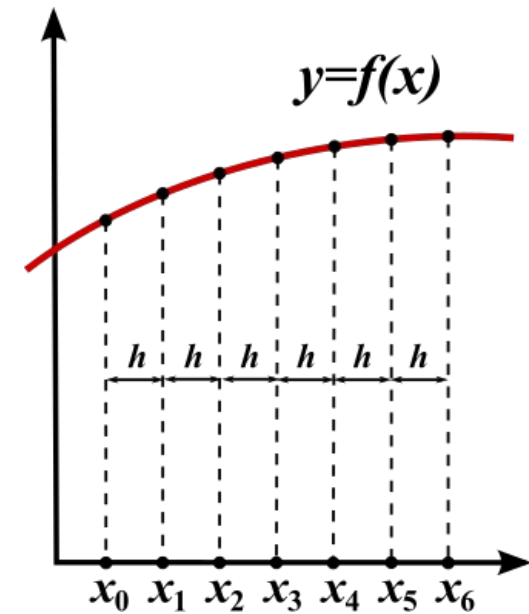
For thermally ideal gases we have $T = pv/R$, with R constant depending on the particular gas. We consider gases obeying the ideal thermal EOS $pV = nRT$, where R is the universal gas constant $R = 8.134 \times 10^3$ J/kilomole/K and T is measured in K (kelvins).

The initial–value problem for the special case of the linear advection equation is given with

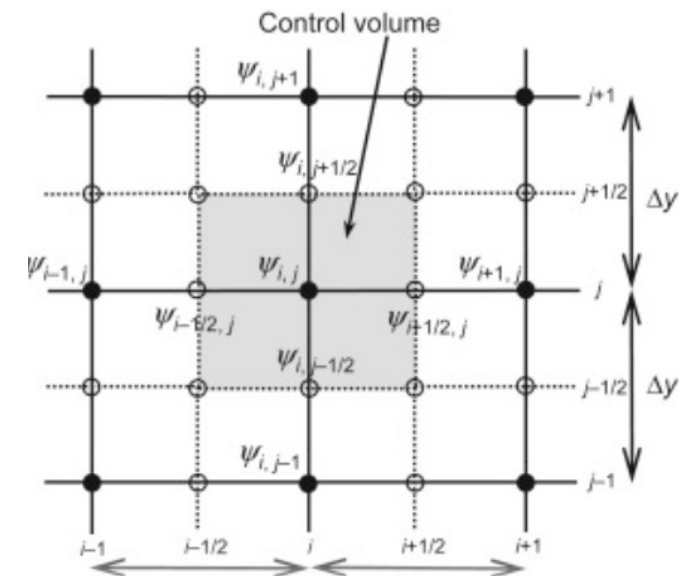
$$\left. \begin{array}{l} \text{PDE: } u_t + au_x = 0, \quad -\infty < x < \infty, \quad t > 0. \\ \text{IC: } \quad \quad \quad u(x, 0) = u_0(x), \end{array} \right\} \quad (2.32)$$

where a is a constant wave propagation speed. The initial data at time $t = 0$ is a function of x alone and is denoted by $u_0(x)$.

Finite difference method: numerical technique for solving differential equations by approximating derivatives with finite differences. The spatial domain (and time domain in time-dependent problems) is discretized, or broken into a finite number of intervals, and the values of the solution at the end points of the intervals are approximated by solving algebraic equations containing finite differences and values from nearby points. In a consequence, ordinary differential equations (ODE) or partial differential equations (PDE), which may be nonlinear, are converted into a system of linear equations that can be solved by matrix algebra techniques.



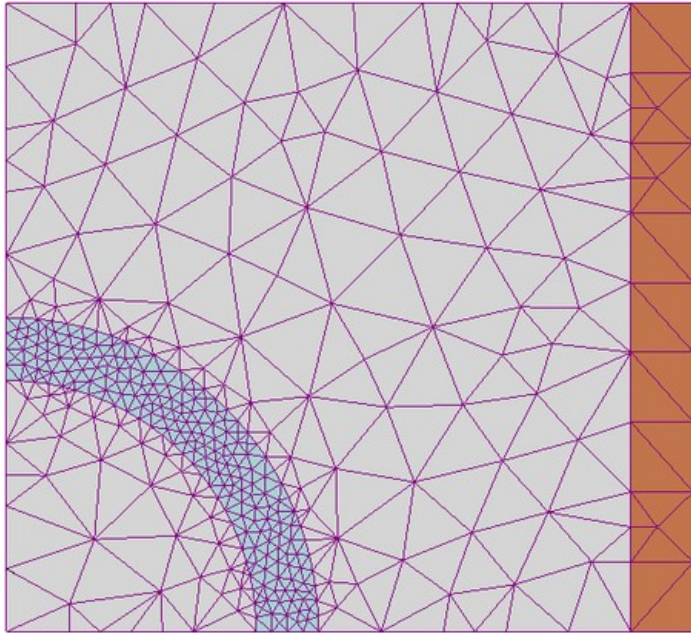
Finite volume method: the name refers to the small volume surrounding each node point on a mesh. Volume integrals in a partial differential equation that contain a divergence term are converted to surface integrals, using the divergence theorem. These terms are then evaluated as fluxes at the surfaces of each finite volume. Because the flux entering a volume is identical to the flux exiting the neighbor volume, finite volume methods are conservative. Finite volume method is easily formulated to allow for unstructured meshes.



This is a conservative finite volume method which solves exact or approximate Riemann problems at each inter-cell boundary. In its basic form (1959), Godunov's method is first order accurate in both space and time, yet can be used as a base scheme for developing higher-order methods. $U(x)$ is approximated by \bar{U}_{ijk} . This is the piece-wise constant approximation where the whole cell is assumed to have constant values for each variable in the vector of conserved quantities.

At the interface between each cell we then have a discontinuity, a left and right state, U_R and U_L , with corresponding left and right fluxes from which we need to produce a single vector of fluxes. This is what is referred to as the Riemann problem. In one dimension, it consists of two fluids with different but constant states separated by an imaginary membrane. The membrane is then removed and the system evolves in time. We are then interested in what the fluxes are at the location of this membrane at some later time after the system begins to evolve.

Finite element method: a large system is subdivided into simpler parts called finite elements. A mesh is constructed for the object: the numerical domain for the solution, which has a finite number of points. With a given boundary values, this finally results in a system of algebraic equations. The method approximates the unknown function over the domain. The simple equations that model these finite elements are then assembled into a larger system of equations that models the entire problem. The solution is approximated by minimizing an associated error function via the calculus of variations.

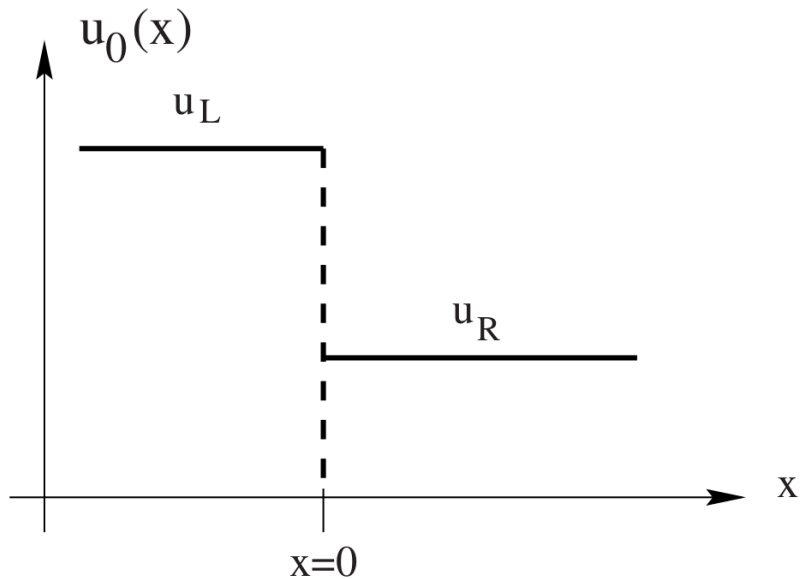


Riemann problem

Riemann problem is a special problem where

$$\left. \begin{array}{l} \text{PDE:} \quad u_t + au_x = 0 . \\ \text{IC:} \quad u(x, 0) = u_0(x) = \begin{cases} u_L & \text{if } x < 0 , \\ u_R & \text{if } x > 0 , \end{cases} \end{array} \right\} \quad (2.40)$$

With two constant values u_L (left) and u_R (right), as shown in Fig.2.2.below.

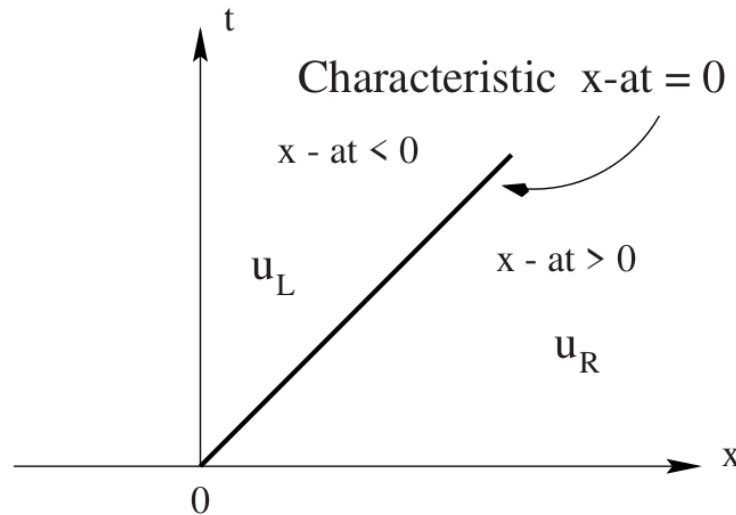


The initial data has a discontinuity at $x = 0$. IVP (2.40) is the simplest initial–value problem. The trivial case would be for $u_L = u_R$.

Fig. 2.2. Illustration of the initial data for the Riemann problem. At the initial time the data consists of two constant states separated by a discontinuity at $x = 0$

Riemann problem

We expect any point on the initial profile to propagate a distance $d = at$ in time t . In particular, we expect the initial discontinuity at $x = 0$ to propagate a distance $d = at$ in time t . The particular characteristic curve $x = at$ will then separate those characteristic curves to the left, on which the solution takes on the value u_L , from those curves to the right, on which the solution takes on the value u_R ; see Fig. 2.3.



The solution of the Riemann problem can be represented in the x - t plane. Through any point x_0 on the x -axis we can draw a characteristic. For the constant a , these are all parallel to each other. For the solution of the Riemann problem the characteristic passing through $x = 0$ is the only one across which the solution changes.

Fig. 2.3. Illustration of the solution of the Riemann problem in the x - t plane for the linear advection equation with positive characteristic speed a

The solution of the Riemann problem (2.40) is simply

$$u(x, t) = u_0(x - at) = \begin{cases} u_L & \text{if } x - at < 0, \\ u_R & \text{if } x - at > 0. \end{cases} \quad (2.41)$$

Riemann problem

We had the simplest PDE of hyperbolic type, the linear advection, with constant wave propagation speed. If we extend the analysis to sets of m hyperbolic PDEs of the form

$$\mathbf{U}_t + \mathbf{A}\mathbf{U}_x = \mathbf{0} , \quad (2.42)$$

where the coefficient matrix \mathbf{A} is constant, with the assumption of hyperbolicity \mathbf{A} has m real eigenvalues λ_i and m linearly independent eigenvectors \mathbf{K}^i , $i = 1, \dots, m$.

We study the Riemann problem for the hyperbolic, constant coefficient system (2.42). This is the special IVP

$$\left. \begin{array}{l} \text{PDEs: } \mathbf{U}_t + \mathbf{A}\mathbf{U}_x = \mathbf{0} , \quad -\infty < x < \infty , \quad t > 0 , \\ \text{IC: } \quad \mathbf{U}(x, 0) = \mathbf{U}^{(0)}(x) = \begin{cases} \mathbf{U}_L & x < 0 , \\ \mathbf{U}_R & x > 0 \end{cases} \end{array} \right\} \quad (2.54)$$

and is a generalisation of the IVP (2.32). We assume that the system is *strictly hyperbolic* and we order the real and distinct eigenvalues as

$$\lambda_1 < \lambda_2 < \dots < \lambda_m . \quad (2.55)$$

Riemann problem

The structure of the solution of the Riemann problem (2.54) in the x - t plane is depicted in Fig. 2.4. It consists of m waves emanating from the origin, one for each eigenvalue λ_i . Each wave i carries a jump discontinuity in \mathbf{U} propagating with speed λ_i . Naturally, the solution to the left of the λ_1 -wave is simply the initial data \mathbf{U}_L and to the right of the λ_m -wave is \mathbf{U}_R . The task is to find the solution in the wedge between the λ_1 and λ_m waves. As the eigenvectors K^1, \dots, K^m are linearly independent, we can expand the data \mathbf{U}_L , constant left state, and \mathbf{U}_R , constant right state, as linear combinations of the set K^1, \dots, K^m .

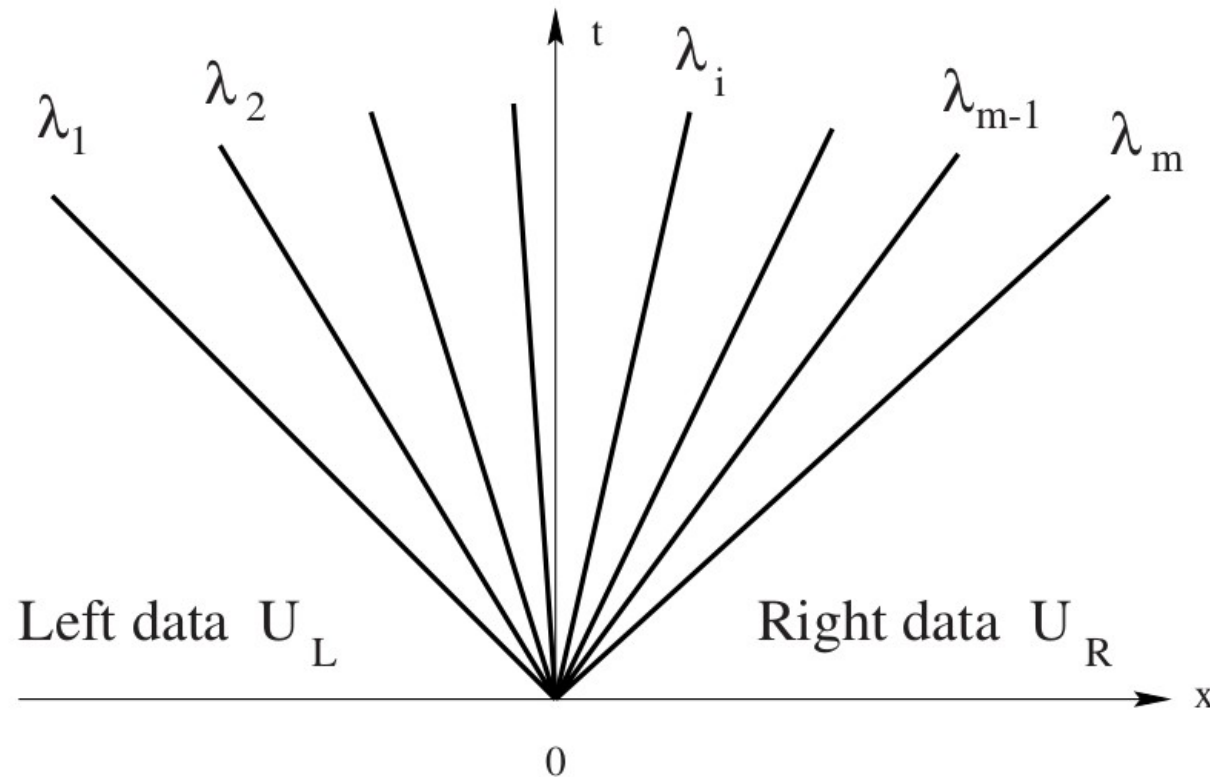


Fig. 2.4. Structure of the solution of the Riemann problem for a general $m \times m$ linear hyperbolic system with constant coefficients

$$\mathbf{U}_L = \sum_{i=1}^m \alpha_i \mathbf{K}^{(i)}, \quad \mathbf{U}_R = \sum_{i=1}^m \beta_i \mathbf{K}^{(i)}, \quad (2.56)$$

with constant coefficients α_i, β_i , for $i = 1, \dots, m$. Formally, the solution of the IVP (2.54) is given by (2.53) in terms of the initial data $w_i^{(0)}(x)$ for the characteristic variables and the right eigenvectors $\mathbf{K}^{(i)}$. Note that each of the expansions in (2.56) is a special case of (2.53). In terms of the characteristic variables we have m scalar Riemann problems for the PDEs

$$\frac{\partial w_i}{\partial t} + \lambda_i \frac{\partial w_i}{\partial r} = 0, \quad (2.57)$$

with initial data obtained by comparing (2.56) with (2.53), that is

$$w_i^{(0)}(x) = \begin{cases} \alpha_i & \text{if } x < 0, \\ \beta_i & \text{if } x > 0, \end{cases} \quad (2.58)$$

for $i = 1, \dots, m$. From the previous results, see equation (2.50), we know that the solutions of these scalar Riemann problems are given by

$$w_i(x, t) = w_i^{(0)}(x - \lambda_i t) = \begin{cases} \alpha_i & \text{if } x - \lambda_i t < 0, \\ \beta_i & \text{if } x - \lambda_i t > 0. \end{cases} \quad (2.59)$$

For a given point (x, t) there is an eigenvalue λ_I such that $\lambda_I < \frac{x}{t} < \lambda_{I+1}$, that is $x - \lambda_i t > 0 \forall i$ such that $i \leq I$. We can thus write the final solution to the Riemann problem (2.54) in terms of the original variables as

$$\mathbf{U}(x, t) = \sum_{i=I+1}^m \alpha_i \mathbf{K}^{(i)} + \sum_{i=1}^I \beta_i \mathbf{K}^{(i)}, \quad (2.60)$$

where the integer $I = I(x, t)$ is the maximum value of the sub-index i for which $x - \lambda_i t > 0$.

The Riemann problem can be solved exactly in some cases. A common test problem for computational fluid codes is the Sod shock tube problem, Sod (1978), a specific case of the Riemann problem which has a semi-analytical solution. You started PLUTO learning with this problem. However, such methods are usually time consuming, and if they have to be computed at every cell interface for every time step, it becomes impractical. It is much easier, and usually nearly as effective to use an approximate solution.

Courant-Friedrichs-Lewy condition: Richard Courant, Kurt Friedrichs, and Hans Lewy described it in their 1928 paper.

If a wave is moving across a discrete spatial grid and we want to compute its amplitude at discrete time steps of equal duration, this duration must be less than the time for the wave to travel to neighbor grid points. If we decrease the grid point separation, the upper limit for the time step also decreases.

$$\frac{\partial w}{\partial t} = u \frac{\partial w}{\partial x}.$$

- In the 1D case, for a quantity w The CFL condition then the dimensionless number C is the Courant number, u is the velocity the time step and length intervals

$$C = \frac{u \Delta t}{\Delta x} \leq C_{\max}$$

are Δt and Δx . The value of C_{\max} changes with the method discretization-it also depends if the method is explicit or implicit. If explicit (time-marching) solver is used then typically $C_{\max} = 1$. Implicit (matrix) solvers are usually less sensitive to numerical instability and so larger values of C_{\max} may be tolerated.

- In 2D: $C = \frac{u_x \Delta t}{\Delta x} + \frac{u_y \Delta t}{\Delta y} \leq C_{\max}$

- In nD:

general CFL condition for the n -dimensional case

$$C = \Delta t \left(\sum_{i=1}^n \frac{u_i}{\Delta x_i} \right) \leq C_{\max}.$$

Euler's method and the improved Euler's method are the simplest examples of a whole family of numerical methods to approximate the solutions of differential equations called Runge-Kutta methods. A numerical technique (year ~1900) used to solve an ordinary differential equation of the form $dy/dx=f(x,y)$, $y(x_0)=y_0$

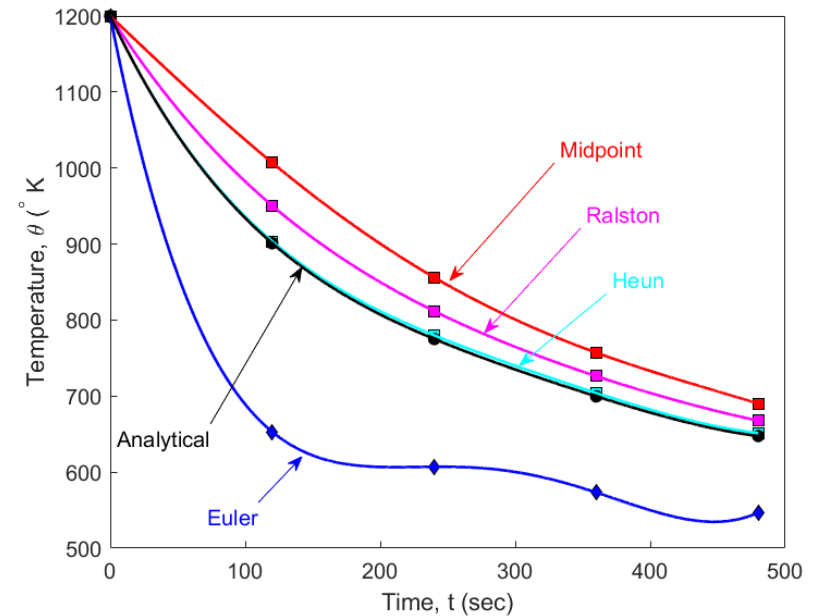
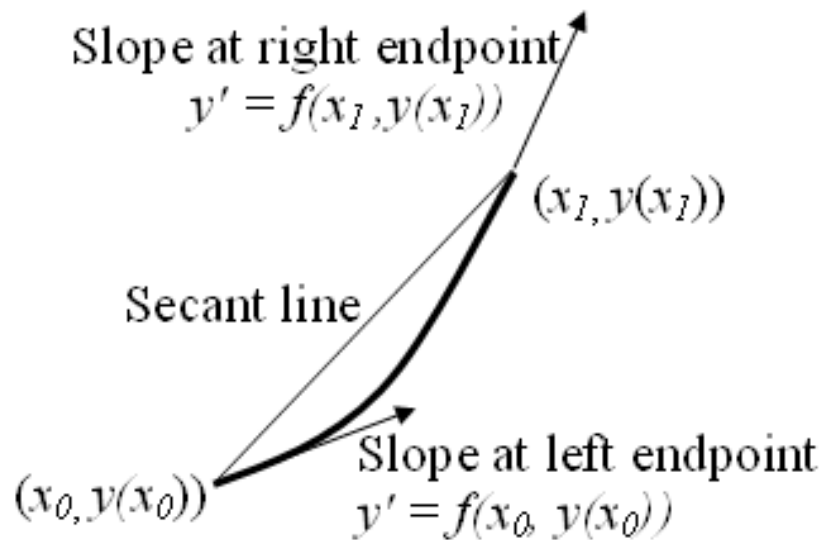
Euler's method is the first member of RK-solvers family: $y_{i+1}=y_i+f(x_i,y_i)h$ with $y(x_0)=y_0$ it is $h=x_{i+1}-x_i$, from the Taylor series, $dy/dx=f(x,y)$, we have

$$y_{i+1}=y_i + f(x_i,y_i)(x_{i+1}-x_i) + 1/2!f'(x_i,y_i)(x_{i+1}-x_i)^2 + 1/3!f''(x_i,y_i)(x_{i+1}-x_i)^3 + \dots$$

so that Euler's method can be considered a Runge-Kutta 1st order method.

The second order would, obviously, include one more term of the Taylor series:

$$y_{i+1}=y_i+f(x_i,y_i)h+1/2!f'(x_i,y_i)h^2$$



Comparison of the solutions for a particular problem.

The higher orders are approximating and simplifying the steps, where possible.

- RK3: To approximate the solution of $dy/dx=f(x,y)$, $y(x_0)=y_0$
compute $x_1=x_0+h$, $k_1=f(x_0,y_0)$, $k_2=f(x_0+h,y_0+hk_1)$, $k_3=f[x_0+h/2, y_0+h(k_1+k_2)/4]$
 $y_1=y_0+h(k_1+k_2+4k_3)/6$, then $y(x_1)\approx y_1$
- It uses the improved Euler method to find an approximate midpoint of the secant line and then takes a weighted average of the slopes at the left and right endpoints and the midpoint. If $f(x,y)$ is a function of x alone, $f(x)$, solving the differential equation $dy/dx=f(x)$ is just evaluating the integral $\int f(x)dx$ and then explored what coefficients could be set to zero. In this case, the third order Runge-Kutta method is the same as Simpson's rule for numerical approximation of integral.

The 4th order, RK4 is most efficient and most used one for the higher orders. It is accurate up to seven digits after the decimal point in some cases. In the worst case, it is accurate up to two digits after the decimal point.

$$\begin{cases} y' = f(t, y) \\ y(t_0) = \alpha \end{cases}$$

Define h to be the time step size and $t_i = t_0 + ih$. Then the following formula

$$w_0 = \alpha$$

$$k_1 = hf(t_i, w_i)$$

$$k_2 = hf\left(t_i + \frac{h}{2}, w_i + \frac{k_1}{2}\right)$$

$$k_3 = hf\left(t_i + \frac{h}{2}, w_i + \frac{k_2}{2}\right)$$

$$k_4 = hf(t_i + h, w_i + k_3)$$

$$w_{i+1} = w_i + \frac{1}{6}(k_1 + 2k_2 + 2k_3 + k_4)$$

computes an approximate solution, that is $w_i \approx y(t_i)$.

Magnetic Kluźniak-Kita disk solution (MKK)

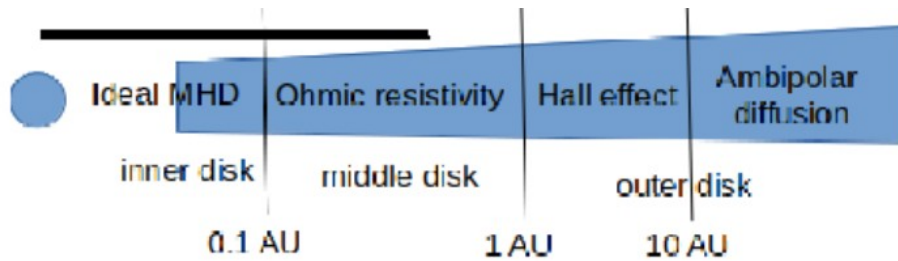


Fig. 1. Illustration of the reach of the inner, middle and outer disk regions in the case of Young Stellar Objects. In the innermost disk region the disk is in the ideal MHD regime. Further away from the star, in the middle disk region, the Ohmic resistivity adds to the viscous dissipation. In the outer disk, which we do not analyze here, other resistive terms prevail in the induction equation. Radial extension of the physical domain in our simulations is indicated with the horizontal thick black solid line.

We work with Ohmic resistivity; in the YSOs disk this is valid only in the inner part of the disk.

$$\frac{\partial \rho}{\partial t} + \nabla \cdot (\rho \mathbf{v}) = 0$$

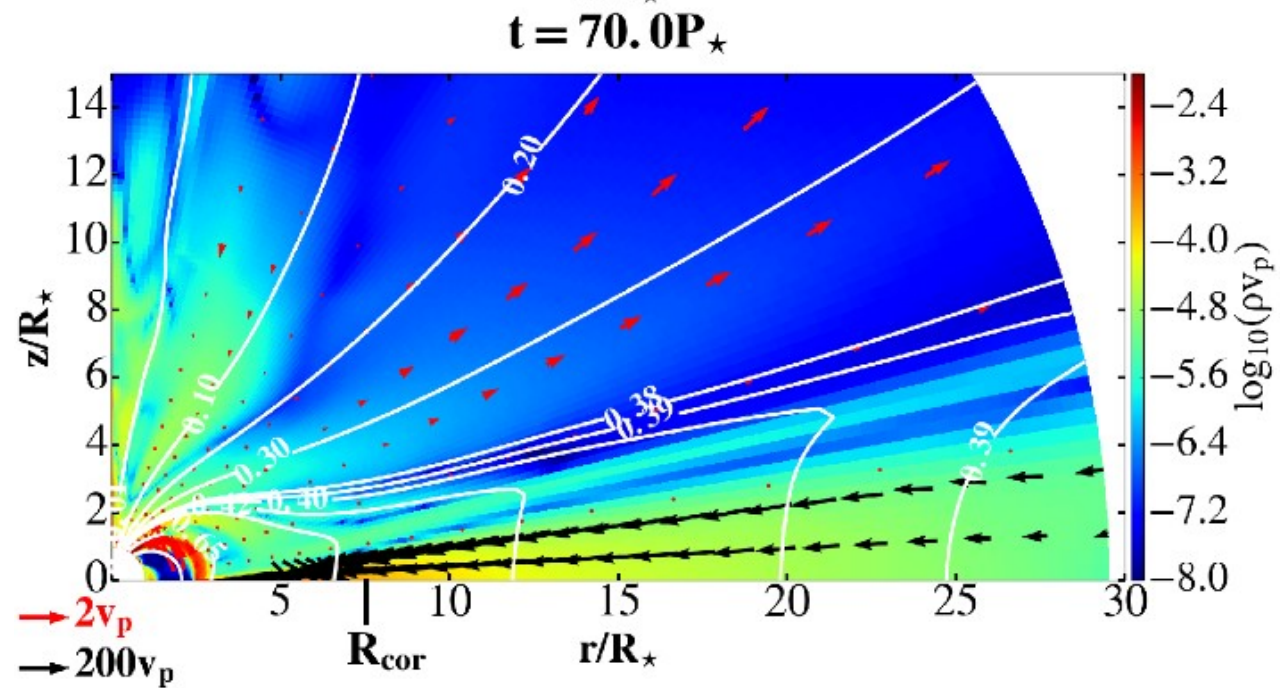
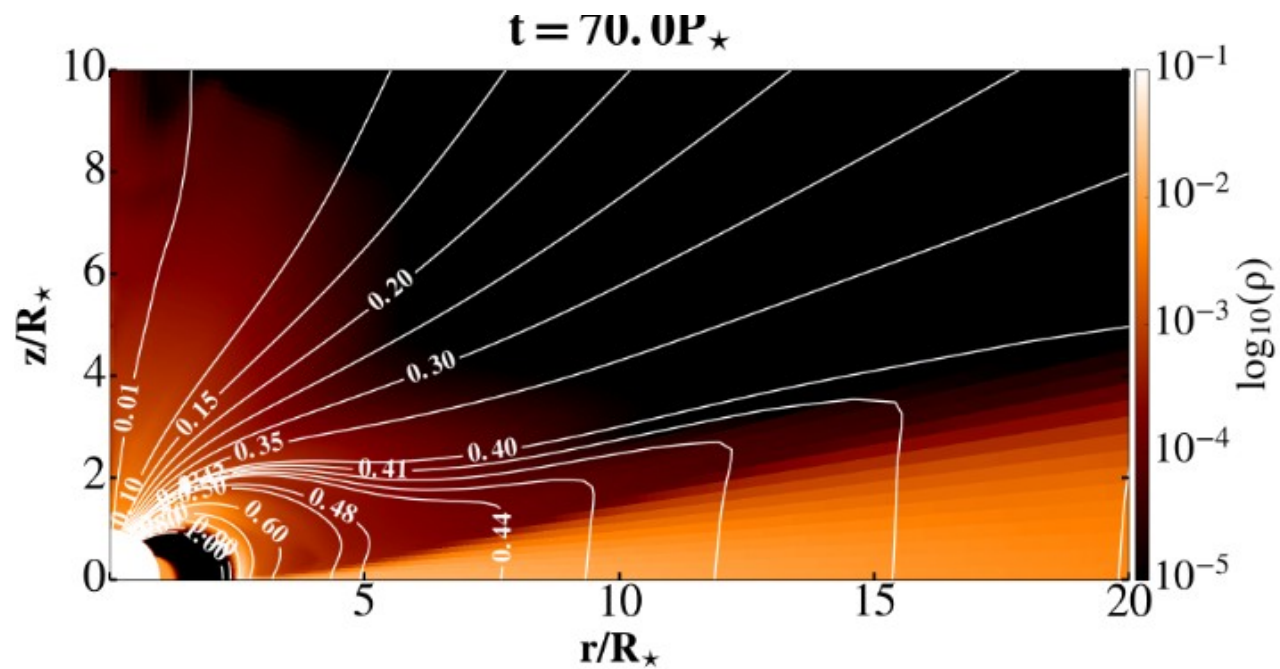
$$\frac{\partial \rho \mathbf{v}}{\partial t} + \nabla \cdot \left[\rho \mathbf{v} \mathbf{v} + \left(P + \frac{\mathbf{B} \cdot \mathbf{B}}{8\pi} \right) \mathbf{I} - \frac{\mathbf{B} \mathbf{B}}{4\pi} - \boldsymbol{\tau} \right] = \rho \mathbf{g}$$

$$\frac{\partial E}{\partial t} + \nabla \cdot \left[\left(E + P + \frac{\mathbf{B} \cdot \mathbf{B}}{8\pi} \right) \mathbf{v} - \frac{(\mathbf{v} \cdot \mathbf{B}) \mathbf{B}}{4\pi} \right] + \nabla \cdot \left[\underbrace{\eta_m \mathbf{J} \times \mathbf{B} / 4\pi - \mathbf{v} \cdot \boldsymbol{\tau}}_{\text{heating terms}} \right] = \rho \mathbf{g} \cdot \mathbf{v} - \underbrace{\Lambda}_{\text{cooling}}$$

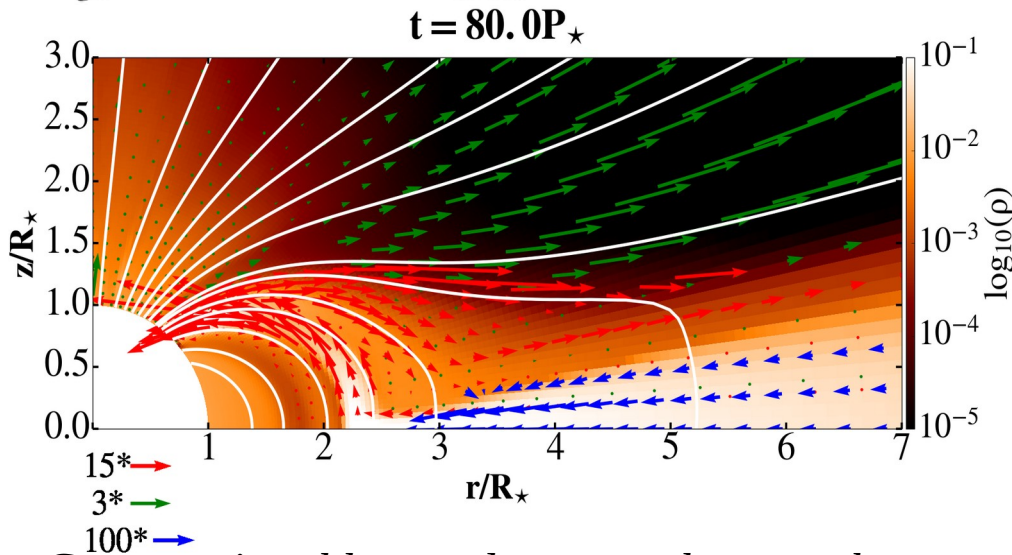
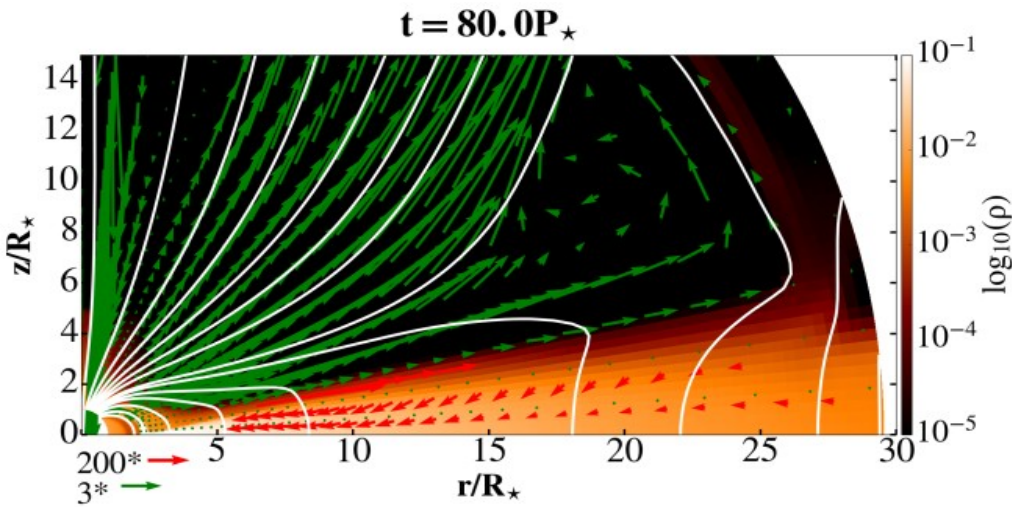
$$\frac{\partial \mathbf{B}}{\partial t} + \nabla \times (\mathbf{B} \times \mathbf{v} + \eta_m \mathbf{J}) = 0$$

We search for the quasi-stationary state solutions, assuming that all the heating is radiated away from the disk. This is why in the “Atlas” and following papers, done with PLUTO v.4.1 the dissipative viscous and resistive terms are not present in the energy equation, nor are the cooling terms. We still solve the equations in the non-ideal MHD regime, because of the viscous terms in the momentum equation, and the Ohmic resistive term in the induction equation. You will be solving viscous and resistive MHD equations with all the terms and with the cooling source term.

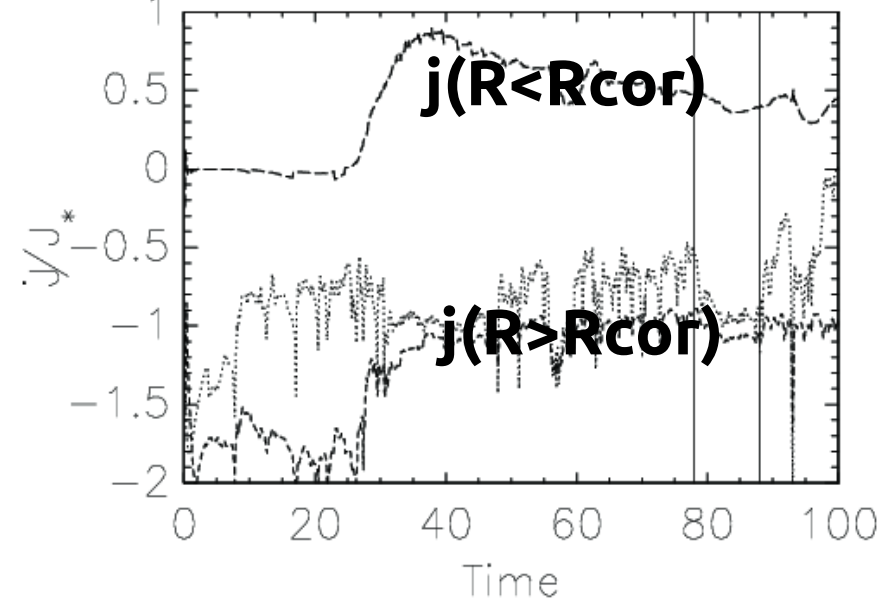
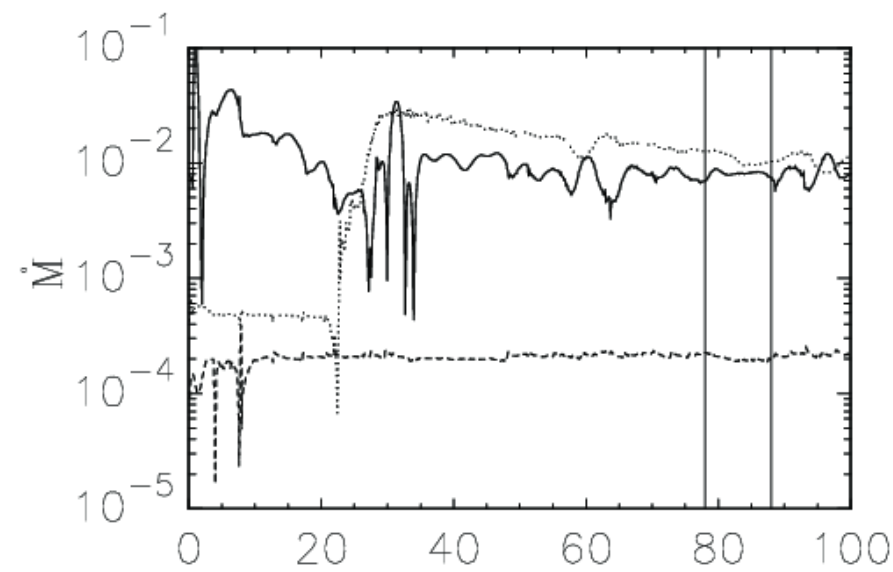
Example of a solution with 500 Gauss



Star-disk magnetospheric interaction (SDMI) simulations

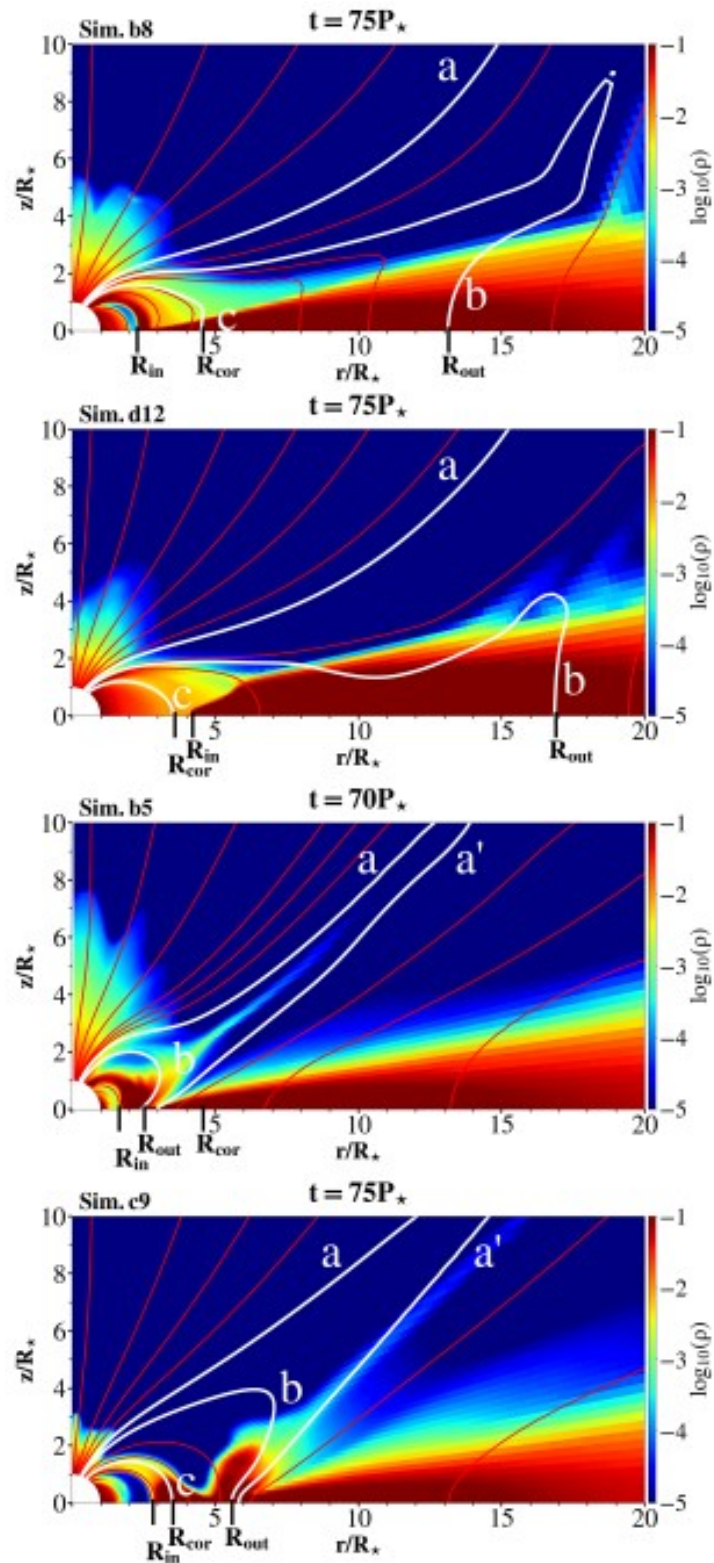


Computational box and a zoom closer to the star after 80 stellar rotations, to visualize the accretion column and the magnetic field lines (white solid lines), connected to the disk beyond the corotation radius $R_{\text{cor}} = 2.92 R_{\star}$. In color is shown the density, and vectors show velocity, with the different normalization in the disk, column and stellar wind.



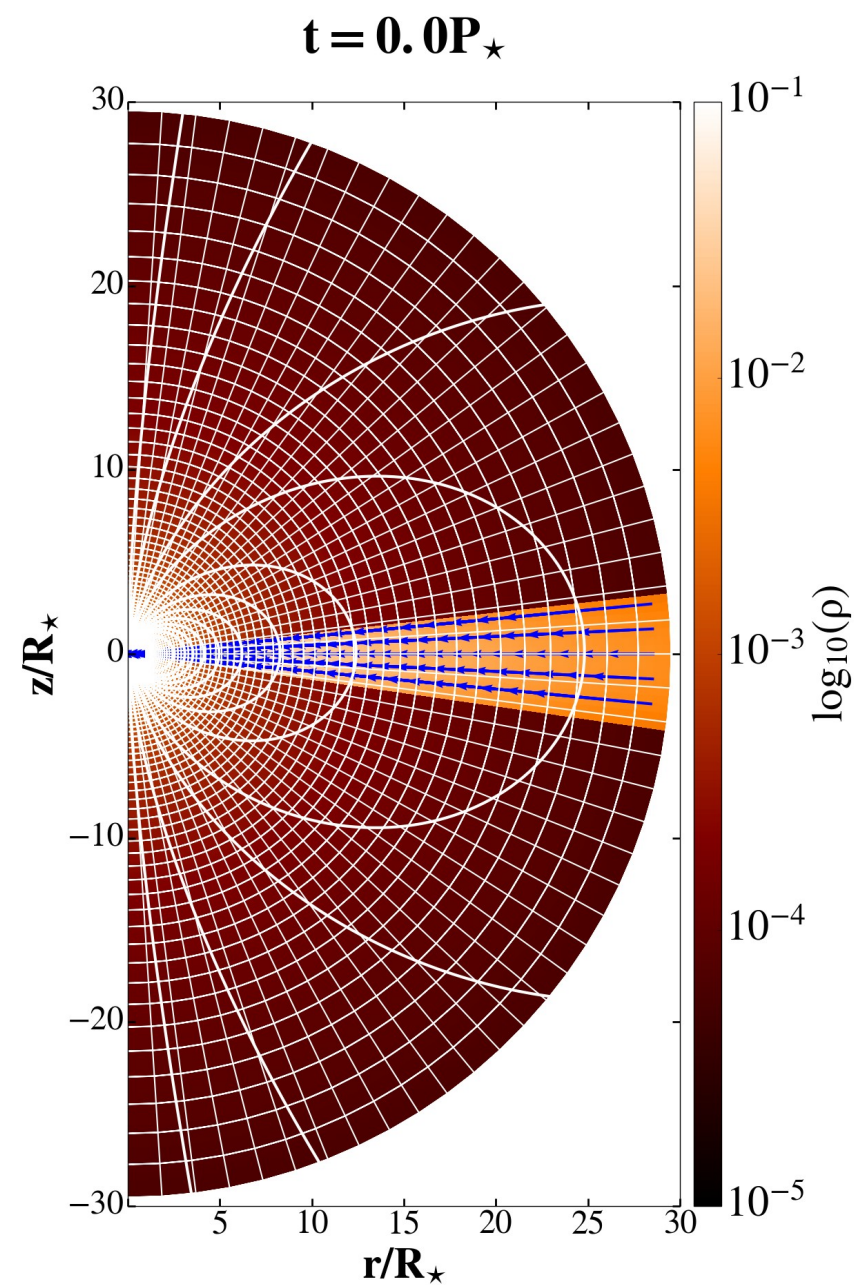
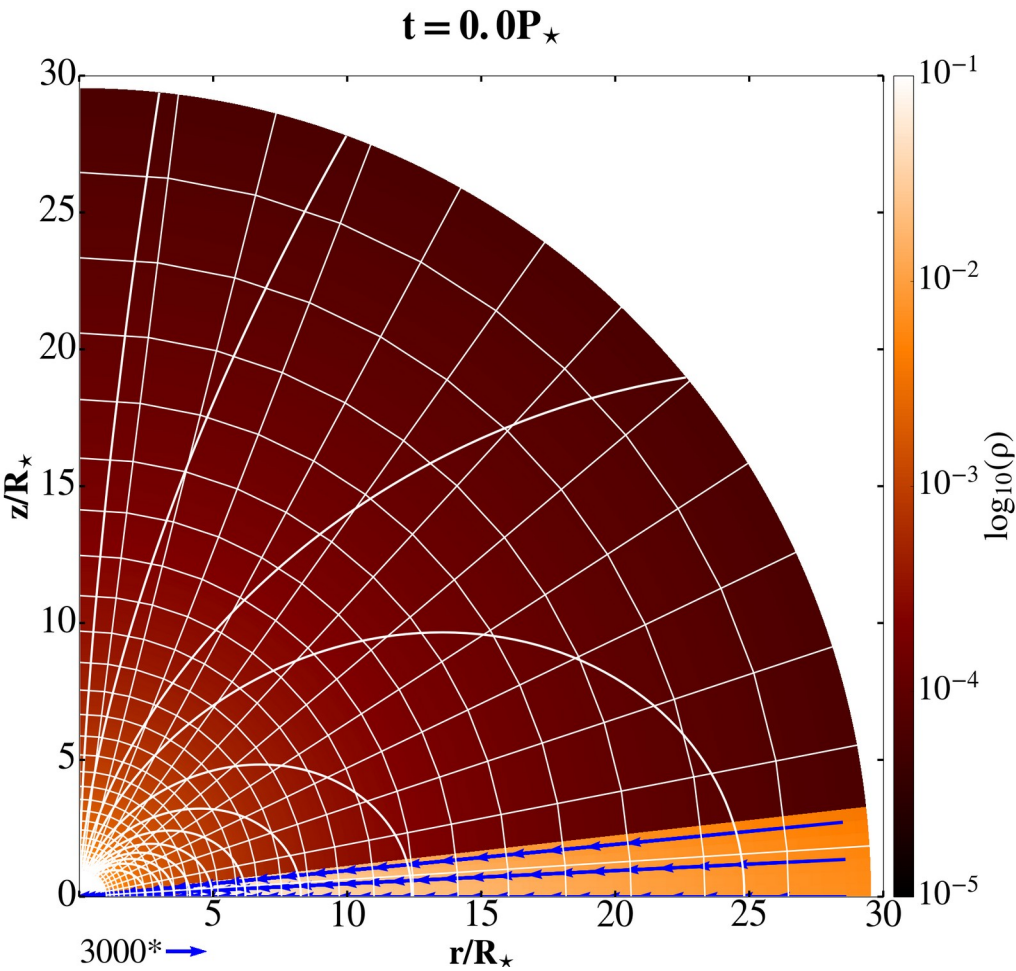
Time dependence of the mass and angular momentum fluxes in the various components in our simulations with marked the time interval in which the average for the quasi-stationarity is computed.

Types of solutions in “Atlas”



- 4 different cases if we consider the position of R_{cor} in the case with conical outflow.
- In general, faster stellar rotation prevents the accretion column formation.
- In the bottom panels resistivity $\alpha_m=0.1$ and $\Omega_s=0.1$, a conical outflow is formed.

Star-disk simulations with magnetic field



- We add the magnetic field to the HD solution
- Stellar surface is a rotating boundary condition at the origin of the spherical computational domain. We assume the star to be a magnetized rotator. The initially non-rotating corona is in a hydrostatic balance.

Numerical methods in PLUTO for star-disk interaction

•I already showed, and will show again where is definition of each of the setup entries in the code, here is an example of what you can usually read in the description of a setup:

- Simulations were performed using the second-order piecewise linear reconstruction.
- Van Leer* limiter, which is more diffusive and enhances stability, is used in density and magnetic field and a *minmod* (monotonized central differences) limiter in pressure and velocity.
- An approximate Roe solver (hlld in the pluto options) was used, with a modification in the `flag_shock` subroutine: flags were set to switch to more diffusive hll solver when the internal energy was lower than 1% of the total energy, instead of switching in the presence of shocks.
- The second-order time-stepping (RK2) was employed.
- $\nabla \cdot \mathbf{B} = 0$ was maintained by the constrained transport method.
- The magnetic field was evolved with the split-field option, so that only changes from the initial stellar magnetic field were evolved in time. This means that in the final results, one has to add magnetic dipole (or other initial field) to the solution from the code.
- The power-law cooling is introduced to account for the disk dissipative heating. Physically it is good enough to represent bremsstrahlung. There are other cooling functions in PLUTO, one can also import a table of values, not necessarily a function.

Setup of magnetic runs-changes in pluto.ini and definitions.h

```
I pluto.ini (Modified)(ini) Row 27 Col 19 1:29 Ctrl-K H for help
Solver      hll
[Boundary]
X1-beg      userdef
X1-end      userdef
X2-beg      axisymmetric
X2-end      eqtsymmetric
X3-beg      outflow
X3-end      outflow
[Static Grid Output]
uservar     3 nu num Te
dbl         6.279 -1 single_file
flt         -1.0 -1 single_file
vtk         6.279 -1 single_file
tab         -1.0 -1
dbl.h5      -6.279 -1
ppm         -1.0 -1
png         -1.0 -1
log         100
analysis    -1.0 -1
[Chombo HDF5 output]
Checkpoint_interval -1
Plot_interval  1.0
[Parameters]
ALPHAM      0.4
MU          0.07
```

```
I A definitions.h (c) Row 1 Col 1 1:38 Ctrl-K H for help
#define PHYSICS MHD
#define DIMENSIONS 2
#define COMPONENTS 3
#define GEOMETRY SPHERICAL
#define BODY_FORCE VECTOR
#define FORCED_TURB NO
#define COOLING NO
#define RECONSTRUCTION LINEAR
#define TIME_STEPPING RK2
#define DIMENSIONAL_SPLITTING NO
#define NTRACER 1
#define USER_DEF_PARAMETERS 9

/* -- physics dependent declarations -- */
#define EOS IDEAL
#define ENTROPY_SWITCH NO
#define DIVB_CONTROL CONSTRAINED_TRANSPORT
#define BACKGROUND_FIELD YES
#define AMBIPOLAR_DIFFUSION NO
#define RESISTIVITY NO
#define HALL_MHD NO
#define THERMAL_CONDUCTION NO
#define VISCOSITY EXPLICIT
#define ROTATING_FRAME NO

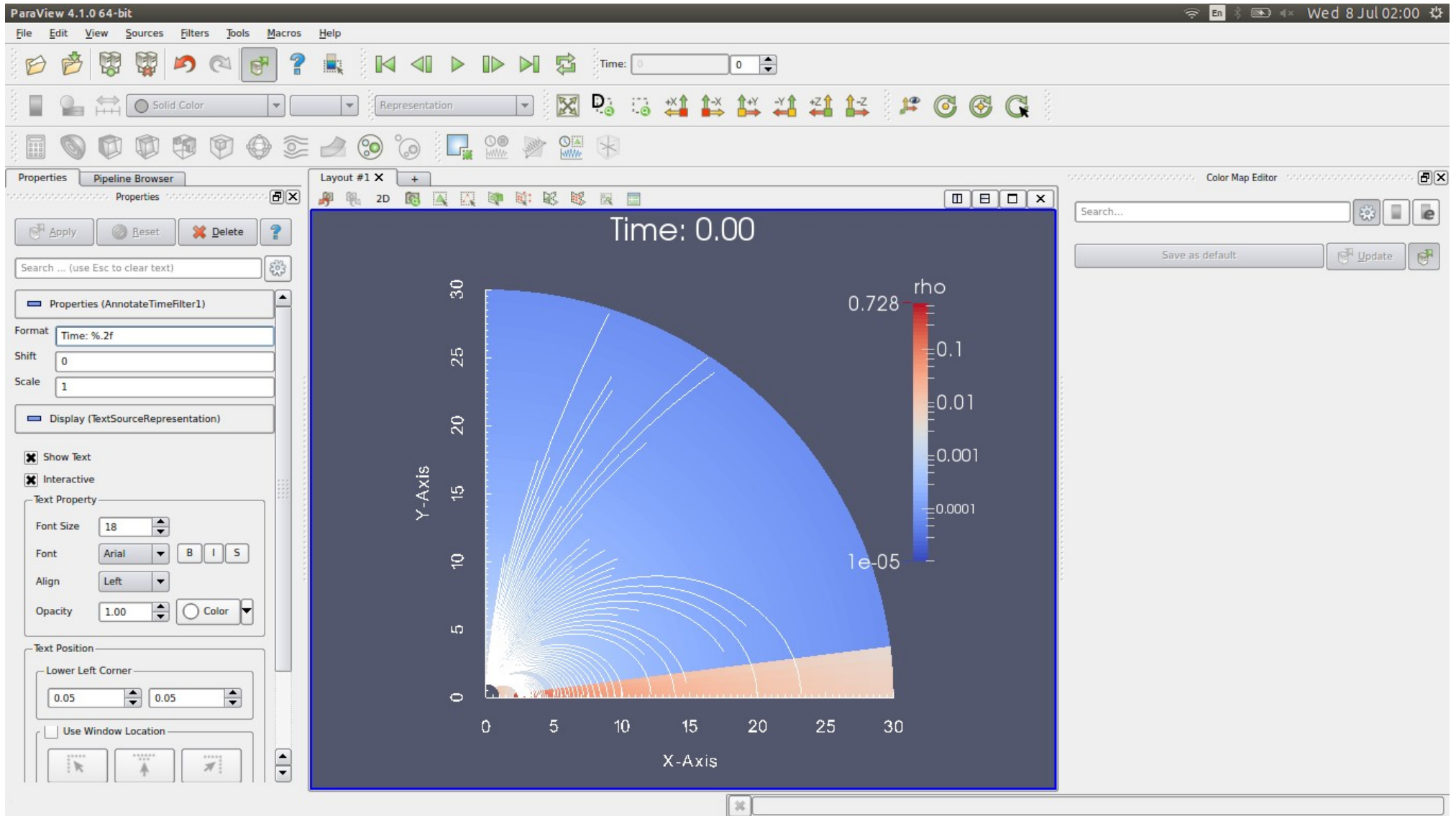
/* -- user-defined parameters (labels) -- */
#define ALPHAM 0
#define MU 1
#define TEMPF 2
#define RHOC 3
#define RD 4
#define EPS 5
```

Setup of magnetic dipole and multipoles in init.c

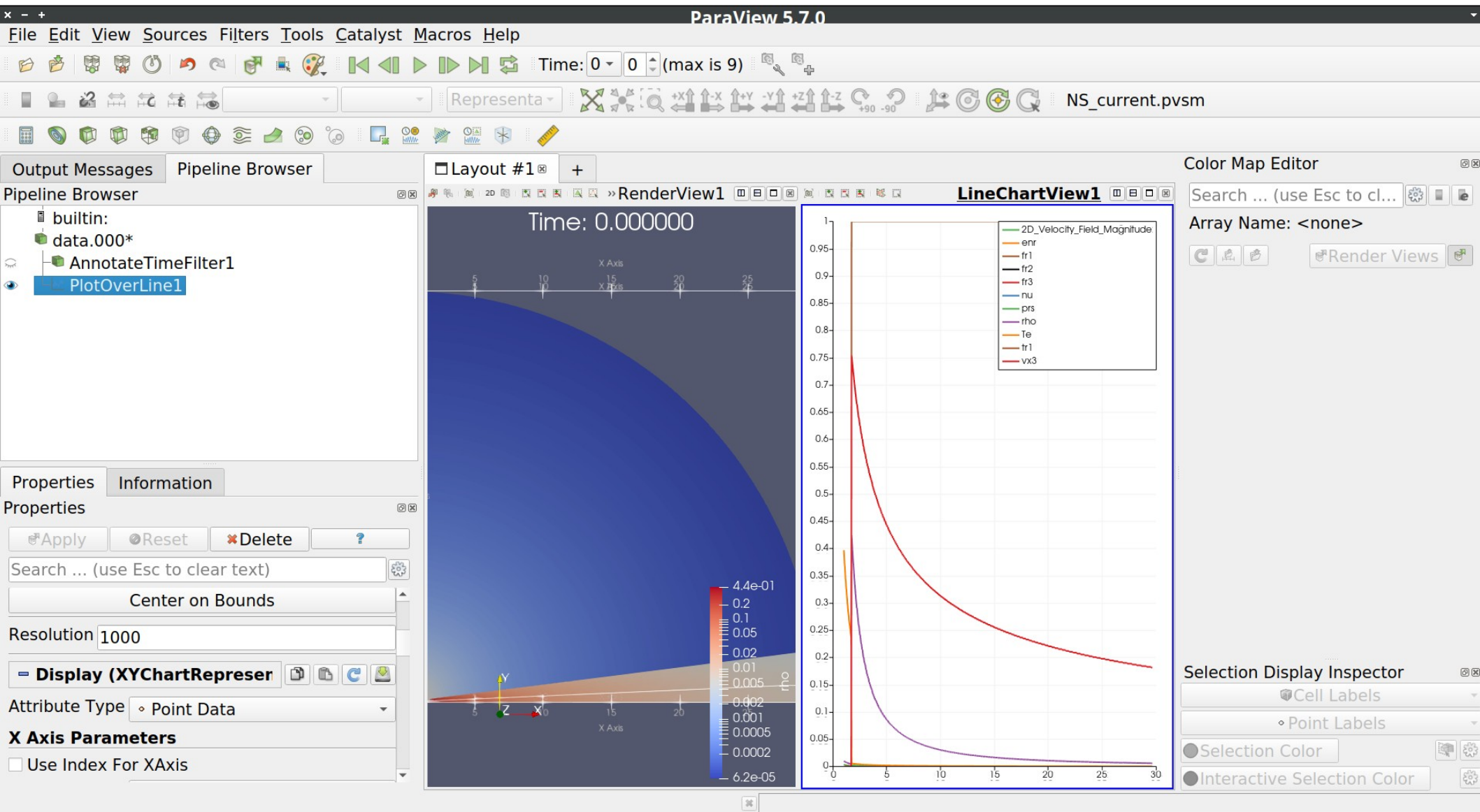
```
I A init.c (c) void UserDefBoundary (const Data *d, RBox *box, int side, Row 146 Col 1 4:22 Ctrl-K H for help)
#if PHYSICS == MHD
/* ***** */
void BackgroundField (double x1, double x2, double x3, double *B0)
/*
 *
 * PURPOSE
 *
 * Define the component of a static, curl-free background
 * magnetic field.
 *
 *
 * ARGUMENTS
 *
 * x1, x2, x3 (IN) coordinates
 *
 * B0 (OUT) vector component of the background field.
 *
 *
 * ***** */
{
/* dipole */
B0[0] = 2.*g_inputParam[MU]*cos(x2)/(x1*x1*x1);
B0[1] = g_inputParam[MU]*sin(x2)/(x1*x1*x1);
B0[2] = 0.0;
}
#endif
```

```
{
/* dipole */
B0[0] = 2.*g_inputParam[MU]*cos(x2)/(x1*x1*x1);
B0[1] = g_inputParam[MU]*sin(x2)/(x1*x1*x1);
B0[2] = 0.0;
/* */
/* quadrupole
B0[0] = 3.0/2.0*g_inputParam[MU]*(3.0*cos(x2)*cos(x2)-1.0)/(x1*x1*x1*x1);
B0[1] = 3.0*g_inputParam[MU]*cos(x2)*sin(x2)/(x1*x1*x1*x1);
B0[2] = 0.0;
*/
/* octupole
B0[0] = 2.0*g_inputParam[MU]*(5.0*cos(x2)*cos(x2)*cos(x2)-3.0*cos(x2))/(x1*x1*x1*x1*x1);
B0[1] = 0.5*g_inputParam[MU]*(15.0*cos(x2)*cos(x2)*sin(x2)-3.0*sin(x2))/(x1*x1*x1*x1*x1);
B0[2] = 0.0;
*/
}
```


Visualization of Bp lines with Paraview

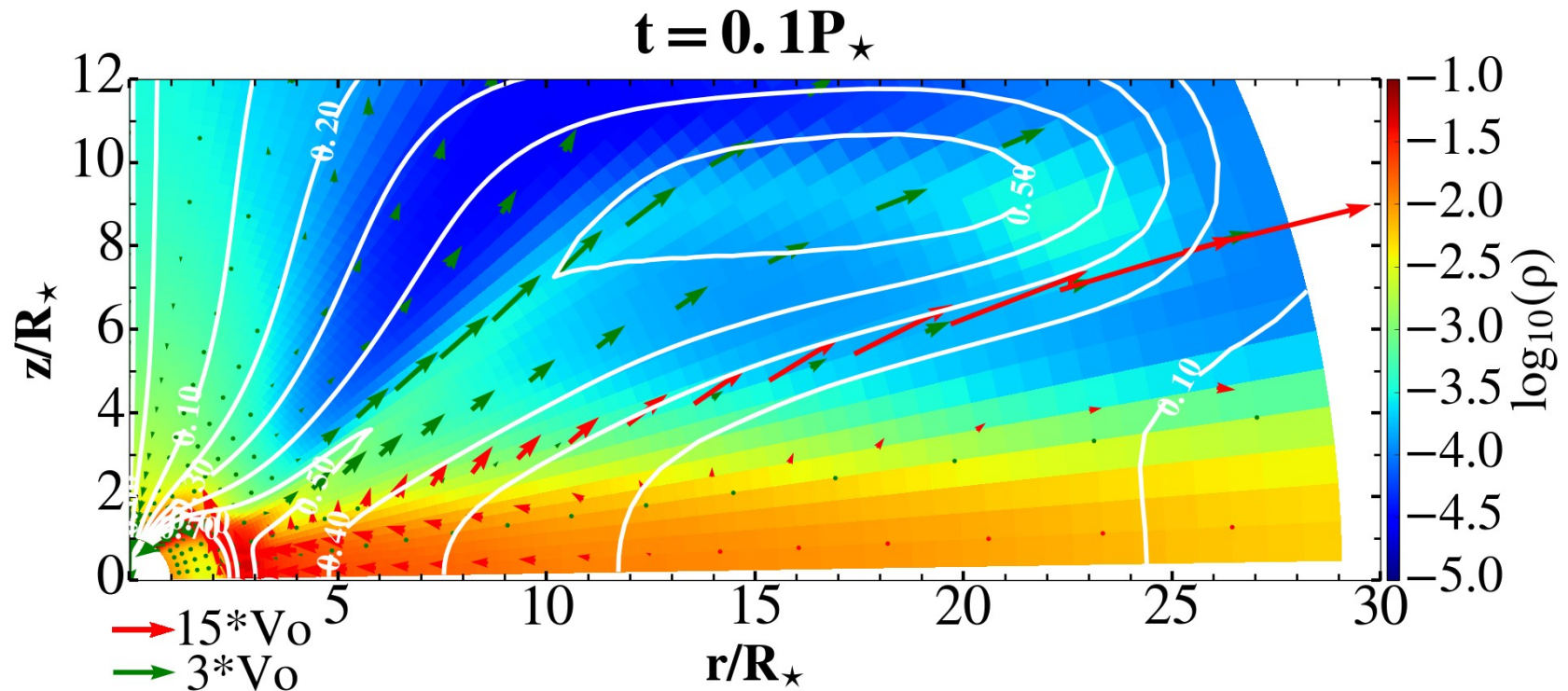


Analysis with paraview



Python script for visualization

- mc_veloclect.py , python ver.3.5 and newer.
- Density in logarithmic color grading.
- Vectors of velocity. Remember to show normalization, I normalize to Keplerian velocity at the stellar equator ($R=1$).
- Magnetic field lines-plots with $A\phi$ isocontours-they are parallel to B_p field lines. Magnetic field lines could be plotted also with B_p streamlines, but I did not do it here.



Summary of the Lect. 5

- Riemann problem, Finite difference, Godunov's method, volume and elements methods, CFL condition, RK2, RK3, ...
- Setup and running of 2.5D MHD KK disc in PLUTO
- Analysis of the results from 2.5D magnetic runs with Paraview
- Python script for visualization

Outline, Lect.6 : Continuation of numerics essentials, astrophysical jets

- Approximate Riemann solvers: HLL, HLLC, HLLD
- Reconstruction methods, MHD numerics
- Astrophysical jets, simulations of jets from disc as a b.c. and with the disc evolution included
- Streamlines in Paraview in 2D and 3D

We had the figure with waves and eigenvalues, which is used in publications to illustrate the Riemann problem and approximate Riemann solvers:

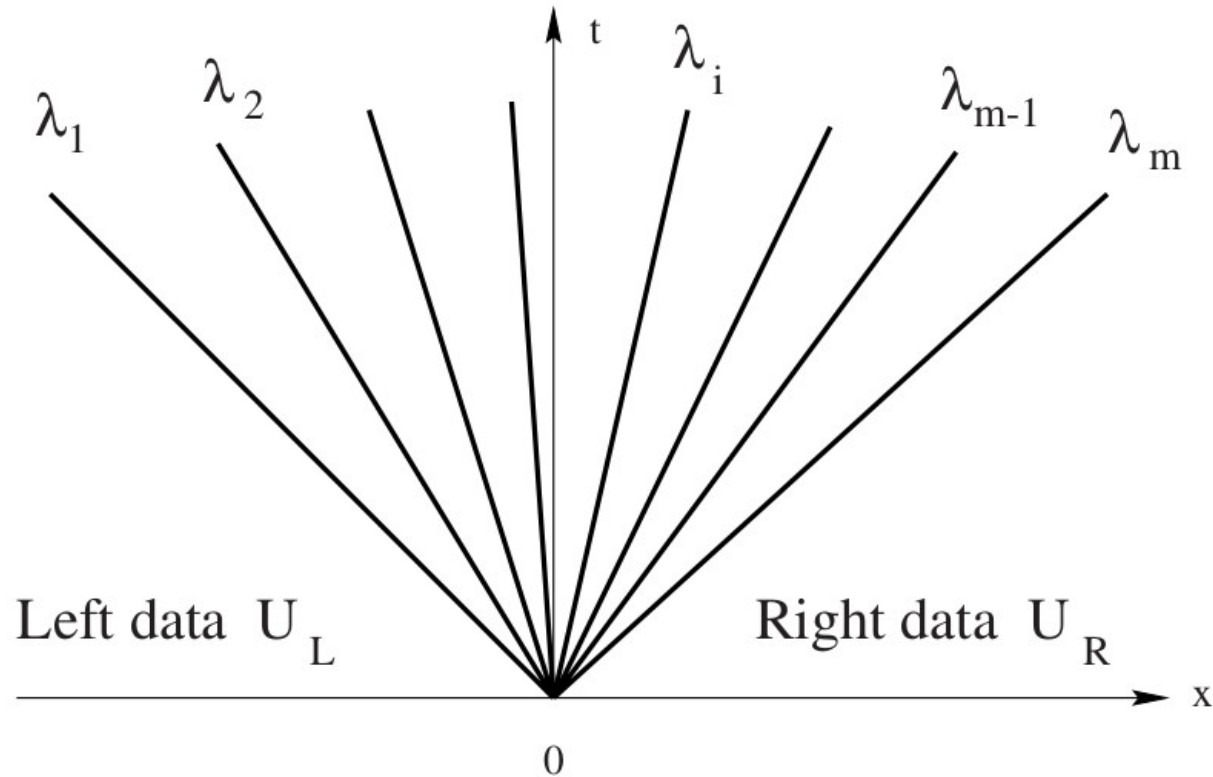


Fig. 2.4. Structure of the solution of the Riemann problem for a general $m \times m$ linear hyperbolic system with constant coefficients

FROM PHD THESIS OF D. ABARCA, CAMK, (2021): One strategy for coming up with approximate Riemann solvers is to approximate the solution by the superposition of a number of waves moving left and right after the system begins to evolve in time. A **two-wave solution** which uses the maximum and minimum velocity signals was proposed by Harten et al. (1983) hereby referred to as the **HLL** Riemann solver. If the maximum and minimum signal velocities (or maximum left and right moving signal speeds), S_R and S_L , respectively, can be computed (there are a number of ways to do this), then the HLL Riemann solver gives, for left and right fluxes,

$$\mathbf{F}_{\text{HLL}} = \begin{cases} \mathbf{F}_L & 0 < S_L \\ \frac{S_R \mathbf{F}_L - S_L \mathbf{F}_R + S_L S_R (\mathbf{U}_R - \mathbf{U}_L)}{S_R - S_L} & S_L \leq 0 \leq S_R \\ \mathbf{F}_R & S_R < 0 \end{cases}$$

If the minimum signal velocity, S_L is positive, this means all waves should be moving to the right and so one can use the flux corresponding to the left side of the interface. If the maximum signal velocity is negative, then the opposite is true and all waves move to the left, so we take the flux from the right. The intermediate case takes a combination of fluxes weighted by the wavespeeds with the addition of a term that computes the overlap of the left and right conserved quantities.

HLL is used extensively due to its simplicity while still producing meaningful results, but **many other Riemann solvers exist**. There is a third type of wave in ordinary hydrodynamics which HLL does not consider: the contact discontinuity corresponding to a jump in density without a corresponding jump in pressure. HLL is unable to provide satisfactory solutions when the contact discontinuity becomes important and a **three wave Riemann solver** was proposed by Toro (2009) (**HLLC**) which includes it. In MHD and GRMHD one also has to consider Alfvén and magnetosonic waves. These wave speeds can be used in the HLL or HLLC Riemann solvers but more accuracy is achieved by considering even more intermediate states as in the **HLLD** Riemann solver (Miyoshi and Kusano 2005) which **assumes a five wave solution** at the interface.

Reconstruction methods

Godunov method is zeroth order accurate in space. We can do better by moving from a piecewise constant approximation for a flux \mathbf{U} to a piece-wise linear approximation. It is difficult to compute the fluxes as function of the conserved quantities; easier is to use a different set of variables, the primitives, \mathbf{P} . They are usually naturally well-defined quantities such as density, velocity, and internal energy, with straightforward, analytical expressions for $\mathbf{F}(\mathbf{P})$ and $\mathbf{U}(\mathbf{P})$. But we must also perform the inversion from conserved to primitive variables, $\mathbf{P}(\mathbf{U})$. In ordinary HD it is easy, but with additional physics, it gets very complicated. In GRMHD it is necessary to perform the inversion numerically, e.g. with a Newton-Raphson method.

If $\mathbf{F}(\mathbf{P})$, $\mathbf{U}(\mathbf{P})$, and $\mathbf{P}(\mathbf{U})$ can be computed, we can reconstruct the primitive variables at the cell interfaces. When computing slopes $\Delta P_i / \Delta x$, not to introduce new maxima and minima into the approximate solution of \mathbf{U} (and, consequently, \mathbf{P}), which would cause the instability of the numerical scheme, with spurious oscillations in the solution which would grow in time, we need to use a total variation diminishing (TVD) scheme. Usually it is done with a slope limiter which adjusts the computed slopes to prevent the formation of new maxima and minima.

- One such scheme is the generalized *minmod* van Leer (1979) slope limiter, which produces a modified slope.
- Another scheme, the minmod slope limiter, is actually a one-parameter mix between the more diffusive *van Leer* scheme (van Leer 1974) and the more accurate (but less stable) monotized central scheme (van Leer 1977).

Slope-limiters have the additional function of preserving large discontinuities in the fluid across cell interfaces. Numerical schemes which include these limiters are referred to as *shock capturing schemes*.

- With Maxwell's equations we often have to depart from the conservation laws which are holding for fluids. The best example is the $\nabla \cdot \mathbf{B} = 0$ condition, which imposes additional constraint on \mathbf{B} .
- To solve this issue and prevent increase in non-physical component of the magnetic field, various methods were invented.
- The simplest way was to simply remove the unphysical component by using the Helmholtz theorem, saying that any vector field \mathbf{B}' can be written as a sum of the curl and gradient of two other fields: $\mathbf{B}' = \nabla \times \mathbf{A} + \nabla \phi$. If we take the gradient of this expression, we obtain the Poisson equation $\nabla \cdot \mathbf{B}' = \nabla^2 \phi$, which we can solve for ϕ , giving us a divergence-free field $\mathbf{B} = \mathbf{B}' - \nabla \phi = \nabla \times \mathbf{A}$. The solution is neat, but we need to solve the Poisson equation often, which comes with a large computational cost. There are many methods for approximating this, but the idea is similar—these are the “*divergence cleaning*” methods.
- Another, more precise, or actually *exact* method, is the Constrained Transport (CT) method, (Evans&Hawley, 1988) which keeps the $\nabla \cdot \mathbf{B}$ constant...but you have to start with the $\nabla \cdot \mathbf{B} = 0$ field—which is not always true or easy. It involves computing the induced electric field $\mathbf{E} = \mathbf{v} \times \mathbf{B}$ at four locations for each component of \mathbf{B} around every point and evolving \mathbf{B} with a finite difference in \mathbf{E} . Any round-off errors are canceled out, so we stay with divergence-less \mathbf{B} .
- For this computation a staggered grid was originally used, with \mathbf{B} computed in the center of the cell faces, and the four values of \mathbf{E} in the cell corners. So one needs two grids.
- Later in Tóth (2000) flux-interpolated constrained transport (flux-CT) method, the values of \mathbf{B} and \mathbf{v} are computed at cell centers and then interpolated to the cell faces, where the field is evolved and then interpolated back to the cell centers.

Jet launching and propagation

- We are still searching for the way to explain not only how the stars are slowed down, but also to the tightly related mechanism: how astrophysical jets are launched and collimated.
- For the jet propagation and collimation, we do not need the launching part, we just assume they are launched, input some surface as a b.c. and follow the flow. But we have to be careful about some characteristic surfaces in such flows when setting them. This is a good example.

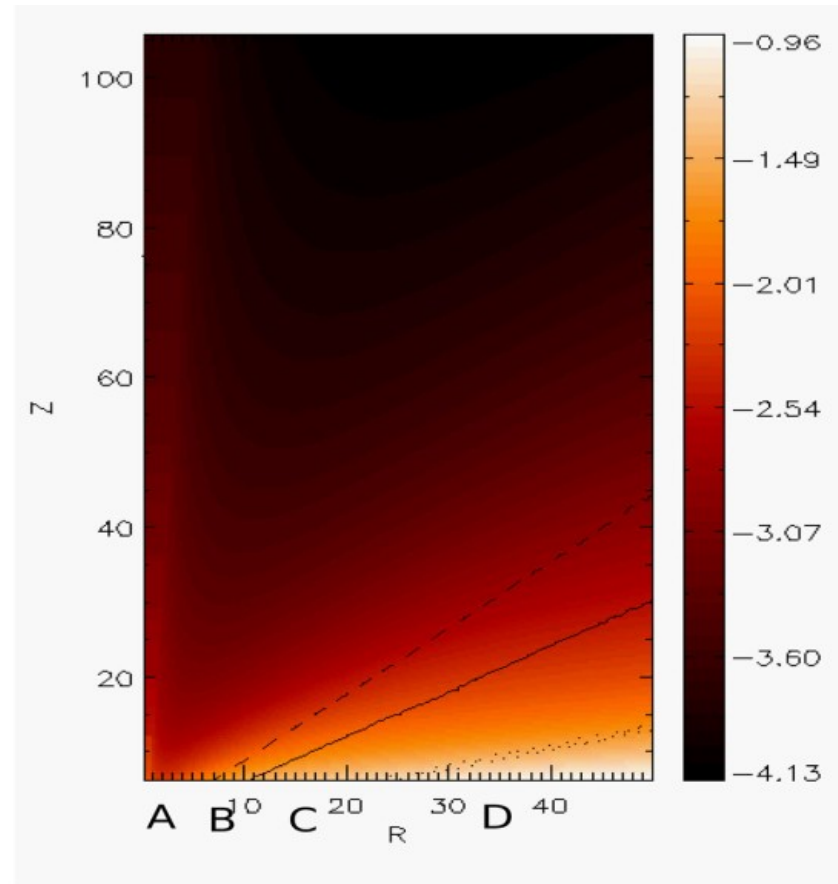


Figure 1. Initial conditions in our simulations, with marked inner- Z boundary regions of interest for the setup of boundary conditions. To avoid reflection from the outer- R boundary, we actually set our computational box three times larger in R -direction, and then analyse results only in the $R \times Z = (128 \times 256)$ grid cells = $([0, 50] \times [6, 106])R_0$ portion of the domain. If not stated otherwise, all the results in this paper are shown at such resolution. In all the plots, the density is shown in a logarithmic colour scale, and the three critical surfaces are plotted in dashed, solid and dotted lines, for fastmagnetosonic, Alfvén and slow magnetosonic waves, respectively. Labels A, B, C and D mark portions of the inner- Z boundary where the flow is superfast magnetosonic, super-Alfvénic, supersonic and subsonic, respectively.

Jet propagation

- Results strongly depend on resistivity.

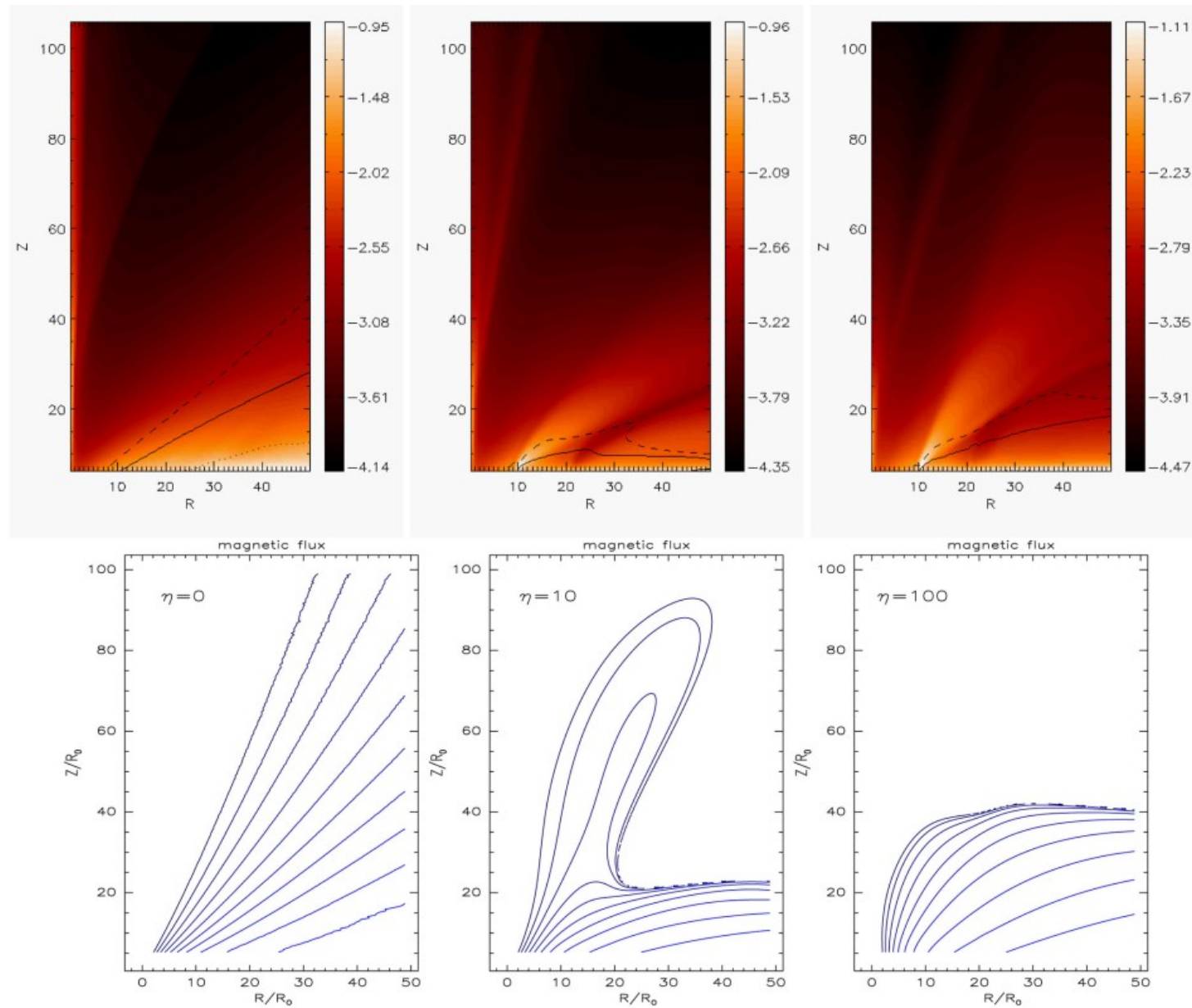
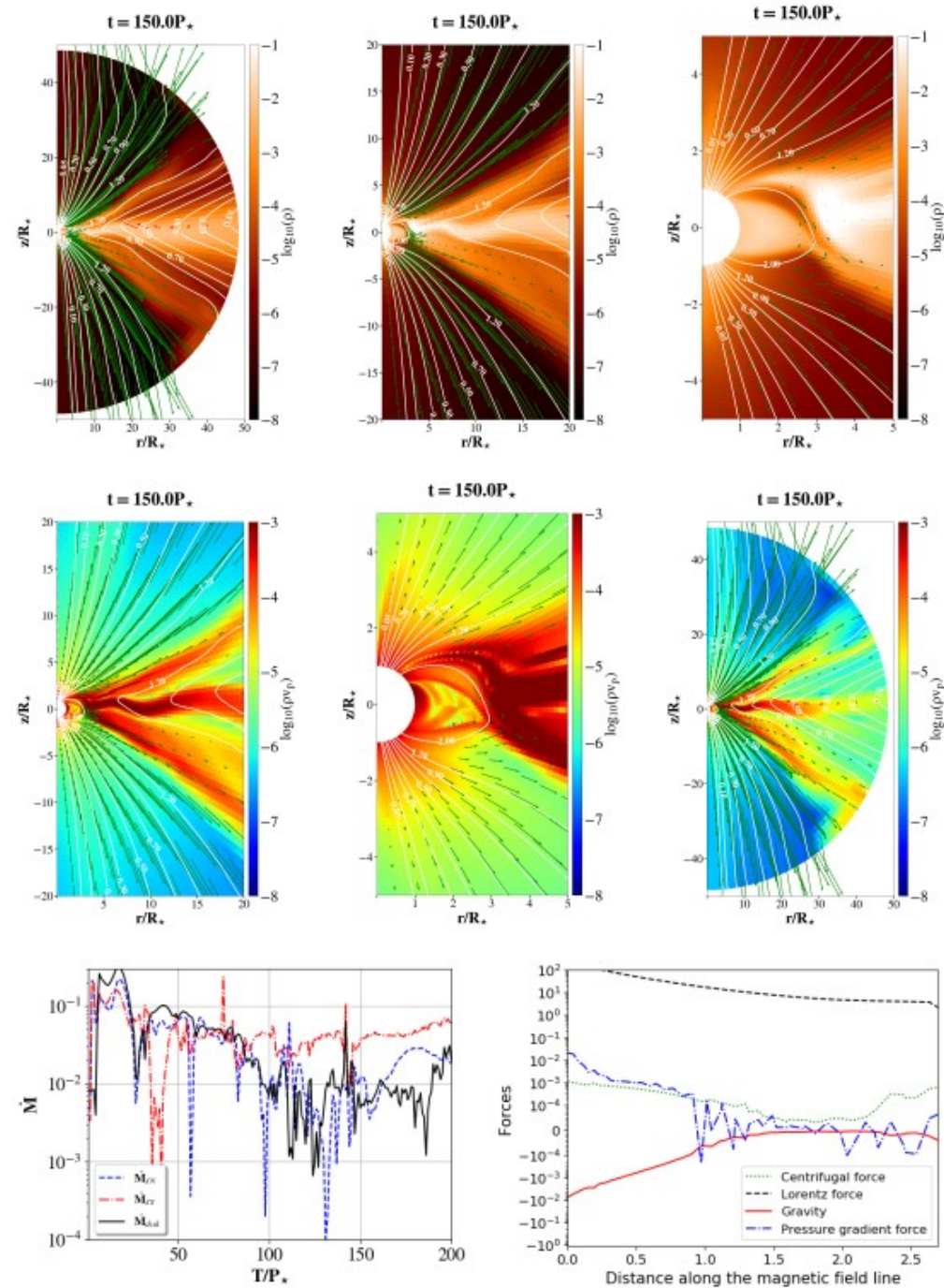


Figure 3. Illustration of the effect of resistivity on the density in the outflow. Top panels: in the left-hand panel, the quasi-stationary state solutions in the ideal-MHD case are shown, and in the middle and right-hand panels, solutions with large and very large resistivity, $\eta = 10$ and 100 are shown. Solutions with

Jet launching

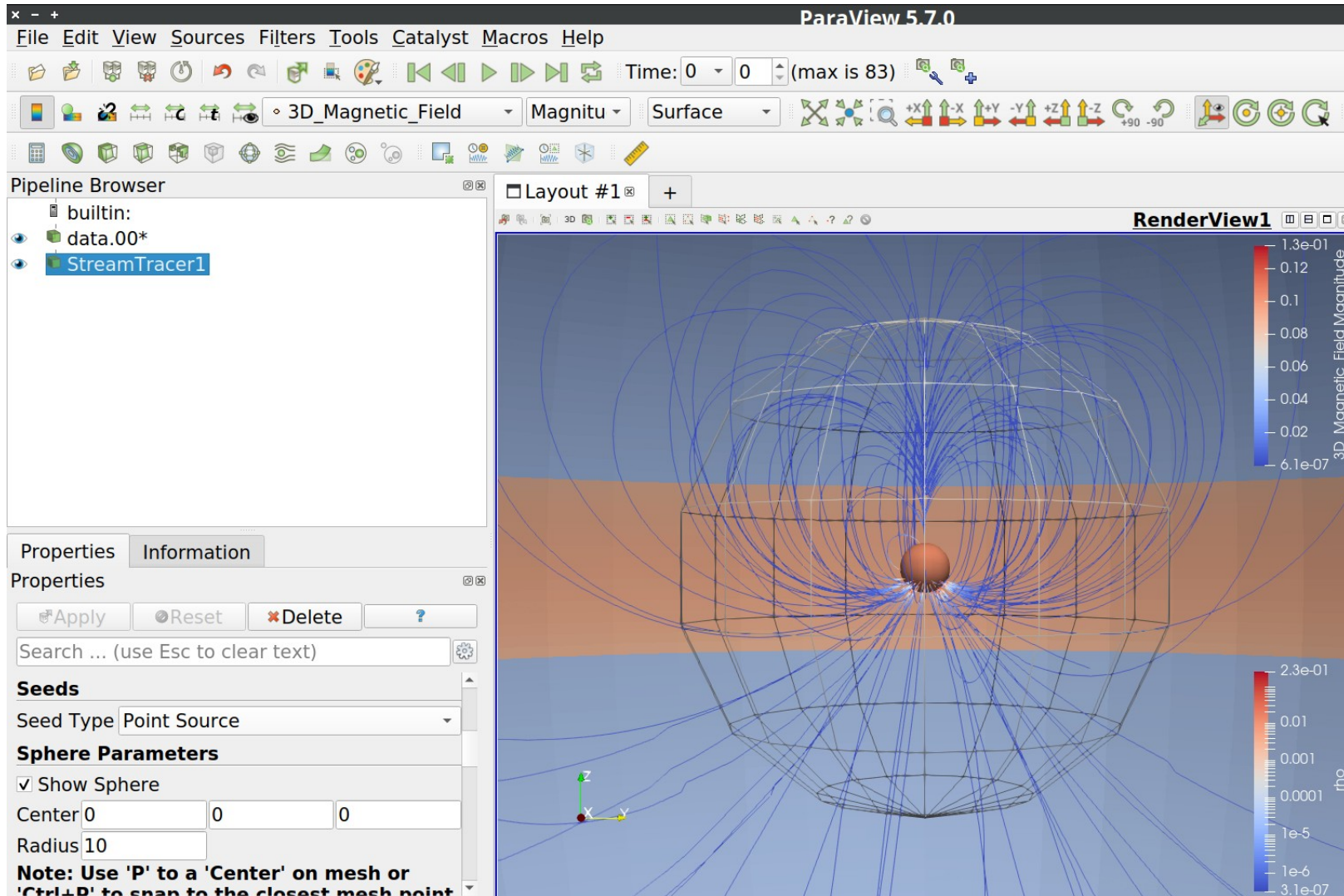
$$0.17 \quad B_* = 1000 \text{ G}, \quad \Omega_*/\Omega_{\text{br}} = 0.8, \quad \alpha_m = 0.4$$

When we include the disc, all the hell get loose, equations are having fun with us! This still waits for your contribution, even in 2D we did investigate it enough, yet, and in 3D we just scratched the surface. Internal report by a Master student looked like few tens of pages of this:



Paraview streamlines

In 2D you use a line to seed the streamlines, in 3D, better is to use a point source and a sphere around it-you can move the sphere around and choose the set of streamlines which you want to show.



Summary of the Lect. 6

- Approximate Riemann solvers: HLL, HLLC, HLLD
- Reconstruction methods, MHD numerics
- Astrophysical jets, simulations of jets from disc as a b.c. and with the disc evolution included.
- Streamlines in Paraview in 2D and 3D

Outline, Lect.7 : PLUTO modules, post-processing of the results

- Different modules in PLUTO, cooling versus radiative transfer
- Hot discs
- Post-processing of the results, DUSTER
- Python script for analysis

PLUTO physics modules, equations

6.1 The HD Module

The HD module may be used to solve the Euler or the Navier-Stokes equations of classical fluid dynamics. The relevant source files and definitions for this module can be found in the Src/HD directory.

With the HD module, **PLUTO** evolves in time following system of conservation laws:

$$\frac{\partial}{\partial t} \begin{pmatrix} \rho \\ \mathbf{m} \\ E_t + \rho\Phi \end{pmatrix} + \nabla \cdot \begin{pmatrix} \rho\mathbf{v} \\ \mathbf{m}\mathbf{v} + p\mathbf{l} \\ (E_t + p + \rho\Phi)\mathbf{v} \end{pmatrix}^T = \begin{pmatrix} 0 \\ -\rho\nabla\Phi + \rho\mathbf{g} \\ \mathbf{m} \cdot \mathbf{g} \end{pmatrix} \quad (6.1)$$

where ρ is the mass density, $\mathbf{m} = \rho\mathbf{v}$ is the momentum density, \mathbf{v} is the velocity, p is the thermal pressure and E_t is the total energy density:

$$E_t = \rho e + \frac{\mathbf{m}^2}{2\rho}. \quad (6.2)$$

An equation of state provides the closure $\rho e = \rho e(p, \rho)$.

The source term on the right includes contributions from body forces and is written in terms of the (time-independent) gravitational potential Φ and the acceleration vector \mathbf{g} (§5.4).

6.2 The MHD Module

The MHD module is suitable for the solution of ideal or resistive (non-relativistic) magnetohydrodynamical equations. Source and definition files are located inside the Src/MHD directory.

With the MHD module, **PLUTO** solves the following system of conservation laws:

$$\begin{aligned}
 \frac{\partial \rho}{\partial t} + \nabla \cdot (\rho \mathbf{v}) &= 0 \\
 \frac{\partial \mathbf{m}}{\partial t} + \nabla \cdot \left[\mathbf{m} \mathbf{v} - \mathbf{B} \mathbf{B} + \mathbf{I} \left(p + \frac{\mathbf{B}^2}{2} \right) \right]^T &= -\rho \nabla \Phi + \rho \mathbf{g} \\
 \frac{\partial \mathbf{B}}{\partial t} + \nabla \times (c \mathbf{E}) &= 0 \\
 \frac{\partial (E_t + \rho \Phi)}{\partial t} + \nabla \cdot \left[\left(\frac{\rho \mathbf{v}^2}{2} + \rho e + p + \rho \Phi \right) \mathbf{v} + c \mathbf{E} \times \mathbf{B} \right] &= \mathbf{m} \cdot \mathbf{g}
 \end{aligned} \tag{6.4}$$

where ρ is the mass density, $\mathbf{m} = \rho \mathbf{v}$ is the momentum density, \mathbf{v} is the velocity, p is the gas (thermal) pressure, \mathbf{B} is the magnetic field² and E_t is the total energy density:

$$E_t = \rho e + \frac{\mathbf{m}^2}{2\rho} + \frac{\mathbf{B}^2}{2}. \tag{6.5}$$

where an additional equation of state provides the closure $\rho e = \rho e(p, \rho)$ (see Chapter 7). The source term on the right includes contributions from body forces and is written in terms of the (time-independent) gravitational potential Φ and the acceleration vector \mathbf{g} (see §5.4).

In the third of Eq. (6.4), \mathbf{E} is the electric field defined by the expression

$$c \mathbf{E} = -\mathbf{v} \times \mathbf{B} + \frac{\eta}{c} \cdot \mathbf{J} + \frac{\mathbf{J}}{ne} \times \mathbf{B} \quad \left(\mathbf{J} = c \nabla \times \mathbf{B} \right) \tag{6.6}$$

where the first term is the convective term, the second term is the resistive term (η denotes the resistivity tensor. see §8.2) while the third term is the Hall term (§8.1). Note that the speed of light c never enters

PLUTO physics modules, equations

6.3 The RHD Module

The RHD module implements the equations of special relativistic fluid dynamics in 1, 2 or 3 dimensions. Velocities are always assumed to be expressed in units of the speed of light. The special relativistic module comes with 2 different equations of state, and it also works in curvilinear coordinates. Gravity in Newtonian approximation can also be incorporated. The relevant source files and definitions for this module can be found in the Src/RHD directory.

The special relativistic module evolves the conservative set U of state variables

$$U = \left(D, m_1, m_2, m_3, E_t \right)^T$$

where D is the laboratory density, $m_{x1,x2,x3}$ are the momentum components, E_t is the total energy (including contribution from the rest mass). The evolutionary conservative equations are

$$\frac{\partial}{\partial t} \begin{pmatrix} D \\ \mathbf{m} \\ E_t \end{pmatrix} + \nabla \cdot \begin{pmatrix} D\mathbf{v} \\ \mathbf{m}\mathbf{v} + p\mathbf{l} \\ \mathbf{m} \end{pmatrix}^T = \begin{pmatrix} 0 \\ \mathbf{f}_g \\ \mathbf{v} \cdot \mathbf{f}_g \end{pmatrix}$$

where \mathbf{v} is the velocity, p is the thermal pressure. Primitive variables V always include the rest-mass density ρ , three-velocity $\mathbf{v} = (v_{x1}, v_{x2}, v_{x3})$ and pressure p . With PLUTO 4.4, the acceleration term \mathbf{f}_g is treated consistently³ with the formalism of [Tau48]. If \mathbf{a} is the acceleration vector,

$$\mathbf{f}_g = \rho\gamma^2 [\gamma^2 \mathbf{v} (\mathbf{v} \cdot \mathbf{a}) + \mathbf{a}] . \quad (6.12)$$

PLUTO physics modules, equations

6.4 The RMHD Module

The RMHD module implements the equations of (ideal) special relativistic magnetohydrodynamics in 1, 2 or 3 dimensions. Velocities are always assumed to be expressed in units of the speed of light. Source and definition files are located inside the Src/RMHD directory.

The RMHD module solves the following system of conservation laws:

$$\frac{\partial}{\partial t} \begin{pmatrix} D \\ \mathbf{m} \\ E_t \\ \mathbf{B} \end{pmatrix} + \nabla \cdot \begin{pmatrix} D\mathbf{v} \\ w_t\gamma^2\mathbf{v}\mathbf{v} - \mathbf{b}\mathbf{b} + p_t \\ \mathbf{m} \\ \mathbf{v}\mathbf{B} - \mathbf{B}\mathbf{v} \end{pmatrix}^T = \begin{pmatrix} 0 \\ \mathbf{f}_g \\ \mathbf{v} \cdot \mathbf{f}_g \\ 0 \end{pmatrix} \quad (6.13)$$

where D is the laboratory density, \mathbf{m} is the momentum density, E is the total energy (including contribution from the rest mass) while \mathbf{f}_g is an acceleration term (see [6.3](#)).

Primitive variables are similar to the RHD module but they also contain the magnetic field, $\mathbf{V} = (\rho, \mathbf{v}, p, \mathbf{B})$. The relation between \mathbf{V} and \mathbf{U} is

$$\begin{aligned} D &= \gamma\rho \\ \mathbf{m} &= w_t\gamma^2\mathbf{v} - b^0\mathbf{b} \\ E_t &= w_t\gamma^2 - b^0b^0 - p_t \end{aligned} \quad , \quad \begin{cases} b^0 = \gamma\mathbf{v} \cdot \mathbf{B} \\ \mathbf{b} = \mathbf{B}/\gamma + \gamma(\mathbf{v} \cdot \mathbf{B})\mathbf{v} \\ w_t = \rho h + \mathbf{B}^2/\gamma^2 + (\mathbf{v} \cdot \mathbf{B})^2 \\ p_t = p + \frac{\mathbf{B}^2/\gamma^2 + (\mathbf{v} \cdot \mathbf{B})^2}{2} \end{cases}$$

PLUTO physics modules, equations

A note on public vs. non-public modules.

Besides the official code release, a few modules have not yet been made available with the standard public version, as they are still under active development or testing stage. In other circumstances, a private module may have been implemented under specific collaboration policies, which do not grant its public distribution. These non-offical modules include:

- Lagrangian Particle Module
(Developers: B. Vaidya [*bvaidya@iiti.ac.in*], D. Mukherjee [*dipanjan@iucaa.in*]);
- Dust Module
(Developers: A. Mignone [*mignone@to.infn.it*], M. Flock [*flock@mpia.de*]);
- Relativistic Resistive MHD
(Developers: A. Mignone [*mignone@to.infn.it*], G. Mattia [*mattia@mpia.de*]);

Distribution, private sharing and usage of these modules is permitted only in the form of a collaboration between our partner institutions network, requiring co-authorship from at least one of the module developers.

6.5 The Resistive RMHD (*ResRMHD*) Module

Note: This module is not part of the public code release, see “Terms & Conditions of Use” at the beginning of this guide

The ResRMHD module deals with the non-ideal relativistic MHD equations using the approaches discussed in [MMBD19](#). Source and definition files are located inside the Src/ResRMHD directory.

The set of resistive relativistic equations arising from the time and space split of the covariant are, in vectorial form,

$$\begin{aligned}
 \frac{\partial D}{\partial t} + \nabla \cdot (D\mathbf{v}) &= 0, \\
 \frac{\partial \mathbf{m}}{\partial t} + \nabla \cdot (w\mathbf{u}\mathbf{u} + p\mathbf{l} + \mathbb{T}) &= 0, \\
 \frac{\partial \mathcal{E}}{\partial t} + \nabla \cdot \mathbf{m} &= 0, \\
 \frac{\partial \mathbf{B}}{\partial t} + \nabla \times \mathbf{E} &= 0, \\
 \frac{\partial \mathbf{E}}{\partial t} - \nabla \times \mathbf{B} &= -\mathbf{J},
 \end{aligned} \tag{6.14}$$

where \mathbf{l} is the identity matrix and the fluid conserved variables are the density $D = \rho\gamma$ as measured in the laboratory frame, the total momentum density $\mathbf{m} = w\gamma\mathbf{u} + \mathbf{E} \times \mathbf{B}$, and the total energy density

$$\mathcal{E} = w\gamma^2 - p + \mathcal{P}_{\text{EM}}. \tag{6.15}$$

In the expressions above, $w = \varepsilon + p$ is the specific enthalpy and $\mathcal{P}_{\text{EM}} = (E^2 + B^2)/2$ denotes the EM energy density. Finally,

$$\mathbb{T} = -\mathbf{E}\mathbf{E} - \mathbf{B}\mathbf{B} + \frac{1}{2}(E^2 + B^2)\mathbf{l} \tag{6.16}$$

7. Equation of State

In the current implementation, **PLUTO** describes a thermally ideal gas obeying the *thermal* Equation of State (EOS)

$$p = nk_B T = \frac{\rho}{m_u \mu} k_B T \quad (7.1)$$

where p is the pressure, n is the total particle number density, k_B is the Boltzmann constant, T is the temperature, ρ is the density, m_u is the atomic mass unit and μ is the mean molecular weight. The thermal EOS describes the thermodynamic state of a plasma in terms of its pressure p , density ρ , temperature T and chemical composition μ . Eq. (7.1) is written in CGS physical units. Using code units for p and ρ while leaving temperature in Kelvin, the thermal EOS is conveniently re-expressed as

$$p = \frac{\rho T}{\mathcal{K} \mu} \quad \iff \quad T = \frac{p}{\rho} \mathcal{K} \mu \quad \left(\text{where } \mathcal{K} = \frac{m_u v_0^2}{k_B} \right) \quad (7.2)$$

where \mathcal{K} is the **KELVIN** macro which depends explicitly on the value of `UNIT_VELOCITY`.

8. Nonideal Effects

In this chapter we give an overview of the code capabilities for treating dissipative (or diffusion) terms which, at present, include

- Hall MHD (MHD), described in §8.1
- Resistivity (MHD), described in §8.2
- Thermal conduction (HD, MHD), described in §8.3
- Viscosity (HD, MHD), described in §8.4

Each modules can be individually turned on from the physics sub-menus accessible via the Python script.

9. Optically Thin Cooling

PLUTO can include time-dependent optically thin radiative losses in a fractional step formalism in which the hydrodynamical evolution and the source step are solved separately using operator splitting. This preserves 2^{nd} order accuracy in time if both the advection and source steps are at least 2^{nd} order accurate. During the cooling source step, specifically, **PLUTO** solves the internal energy and chemical reaction network equations

$$\begin{cases} \frac{\partial(\rho e)}{\partial t} = -\Lambda(n, T, \mathbf{X}) \\ \frac{\partial \mathbf{X}}{\partial t} = \mathbf{S}(\mathbf{X}, T) \end{cases} \quad (9.1)$$

where Λ is a cooling (or heating) term, \mathbf{X} is an array of fractional abundances (typically ion or molecule number fractions) and \mathbf{S} is a reaction source term. The right-hand side of Equations (9.1) is implemented in the function `Src/Cooling/<COOLING>/radiat.c` of each corresponding cooling module, except for the `POWER_LAW` cooling where integration is performed analytically. The user can select one among several different cooling module by setting the `COOLING` flag during the python script:

- `POWER_LAW`: power-law cooling, see §9.1
- `TABULATED`: only the equation for the internal energy with a tabulated cooling function $\Lambda(T)$ is provided. No chemical network, see §9.2
- `SNEq`: cooling function for atomic hydrogen, $\mathbf{X} = \{X_{HI}\}$, including ionization, recombination and collisionally excited emission lines, §9.3
- `H2_COOL`: cooling function for atomic and molecular and atomic hydrogen, $\mathbf{X} = \{X_{H2}, X_{HI}, X_{HII}\}$, including ionization, recombination and collisionally excited emission lines, §9.4
- `MINEq`: cooling function for atomic and molecular and atomic hydrogen treating the time-dependent ionization state of the plasma, $\mathbf{X} = \{X_H, X_{He}, X_C, X_N, X_{Ne}, X_O, X_S\}$, see §9.5

Cooling modules are implemented inside the `Src/Cooling` directory and require three dimensional constants to be correctly initialized. Dimensional constants are essential to scale data values to cgs physical units as explained in §5.1.1

Other variables are introduced to control crucial parameters such as the maximum allowed cooling rate in each time step, or the cutoff temperature:

- `g_maxCoolingRate`: limit the time step so that the maximum fractional thermal losses cannot exceed `g_maxCoolingRate`. In general $0 < g_maxCoolingRate < 1$; the default is 0.1.
- `g_minCoolingTemp`: sets the cut-off temperature below which cooling is artificially set to 0.

9.1 Power-Law Cooling

Power-law cooling is the most simple form of cooling, where the loss term in the internal energy equation becomes:

$$\Lambda = a_r \rho^2 T^\alpha \quad (9.2)$$

There are no new species when this form of cooling is selected. When an ideal equation of state is used, the source step becomes

$$\frac{dp}{dt} = -(\Gamma - 1) a_r \rho^{2-\alpha} p^\alpha (\mathcal{K}\mu)^\alpha$$

and since density is not affected during this step, integration is done analytically:

$$p^{n+1} = \begin{cases} \left[(p^n)^{1-\alpha} - \Delta t C (1-\alpha) \right]^{\frac{1}{1-\alpha}} & \text{for } \alpha \neq 1 \\ p^n \exp(-C \Delta t) & \text{for } \alpha = 1 \end{cases} \quad (9.3)$$

where $C = (\Gamma - 1) a_r \rho^{2-\alpha} (\mathcal{K}\mu)^\alpha$ is a constant.

The default power law accounts for bremsstrahlung cooling by solving

$$\frac{dp_{\text{cgs}}}{dt_{\text{cgs}}} = -(\Gamma - 1) \frac{a_{\text{br}}}{\mu^2 m_H^2} \rho_{\text{cgs}}^2 \sqrt{T(K)} \quad \implies \quad \frac{dp}{dt} = -C \rho^2 \sqrt{\frac{p}{\rho}} \quad (9.4)$$

with p , t and ρ given in code units and

$$C = a_{\text{br}} \frac{\Gamma - 1}{(k_B \mu m_H)^{3/2}} \frac{\rho_0 L_0}{v_0^2}$$

where ρ_0 , v_0 and L_0 are the reference density, velocity and length defined in §5.1.1 and $a_{\text{br}} = 2 \cdot 10^{-27}$ in expressed in c.g.s. units. The implementation of this cooling step, with $\alpha = 1/2$, can be found under `Src/Cooling/Power_Law/cooling.c`.

9.2 Tabulated Cooling

The tabulated cooling module provides a way to solve the internal energy equation

$$\Lambda = n^2 \tilde{\Lambda}(T), \quad \text{with} \quad n = \frac{\rho}{\mu m_u} \quad (9.5)$$

when the cooling/heating function $\tilde{\Lambda}(T)$ is not known analytically but rather is available as a table sampled at discrete (not necessarily equidistant) points, i.e., $\tilde{\Lambda}_j \equiv \tilde{\Lambda}(T_j)$. In order to use this module, the user must provide a two-column ascii files in the working directory named `cooltable.dat` of the form

```
.      .  
.      .  
T(j)   Lambda(j)  
.      .  
.      .  
.      .
```

with the temperature expressed in Kelvin and the cooling/heating function $\tilde{\Lambda}$ in `ergs.cm3/s`. An example of such file `1` can be found in `Src/Cooling/Tab/cooltable.dat`. As usual, the dimensionalization is done automatically by the cooling module, once `UNIT_DENSITY`, `UNIT_LENGTH` and `UNIT_VELOCITY` have been defined in `Init()`.

Alternatively, the `TABULATED` cooling module can be used to provide a user-defined cooling function,

$$\Lambda = \Lambda(\mathbf{V}), \quad (9.6)$$

where \mathbf{V} is a vector primitive variables. The explicit dependence of Λ can be given by i) copying `Src/Cooling/Tab/radiat.c` into your local working directory and ii) make the appropriate changes.

10.3 The RADIATION Module

The RADIATION module couples the conservation laws of relativistic/nonrelativistic HD/MHD to a system of frequency- and angle-averaged radiation transport equations computing the evolution of the radiation energy density, E_r , and the three components of the radiation flux, \mathbf{F}_r . We normalize the latter by c in such a way that all radiation fields are measured in energy density units. Assumptions and implementation details are summarized in [MM19] (relativistic version) and [MKFM21] (nonrelativistic version).

In the nonrelativistic modules (HD/MHD), ignoring extra source terms (e.g., viscosity), the resulting system of equations takes the form

$$\begin{aligned}
 \frac{\partial \rho}{\partial t} + \nabla \cdot (\rho \mathbf{v}) &= 0 \\
 \frac{\partial \mathbf{m}}{\partial t} + \nabla \cdot \left[\mathbf{m} \mathbf{v} - \mathbf{B} \mathbf{B} + \mathbf{l} \left(p + \frac{\mathbf{B}^2}{2} \right) \right]^T &= -\rho \nabla \Phi + \rho \mathbf{g} + \mathbf{G} \\
 \frac{\partial \mathbf{B}}{\partial t} + \nabla \times (c \mathbf{E}) &= 0 \\
 \frac{\partial (E_t + \rho \Phi)}{\partial t} + \nabla \cdot \left[\left(\frac{\rho v^2}{2} + \rho e + p + \rho \Phi \right) \mathbf{v} + c \mathbf{E} \times \mathbf{B} \right] &= \mathbf{m} \cdot \mathbf{g} + c G^0 - \nabla \cdot \mathbf{F}_{\text{Irr}} \\
 \frac{1}{\hat{c}} \frac{\partial E_r}{\partial t} + \nabla \cdot \mathbf{F}_r &= -G^0 \\
 \frac{1}{\hat{c}} \frac{\partial \mathbf{F}_r}{\partial t} + \nabla \cdot \mathbb{P}_r &= -\mathbf{G}
 \end{aligned} \tag{10.6}$$

(see Eq. (6.4)), while in the relativistic modules (RHD/RMHD), the resulting system is

$$\frac{\partial}{\partial t} \begin{pmatrix} D \\ \mathbf{m} \\ E_t \\ \mathbf{B} \\ E_r \\ \mathbf{F}_r \end{pmatrix} + \nabla \cdot \begin{pmatrix} D \mathbf{v} \\ w_t \gamma^2 \mathbf{v} \mathbf{v} - \mathbf{b} \mathbf{b} + \mathbf{l} p_t \\ \mathbf{m} \\ \mathbf{v} \mathbf{B} - \mathbf{B} \mathbf{v} \\ \mathbf{F}_r \\ \mathbb{P}_r \end{pmatrix}^T = \begin{pmatrix} 0 \\ \mathbf{G} \\ G^0 - \nabla \cdot \mathbf{F}_{\text{Irr}} \\ 0 \\ -G^0 \\ -\mathbf{G} \end{pmatrix} \tag{10.7}$$

(see Eq. (6.13)). In all cases, the components of the radiation pressure tensor, \mathbb{P}_r , are defined as a function of (E_r, \mathbf{F}_r) via the M1 closure by [Lev84] as

$$P^{ij} = E_r \left(\frac{1 - \xi}{2} \delta^{ij} + \frac{3\xi - 1}{2} n^i n^j \right), \quad \xi = \frac{3 + 4f^2}{5 + 2\sqrt{4 - 3f^2}}, \tag{10.8}$$

where $\mathbf{n} = \mathbf{F}_r / |\mathbf{F}_r|$, $f = |\mathbf{F}_r| / E_r$, and δ^{ij} is the Kronecker delta. The radiation-matter interaction terms (G^0, \mathbf{G}) are defined by boosting into the Eulerian frame their comoving values, given by

$$(G^0, \mathbf{G})_{\text{comov}} = \rho \left[\kappa (E_r - a_R T^4), (\kappa + \sigma) \mathbf{F}_r \right]_{\text{comov}}. \tag{10.9}$$

In this equation, κ and σ are the frequency-averaged absorption and scattering coefficients, respectively, $a_R = 4\sigma_{\text{SB}}/c$ is the radiation constant, and T is the fluid's temperature.

The reduced speed of light, \hat{c} , is introduced in the nonrelativistic equations to reduce the overhead of the explicit integration of radiation transport terms. Additional speedup is achieved by splitting the integration of radiation and MHD fields, applying substepping to integrate the radiation subsystem. The computational cost can be minimized by the user by setting \hat{c}/c to the smallest value that does not alter the resulting dynamics (see [MKFM21]).

Heating by external (e.g., stellar) sources of irradiation not included in the (E_r, \mathbf{F}_r) radiation field can be added as a user-defined source term depending on an external irradiation flux, \mathbf{F}_{Irr} (see §10.3.1).

10.3.1 Using the module

The RADIATION module can be switched on by setting the RADIATION switch to YES in the HD, MHD, RHD, or RMHD sub-menus. The relativistic version is compatible with AMR. The nonrelativistic version is compatible with the ROTATING.FRAME option and usual nonideal options such as VISCOSITY, which are applied during the HD/MHD step.

The radiation fields are initialized in `Init ()` or `InitDomain ()` using the indices ENR, FR1, FR2, and FR3 (see Table 10.1). Although these indices can be used in any coordinate system, an alternative set can be used in curvilinear coordinates to avoid confusion (see columns 2-4 in Table 10.1). Boundary conditions for (E_r, \mathbf{F}_r) can be defined either in `pluto.ini`, in which case they coincide with those assigned to (ρ, v) , or in `UserDefBoundary ()` if the boundary is set as `userdef`.

Three possible Riemann solvers can be selected for the explicit integration of radiation fluxes. The solver for the radiation subsystem is defined independently from the HD/MHD solver by setting the `RadSolver` tag in the `[Solver]` block of `pluto.ini`, as described in §4.4. All reconstruction methods available in PLUTO can be used. Additional integration options can be found in Table C.1.

Index	Cylindrical	Polar	Spherical	Quantity
ENR	-	-	-	radiation energy density
FR1	iFRR	iFRR	iFRR	x_1 -radiation flux
FR2	iFRZ	iFRPHI	iFRTH	x_2 -radiation flux
FR3	iFRPHI	iFRZ	iFRPHI	x_3 -radiation flux

Table 10.1: Additional array indices used for labeling primitive variables in the RADIATION module.

External irradiation can be switched on by defining IRRADIATION as YES in `definitions.h`. The divergence of the irradiation flux, $\nabla \cdot \mathbf{F}_{\text{Irr}}$, must then be computed in a local file `irradiation.c`, stored in both primitive and conserved fields using the index FIR. A template for this file is provided in `Src/Radiation/irradiation.c` (see also the Disk-Planet test in `Test.Problems/Radiation/Nonrelativistic/HD-Disk-Planet/`). The term $\nabla \cdot \mathbf{F}_{\text{Irr}}$ is only computed at startup if IRRADIATION_UPDATE is defined as NO in `definitions.h`; otherwise, it is computed at each hydro step by default.

10.3.1.1 Constants and units

The RADIATION module depends on the following constants, which can be defined either in `Init ()` or `InitDomain ()`:

- `g_radiationConst` (double, default: 1): the radiation constant, $a_R = 4\sigma_{\text{SB}}/c$.
- `g_idealGasConst` (double, default: 1): the ideal gas constant, c_I , determining the gas temperature in code units as $T = c_I p/\rho$.

In the nonrelativistic version, the following constants must also be specified:

- `g_radC` (double, default: 1): the speed of light, c .
- `g_reducedC` (double, default: 1): the reduced speed of light, \hat{c} .

If constant opacities are used (see §10.3.1.2), they must be defined as follows:

- `g_absorptionCoeff` (double, default: 0): the absorption opacity, κ .
- `g_scatteringCoeff` (double, default: 0): the scattering opacity, σ .

10.3.1.2 Opacities

The opacity coefficients κ and σ in Eq. (10.9) can be defined either as constants (see §10.3.1.1) or as user-defined functions of the primitive fields. The latter option is selected by defining `RADIATION_VAR_OPACITIES` as `YES` in `definitions.h` and defining in `init.c` a function `UserDefOpacities()` of the form

```
void UserDefOpacities(double *v, double *abs, double *scat) ,
```

where `*v` is a pointer to a vector of primitive variables, while `*abs` and `*scat` are pointers used to store the resulting absorption and scattering coefficients. As an example, Kramers' opacity law $\kappa \propto \rho T^{-7/2}$ with $\sigma = 0$ can be defined as follows:

```
#if RADIATION_VAR_OPACITIES
void UserDefOpacities (double *v, double *abs, double *scat)
{
    double T ;

    T = GetTemperature (v[RHO],v[PRS]) ;

    *scat = 0.0 ;
    *abs = v[RHO] * pow(T,-3.5) ;
}
#endif
```

In this example, the gas temperature is computed as $T = c_I p / \rho$ by means of the built-in function `GetTemperature()`:

```
void GetTemperature(double rho, double prs) .
```

Another built-in function, particularly useful to define initial conditions in local thermal equilibrium, is `Blackbody()`:

```
void Blackbody(double temperature) ,
```

which returns the value of $a_R T^4$ taking as input the value of T .

Note: To achieve good accuracy in both the optically thick and optically thin limits, the terms between brackets in Equation (10.9) are commonly defined as $[\kappa_P(E_r - a_R T^4), \chi_R \mathbf{F}_r]$, where κ_P is the Planck-averaged absorption opacity and χ_R is the Rosseland-averaged total (absorption+scattering) opacity. To do this, κ must be defined as κ_P , and σ must be defined as $\chi_R - \kappa_P$.

Hot discs

The simulations up to now were with **cold** thin discs. This is physically correct for proto-planetary discs around YSOs, but if we rescale the results to the WD, NS or BH case, the disc is hot. With this year interns during the Summer program in CAMK, I started preparing the setup for hot discs. The only change is actually to change the polytropic index in PLUTO setup: by default, it is $\gamma=5/3$, which is for adiabatic processes. For isothermal it would be $\gamma=1$, and for hot discs we expect something between like $\gamma=4/3$. So, in `init.c` we have to set such values, by setting `g_gamma`.

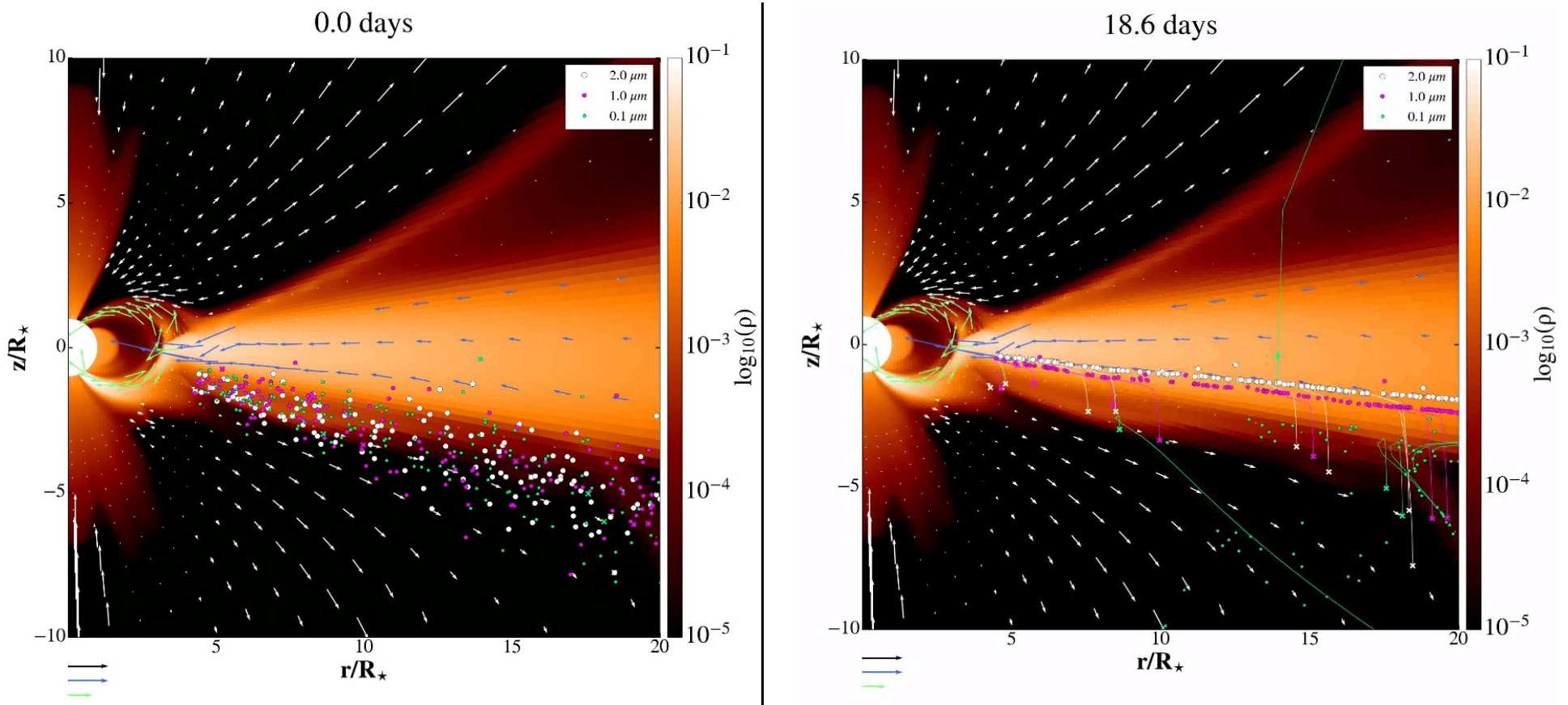
```
I A init.c (Modified)(c) void Init (double *v, double x1, double x2, double x3)
{
    double coeff, eps2, pc, rcyl;
    double br, bth;
    double lambda;
    double xhi2, Rco;
    g_gamma=4./3.; //ccm150824--we change from PLUTO default g_gamma=5./3.

    rcyl=x1*sin(x2);
    eps2=g_inputParam[EPS]*g_inputParam[EPS];
    // coeff=2./5./eps2*(1./x1-(1.-5./2.*eps2)/rcyl);
    //ccm230824:
    coeff=(g_gamma-1.)/g_gamma/eps2*(1./x1-(1.-eps2*g_gamma/(g_gamma-1.))/rcyl); //coeff=rho_d/rho_d0

    lambda=11./5./(1.+64./25.*g_inputParam[ALPHAV]*g_inputParam[ALPHAV]);
    /* initial non-rotating adiabatic corona in hydrostatic equilibrium */
    v[RHO] = g_inputParam[RHOC]*pow(x1,-1./(g_gamma-1.));
    v[PRS] = (g_gamma-1.)/g_gamma*g_inputParam[RHOC]*pow(x1,-g_gamma/(g_gamma-1.));
    pc=v[PRS]; //coronal pressure
    v[VX1] = 0.0;
    v[VX2] = 0.0;
    v[VX3] = 0.0;
    /* Keplerian adiabatic disk in vertical pressure equilibrium with the
       adiabatic corona, as given by Kluzniak & Kita (2000) */
    v[PRS]=eps2*pow(coeff,g_gamma/(g_gamma-1.));
    if (v[PRS] >= pc && rcyl > g_inputParam[RD])
    {v[RHO] = pow(coeff,1./(g_gamma-1.));
    v[PRS]=eps2*pow(coeff,g_gamma/(g_gamma-1.));
    v[VX1] = -g_inputParam[ALPHAV]/sin(x2)*eps2*(10.-32./3.
    *lambda*g_inputParam[ALPHAV]*g_inputParam[ALPHAV]
    -lambda*(5.-1./(eps2*tan(x2)*tan(x2)))/sqrt(rcyl);
    v[VX3] = (sqrt(1.-5./2.*eps2)+2./3.*eps2
    *g_inputParam[ALPHAV]*g_inputParam[ALPHAV]
    *lambda*(1.-6./(5.*eps2*tan(x2)*tan(x2)))/sqrt(rcyl);
    v[TRC] = 1.0; /* Track the disc material */
    }
    else
    {v[PRS]=(g_gamma-1.)/g_gamma*g_inputParam[RHOC]*pow(x1,-g_gamma/(g_gamma-1.));
    v[TRC] = 0.0; /* Track the corona */
    }
}
```

“STARDUST”: Dusty disk in Young Stellar Objects

During a Summer Student Program, C. Turski wrote the Python script “DUSTER” for post-processing of the quasi-stationary results in my star-disk solutions. He added the dust particles and computed their movement in the disk-corona solution as a background. The results are used to model dust distribution in the disk.



$$\ddot{\vec{r}} = -G \frac{M_\star}{r^3} \vec{r} - \frac{\rho_{\text{gas}}}{\rho_{\text{gr}}} \frac{c_s}{a} (\dot{\vec{r}} - \vec{v}_{\text{gas}}) + \beta G \frac{M_\star}{r^2}$$

$$\beta = 0.4 \frac{L_\star}{L_\odot} \frac{M_\odot}{M_\star} \frac{3000 \frac{\text{kg}}{\text{m}^3}}{\rho_{\text{gr}}} \frac{\mu\text{m}}{a}, \quad R_{\text{in}} = 0.0344 \Psi \left(\frac{1500\text{K}}{T_{\text{gr}}} \right)^2 \sqrt{\frac{L_{\text{tot}}}{L_\odot}} [\text{AU}],$$

Summary of the Lect. 7

- Different modules in PLUTO, cooling versus radiative transfer
- Hot discs
- Post-processing of the results, DUSTER
- Python script for analysis

Outline, Lect.8 : Pseudo-Newtonian potentials for BHs, NkS, Star-Planet²²⁵ simulations setup

- Pseudo-Newtonian potential and its use in numerical simulations of compact objects
- Simulations of thin disk or torus around a black hole in Paczynski-Wiita potential
- Simulations of thin disk around a naked singularity in pseudo-Newtonian potential for Reissner-Nordstrom metric.
- Star-planet simulations
- Running jobs on a Linux cluster

The name "black hole" is catchy, but misleading. These are not "holes", at least not empty ones: in fact, it is a large mass gathered in some volume (not necessarily large density). The escape velocity for these objects is greater than the speed of light!

The possibility of their existence is not news: we know that Romer in 1676 measured the finite speed of light quite accurately by observing Jupiter's satellites - for this a telescope was needed, the distances on earth are too small for primitive methods of measuring the speed of light - unless we know optics, but then we will already have a telescope... From the concept of the finite speed of light to the above-mentioned escape velocity and the conclusion that objects of sufficiently large mass could retain light is not far - this is how John Michell concluded in 1783: ***“If the semi-diameter of a sphere of the same density as the Sun in the proportion of five hundred to one, and by supposing light to be attracted by the same force in proportion to its [mass] with other bodies, all light emitted from such a body would be made to return towards it, by its own proper gravity.”***

The first description as "dark stars" followed from the invisibility of such objects. That inspiring description turned out to be physically incorrect: in Einstein's gravity, the curvature of space-time causes the curvature of the path of a light ray that does not change speed. But the fact that these objects are dark remains - John Wheeler called such objects "black holes" in a lecture in 1968, and that name remains to this day.

Naked singularities are also not something new: the solutions of the equations from which they "popped out" were published almost simultaneously with the Theory of Relativity (1916) and Schwarzschild's solutions for a non-rotating black hole (1916). The first solution was by Reissner (1916), who gave solutions for the electric charged, non-rotating black holes, and soon others arrived, including Nordström (1918), so such objects are now called Reissner-Nordström (RN) naked singularities.

The next step came only in the 1960s, with solutions for rotating, uncharged (Kerr 1963) and charged (Kerr-Newman, 1965) black holes. Very fast rotating black holes can become naked singularities and have no charge, which is more physically realistic - black holes are difficult to charge electrically, it is generally accepted that they should be electrically neutral. This was also the main reason why these solutions, although simple, are not better known, they remained as an exercise for beginners - I performed them on a couple of pages for the exercise of Christoffel symbols, I recommend them to doctoral students to refresh the General Theory of Relativity – I suggest to do it on paper, without using Maple or similar computer packages.

The Reissner-Nordström solutions, which are relatively simple, are nevertheless useful because they are mathematically identical in many properties to much more complicated solutions for rotating objects. That's why we started to study them in a pseudo-Newtonian approach, so that we can run simulations faster and do the first checks of ideas, which we can then study in more detail in relativistic simulations, which are more demanding.

The first exact solutions in GR

Schwarzschild metric (1916) for nonrotating BHs

$$ds^2 = \left(1 - \frac{2M}{r}\right) dt^2 - \left(1 - \frac{2M}{r}\right)^{-1} dr^2 - r^2 (d\theta^2 + \sin^2 \theta^2 d\phi^2).$$

Reissner-Nordström metric for nonrotating **charged** BHs, or, if $Q > M$, naked singularities (1916, 1918)

$$ds^2 = f(r) dt^2 - \frac{1}{f(r)} dr^2 - r^2 (d\theta^2 + \sin^2 \theta^2 d\phi^2), \quad (13)$$

$$\text{with } f(r) = 1 - \frac{2M}{r} + \frac{Q^2}{r^2} \equiv 1 - 2\frac{M}{r} + q^2 \frac{M^2}{r^2}. \quad (14)$$

Q is the electric charge of the gravitating body, and we define the dimensionless charge parameter $q = Q/M$.

Pseudo-Newtonian potentials

In a classical Newtonian description, we can describe the motion of a test particle of unit mass in the orbital plane $\theta = \pi/2$ around a much larger point mass M as a motion in the central gravitational potential $\Phi(r) = -GM/r$. The energy equation is:

$$E = \frac{1}{2}(v_r^2 + v_\phi^2) + \Phi(r). \quad (1)$$

Introducing the effective potential $U_{\text{eff}}(r, L) = \Phi(r) + L^2/(2r^2)$, we can write:

$$E - \frac{1}{2}v_r^2 = U_{\text{eff}}(r, L), \quad (2)$$

where E , L and v_r are the total energy, angular momentum and radial velocity, respectively.

For the circular orbits, the condition $(\partial U_{\text{eff}}/\partial r)_L = 0$ is satisfied, so that we obtain the condition:

$$\frac{\partial \Phi(r)}{\partial r} - \frac{L^2}{r^3} = 0. \quad (3)$$

Paczyński & Wiita (1980), for a non-rotating BH:

$$\frac{d}{dr} \left(\frac{1}{1 - 2M/r} \right) + \frac{2\ell}{r^3} = 0. \quad (10)$$

Employing $r/(r - 2M) = 2M/(r - 2M) + 1$, we can write:

$$\frac{d}{dr} \left(1 + \frac{2M}{r - 2M} \right) + \frac{2\ell}{r^3} = 0 \Rightarrow \frac{d}{dr} \left(\frac{2M}{r - 2M} \right) + \frac{2\ell^2}{r^3} = 0. \quad (11)$$

Comparison with the Eq. 3 gives the pseudo-Newtonian potential

$$V_{\text{PW}} = -\frac{M}{r - 2M}. \quad (12)$$

The Keplerian angular momentum $\ell = \sqrt{Mr^3}/(r - 2M)$ in the PW potential is the same as in its exact Schwarzschild GR solution, but the value of the Keplerian angular velocity is different: $\Omega_{\text{K,PW}} = \text{fix it } \sqrt{M/r^3}/(r - 2GM/r)$, while in the Schwarzschild solution it is the usual Newtonian $\Omega_{\text{K}} = \sqrt{GM/r^3}$

Kluźniak & Lee (2002), for a more exact rendering of PW:

$$\Phi(r) = \left(\frac{GM}{3r_G} \right) [1 - e^{3r_G/r}]$$

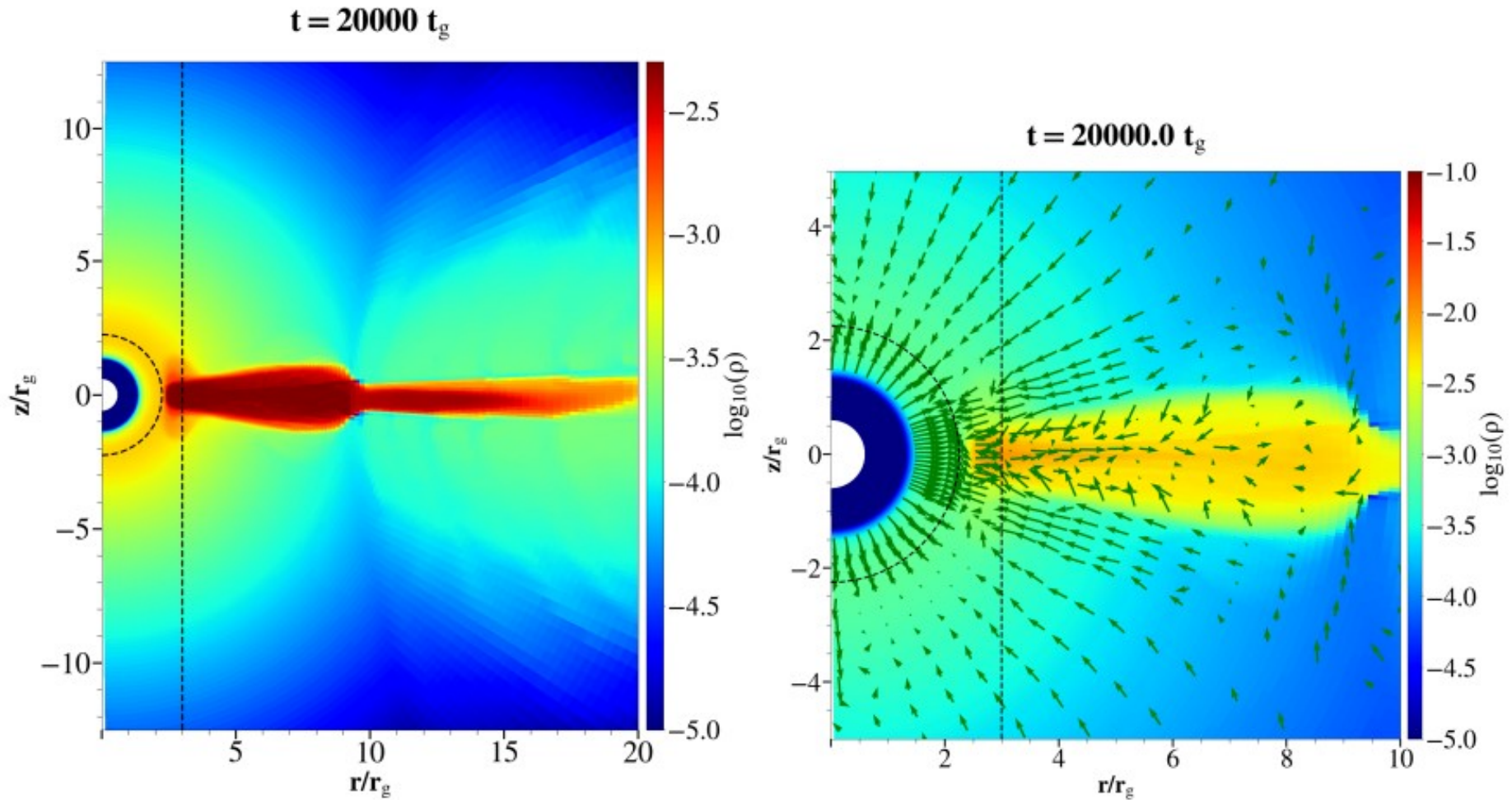


Fig. 2. Gas density in the simulation with $q = 1.5$. *Left panel:* a snapshot result at $t=20000 t_g$, where $t_g = r_g/c$. The zero-gravity radius r_0 is marked with the dashed half-circle and the radius, $4r_0/3$, at which test-particle Ω attains a maximum is marked with the straight black dashed line. *Right panel:* a zoom into the inner region of the accretion flow, obtained as an average over the time interval of $t \in [19000, 21000] t_g$. Poloidal gas velocity vectors are indicated with green arrows.

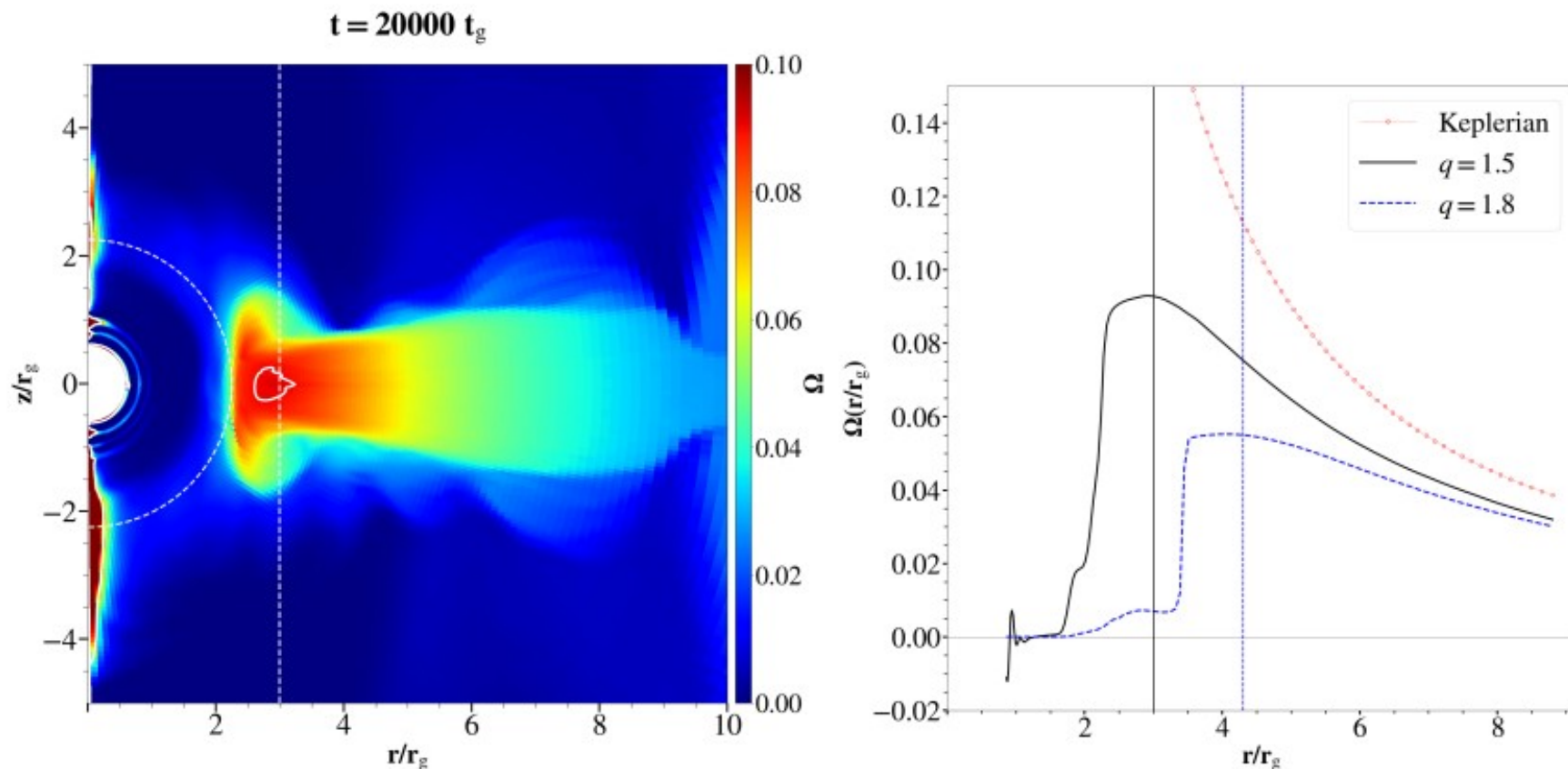


Fig. 3. *Left panel:* the angular velocity $\Omega = v_\phi/(r \cos \theta)$, in the linear color grading at $t = 20000 t_g$ in our simulation with $q = 1.5$. The contour of $\Omega = 0.09/M$ within which the test-particle orbital frequency value of Ω_{\max} at $r/M = 4q^2/3$ is located is shown with the white solid curve. *Right panel:* $\Omega(r)$ in the equatorial plane for the RN metric with $q = 1.5$ and 1.8 , in solid (black) and dashed (blue) lines, respectively. The dotted (red) line follows the Schwarzschild profile of ΩM , and is given for comparison. Vertical lines in the corresponding styles indicate the radial positions of Ω_{\max} test-particle orbital values for $q = 1.5$ and $q = 1.8$. MW: does it make sense to indicate the location of r_0 as well? Maybe with black/blue

Sure, there are many such approximations, each good for its purpose-some characteristic distances or surfaces are usually represented correctly in such pseudo-potentials.

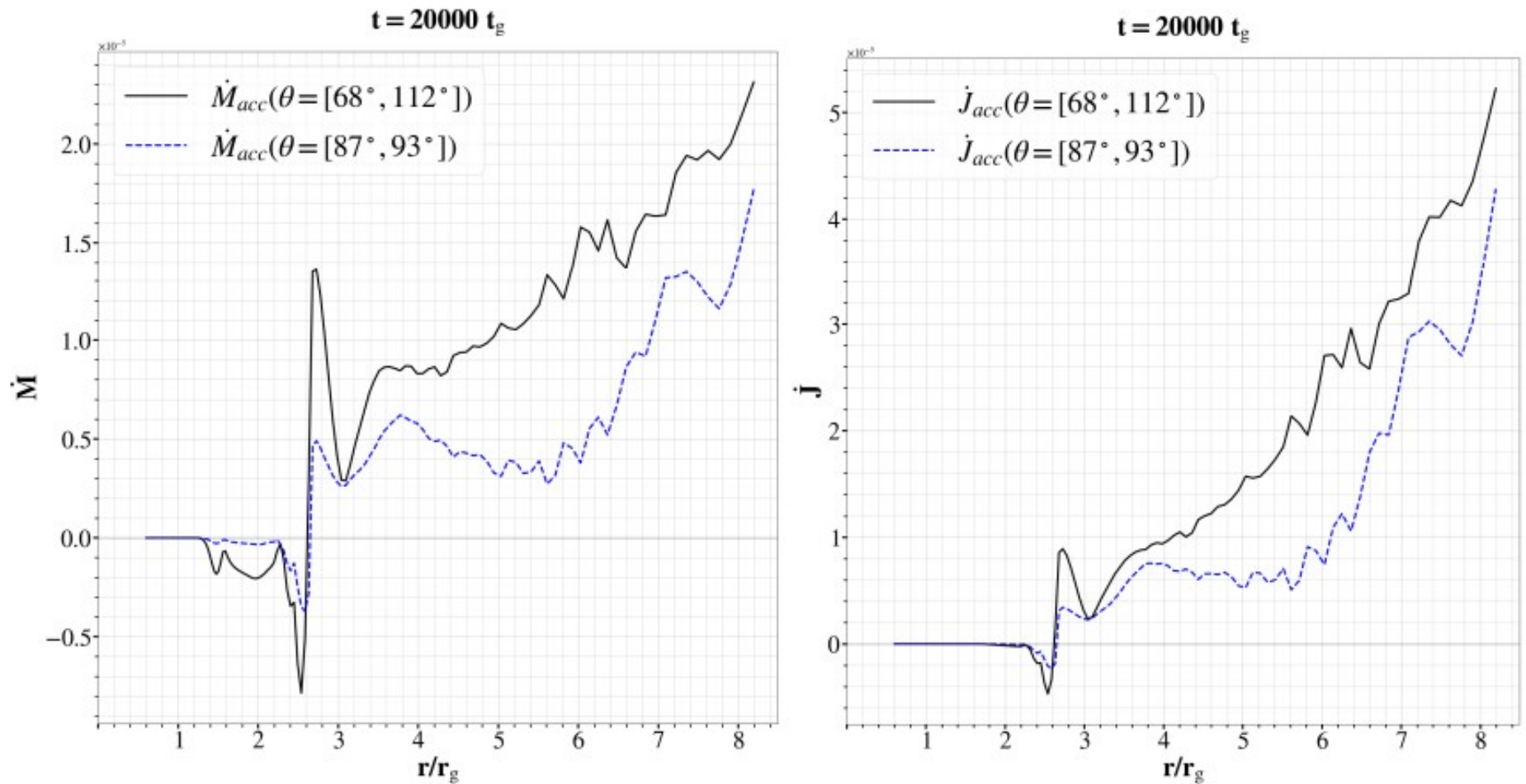


Fig. 4. Values of \dot{M} and \dot{J} computed in two co-latitudinal intervals as assigned in the legends, in dependence of radial distance from the origin in the simulation from Fig. 2, obtained as an average over the time interval of $t \in [19000, 21000] t_g$. MW: Can't the panels be of the same size?

In the SDI setup, at the end of the init.c file, just set the BodyForcePotential instead of BodyForceVector.

```
I A init.c (c) double BodyForcePotential(double x1, double x2, double x3)
* Return the gravitational potential as function of the coordinates.
*
* \param [in] x1 position in the 1st coordinate direction \f$x_1\f$
* \param [in] x2 position in the 2nd coordinate direction \f$x_2\f$
* \param [in] x3 position in the 3rd coordinate direction \f$x_3\f$
*
* \return The body force potential \f$\Phi(x_1,x_2,x_3)\f$.
*
***** */
{
//ccm--060824--uncomment the wanted pseudo-potential
//set in definitions.h #define BODY_FORCE POTENTIAL
//double q;
//q=1.25;
//return -1./(x1-2.);//0.0;//ccm--Paczynski-Wiita
return -(1.0/6.0)*(exp(6.0/x1)-1.0);//KluzniakLee
//return -1./x1+0.5*(q*q/x1/x1);//KluzniakNordstrom
}
#endif
```

Also in the definitions.h file, just set the BodyForcePotential instead of BodyForceVector.

```
I A definitions.h (c)
#define PHYSICS MHD
#define DIMENSIONS 2
#define GEOMETRY SPHERICAL
#define BODY_FORCE POTENTIAL
#define COOLING POWER_LAW
#define RECONSTRUCTION LINEAR
#define TIME_STEPPING RK2
#define NTRACER 1
#define PARTICLES NO
#define USER_DEF_PARAMETERS 9

/* -- physics dependent declarations -- */

#define EOS IDEAL
#define ENTROPY_SWITCH NO
#define DIVB_CONTROL DIV_CLEANING
#define BACKGROUND_FIELD YES
#define AMBIPOLAR_DIFFUSION NO
#define RESISTIVITY EXPLICIT
#define HALL_MHD NO
#define THERMAL_CONDUCTION NO
#define VISCOSITY EXPLICIT
#define ROTATING_FRAME NO

/* -- user-defined parameters (labels) -- */

#define ALPHAM 0
Joe's Own Editor 4.6 (utf-8) ** Type Ctrl-K Q to exit or
```

The magnetic field strength could be much smaller if

```
I pluto.ini (Modified)(ini)
uservar      3 nu num Te
dbl          6.283 -1  single_file
flt          -1.0  -1  single_file
vtk          6.283  -1  single_file
tab          -1.0  -1
dbl.h5       -6.283  -1
ppm          -1.0  -1
png          -1.0  -1
log          10
analysis     -1.0  -1

[Chombo HDF5 output]

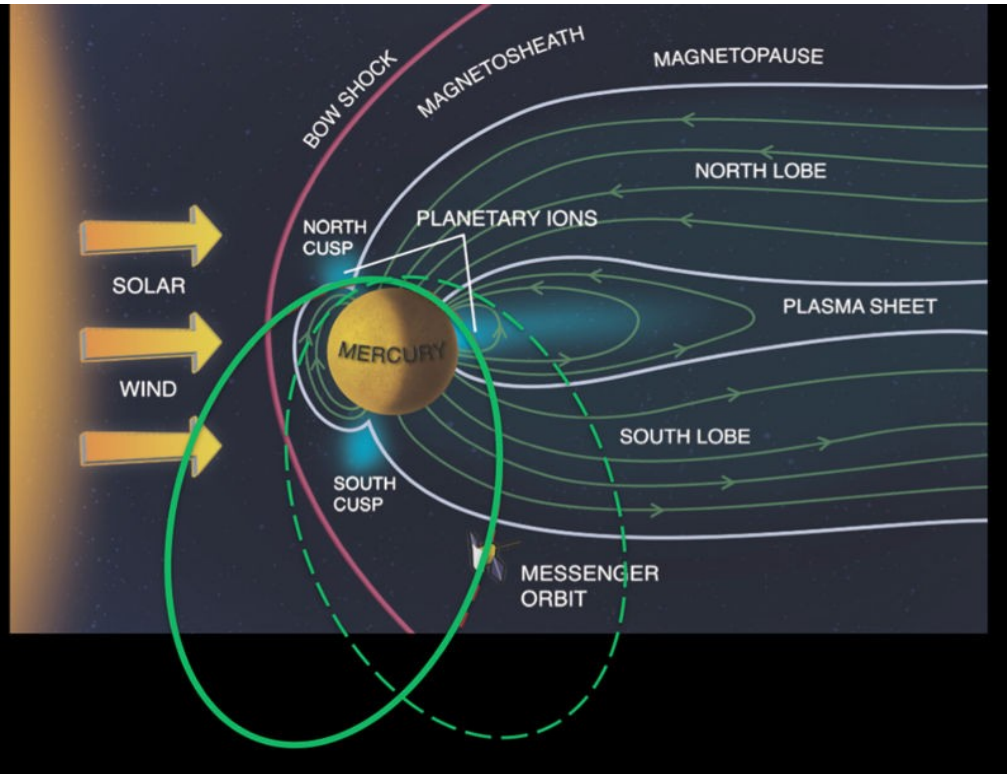
Checkpoint_interval -1
Plot_interval      1.0

[Parameters]

ALPHAM           0.1
MU               0.0007
TEMPF           300.0
RHOC             0.01
RD              4.0
EPS              0.1
OMG              0.0
ALPHAV           0.4
DFLOOR          5.e-7
```

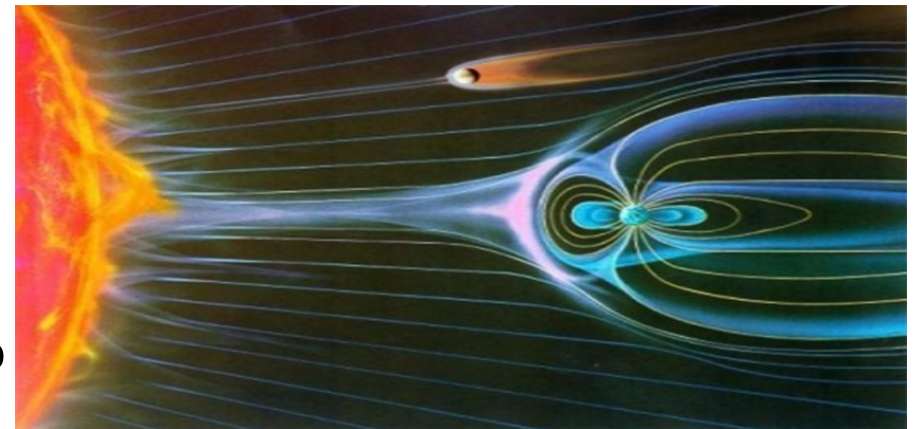
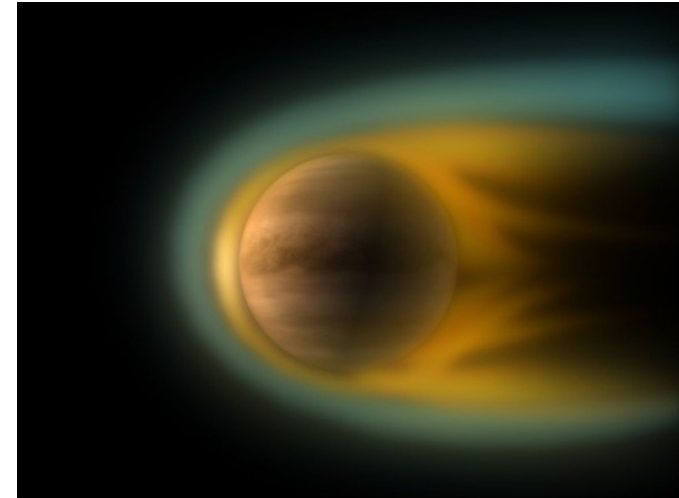
We will simulate star-planet magnetospheric interaction for a practical reason: auroras are found on most of the planets in the Solar system.

Mercury



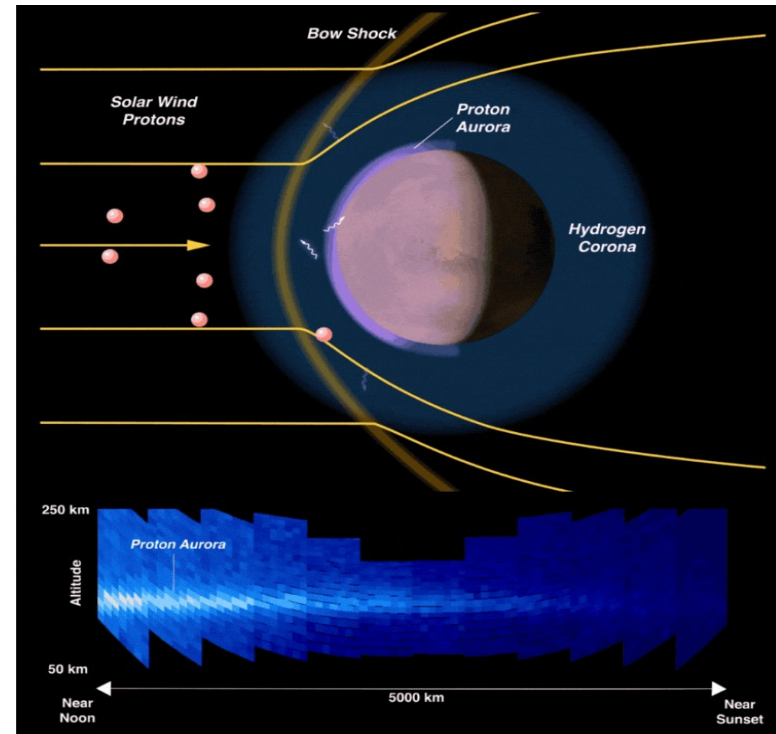
Mercury magnetic field is well measured thanks to Messenger probe. Its aurora is similar to Earth's.

Venus

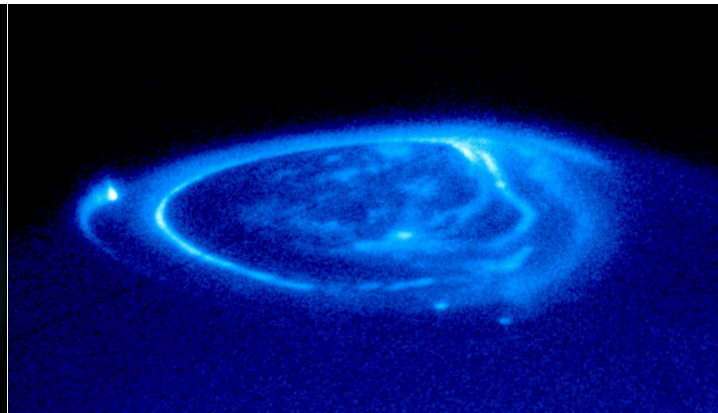
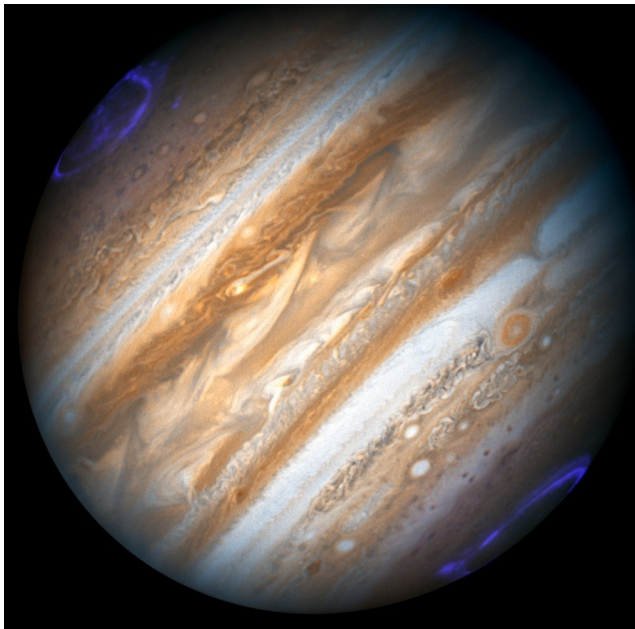


Venus has smaller aurora towards Sun than Earth, here I show a comparison.

Even in the planets like Mars, which do not have significant magnetic field, we observe aurora, formed as a result of interaction of particles-here mostly protons- from the solar wind shock where the planet moves through the wind. It is most visible at the sunny side of the planet.



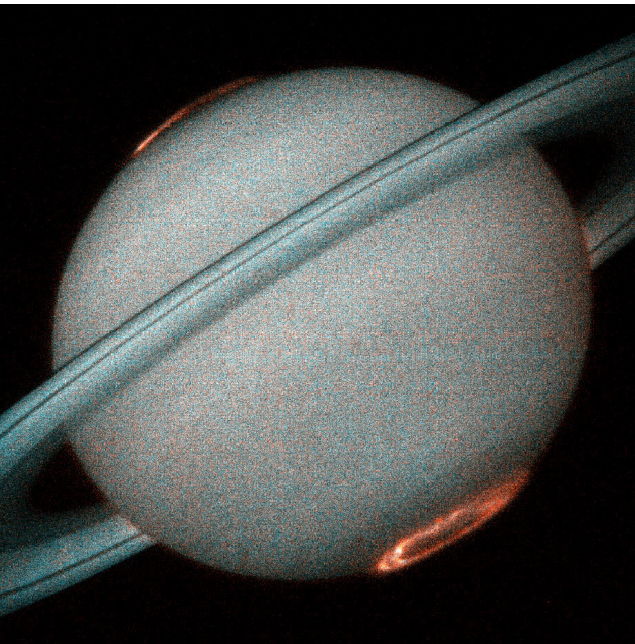
Aurora is observed also on Jupiter and Saturn. On the gas planets aurora is visible mostly in ultra-violet, so we can observe it from outside our atmosphere.



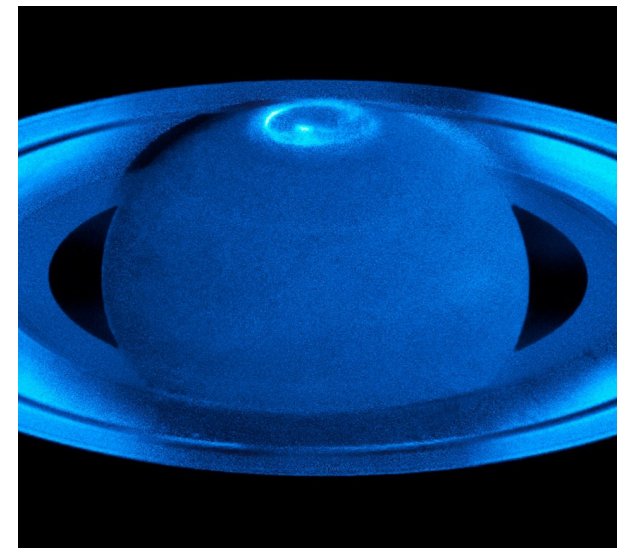
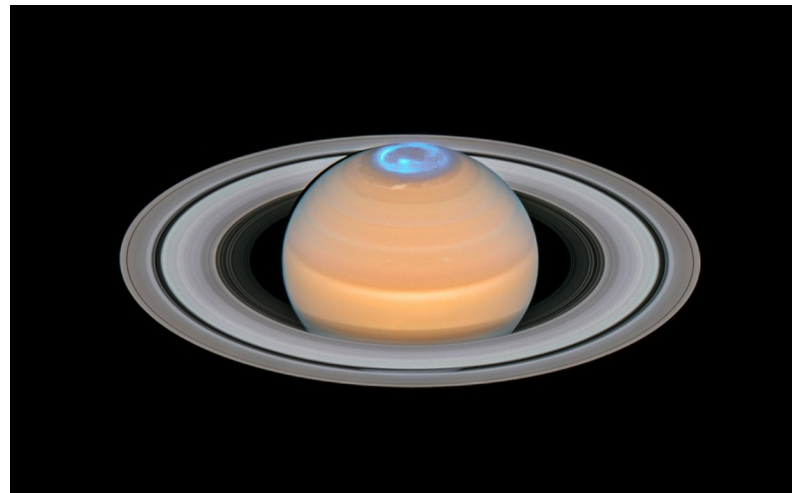
Spots in aurora on Jupiter are magnetically connected with its satellites: the spot on the left side is connected with Io, bottom two with Ganymede and Europe.



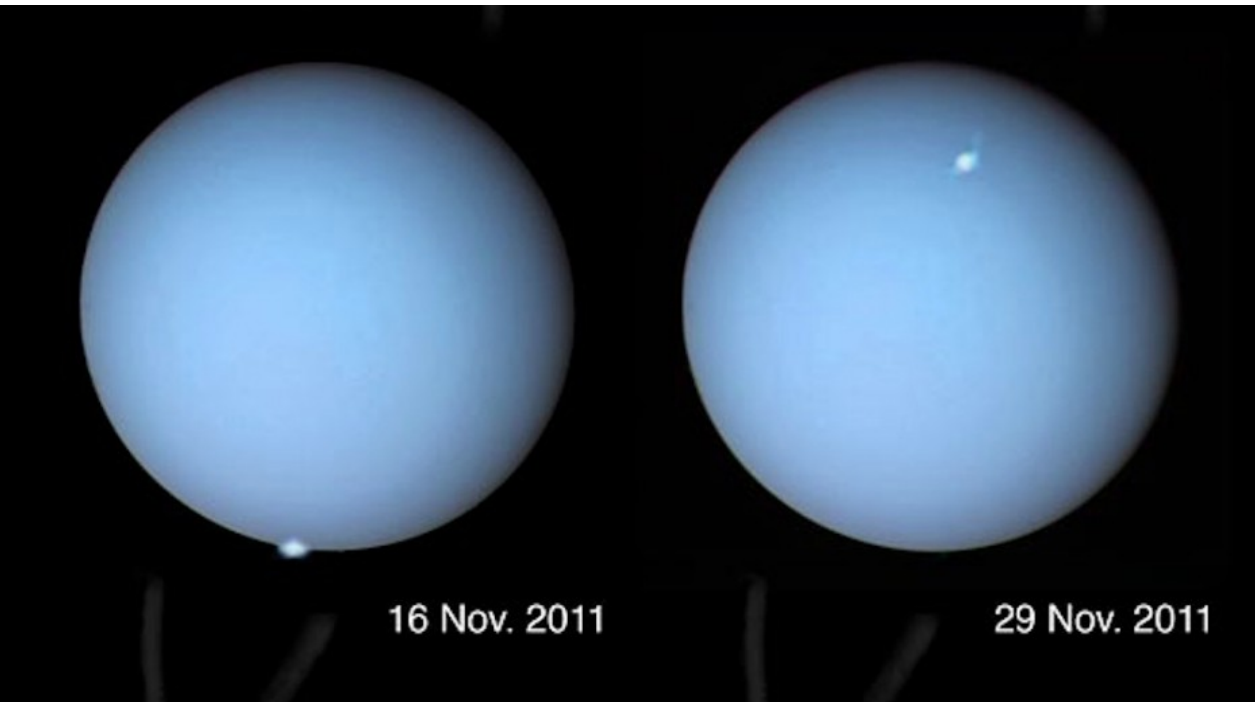
JWST's capture of aurora on Jupiter



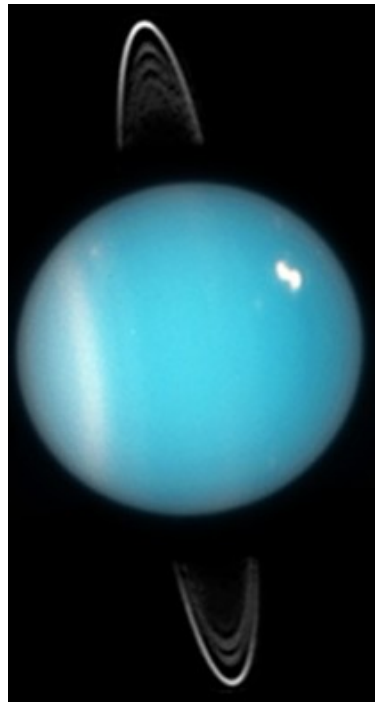
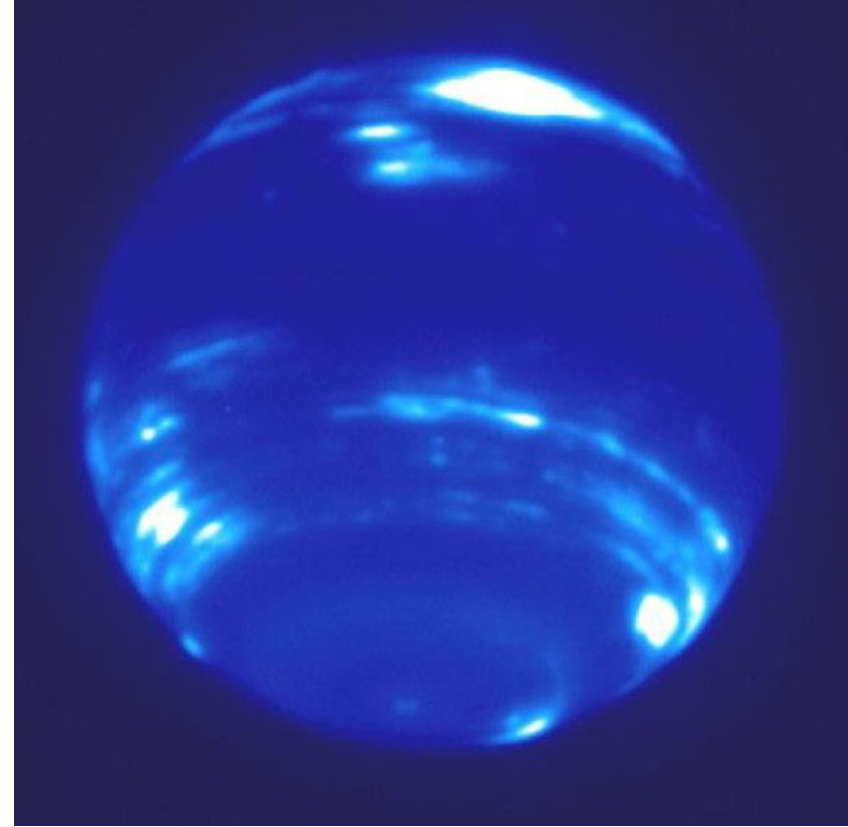
Saturn also features polar aurora:



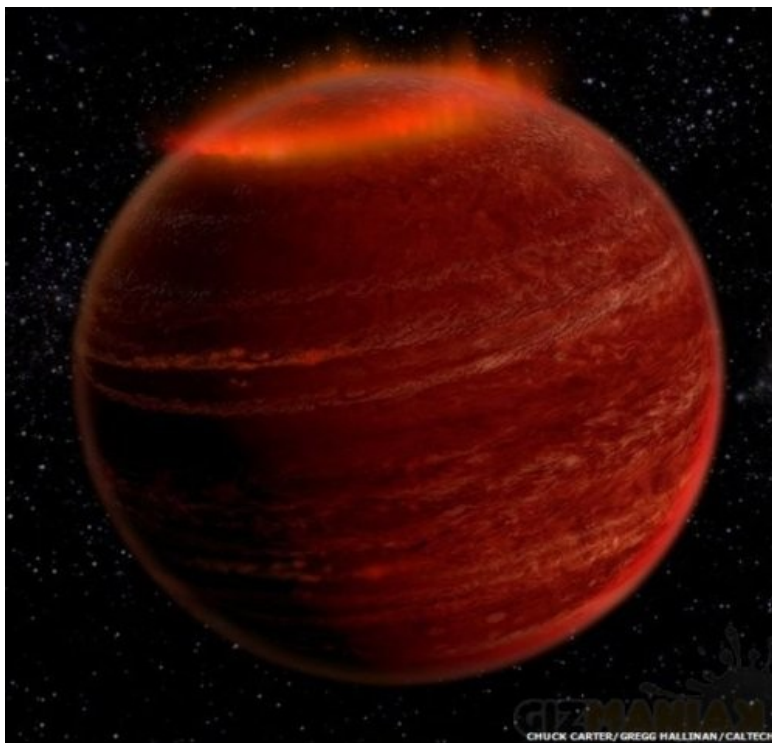
HST observed auroras on Uranus:



And Keck on Neptune:



- As for now, we have an observation of extrasolar aurora on a brown dwarf LSR J1835+3259, 18 lyrs from us, in Lyra. There are more of similar objects which show characteristic spectral features which point to aurora. Shown is an artist impression, not the real observation. It is reddish aurora, from more hydrogen in the atmosphere, and about million times more intense, because of larger magnetic field.
- Such an aurora should also be of different nature, because there is no other star for producing the stellar wind.
- A model for aurora requires a continuously replenished body of plasma within the magnetosphere. This mass-loading can be achieved in multiple ways, including interaction with the interstellar medium, a volcanically active orbiting planet or magnetic reconnection at the photosphere. Alternatively, an orbiting planetary body embedded within the magnetosphere could provide magnetospheric interaction.



In the cases of **exoplanets**, we also expect auroras, and we can use the same simulations and make the predictions for different kinds of planets.

In the cases of **planets around pulsars**, which were actually the first observed exoplanets, we can expect similar effects. Because of much larger field involved, they could behave different from usual planet aurora.

Here we try to make the first such model, by introducing necessary modifications in our star-planet interaction setup.

- In a series of works by Varela et al. (e.g. A&A, 616, A182, 2018; A&A 659, A10, 2022) are given numerical simulations of planetary magnetospheric response in extreme solar wind conditions, using the PLUTO code.
- Such simulations are valid for Earth and exoplanets.
- We use this setup as a template for the much larger magnetic field of pulsar.

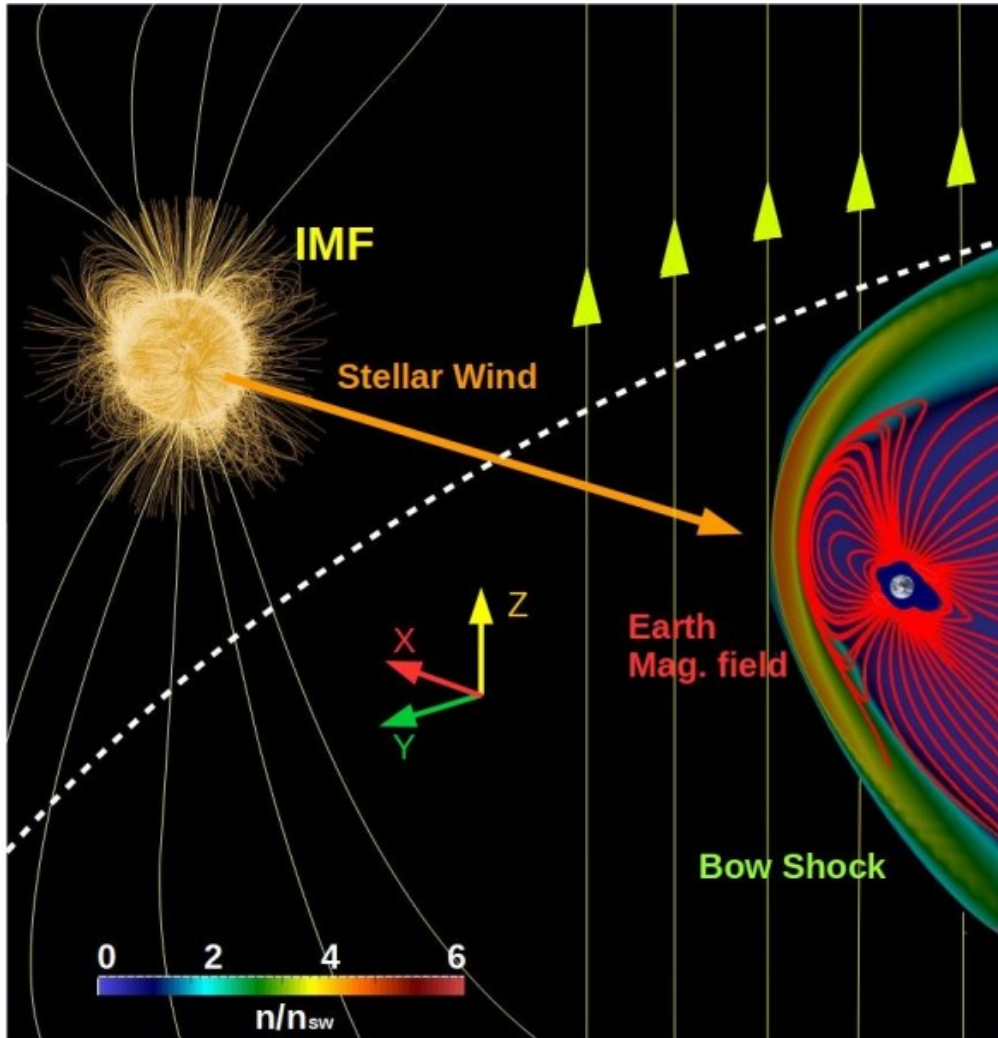


Fig. 1. 3D view of a typical simulation setup. We show the density distribution (color scale), Earth magnetic field lines (red lines), and IMF (yellow lines). The yellow arrows indicate the orientation of the IMF (northward orientation). The dashed white line shows the beginning of the simulation domain (the star is not included in the model).

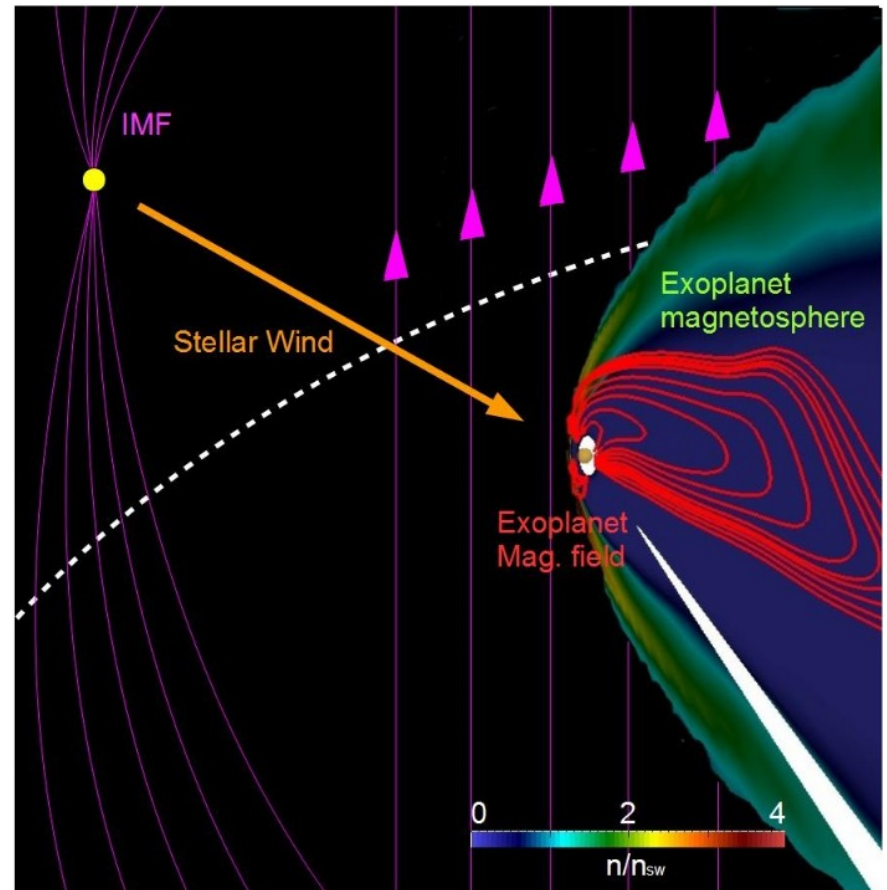


Fig. 1. 3D view of the system. Density distribution (color scale), field lines of the exoplanet magnetic field (red lines) and IMF (pink lines). The arrows indicate the orientation of the IMF (Northward orientation). Dashed white line shows the beginning of the simulation domain.

Numerical simulations of Sun-Mercury interaction

Similar study was also done for Mercury, where we have a wealth of data from Mariner 10 mission, which measured the dipole moment, and later Messenger mission, which provided more precise measurements for the multipolar representation.

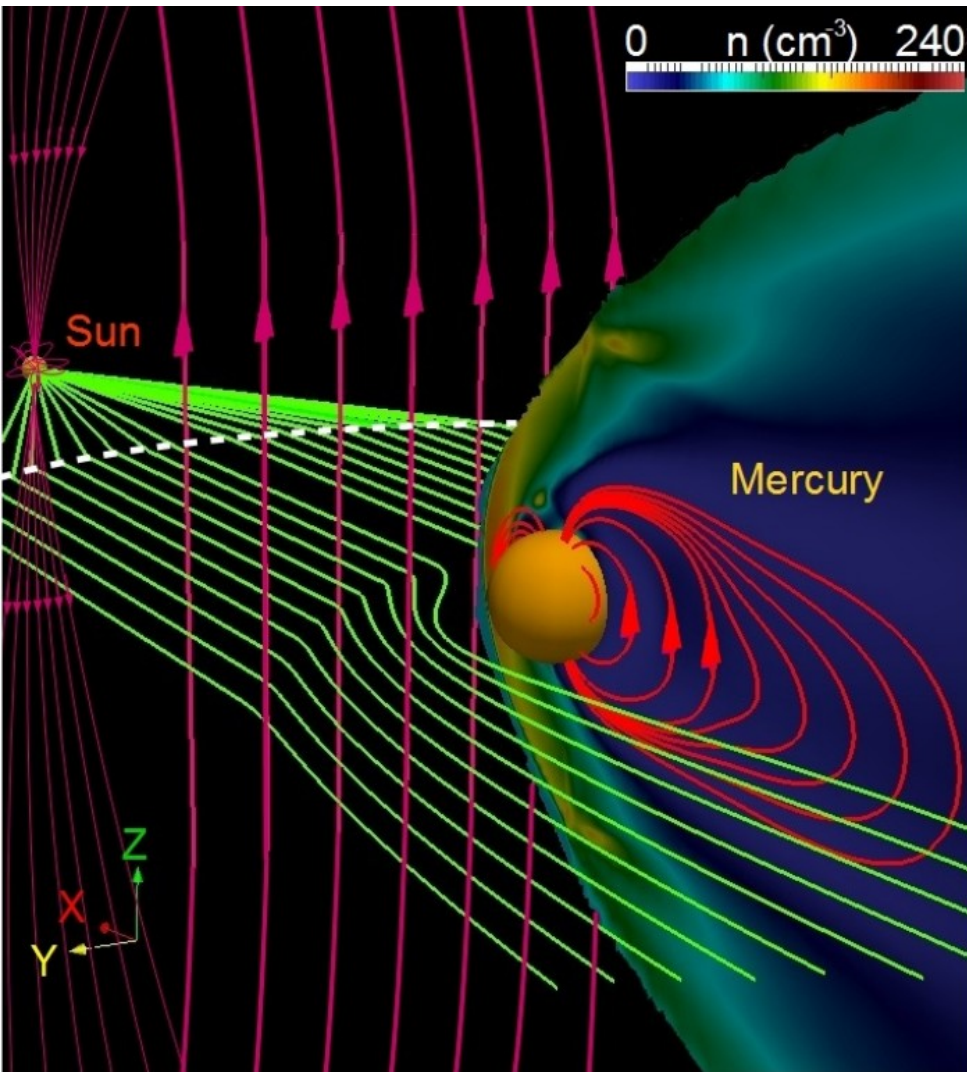


Fig. 1. 3D view of the system. Density distribution (color scale), field lines of the Hermean magnetic field (red lines), IMF (pink lines) and solar wind stream lines (green lines). The arrows indicate the orientation of the Hermean and interplanetary magnetic fields (case Bz). Dashed white line shows the beginning of the simulation domain.

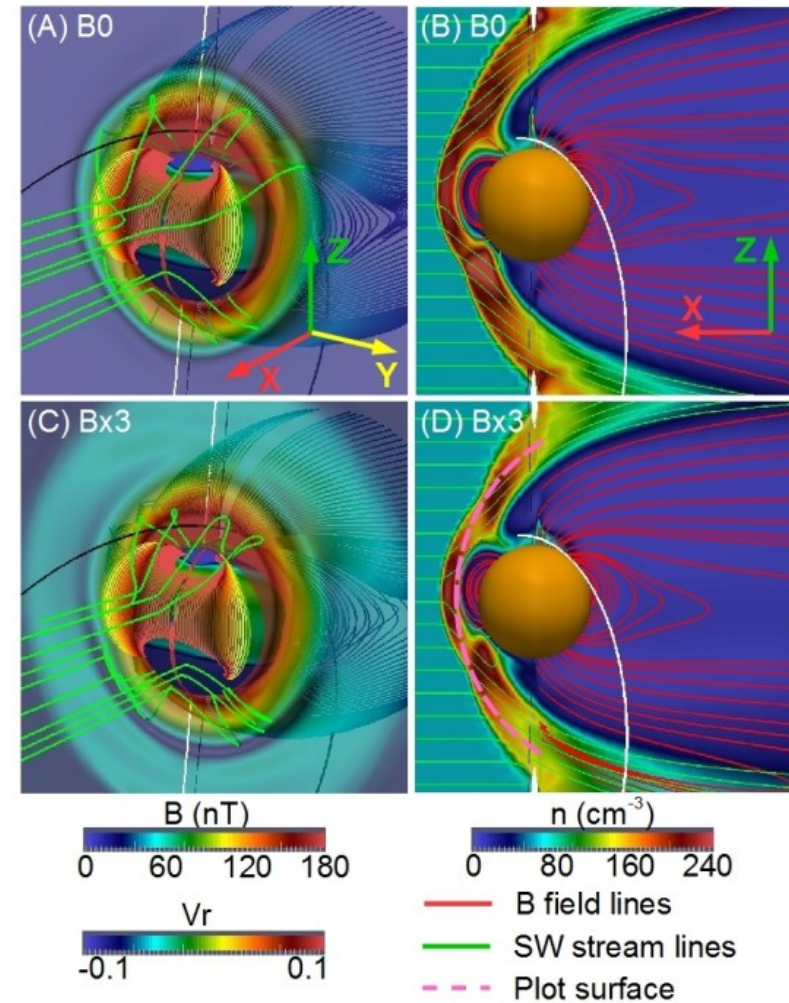


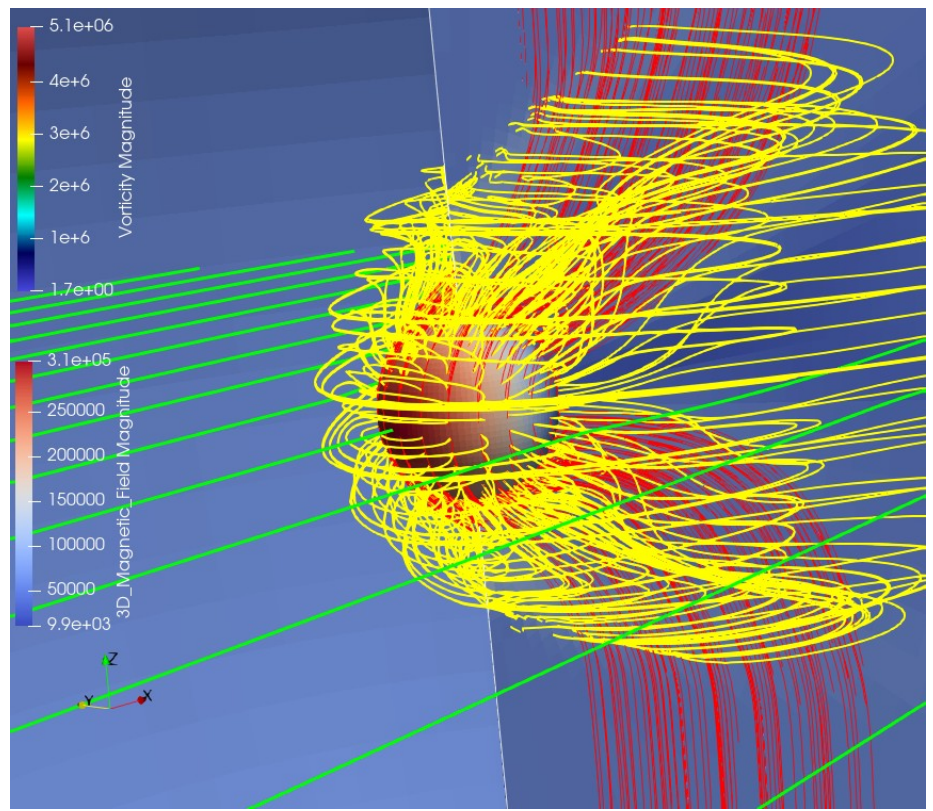
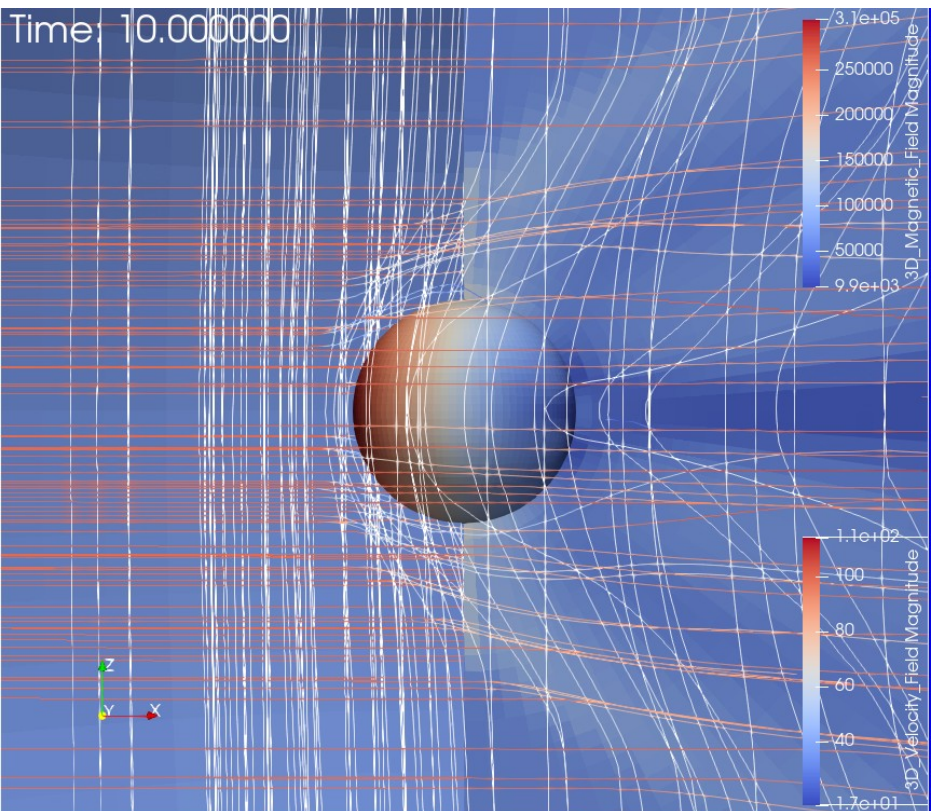
Fig. 2. Hermean magnetic field lines with the intensity imprinted on the field lines by a color scale for the reference case (A) and simulation Bx3 (C). Magnetic field intensity at the frontal plane $X = 0.3R_M$. SW stream lines (green). Inflow/outflow regions on the planet surface (blue/red). Polar plot of the density distribution (displaced $0.1R_M$ in Y direction) for the reference case (B) and simulation Bx3 (D). Dashed pink curve indicates the surface plotted in figures 3 and 4.

I show preliminary results in our simulations with NS parameters. We are increasing the stellar magnetic field in the simulations-to accommodate for the large field we increase the density of the interplanetary medium, local magnetic field strength near the planet and stellar wind velocity. We probe for the different planetary surface boundary conditions (conducting, ferromagnetic) - this is potentially interesting for the planetary study: planets around NS could have some extreme physical properties.

Conducting planet ($B_{\text{planet}}=0$):

$B_{\text{sw}}=3.0$, $V_{\text{sw}}=1.e9$

Currents (yellow), V_{sw} (green), mag.field (red)

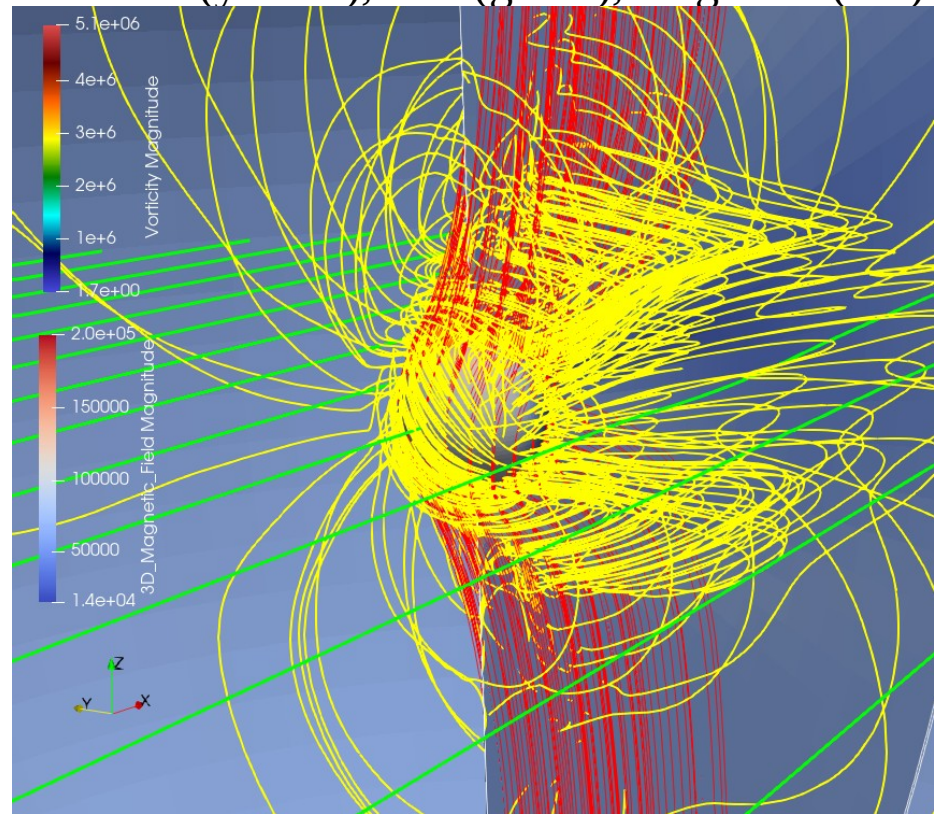
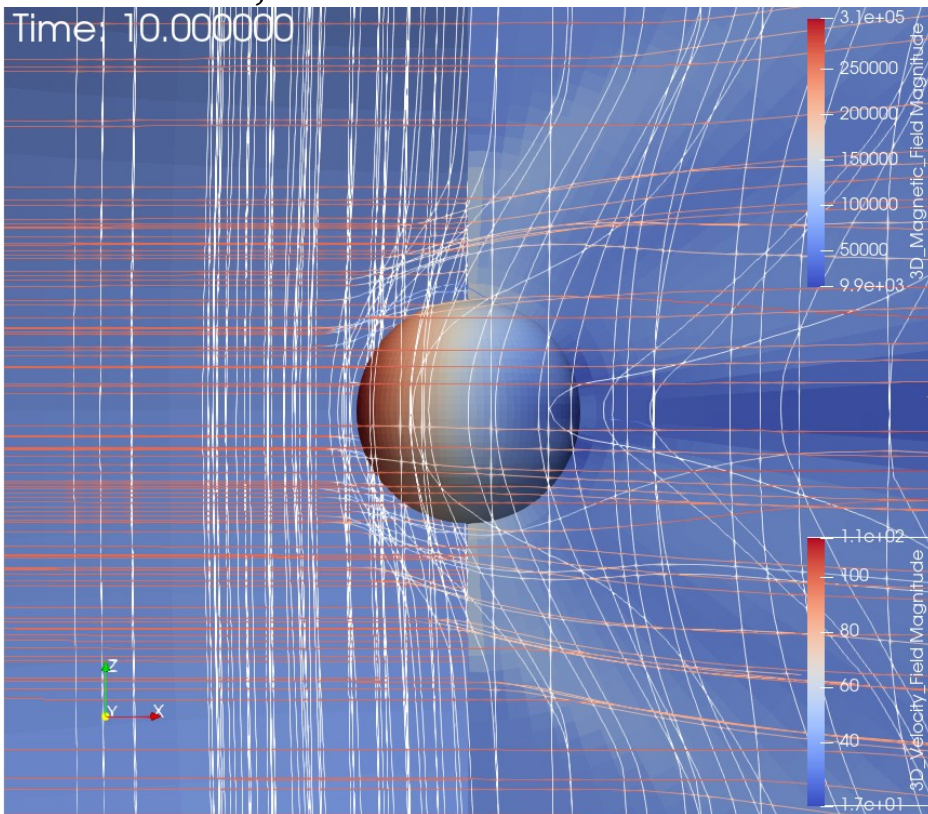


For the conducting planet atmosphere case, electric current loops remain close to the planet surface.

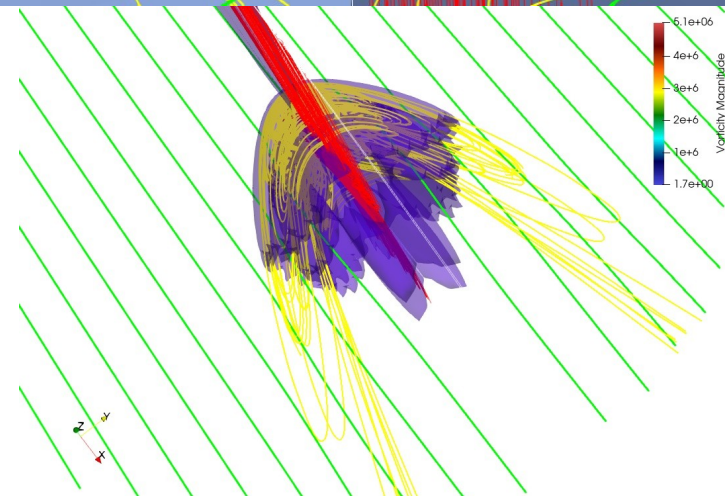
In the case of ferromagnetic planet surface, results are different, currents point to an extended dipolar *electric field* structure. Work is in progress to understand the possible auroral effects.

$B_{sw}=3.0$, $V_{sw}=1.e9$

Currents (yellow), V_{sw} (green), mag.field (red)

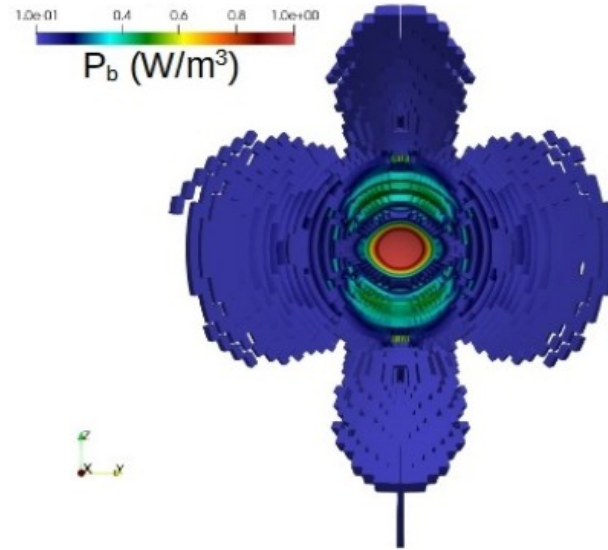
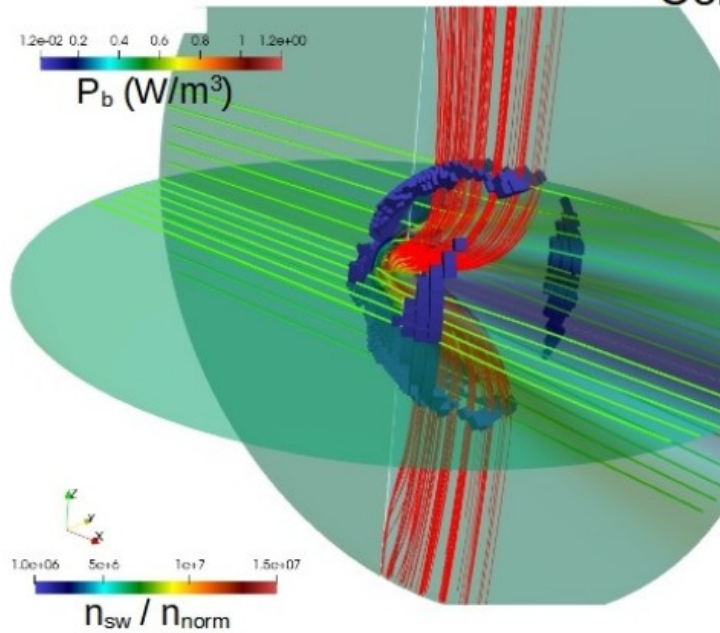


Equatorial view-Alfven “wings”:

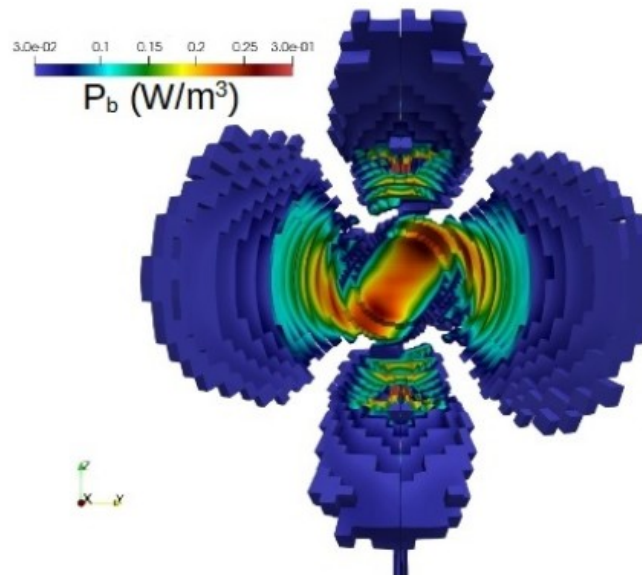
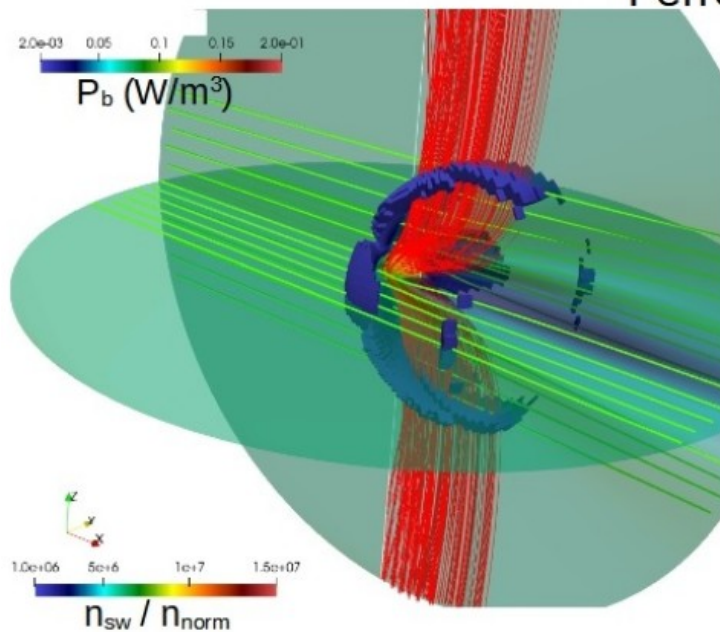


Radio emission from non-magnetic planets

Conductor



Ferromagnetic



Left panels: Iso-volume of Poynting flux divergence in cases with non-magnetic planet. Red lines are the magnetic field lines and green lines are the velocity streamlines of stellar wind.

Right panels: Mag. power in the same cases. A surface with the maximum radiated power is located in the nose of the bow shock, because of bending and compression of inter-planetary magnetic field.

- El.mag. emission is 100 million times more intense than in the Sun-Earth case.
- We suggest that it could be observable even with the current instruments.

```
x - + Terminal - miki@miki: ~
File Edit View Terminal Tabs Help
I pluto.ini (ini)
[[Grid]
X1-grid      2      3.0      8      u      3.2      128      u      30
X2-grid      1      0.0     48      u      3.14
X3-grid      1      0.0     96      u      6.28

[Chombo Refinement]
Levels              4
Ref_ratio           2 2 2 2 2
Regrid_interval    2 2 2 2
Refine_thresh       0.3
Tag_buffer_size     3
Block_factor        4
Max_grid_size       32
Fill_ratio          0.75

[Time]
CFL                 0.5
CFL_max_var         1.1
tstop               0.1
first_dt            1.e-5

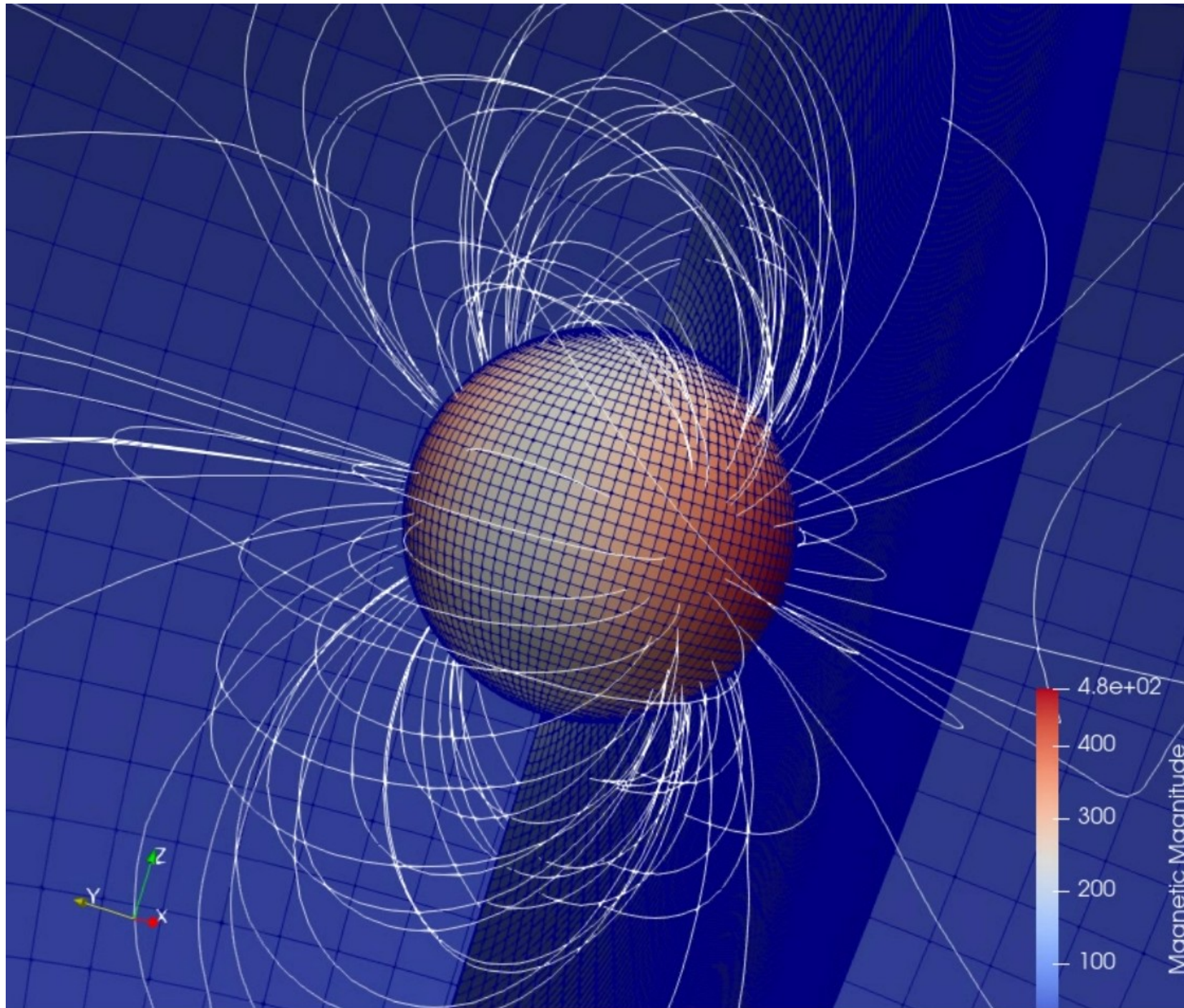
[Solver]
Solver              hll
```

```
x - +
Terminal - miki@mikic: ~/Pluto442/RunEarth1
File Edit View Terminal Tabs Help
I A init.c (c)
/* ////////////////////////////////////// */
/*!
 \file
 version 2.0
 \Mercury magnetosphere.
 \author J.Varela, Miki and V. Reville
 \date 26/05/2017

 \modified by miki for PLUTO 4.4
 \date 12/01/2022
*/
/* ////////////////////////////////////// */
#include "pluto.h"

/* ***** */
void Init (double *v, double x1, double x2, double x3)
/*
 *
 ***** */
{
 int i, j, k;
 double r, R, z, slp, slp2, slp3, v1, v2, v3, bbb1, bbb2, bbb3, bd, b_f, gam, Mn, ddip;
 double cqdr, cdip, coct, sixt, Tp, vs_p;
 double beta, bx_w, by_w, bz_w, vx_w, vy_w, vz_w, va, bdip, in_b, rd, pi, vs, bs;
 double ddi, rho_sw, B_norm, P_norm, T_norm, r_sw_c, r_sc, r_in, in_s;
 double AA, BB;
 double xc1, xc2, xc3;
```

Star-planet: a good exercise for simulations and plots in 3D ⁴⁸



- Usually Linux clusters and supercomputers use management and queuing system. I will describe two of them, which work in a similar way. Think of them just as an expanded command for running your job.
 - **SLURM** - a free one, became quite reliable so one does not need to pay for management, which could come with a significant cost. After creating a `slurm_job_file`, execute `sbatch slurm_job_file`. Most often used commands: `sbatch`, `squeue`, `scancel`.
 - **PBS** – (Portable Batch System), there are Open (free) and Pro (not free) versions, also very similar is its fork, **TORQUE**. After creating a PBS or TORQUE job script `pbs_job_file`, execute in terminal: `qsub pbs_job_file`.
Most often used commands are: `qsub`, `qstat`, `qdel`, `qmgr` and `xpbs`, `pbsjobs` (located in `/home/Tools/bin`) for additional detail about queued and running jobs.

```
miki@chuck: /work/chuck/miki/Pluto/RuchiNewStart1
I A qpluto.sh (sh) Row
#! /bin/bash -l
#SBATCH -J pluto41
#SBATCH -N 6
#SBATCH --ntasks-per-node=16
#SBATCH --mem-per-cpu=500MB
#SBATCH --time=5-00:00:00
#SBATCH -p para
#SBATCH --output="out.txt"
#SBATCH --error="err.txt"
#SBATCH -A camk
#SBATCH --mail-type=END
cd /work/chuck/miki/Pluto/RuchiNewStart1
module purge
module add mpi/mvapich2-2.2-x86_64
#just a serial task (step)
#srun -n 1 mpicc make
srun --mpi=pmi2 ./pluto -restart 540
```

```
miki@gate:tiara/ara/data/miki/Pluto/Saclay/M3a3DRmax50
I A qpluto (Modified)(sh) $MPICH HOM Row 29 Col 1 4:54 Ctrl-K H for
#PBS -N pluto
##### Output files #####
##PBS -o pluto.out
#PBS -e pluto.err
##### Number of nodes and cores #####
#PBS -l nodes=12:ppn=8
##### Queue name #####
#PBS -q medium
##### Sends mail to yourself when the job begins and ends #####
##PBS -M miki@tiara.sinica.edu.tw
###PBS -m be
##### Specific the shell types #####
###PBS -S /bin/bash
##### Enter this job's working directory #####
cd $PBS_O_WORKDIR
##### Load modules to setup environment #####
. /etc/profile.d/modules.sh
module purge
module load mpich
##### Run your jobs with parameters #####
if [ -n "$PBS_NODEFILE" ]; then
  if [ -f $PBS_NODEFILE ]; then
    NPROCS=`wc -l < $PBS_NODEFILE`
  fi
fi
$MPICH_HOME/bin/mpirun -machinefile $PBS_NODEFILE -np $NPROCS ./pluto -restart 42
```

Summary of the Lect. 8

- Pseudo-Newtonian potential and its use in numerical simulations of compact objects
- Simulations of thin disk or torus around a black hole in Paczynski-Wiita potential
- Simulations of thin disk around a naked singularity in pseudo-Newtonian potential for Reissner-Nordstrom metric.
- Star-planet simulations
- Running jobs on a Linux cluster

Thank you!

